NOVEL IMIDAZOLE AND IONIC LIQUID-BASED PLATFORMS AS MEDIA FOR CO_2 CAPTURE APPLICATIONS

by

MATTHEW SAMUEL SHANNON

JASON E. BARA, COMMITTEE CHAIR

C. HEATH TURNER
CHRISTOPHER S. BRAZEL
ERIC S. CARLSON
DANIEL T. DALY

A DISSERTATION

Submitted in partial fulfillment of the requirements
for the degree of Doctor of Philosophy in the
Department of Chemical and Biological Engineering
in the Graduate School of
The University of Alabama

TUSCALOOSA, ALABAMA

2014

ABSTRACT

The objective of this extensive research project was to investigate imidazoles as potential solvents for acid gas removal applications. Imidazoles are integral starting materials and neutral analogs for the synthesis and production of imidazolium-based ionic liquids (ILs) and virtually have not been explored as candidates for novel, CO_2 capture media. *N*-functionalized imidazoles also provide a similar platform as seen in ILs as tunable structures that govern physical and chemical properties leading towards lower volatilities, lower viscosities, higher CO_2 uptake, etc. Physical properties (including density, viscosity, and gas solubilities) of *N*-functionalized imidazoles were recorded providing an initial database for comparisons to commercially-available organic solvents and imidazolium-based ILs. These results show that some novel *N*-functionalized imidazoles contend with common organic solvents for CO_2 separations in terms of dynamic processing properties (i.e. viscosity and CO_2 uptake). Imidazoles and ILs also provide a non-volatile media in which fugitive emissions and evaporative losses during solvent regeneration are reduced significantly.

Chemical simulations and calculations via COSMOtherm software were also employed to rapidly predict thermophysical properties of these imidazoles and ILs, providing a means of screening of such novel solvents to be optimized for CO_2 separation processes. In the concluding chapters of this dissertation, continued research with the *N*-functionalized imidazole platform are noted, including areas of hybrid solvents, multiply-substituted, isomeric compounds, and imidazole-based polymeric media for acid scavenging (CO_2, SO_2, etc).

DEDICATION

This dissertation is dedicated to those who have inspired me, encouraged me, and instructed me in everything up to this point in my career, as well as with life lessons that have brought me much success and motivation so far. To my loving parents and brother who have been with me all of my life and watched me grow into the man I have become, reassuring me through the highs and lows of life. To all of the classmates, coworkers, advisors, and life-long friends I have made throughout this whole process and will always have a special place in my heart as I continue on with what life has to offer in the near future. And last but not least, to the love of my life, my fiancé and soon-to-be wife for making all of this hard work and journey worth the while. I look forward to our bright and joy-filled life together and am excited for the many years to come.

ACKNOWLEDGMENTS

I would like to express my appreciation and gratitude to all of my friends and colleagues who have inspired and supported me both personally and professionally in pursuit of my PhD. First and foremost, I would like to give a special thank you to my graduate advisor, Dr. Jason E. Bara, who has maintained an excellent level of supervision, advisement, and patience throughout all of my work at The University of Alabama. He has always been there to personally drive me and push me to uphold a higher standard of excellence and work, while always remaining an enthusiastic mentor and friend through our research and collaboration together.

I would also like to thank my committee members, Dr. C. Heath Turner, Dr. Christopher S. Brazel, Dr. Eric S. Carlson, and Dr. Daniel T. Daly, for all of their cooperation, guidance, and suggestions. I have to give a huge thank you and show gratitude to the Department of Chemical and Biological Engineering for allowing me the opportunity to pursue my PhD.

I must express my love and appreciation towards my parent, family, and fiancé for their continuous sacrifices and belief in me and my life goals. This journey would not have been possible without them motivating me to pursue and achieve my personal ambitions.

I would also like to recognize my fellow doctoral research group, Jeffrey Horne and John Whitley, as well as my colleagues, Brian Flowers and Chuntian Hu, for their hard work and dedication in the lab, classroom, and office, making the work environment very comfortable and enjoyable and memorable.

TABLE OF CONTENTS

LIST OF TABLES

LIST OF FIGURES

CHAPTER ONE

INTRODUCTION

With an ongoing emphasis on reducing greenhouse gas emissions to the atmosphere and our ecosystem, continuous research endeavors are in pursuit for novel alternative technologies and approaches to mitigate fugitive greenhouse gas (GHG) emissions. Leading scientists and contributors to research in atmospheric and climate variations strongly agree that CO_2 emissions contribute to nearly half of current global warming conditions.[1-3] The average atmospheric CO_2 concentration has increased from 275 to 387 ppm within the last century, with climate models suggesting CO_2 emissions to double by the year 2100 and increase the current global temperature by 2-4^{o}C.[2,4] The leading source for the rise in anthropogenic CO_2 emissions is due to the increase in burning of fossil fuels, accounting for 94.6% of U.S. CO_2 emissions in 2009, according the EPA.[5] It has also been estimated that global emissions will increase from 9 to 32 Gton per year by 2050, with coal-fired power plants being the leading cause of the increase in CO_2 emissions.[2] As coal is still one of the cheapest and readily-available commodities for burning to produce electricity, it is inevitable that this process is will continue to be utilized as electricity demands will inherently increase in the future.

Novel processes and techniques for CO_2 capture and sequestration (CCS) from these large point sources have been suggested and explored to be effectively employed to remove CO_2 from coal-fired power plant flue gas, where the captured CO_2 is compressed and stored in subterranean geological sites. This stored CO_2 presents innovative uses, including enhanced oil recovery (EOR), in which CO_2 is injected into semi-depleted oil reservoirs to efficiently and economically recover crude oil that is viscous and not easily accessible. However, the Department of Energy has set stringent and specific requirements for proposed and novel techniques for CCS applications: 90% of CO_2 emissions must be captured with a purity of at least 90%, and not to increase the current cost of electricity (COE) by more than 30%.[6] The most readily-available technology utilized for CO_2 separations in the natural gas industry is aqueous amine solvents (e.g. aqueous monomethanolamine (MEA)). However, this technology along with other common organic solvents is not feasible or practical to scale up to process the vast bulk gas (e.g. N_2, CO_2, etc.) flow rate from power plants and other industrial sources.

Our studies explore the concept of employing the imidazole-platform as novel chemical solvent and polymeric media for CO_2 separation applications for both post-combustion capture and natural gas processing, as presented in the following eight chapters. In Chapter Two, initial experimental investigations

of alkylimidazoles and comparisons to imidazolium-based ionic liquids are presented. Chapter Three relates current and aforementioned ionic liquid solvents explored in research and compares CO_2 separation performance and presents the novelty of imidazoles for such separations of CO_2 and other acid gases (e.g. SO_2, H_2S). Chapter Four shows experimental evaluations of aforementioned alkylimidazoles for CO_2/CH_4 separations along with solubility temperature dependence. Comparisons of these novel solvents and ILs are made to that of the thermophysical properties of common organic solvents for gas separations. In Chapter Five, ionic liquids and their CO_2 solubilities are modeled via COSMOTherm software package and correlated to molar volume (V_m) and fractional free volume (*FFV*) for an underlying relationship and dependence that governs solvent properties based on cation and anion systematic structures. Properties of alkylbenzimidazoles are presented in Chapter Six for CO_2 and SO_2 separations as another analogous structure and precursor to common ILs. Chapter Seven explores the concept of functionalizing the imidazole solvent platform with polar substituents (e.g. oligo(ethylene glycol) units) and compared to that of the properties and performance of 1-*n*-alkylimidazoles for CO_2/CH_4 separations. Chapter Eight reflects the first reported characterization of SO_2 solubility in *N*-functionalized imidazoles and the resulting molar complex at ambient conditions, verified via molecular-level calculations and measured SO_2 binding energies. Chapter Nine presents the concept of imidazole-based polymers and co-polymers for fixed media CO_2 separations, along with novel electrolyte polymeric materials and proposed synthesis. The imidazole structure with its nucleophilic behavior possesses possibilities for facilitated transport via bicarbonate formation for post-combustion capture applications and the ability to readily form ionic species as novel poly(ILs).

CHAPTER TWO

[†]Properties of Alkylimidazoles as Solvents for CO_2 Capture and Comparisons to Imidazolium-based Ionic Liquids

Matthew S. Shannon & Jason E. Bara*

Department of Chemical & Biological Engineering

The University of Alabama, Tuscaloosa, AL USA 35487-0203

Abstract

Density, viscosity and CO_2 solubility of a series of ten 1-*n*-alkylimidazoles with chain lengths ranging from methyl (C_1) to tetradecyl (C_{14}) were characterized. Density and viscosity values were comparable to many common organic solvents over a temperature range of 20 – 80°C. The measured data were utilized to develop empirical models for these physical properties with respect to temperature and the contribution of the *n*-alkyl chain. Solubility of CO_2 in 1-*n*-alkylimidazoles at ambient temperature (25°C) and low pressures (3 – 7 atm) was found to be less than most common organic solvents, even though the 1-*n*-alkylimidazole motif offers opportunities to tune the molecule's solubility parameter. This effect was attributed to lower fraction free volume (FFV) that is available in molecules with systematically variable side chains. 1-*n*-alkylimidazoles were less dense than most 1-*n*-alkyl-3-methylimidazolium-based ILs, with differences ranging from 10 – 50%, based on contributions to increased density from the anion. However, much larger differences in viscosities were observed between the two classes of compounds, with ILs at least an order of magnitude more viscous than their neutral 1-*n*-alkylimidazole counterparts. Solubility levels of CO_2 were similar in both types of solvents indicating that no advantage (or disadvantage) in CO_2 uptake is achieved by transforming a neutral 1-*n*-alkylimidazole to a charged IL solvent. While CO_2 solubility levels in each are insufficient to provide a viable solvent for post-combustion CO_2 capture applications, 1-*n*-alkylimidazoles can be used in combination with amines as a low-volatility, high capacity solvent to capture CO_2, using only inexpensive and readily available components. The viscosity of a highly CO_2-rich liquid phase formed between monoethanolamine (MEA) and 1-butylimidazole was found to be 85 – 100 cP at 298 K, which is less viscous than many neat ILs. Initial data indicate 1-butylimidazole has a synergistic effect on CO_2 capture as the solution can easily exceed the stoichiometric limitations of 2 moles of MEA per 1 mole of CO_2. Thus, while certainly more volatile than IL-based analogues, 1-*n*-alkylimidazole solvents may offer some unique capabilities and advantages in CO_2 capture processes.

Keywords

Alkylimidazole solvents, CO_2 capture, imidazolium-based ionic liquids, gas separation processes, clean energy

[†]*Industrial & Engineering Chemistry Research, 2011, 50, 8665-8677*.

2.1 Introduction: The two most important features of ionic liquids (ILs) that have driven research into their use as solvents for engineering separations have been their very low to virtually negligible vapor pressures[1] (< 10 mbar at 300°C)[2] and tunable structures/properties.[3] The lack of a vapor pressure is a desirable characteristic in many separations applications,[4] as solvent losses due to evaporation are unlikely to occur and volatile solutes may be recovered cleanly without residual solvent entrainment. The ability to tune the structure of an IL enables a certain degree of control over physical properties[3] such as density, viscosity, heat capacity, hydrophobicity, etc. and thermodynamic properties such as CO_2 solubility[5] and heats of solution.[6] ILs present many potential advantages over conventional organic solvents and water, and consequently have created new opportunities to reconsider conventional chemical engineering processes.[4]

ILs, however, will likely remain inherently more expensive to manufacture than conventional organic solvents due to the cost of starting materials, the number of reaction steps needed and – depending on the end use – the degree of purification required (e.g. higher purity required for electrochemical applications than solvents for gas processing).[7] The increased cost of an IL-based solvent may be justifiable in applications where major process advantages/simplifications were obtained via improved solvent performance, minimized evaporative losses and/or increased solvent lifetime.[4]

While the lack of an appreciable vapor pressure is a quality associated with ILs, it may come at the expense of other physical properties, especially viscosity.[8] Solvent viscosity is an important consideration for separations applications, as increased viscosity typically correlates with decreased diffusion rates which negatively impact mass and heat transfer.[9, 10] Virtually all ILs are at least an order of magnitude more viscous than common organic solvents and H_2O at the same temperature.[11] However, other IL physical properties, such as density, heat capacity and surface tension are usually within the ranges exhibited by conventional organic solvents.[12]

The removal of CO_2 from the flue gas of coal-fired power plants, known as post-combustion CO_2 capture,[13] has been an area where ILs have received a great deal of attention as non-volatile solvents. However, the solubility of CO_2 in most ILs, like organic solvents, is largely physical in nature.[5] Consequently, most ILs lack the necessary carrying capacity for CO_2 to economically scrub 90% of CO_2 from low partial pressure (~2 psia) flue gas streams, with CO_2 capacities on the order of 1% or less relative to conventional aqueous amine solvents.[14] In order to improve CO_2 uptake in IL-based solvents, ILs featuring acetate (OAc) anions[15-18] and amine-functionalized "task-specific" ILs (TSILs) have been examined.[19] While both approaches enable much greater CO_2 capacity relative to other ILs lacking these functionalities, a much

more intensive synthetic method was required and/or dramatically increased solvent viscosities were observed in the CO_2-rich state.[20]

If the goal of designing ILs solvents is to eliminate volatility while achieving one or more desired physical, thermodynamic or chemical properties, then the trade-offs and benefits associated with using an IL-based approach must be assessed.[4] If the key property(ies) of interest is similar to that of the organic solvent which is being replaced, then a technical assessment of switching to an IL-based solvent is relatively straightforward. However, when the magnitude of the key property(ies) of interest deviates significantly from conventional solvents (e.g. viscosity), more thorough consideration must be given to the impact on process operation and whether the use of an IL can be supported within the existing process design. Increased viscosities may result in decreased mass and heat transfer rates which can require larger unit operations such as absorption columns and heat exchangers.[10]

In assessing the viability of an IL as a solvent for industrial separations processes, several key questions must be asked:

- Will the replacement cost of the non-volatile IL solvent with non-ideal physical properties still provide sufficient technical and economic benefits to warrant modifying the current process or designing/constructing a new process around the properties of the IL?
- Might a hybrid approach be taken where the IL is combined with one or more non-IL components to achieve the desired solvent performance?
- For separations involving (reversible) chemical reactions, are strategies available to produce an IL *in situ*, whereby an IL is a reaction product or intermediate (reversibly) generated from non-IL starting materials?

While many works have considered imidazolium-based ionic liquids (ILs) (Figure 2.1a) for existing and emerging separation applications such as CO_2 capture, virtually no attention has been given to the use of *N*-functionalized imidazoles (Figure 2.1b) from which these ILs are derived. *N*-functionalized imidazoles are also a modular system in that the 'R' group can be chosen from a nearly endless array of functionalities. Many *N*-functionalized imidazoles exist as liquids at room temperature,[21] potentially making them useful as solvents in many of the same separation applications that have been proposed for ILs.[22] More complex imidazoles derivatives featuring substitutions at one or more of the three carbon positions in the 5-membered ring are also well-known. A distinguishing feature of *N*-functionalized imidazoles is the presence of a "pyridine-like" nitrogen center (opposite the functionalized or "pyrrole-like" nitrogen) which can act as a Bronsted base or proton (H^+) acceptor (Scheme 1a).[23] This pyridine-like nitrogen is key to the formation of imidazolium salts (Scheme 1b), however this transformation results in the loss of Bronsted basicity.

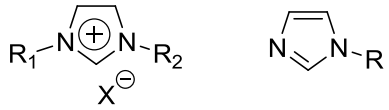

Figure 2.1: Structures of (a) imidazolium-based ILs and (b) *N*-functionalized imidazoles.

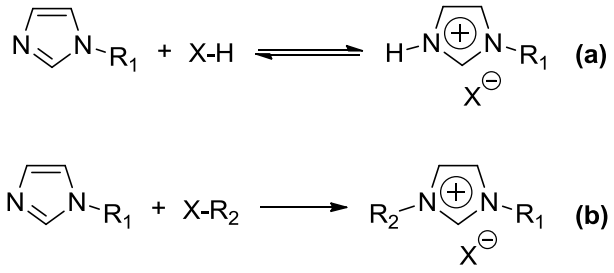

Scheme 1: (a) *N*-functionalized imidazole reacting as Bronsted base and (b) permanent quaternizatoin of *N*-functionalized imidazole with alkyl halide to produce an imidazolium salt.

Very limited physical property data (e.g. density, viscosity, vapor pressure) currently exist for *N*-functionalized imidazoles, even for the simplest 1-*n*-alkylimidazole compounds (e.g. 1-methylimidazole, 1-butylimidazole, etc.). Vapor pressure data may be garnered from reports on the distillation of *N*-functionalized imidazoles as a means of purification in certain chemical syntheses. This is in distinct contrast to imidazolium-based ILs, where density and viscosity properties have been characterized for perhaps at least several hundred compounds.[11, 12] Thus, in order to compare how *N*-functionalized imidazoles might perform relative to their imidazolium-based IL analogues, fundamental experimentation and studies are needed to generate baseline physical property data.

In this work, we present the first known characterization of the density, viscosity and CO_2 solubility properties of a series of ten 1-*n*-alkylimidazole compounds. Each property was found to have a strong relationship to the length of the alkyl substituent. For density and viscosity, empirical models were developed to relate these properties to temperature and the length of the alkyl chain. CO_2 solubility in 1-*n*-alkylimidazole compounds could be related to calculated Hildebrand solubility parameters, with CO_2 solubility decreasing with decreasing solubility parameter. Relative to imidazolium-based ILs, 1-*n*-alkylimidazoles can offer reductions in viscosity of up to 2 orders of magnitude. CO_2 solubility in 1-*n*-alkylimidazoles was slightly greater (~10-20%) when compared to imidazolium-based ILs, though the values measured are less than those exhibited by common polar organic solvents.[24] However, the CO_2 capacity of 1-*n*-alkylimidazoles could be improved by blending with an amine, as demonstrated with a mixture of 1-

butylimidazole and monoethanolamine (MEA) in the presence of low pressure CO_2. It was found that this combination of an *N*-functionalized imidazole and a 1^o amine could exceed the stoichiometric limitation of 2:1 moles amine per mole of CO_2, while the viscosity of the CO_2-rich solvent was < 100 cP at 25 ^oC. These initial studies indicate that the intrinsic properties of 1-*n*-alkylimidazole solvents, though more volatile than ILs, may offer performance improvements relative to ILs and TSILs in CO_2 capture applications.

2.2 Experimental:

2.2.1 Materials: 1-methylimidazole (1) was obtained from Sigma-Aldrich (Milwaukee, WI USA) and used without further purification. 1-*n*-alkylimidazoles (2 – 10) were synthesized in our laboratory from sodium imidazolate (NaIm) and a corresponding alkyl bromide as detailed in other works.[21, 25] The 1-*n*-alkylimidazoles produced in this reaction were purified by dissolving the crude product in a 50:50 (vol:vol) mixture of EtOAc/hexanes, drying over $MgSO_4$, passing the solution through a plug of Al_2O_3, removing the solvent and drying the final product under dynamic vacuum (< 1 torr) for at least 2 hours. All compounds were obtained as pale, yellow oils.

Research Grade CO_2 was purchased from AirGas (Radnor, PA USA). Certain 1-*n*-alkylimidazoles with odd numbered side chains (heptyl, nonyl, undecyl and tridecyl) were excluded from this study due to high cost and/or limited availability of suitable alkyl halides or other starting materials needed for their synthesis. It is also worth noting that we previously reported that 1-tetradecylimidazole has a melting point near room temperature, though can exist as a supercooled liquid for extended periods of time prior to crystallizing.[21]

2.2.2 Density Measurements: Density values for each 1-*n*-alkylimidazole were obtained using a Mettler Toledo DM45 DeltaRange density meter, which operates via electromagnetically induced oscillation of a glass U-form tube, with automatic compensation for variations in atmospheric pressure. The density meter can measure liquid samples within the range of 0 – 3 g/cm^3 with a minimal sample size of 1.2 cm^3. The accuracy of the density meter measurements is ±0.00005 g/cm^3 for all operating temperatures. Densities of 1-*n*-alkylimidazoles were recorded over a temperature range of 20 - 80°C at 10°C increments, for a total of seven density measurements per compound. As suggested by the manufacturer, the unit was washed between every run with deionized H_2O, followed by an acetone rinse, and then dried by air flow. The density reading of the clean, empty cell was verified to be consistent with that of air at 20°C (0.00120 g/cm^3) before continuing to the next sample. The accuracy of the instrument was verified through use of H_2O standards provided by the manufacturer.

2.2.3 Viscosity Measurements: Viscosity data were obtained using a Brookfield DV-II+ Pro viscometer. The viscosity measurement is based on a torque value and shear rate of a certain sized spindle in contact with a pre-determined amount of fluid. As recommended by the manufacturer, the "ULA" spindle and jacketed sample cell was used for these relatively low viscosity liquids (< 25 cP), which required a minimum sample size of approximately 16 cm^3. The viscometer accuracy is ±1% of the reading for torque measurement with a repeatability of ±0.2% of the reading. The viscosity of each 1-*n*-alkylimidazole was measured at ten temperatures within the range of 20 – 80°C. The temperature of the jacketed sample chamber was controlled via the Brookfield TC-602P circulating bath, which has an operating range of -20 – 200°C and a temperature stability of ± 0.01°C. The sample cell was cleaned between every run by rinsing with deionized water and acetone, followed by air drying. The viscometer was re-zeroed between runs as suggested by the manufacturer and the accuracy of the instrument was verified by measuring the viscosities of water and diethylene glycol, which span the range of viscosities exhibited by the 1-*n*-alkylimidazole solvents.

2.2.4 CO_2 Solubility Measurements: The solubility of CO_2 in each of the 1-*n*-alkylimidazoles was measured using an apparatus (Figure 2.2) constructed from guidelines developed for the natural gas industry.[26]

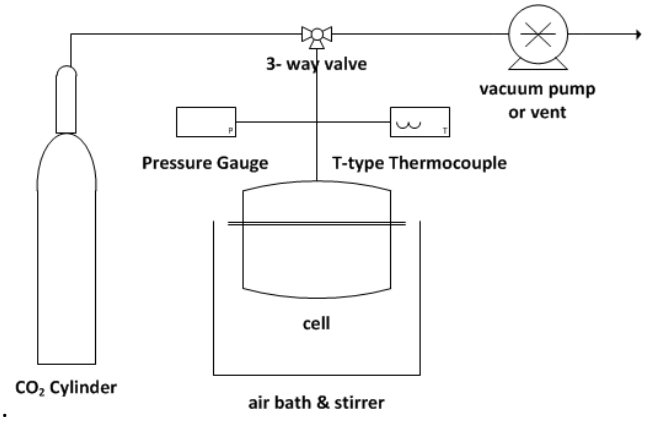

Figure 2.2: Schematic of the gas solubility apparatus.

The cell body was constructed from a 2.5" OD sanitary fitting butt-welded to a corresponding bottom cap. 1/4" VCR and 1/8" tube fittings were welded to the top cap, and a PTFE gasket and spring-loaded clamp were used to seal the vessel. The sanitary fittings, gaskets and clamps were purchased from McMaster-Carr. Swagelok fittings were purchased from Alabama Fluid Systems Technologies (Pelham, AL). Machine work was performed by Engineering Technical Services at the University of Alabama. Welding was performed by McAbee Construction (Tuscaloosa, AL).

Experiments were conducted at ambient temperature (25 ± 0.5°C) and the temperature controlled via air circulation. The unit was checked against published CO_2 solubility data for both physical solvents (imidazolium-based ILs)[5] and a chemical solvent (30 wt% aqueous MEA),[27, 28] providing data consistent with literature reports. Approximately 40 g (~40 – 50 mL) of a 1-*n*-alkylimidazole compound of interest was added to the cell and the weight of solvent recorded using a Mettler Toledo XS6002S Precision Balance, which has a maximum capacity of 6000 g, with an uncertainty of +/- 8 mg. The volume of solvent was calculated using the density values measured in this work. A 1.75" wide stir bar of known volume was added to ensure thorough contact between the gas and liquid phases. The vessel was then sealed and the residual air removed via vacuum until the system pressure was < 5 torr as measured by an MKS Baratron pressure transducer (accuracy of ± 0.5% of the reading) and displayed on a MKS PDR2000A Two-Channel Digital Power Supply/Readout. The transducer was also interfaced with LabView (National Instruments) for digital data acquisition and visual monitoring of system temperature and pressure. The sealed apparatus was then weighed to provide a tare weight prior to adding CO_2, the instrumentation re-connected and then unit secured above a stir plate. CO_2 was added to the cell at pressures between 3 – 7 atm, and the equilibrium pressure and weight of added CO_2 were recorded. Confirmation that equilibrium had been reached was determined via a stable pressure reading (± 2 torr) over at least 10 min on both the digital readout and the data acquisition software interface. Because the solvent viscosities are low, and the vessel was well-stirred, equilibrium was typically achieved in < 30 min. For physical solubility measurements under these conditions, the ratio of the mass of CO_2 absorbed in the liquid relative to the mass of CO_2 remaining in the gas phase was on the order of 1:1 – 2:1. The same ratio was > 10:1 for CO_2 solubility measurements in chemical solvents. Thus, the mass of CO_2 absorbed in the liquid phase was, at a minimum, equal to the mass of CO_2 in the gas phase. Given the scale of the experiments, the mass and pressure data collected were well beyond the lower sensitivity limits of the instrument.

A CO_2 pressure of 3 atm was chosen as a starting point so as to ensure a sufficient mass of CO_2 had been added to be far outside the error of the balance. About 350 – 400 mg of CO_2 per atmosphere of CO_2 pressure were absorbed in 40 mL of solvent. The moles of CO_2 (n_{CO2}) added to the vessel were calculated from the mass increase of the vessel and the molecular weight of CO_2 (44.01 g/mol). Because the compressibility factor of CO_2 is very close to 1.00 under the experimental conditions,[29] the ideal gas law was applied to calculate the moles of CO_2 in the vapor phase (n^v_{CO2}) by subtracting the volume of the stir bar and solvent from that of the empty cell (Eqn.1).[6, 30-32]

$$P_{vapor}(V_{cell} - V_{stirbar} - V_{solvent}) = n^{v}_{CO_2} RT_{vapor} \quad (1)$$

The moles of CO_2 in the liquid phase (n^{l}_{CO2}) were taken to be the moles in the vapor phase subtracted from the total moles of CO_2 added to the cell (Eqn. 2).

$$n^{l}_{CO_2} = n_{CO_2} - n^{v}_{CO_2} \quad (2)$$

The maximum error in repeatability using this technique was found to be ± 4%, which is in line with the error of similar equipment previously described for making similar gas solubility measurements on ILs.[6, 30-33] It was assumed that the solvent density was constant upon addition of CO_2 (i.e. no expansion of the liquid phase). The solvent density is assumed to be constant as the maximum mole fraction of CO_2 in the 1-*n*-alkylimidazole solvents is relatively low (6.5 < x_{CO2} < 15%) at the highest pressure (7 atm). It has been previously shown that the molar volume of 1-methylimidazole expanded <5% when the CO_2 mole fraction in this solvent was ~0.10 at 40°C.[34] As 1-methylimidazole shows the greatest solubility for CO_2 on a moles per volume basis within 1-*n*-alkylimidazole solvents, it can be reasonably assumed that 1-*n*-alkylimidazole solvents with larger pendant groups have less potential for expansion at these relatively low concentrations of CO_2. Based on this phenomenon, constant solvent density was assumed under these experimental conditions in order to simplify calculations. The solubility of CO_2 in each 1-*n*-alkylimidazole was found to be linear in the pressure range examined, and Henry's Law constants for CO_2 (H(atm)) at 25°C were calculated from the mole fraction of CO_2 (x_{CO2}) dissolved at a given pressure (P(atm)) (Eqn. 3).

$$P(atm) = H(atm) \cdot x_{CO_2} \quad (3)$$

Volumetric solubility (S) was calculated as standard cubic centimeters (cm^3(STP)) of CO_2 dissolved per cm^3 of 1-*n*-alkylimidazole (cm^3_{imid}) per atmosphere of pressure, according to Eqn. 4:

$$S = \frac{n^{l}_{CO2} \cdot 22414 \frac{cm^3(STP)}{mol}}{cm^3_{imid} \cdot P(atm)} \quad (4)$$

2.3. Results & Discussion

2.3.1 Densities of 1-n-alkylimidazoles and Empirical Model: The measured density values for 1-*n*-alkylimidazoles over the temperature range of 20 – 80 ^{o}C are presented in Table 2.1.

Table 2.1: Temperature dependent density data (g/cm^3) for 1-*n*-alkylimidazoles (1 – 10).

1-*n*-alkylimidazole	Density (g cm^{-3})						
	Temperature (^{o}C)						
	20	30	40	50	60	70	80
1 – Methyl	1.0353	1.0264	1.0176	1.0087	0.9998	0.9908	0.9818
2 – Ethyl	0.9945	0.9858	0.9771	0.9684	0.9597	0.9509	0.9421
3 – Propyl	0.9729	0.9646	0.9562	0.9479	0.9395	0.9311	0.9227
4 – Butyl	0.9514	0.9434	0.9354	0.9274	0.9194	0.9113	0.9032
5 – Pentyl	0.9389	0.9311	0.9233	0.9156	0.9078	0.8999	0.8921
6 – Hexyl	0.9299	0.9223	0.9146	0.9070	0.8993	0.8917	0.8840
7 – Octyl	0.9115	0.9043	0.8971	0.8898	0.8826	0.8753	0.8680
8 – Decyl	0.9015	0.8944	0.8873	0.8802	0.8732	0.8661	0.8590
9 – Dodecyl	0.8947	0.8878	0.8808	0.8739	0.8670	0.8601	0.8532
10 – Tetradecyl	0.8894	0.8826	0.8757	0.8690	0.8622	0.8554	0.8486

With the exception of 1-methylimidazole in the range of 20 – 50 ^{o}C, all of the measured densities for 1-*n*-alkylimidazoles were less than 1.00000 g/cm^3. For each compound, density was observed to decrease linearly with increasing temperature, and across the entire group of 1-*n*-alkylimidazoles, density decreased with increasing length of the *n*-alkyl substituent. This trend is similar to that observed across families of [$C_n$mim][X] ILs as the length of the 'C_n' chain increases, and can be explained by the dilution of the polar imidazole ring (or ions in the case of ILs) within the bulk by increasing hydrocarbon content.[35] In order to quantify the impact of both temperature and the length of the *n*-alkyl side chain on density, an empirical model was developed. The influence of the side chain was quantified as a "molecular weight parameter" (R'), a dimensionless value relating the molecular weight of the side chain to the molecular weight of the entire molecule (Eqn. 5). Table 2.2 presents R' values for each of the 1-*n*-alkylimidazoles (1 – 10).

$$R' = \frac{MW(n-alkylchain)}{MW(molecule)} \quad (5)$$

Table 2.2: R' Values for each of the 1-*n*-alkylimidazoles examined.

1-*n*-alkylimidazole	MW(g/mol)	R'
1 – Methyl	82.11	0.183
2 – Ethyl	96.13	0.281
3 – Propyl	110.16	0.391
4 – Butyl	124.18	0.460
5 – Pentyl	138.21	0.515
6 – Hexyl	152.24	0.559
7 – Octyl	180.29	0.628
8 – Decyl	208.34	0.678
9 – Dodecyl	236.40	0.716
10 – Tetradecyl	264.45	0.746

As seen in Table 2.2, R' is a moving ratio that would approach unity as the alkyl chain becomes infinitely long. By combining the data in Table 2.1 with the calculated R' values in Table 2.2, a surface plot relating density to temperature and the influence of the side chain was produced (Figure 2.3).

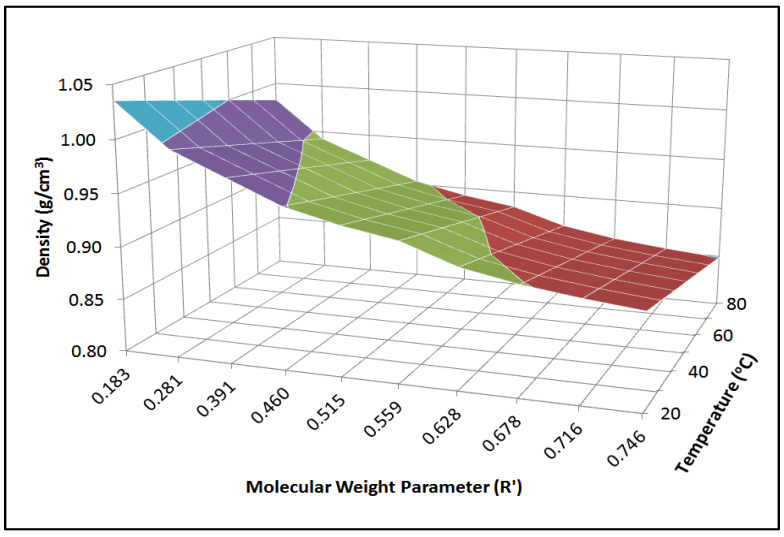

Figure 2.3: Surface plot of 1-*n*-alkylimidazole density relative to temperature (K) and molecular weight parameter (R').

The approximately planar surface in Figure 2.3 was regressed using Matlab to develop an empirical equation describing the densities of 1-*n*-alkylimidazoles as a function of both temperature and molecular weight parameter. By observing the two-dimensional plots of ρ vs. T (constant R') and ρ vs. R' (constant T), a simple linear model was assumed to approximate density (Eqn. 6),

$$\rho(T, R') = AT + BR' + C \tag{6}$$

where ρ [=] g mL^{-1}, T [=] K, A = -7.753x10^{-4} g mL^{-1} K^{-1}, B = -0.239 g mL^{-1}, and C = 1.2926 g mL^{-1}. Using these constants within the two-parameter density model (Eqn. 6) provides an excellent fit (R^2 = 0.9881) and the ability to rapidly and accurately describe density at a given temperature for 1-*n*-alkylimidazoles with side chains as long as tetradecyl.

2.3.2 Viscosities of 1-n-alkylimidazoles and Empirical Model: The measured viscosity values for 1-*n*-alkylimidazoles over the temperature range of 20 – 80 °C are presented in Table 2.3.

Table 2.3: Viscosity data for 1-*n*-alkylimidazoles at temperatures between 20 – 80 °C.

1-*n*-alkylimidazole	Viscosity (cP)									
	Temperature (°C)									
	20	25	30	35	40	45	50	60	70	80
1 – Methyl	1.92	1.77	1.64	1.51	1.40	1.30	1.28	1.24	1.21	1.17
2 – Ethyl	2.22	2.04	1.86	1.70	1.56	1.45	1.34	1.30	1.23	1.22
3 – Propyl	3.17	2.81	2.50	2.26	2.05	1.86	1.69	1.45	1.25	1.23
4 – Butyl	3.95	3.47	3.05	2.71	2.43	2.19	1.99	1.66	1.43	1.42
5 – Pentyl	5.13	4.49	3.89	3.42	3.02	2.70	2.42	2.00	1.68	1.43
6 – Hexyl	5.88	5.07	4.38	3.82	3.37	2.99	2.67	2.18	1.82	1.55
7 – Octyl	9.17	7.77	6.56	5.63	4.87	4.25	3.76	3.00	2.44	2.04
8 – Decyl	13.0	10.8	9.00	7.62	6.50	5.62	4.93	3.86	3.10	2.56
9 – Dodecyl	18.1	15.0	12.4	10.3	8.77	7.52	6.50	5.00	3.95	3.21
10 – Tetradecyl	24.7	20.3	16.6	13.7	11.5	9.73	8.35	6.30	4.92	3.94

As can be seen in Table 2.3, almost all of the measured viscosities for the ten 1-*n*-alkylimidazole compounds were < 10 cP, with 1-tetradecylimidazole as the sole exception where the solvent viscosity was >20 cP below 30°C. For each compound, viscosity was observed to decrease in a non-linear fashion with increasing temperature. Viscosity was strongly correlated to length of the *n*-alkyl substituent, with an order of magnitude difference between the least viscous and most viscous compounds at 20°C, though reducing to a ~3.5x difference at the highest temperature.

As with the density data, an empirical model was developed to quantify the impact of both temperature and the length of the *n*-alkyl chain on the viscosity of 1-*n*-alkylimidazoles, again using R' (Eqn. 5) to quantify the contribution of the *n*-alkyl group. A surface plot relating viscosity to temperature and R' is presented in Figure 2.4.

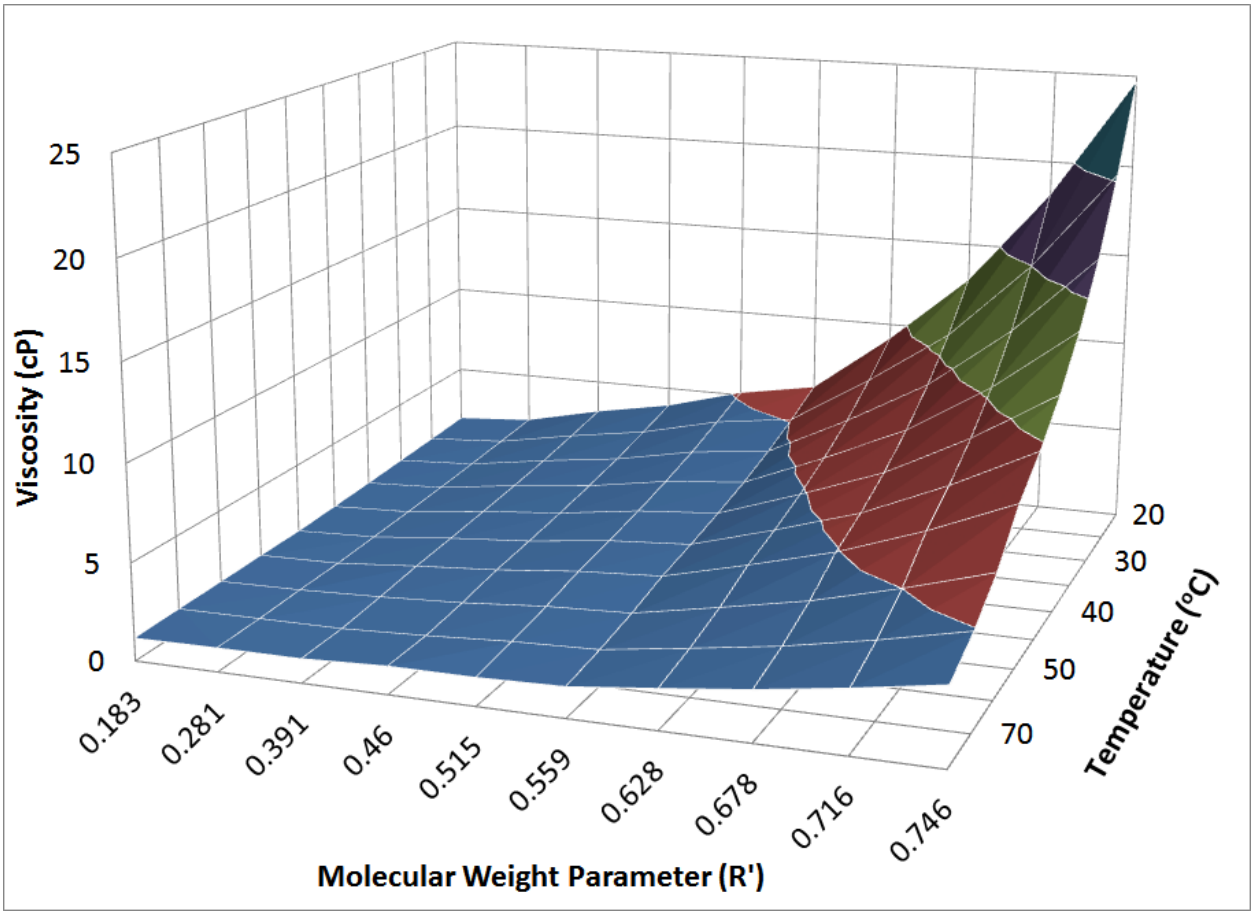

Figure 2.4: Surface plot of alkylimidazole viscosity vs. temperature (K) and molecular weight parameter (R').

Examination of the surface in Figure 2.4 reveals a sharp increase in viscosity at lower temperatures and larger R' values, likely indicating aggregation between long *n*-alkyl chains away from the polar imidazole

ring. This behavior is also typical of [$C_n$mim][X] ILs, with localized phase separation occurring even at relatively short *n*-alkyl chain lengths (e.g. 4 carbons).[36]

A method similar to that used to fit the density data was employed to relate viscosity as a function of temperature and R'. Initially, the viscosities (μ) for each solvent were plotted as a function of temperature, and a linear regression of μ vs. T for each solvent was used to model each curve based upon the Litovitz equation (Eqn. 7). The Litovitz Equation has been successfully applied to modeling the viscosity of imidazolium-based ILs.[37]

$$\mu(T) = A\exp(BT^{-3}) \tag{7}$$

Using the linearized form of this equation (Eqn. 8),

$$\ln\left[\mu(T)\right] = \ln A + BT^{-3} \tag{8}$$

the constants A and B were found for each solvent by plotting $ln|\mu(T)|$ vs. T^{-3}, where B is the slope of the fitted line, and $ln|A|$ is the y-intercept. Table 2.4 contains the A and B values obtained for each of the 1-*n*-alkylimidazoles and the quality of the fit for each line.

Table 2.4: Empirical constants for 1-*n*-alkylimidazoles in Litovitz viscosity model.

	A (cP)	B x 10^{-7} (K^3)	R^2
1 – Methyl	0.57	2.92	0.9119
2 – Ethyl	0.49	3.66	0.9483
3 – Propyl	0.30	5.88	0.9963
4 – Butyl	0.30	6.40	0.9950
5 – Pentyl	0.26	7.54	0.9998
6 – Hexyl	0.26	7.87	0.9999
7 – Octyl	0.27	8.87	0.9999
8 – Decyl	0.29	9.56	0.9999
9 – Dodecyl	0.32	10.2	0.9999
10 – Tetradecyl	0.33	10.9	0.9998

Rather than use tabulated individual *A* and *B* constants for each solvent, further regression was done to fit these constants as functions of R'. A plot of *B* as a function of *R'* (Eqn. 9) revealed that a linear fit was most appropriate.

$$B(R') = mR' + n \tag{9}$$

However, a plot of *A* as a function of *R'* illustrated that a quadratic curve was a more appropriate fit (Eqn. 10).

$$A(R') = a(R' - b)^2 + c \tag{10}$$

From these two regression fits (Eqns. 9 & 10), an overall equation to describe the viscosity of 1-*n*-alkylimidazoles as a function of both temperature and the length of the *n*-alkyl chain was developed using the Litovitz Equation as the primary model (Eqn. 11).

$$\mu(T, R') = (a(R' - b)^2 + c) \cdot \exp((mR' + n)T^{-3}) + p \tag{11}$$

Regressing the surface in Figure 2.4 to the form described by Eqn. 11 provided the six constants (Table 2.5) needed to complete the model viscosity model for 1-*n*-alkylimidazoles, with an excellent fit to the experimental data (R^2 = 0.9978). As with density, the viscosity of 1-*n*-alkylimidazoles can be accurately modeled with temperature and the dimensionless molecular weight parameter (R').

Table 2.5: Empirical constants for Eqn. 11 describing the viscosity of 1-*n*-alkylimidazoles.

Constant	Value	Units
a	3.22	cP
b	0.575	-
c	0.266	cP
m	1.42×10^8	K^3
n	6.67×10^5	K^3
p	-0.252	cP

2.3.3 CO_2 Solubility and Group Contribution Model for Solubility Parameters: Solubility data for CO_2 in 1-*n*-alkylimidazoles at low pressures and 25 ± 0.5°C in terms of Henry's constants (H(atm)) and volumetric solubility (S) are presented in Table 2.6.

Table 2.6: Solubility of CO_2 in 1-*n*-alkylimidazoles at 25 °C.

1-*n*-alkylimidazole	H_{CO2} (atm)	±	S	±
1 – Methyl	109	2	2.71	0.04
2 – Ethyl	97.9	0.6	2.49	0.07
3 – Propyl	88.9	0.3	2.40	0.06
4 – Butyl	77.4	2.0	2.31	0.04
5 – Pentyl	70.0	1.3	2.25	0.03
6 – Hexyl	67.8	0.8	2.18	0.09
7 – Octyl	58.3	0.9	2.11	0.04
8 – Decyl	53.6	0.7	1.99	0.06
9 – Dodecyl	51.7	1.1	1.82	0.06
10 – Tetradecyl	48.6	1.7	1.77	0.04

S [=] cm^3 (STP) cm^{-3} atm^{-1}

Uncertainty represents ±1 standard deviation from the mean

The value of 109 ± 2 atm for the CO_2/1-methylimidazole system at 25°C is comparable to data reported by Brennecke and co-workers at 40 °C,[34] which is the only other known report of CO_2 solubility data for an imidazole solvent. H(atm) values were observed to decrease with increasing chain length, indicating higher mole fractions of CO_2 could be achieved by lengthening the *n*-alkyl chain. However, an analysis of CO_2 solubility built on Henry's constants alone would be inappropriate, as the main reason for the increase in CO_2 mole fraction with increasing *n*-alkyl chain length is simply due to a larger molecular weight of the solvent. Examination of the volumetric solubility of CO_2 (S) reveals that the amount of CO_2 absorbed at a constant pressure by a given volume of a 1-*n*-alkylimidazole actually decreases with increasing chain length. As CO_2 would be expected to be more soluble in polar solvents than in hydrocarbons,[24] diluting the polar imidazole ring with increasing larger alkyl chains can only serve to reduce the overall affinity of the solvent for CO_2. A cursory examination reveals that H(atm) and S values are negatively correlated to the *R'* values reported in Table 2.2.

However, *R'* should not be viewed as an applicable metric for comparing the solubility of CO_2 in either liquid solvents or solid materials (e.g. polymers). A more appropriate unit is the solubility parameter (δ),[24] which is defined as the square root of the cohesive energy density (Eqn. 12),[38] where H_{vap} is the heat of vaporization and V_m is the molar volume of the solvent.

$$\delta = \sqrt{\frac{H_{vap} - RT}{V_m}} \tag{12}$$

While it appears that no data on the heat of vaporization of 1-*n*-alkylimidazoles are available, sufficient vapor pressure date exist for 1-methylimidazole and 1-butylimidazole to calculate the heat of vaporization parameters for these species via the Clausius-Clapeyron Equation (Eqn 13).

$$\ln P = \frac{-H_{vap}}{RT} + c \tag{13}$$

Table 2.7 presents a summary of the data for 1-methylimidazole and 1-butylimidazole as well as other vapor pressure data for 1-*n*-alkylimidazoles reported in the literature.

Table 2.7: Selected literature vapor pressure data for 1-*n*-alkylimidazoles.

1-*n*-alkylimidazole	Temp (^{o}C)	P_{vap} (Torr)	Reference(s)
1 – Methyl	197 – 198	760	*39, 40, 41, 42*
	99	18	*43*
	95	15	*44*
2 – Ethyl	226	760	*39*
3 – Propyl	89.5	18	*45*
4 – Butyl	235	760	*46*
	118.5	15	*45*
	115	12	*39*
5 – Pentyl	119.5	20	*45*
6 – Hexyl	167	30	*47*
	135.5	24	*45*
	94	4	*48*
7 – Octyl	151.5	16	*45*
8 – Decyl	172.5	25	*45*
9 – Dodecyl	199.5	24	*45*
	125	0.08	*48*
10 – Tetradecyl	142	0.001	*48*

The vapor pressure data in Table 2.7 were compiled from a number of sources primarily relating to the preparation of 1-*n*-alkylimidazoles, where distillation was used as a purification technique. Although no study to date has been exclusively devoted to thoroughly characterizing the vapor pressure behavior of any 1-*n*-alkylimidazole, the available data can still provide valuable insight. From Table 2.7, it is apparent that, with the exception of 1-methylimidazole (T_b = 198^{o}C), 1-*n*-alkylimidazoles have normal boiling points >200^{o}C, and volatility is observed to decrease as the *n*-alkyl chain length increases. Almost all of the 1-*n*-alkylimidazoles have vapor pressures less than 20 torr at 120^{o}C, a typical temperature for solvent regeneration in CO_2 capture processes.[13]

A plot of ln(P) vs 1/T (K) was generated to fit the Clausius – Clapeyron Equation (Eqn. 13) to the data in Table 2.7 for 1-methylimidazole and 1-butylimidazole. From the plot, the slopes of the respective lines for 1-methylimidazole and 1-butylimidazole were calculated, yielding H_{vap} values of 55.3 kJ/mol and 56.4 kJ/mol,

respectively. This calculation assumes H_{vap} is constant across the entire temperature range. For general reference and consideration, these calculated latent heats of 1-*n*-alkylimidazoles are larger than many common organic solvents and water.[29]

The calculated H_{vap} data were then applied to Eqn. 12 to calculate δ values for 1-methylimidazole and 1-butylimidazole. Respective V_m values of 79.65 cm^3 mol^{-1} and 131.08 cm^3 mol^{-1} for 1-methylimidazole and 1-butylimidazole at 25°C were calculated from a linear interpolation of the data presented in Table 2.1. 1-methylimidazole and 1-butylimidazole were calculated to have δ values of 25.8 $MPa^{1/2}$ and 20.3 $MPa^{1/2}$, respectively.

Based on these calculations, it can be inferred that the solubility parameters of 1-*n*-alkylimidazoles decrease with increasing length of the *n*-alkyl chain. However, with insufficient vapor pressure data for the other eight compounds, calculation of their respective δ values is not possible using Eqn. 12. However, group contribution methods[38, 49, 50] can be applied to the approximate the solubility parameters of 1-*n*-alkylimidazoles.

A group contribution approach has been applied to calculating the solubility parameters of substances with little or no volatility, where accurate H_{vap} data may difficult or impossible to obtain. This methodology has been traditionally applied to polymers,[50] and more recently, imidazolium-based ILs.[33]

Through a group contribution approach, the solubility parameter of a species (δ_i) is calculated as the sum of the molar attraction constants of each constituent chemical group (F_j) divided by the molar volume of the molecule (V_m) (Eqn. 14).[38, 50]

$$\delta_i = \frac{\sum_j F_j}{V_m} \tag{14}$$

Values for F_j have been tabulated for a variety of simple chemical functionalities and can be found in resources such as the Polymer Handbook.[50] Table 2.8 summarizes the values relevant to this work.

Table 2.8: Tabulated molar attraction constants relevant to this work.

Group	F ($MPa^{1/2}$ cm^3 mol^{-1})
Methyl (-CH_3)	303
Methylene (-CH_2-)	269

However, molar attraction constants for complex and unique groups such as the 5-membered imidazole ring are not readily available.[33] Using the solubility parameters for 1-methylimidazole and 1-butylimidazole calculated from Eqn. 12, the molar attraction constants in Table 2.8, and the molar volumes of these solvents, it is possible to calculate an average molar attraction constant for the 5-membered imidazole ring using Eqn. 14. The values obtained through this calculation are summarized in Table 2.9, where 1-methylimidazole provided the high estimate and 1-butylimidazole provided the low estimate.

Table 2.9: Estimates for the molar attraction constant of the 5-membered imidazole ring.

	F ($MPa^{1/2}$ cm^3 mol^{-1})
High	1749
Low	1549
Average	1649

The range of the molar attraction constant for the imidazole ring presented in Table 2.9 appears reasonable considering the complexity of the 5-membered ring structure and that they are approximately 5x-6x greater than the values in Table 2.8, which each account for only a single carbon atom and its protons. For additional comparison, the molar attraction constant for a terminal nitrile (-C≡N) group is 735 $MPa^{1/2}$ cm^3 mol^{-1},[33, 50] and a molar attraction constant between 1500 – 1800 $MPa^{1/2}$ cm^3 mol^{-1} for a 5-membered ring containing two nitrogen atoms and three carbon atoms seems quite reasonable. Furthermore, a 6-membered phenyl (C_6H_6) ring has a tabulated value of 1400 $MPa^{1/2}$ cm^3 mol^{-1}.[50]

Application of the molar attraction constants in Tables 2.8 and 2.9, to Eqn. 14 provided high, average and low estimates for the solubility parameter of each of the 1-*n*-alkylimidazole. These values are presented in Table 2.10.

Table 2.10: Solubility parameter estimates obtained via group contributions for the 1-*n*-alkylimidazoles examined in this work.

1-*n*-alkylimidazole	V_m (25°C) (cm^3/mol)	δ Estimate ($MPa^{1/2}$)		
		High	Avg	Low
1 – Methyl	79.64	25.8[a]	24.5	23.3
2 – Ethyl	97.09	23.9	22.9	21.8
3 – Propyl	113.72	22.8	21.9	21.0
4 – Butyl	131.08	21.8	21.0	20.3[a]
5 – Pentyl	147.82	21.2	20.5	19.8
6 – Hexyl	164.39	20.7	20.1	19.4
7 – Octyl	198.58	19.8	19.3	18.8
8 – Decyl	232.03	19.3	18.8	18.4
9 – Dodecyl	265.25	18.9	18.5	18.1
10 – Tetradecyl[b]	298.49	18.6	18.3	17.9

[a] corresponds to value calculated from heat of vaporization (Eqn. 12)

[b] In supercooled liquid state at 25°C

Using the calculated δ values in Table 2.10, the volumetric solubility of CO_2 in the series of 1-*n*-alkylimidazoles (Table 2.6) is directly correlated to the solubility parameter. Ideally, CO_2 solubility should reach a maximum as the solubility parameter of the solvent approaches that of CO_2 (δ = 21.8 $MPa^{1/2}$).[24] However, for 1-*n*-alkylimidazoles, solubility is observed to continually decrease as the *n*-alkyl chain is extended, as the molecule effectively becomes much more like a polymer than a small molecule. This effect, according to Lin and Freeman, can be attributable to smaller fraction free volume (FFV) in polymers than in liquids.[24] Thus, while an expected effect of tuning the solubility parameter by extending the alkyl chain length is to improve CO_2 solubility, this is counteracted by reduced FFV and an overall decrease in CO_2 solubility.

2.4. Comparing 1-*n*-alkylimidazoles to [$C_n$mim][X] ILs and Organic Solvents: Tailoring molecules via side chain modifications will inevitably result in trade-offs between certain properties. For 1-*n*-alkylimidazoles, higher CO_2 solubility and lower viscosity come at the expense of greater solvent volatility. Ideally, a solvent platform could be tailored to have both maximum FFV and a low vapor pressure, though data for organic

solvents suggest that greater FFV values directly correlate with increased volatility.[24] However, such trade-offs are not unique to only 1-*n*-alkylimidazoles.

2.4.1 Comparison of Density & Viscosity: For 1-*n*-alkylimidazoles, density is only influenced by the length of the *n*-alkyl chain and temperature. Both increasing temperature and increasing side chain length are observed to decrease density. Trends similar to 1-*n*-alkylimidazoles are also observed for families of [$C_n$mim][X] ILs (e.g. [C_2mim][BF_4], [C_4mim][BF_4], [C_6mim][BF_4]…),[35, 51] however IL density is also strongly influenced by the nature of the anion, across a family with identical cations such as [C_4mim][BF_4], [C_4mim][PF_6], [C_4mim][OTf], etc.[52] While densities of 1-*n*-alkylimidazoles were observed to only vary ~15% between the least and most dense species at a given temperature, densities of ILs can vary more widely.[52] For example, a 30% difference is observed in the densities of [C_4mim][Tf_2N] (ρ = 1.44 g/cm^3) and [C_4mim][dca] (ρ = 1.06 g/cm^3) at 298 K.[52] Even greater spreads are possible with smaller cations such as [C_2mim] or anions with greater fluorination such as bis(perfluoroethylsulfonyl)imide ([beti]). All [$C_n$mim][X] ILs are at least ~10% more dense than their 1-*n*-alkylimidazole analogues at the same temperature.

As the differences in densities between 1-*n*-alkylimidazoles and [$C_n$mim][X] ILs might influence certain process design considerations (e.g. hydrostatic pressure in a vessel, increased mass flow rate), the magnitude of the difference (10 – 50%) is relatively small and within range of many common organic compounds. Common chlorinated organic solvents (e.g. chloroform) are nearly as dense as the most dense ILs, while brominated compounds (e.g. bromoform)[53] can be at least twice as dense as most [$C_n$mim][X] ILs.

While the change in density associated with transitioning from a neutral 1-*n*-alkylimidazole to a [$C_n$mim][X] IL is relatively small, a penalty is exacted on the solvent viscosity. Viscosity increases by an order of magnitude or more when transitioning from the neutral 1-*n*-alkylimidazole to the [$C_n$mim][X] IL. For 1-*n*-alkylimidazoles, viscosity was observed to increase with increasing chain length and decreasing temperature. A similar trend holds for across a family of [$C_n$mim] ILs with the same anion, [X]. However, viscosity differences between ILs with the same [$C_n$mim] cation and different anion species can be quite large, spanning almost an order of magnitude.[11]

Using the NIST ILTHERMO[12] database for [$C_n$mim][X] ILs and the data measured in this work, a plot was generated to compare the relative viscosity regimes of 1-*n*-alkylimidazoles and [$C_n$mim][X] ILs. Figure 2.5 compares the viscosities of 1-*n*-alkylimidazoles to [$C_n$mim][X] with respect to temperature. A plot of the raw data without overlaid regions, and the associated references used to generate Figure 5 are provided in the Supporting Information.

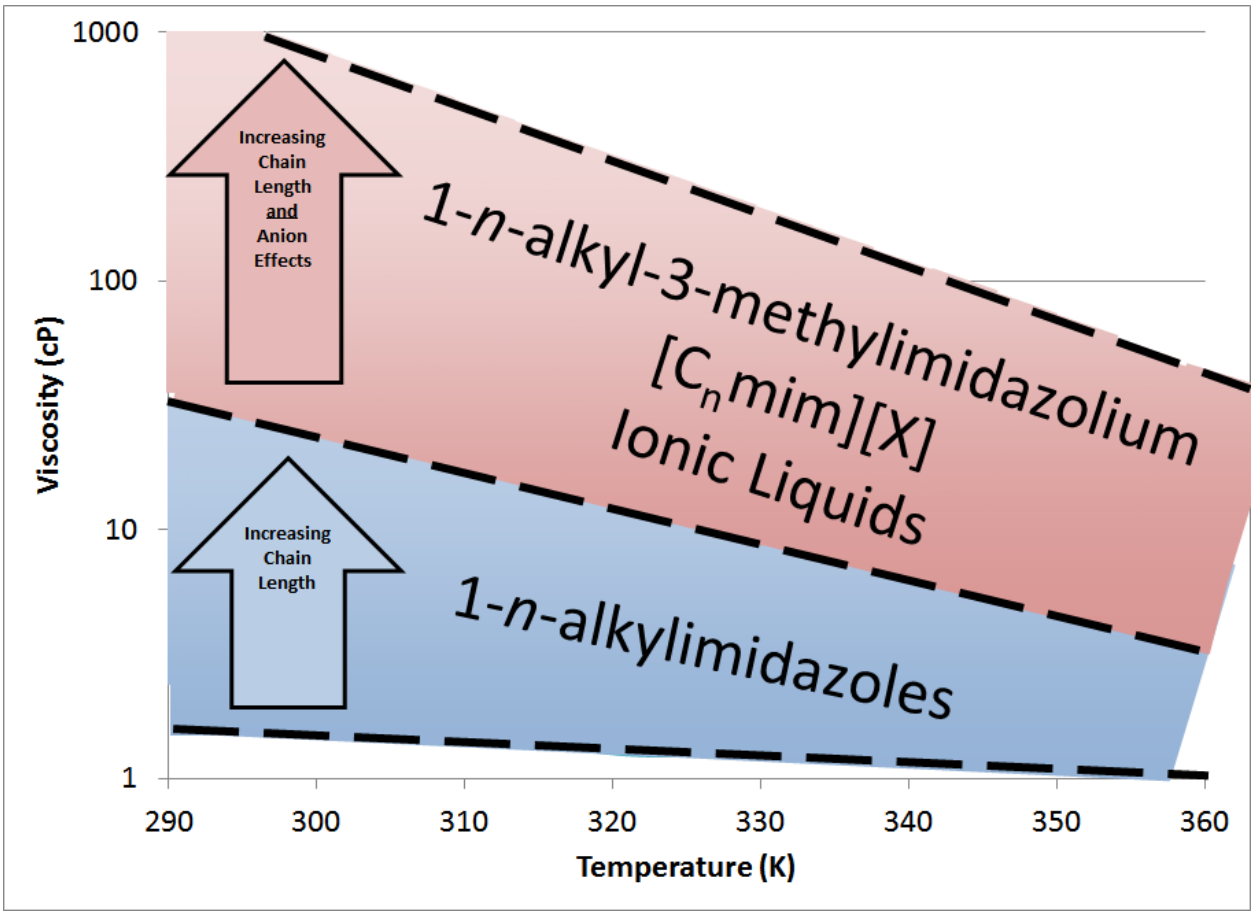

Figure 2.5: Graphical comparison of reported viscosity ranges of 1-*n*-alkylimidazoles (lower, blue) and [$C_n$mim][X] ILs (upper, red).

Figure 2.5 illustrates clearly defined regimes separating the viscosities of 1-*n*-alkylimidazoles and [$C_n$mim][X] ILs. Only a single IL, [C_2mim][dca], can be found near the top of the blue area occupied by 1-*n*-alkylimidazoles. Virtually all [$C_n$mim][X] ILs are at least an order of magnitude more viscous than their analogous 1-*n*-alkylimidazole (e.g. [C_4mim][Tf_2N] relative to 1-butylimidazole). The large differences in viscosities between the two classes of solvents would have significant impacts on process design. As mentioned earlier, increased viscosity correlates with decreased diffusion, which can negatively impact mass and heat transfer rates, and in turn process scale.[10] For mass and/or heat transfer limited processes, 1-*n*-alkylimidazole solvents might be more amenable to use within the existing unit operations and equipment (e.g. absorption columns, heat exchangers), while IL solvents might require certain unit operations to be reconfigured to accommodate for their respective viscosities.

2.4.2 Comparison of CO_2 Solubility & Solubility Trends: A comparison of the data in Table 2.6 to published values for [$C_n$mim][X] ILs indicates that the solubility of CO_2 in most 1-*n*-alkylimidazoles at 298 K and low pressures is similar to that of CO_2 in analogous ILs under similar conditions.[5] However, of all of the compounds examined, 1-methylimidazole exhibited the greatest affinity for CO_2, as the value of S (2.71 cm^3 (STP) cm^{-3} atm^{-1}) is about 10% greater than the largest values observed in [$C_n$mim][X] ILs.[5] Mole fraction data for 1-*n*-alkylimidazoles (Table 2.6), represented as Henry's constants, suggest that ILs can absorb greater mole fractions of CO_2 than 1-*n*-alkylimidazoles under the same temperature and pressure conditions. However, Henry's constants become less useful for comparing the solubility of CO_2 in two or more species if they have disparate molecular weights.

The greater mole fractions observed in ILs than in organic solvents have been attributed to interactions between the anion and CO_2,[54, 55] although the largest mole fractions have been observed in ILs with the largest anions (in terms of MW and molar volume).[5, 30, 33, 54-56] For example, [$C_n$mim][Tf_2N] ILs have been shown to have greater mole fractions (e.g. smaller Henry's constants) and larger volumetric solubility of CO_2 than [$C_n$mim][BF_4] and [$C_n$mim][PF_6] ILs. Thus, for non-chemically complexing anions (e.g. OAc, etc.),[15, 16, 18, 57] a more diffuse charge (larger anion) actually increases solubility relative to a more localized charge (smaller anions). It may thus be inferred that the presence of any charge will ultimately decrease CO_2 volumetric solubility, as evidenced by the measured data which indicate that transformation from the neutral 1-*n*-alkylimidazole to the charged [$C_n$mim][Tf_2N] IL is slightly detrimental to the solubility of CO_2 in the liquid phase. Thus, approaches to design of tailored solvents aimed at enhancing physical solubility of CO_2 appear to be counterproductive when they rely upon the use of large, bulky side chains and/or charged species. The limitations associated with lower physical solubility of CO_2 in designer solvents must be offset by process benefit(s) associated with decreasing or eliminating volatility and/or unique chemistry or selectivity behaviors not available with conventional solvents.

Figure 2.6 is a plot relating the solubility of CO_2 in 1-*n*-alkylimidazoles, [$C_n$mim][Tf_2N] ILs, organic solvents and polymers as a function of solubility parameter (δ). The region around δ=21.8 has been highlighted to illustrate how only relatively small organic molecules are present near the maximum values of CO_2 solubility reported.[24]

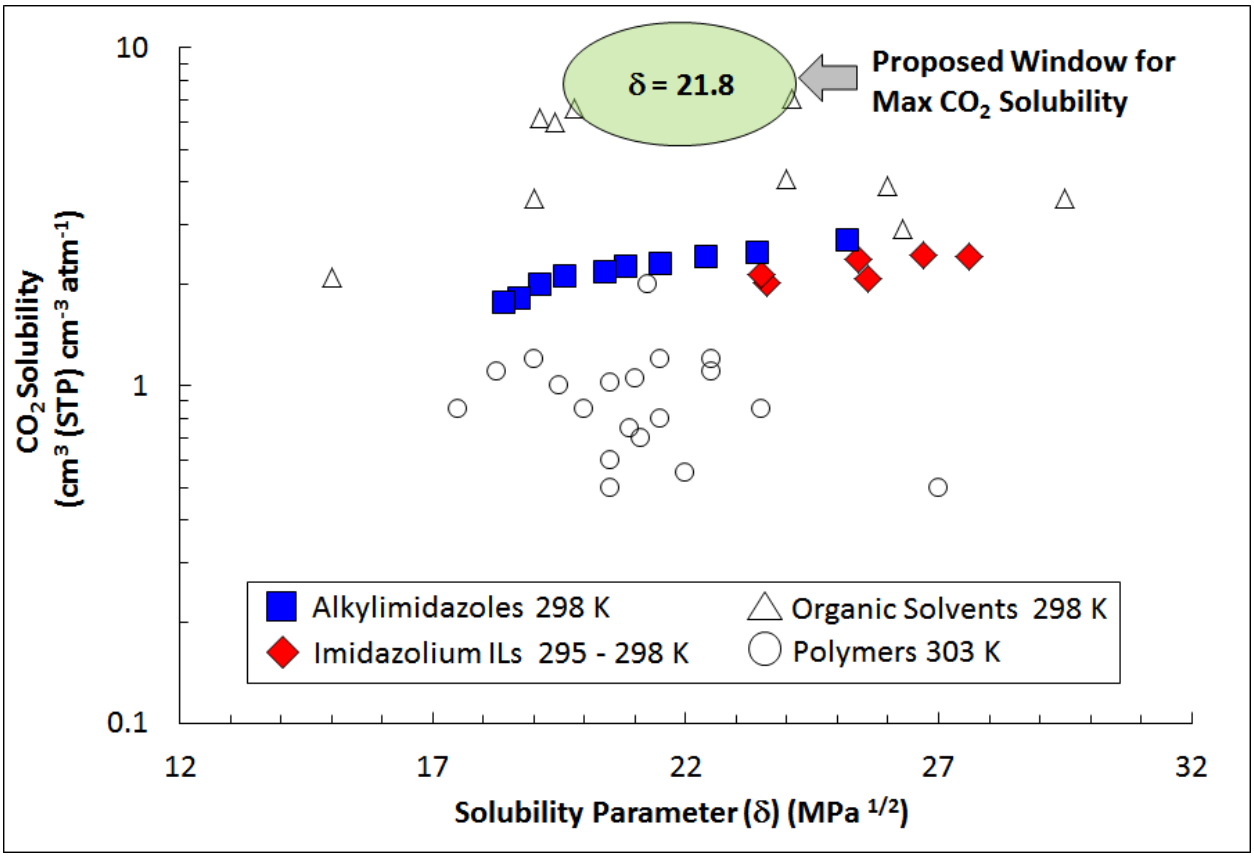

Figure 2.6: Relationships between CO_2 solubility and Hildebrand solubility parameter for alkylimidazoles at 298 K (filled squares), imidazolium-based [$C_n$mim][Tf_2N] ILs at 295 – 298 K (filled diamonds), organic solvents at 298 K (unfilled triangles) and polymers at 303 K (unfilled circles). Partially reproduced from data found in References 24 & 5 .

Lin and Freeman point out that almost all of the organic solvents in Figure 2.6 have FFV values well above 0.21 and all of the polymers are below that value.[24] The trends presented in Figure 2.6 for 1-*n*-alkylimidazoles and [$C_n$mim][X] ILs indicate that these solvents lie in a region straddling that occupied by small organic molecules and polymers. And although Lin and Freeman used Bondi's Group Contribution to estimate FFV,[58] this method cannot be employed for 1-*n*-alkylimidazoles and [$C_n$mim][X] ILs, as van der Waals volumes are not available for the complex constituents of these solvents. However, the trends in Figure 2.6 and the data from the literature indicate that 1-*n*-alkylimidazole and [$C_n$mim][X] solvents should have FFV values near 0.21, and that any major improvements in CO_2 solubility could only be achieved by tailoring the molecules to have larger FFV values.

2.5. 1-*n*-alkylimidazoles as Co-solvents for Post-Combustion CO_2 Capture: Based on the results presented, it is apparent that 1-*n*-alkylimidazoles, along with [$C_n$mim][X] ILs,[5] lack the high levels of CO_2 capacity needed to be viable solvents for post-combustion CO_2 capture processes.[13] Both must be considered "physical" solvents that might find application in removing CO_2 from streams where it is present in high concentrations and high partial pressures, such as in the natural gas industry.[5,59-61] Ideally, a solvent for post-combustion CO_2 capture should have a theoretical loading of at least 100 g CO_2 L^{-1} solvent when the partial pressure of CO_2 in the gas stream is ≤ 2 psia.[13, 62] Such CO_2 capacities are only likely to be achievable through chemical reaction between the solvent and CO_2.[59, 60, 62] Like [$C_n$mim][X] ILs, 1-*n*-alkylimidazoles are not capable of reacting directly with CO_2 in the manner of 1° and 2° amines, wherein an amine first reacts with CO_2 to form a zwitterion, followed by H^+ transfer to a second equivalent of amine to form a carbamate-ammonium salt (Scheme 2).[59, 60]

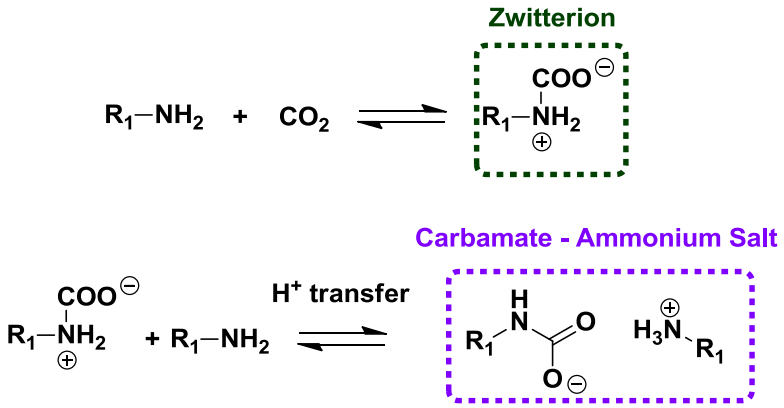

Scheme 2: Reaction between 2 moles of a 1° amine and 1 mole of CO_2 to form a carbamate-ammonium salt.[59, 60]

In aqueous solutions, an additional reaction pathway exists where water combines with CO_2 to form carbonic acid, which is neutralized by amines to form ammonium bicarbonates, and allows for CO_2 loadings to approach 1 mol CO_2 per 1 mol amine.[59, 60] For 1° and 2° amines, the carbamate pathway typically dominates at low CO_2 partial pressures, while the carbonate pathway is prevalent in 3° amines and sterically hindered amines.[59, 60]

The addition of amines to [$C_n$mim][X] ILs has been shown to dramatically increase the capacity of the solvent for CO_2 through the formation of carbamate-ammonium salts via the mechanism shown in Scheme 2.[14] These carbamate-ammonium salts could either remain soluble in the IL or precipitate as a separate phase.[14] However, the IL itself was not observed to participate with amines in the CO_2 capture reactions. In this respect, imidazole co-solvents may present a unique opportunity to utilize amines for CO_2 capture, as it

inherently contains a Bronsted basic, "pyridine-like" nitrogen that could act as an H^+ acceptor.[23] Mixtures of 1-*n*-alkylimidazoles and 1° or 2° amines could be used to create a carbamate-imidazolium salt as a CO_2 capture product, with the 1-*n*-alkylimidazole acting as both chemical and physical solvent. Scheme 3 details potential reaction mechanisms that involve the use of 1-*n*-alkylimidazoles and amines for CO_2 capture.

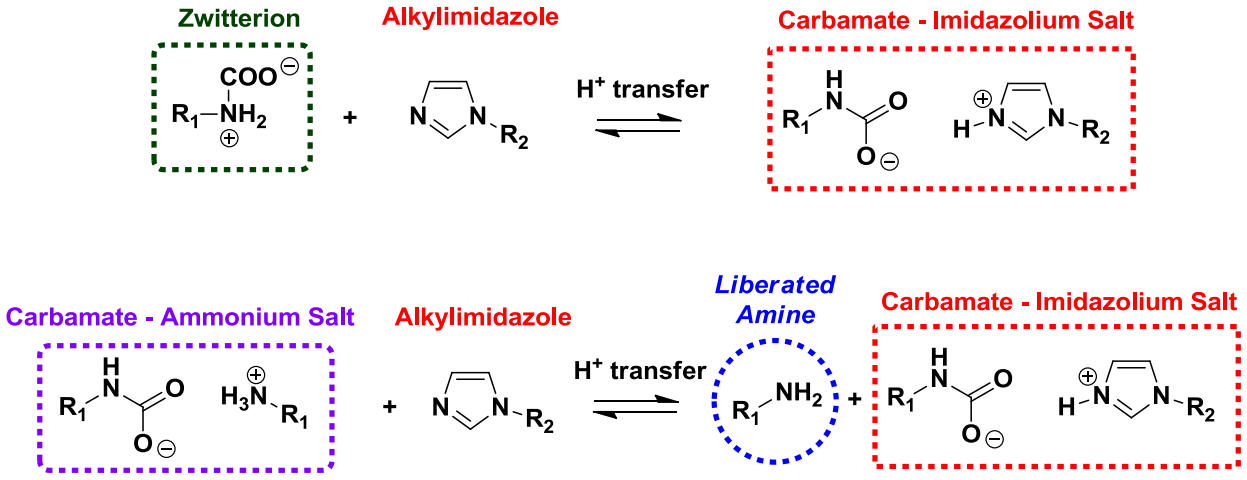

Scheme 3: Two potential mechanisms for CO_2 capture via carbamate-imidazolium salt using a 1-*n*-alkylimidazole with a 1° amine.

The mechanisms in Scheme 3 could be advantageous to a CO_2 capture process in that only one equivalent of a 1° or 2° amine would be required per molecule of CO_2, rather than the 2:1 mechanism shown in Scheme 2. This approach could be useful to more effectively utilize amine-based solvents and limit issues such as corrosion associated with certain concentrated amine solutions.[63]

In order to determine if 1-*n*-alkylimidazoles could be used as solvents/agents for low pressure CO_2 capture applications, the uptake of CO_2 in a mixture of 1-butylimidazole (37.37 g, 158.2 mmol) and MEA (9.968 g, 163.2 mmol) (overall mixture ~80:20 vol/vol) was determined using the same apparatus as described in Section 2.2.4, using a slightly modified experimental procedure. Initially, a stream of CO_2 at ~1000 torr of CO_2 was fed to the cell for several minutes. The valve was then closed and the cell pressure was observed to decay until an equilibrium pressure of 606 torr was achieved. After obtaining the mass of the cell and applying Eqn. 1, it was found that 118 mmol (5.20 g) of CO_2 were absorbed by the liquid phase. This value of 0.725 mol CO_2 / mol MEA represents 145% of the theoretical loading with MEA in a non-aqueous solvent, based on a limiting 2:1 MEA:CO_2 stoichiometry (Scheme 2). For comparison, Jou reported that under similar temperature and pressure conditions, a 30 wt% solution of aqueous MEA exhibited a

loading of ~0.85 mol CO_2 / mol MEA.[27] While the aqueous solvent can achieve a greater loading, modifications to the imidazole structure may improve the equilibrium of the H^+ transfer reaction (Scheme 3) to favor products,[64] and increase CO_2 loadings to levels comparable to aqueous MEA under the same conditions.

The large excess of CO_2 absorbed over theoretical stoichiometry cannot be attributed solely to additional physical solubility of CO_2 in the solvent after the MEA has been consumed. Using the data in Table 2.6, the physical solubility of CO_2 in 1-butylimidazole at the equilibrium pressure of 606 torr would only account for a small portion (~300 mg) of the 1.60 g CO_2 absorbed in excess of MEA stoichiometry (Scheme 2). These data indicate that a secondary reaction pathway exists within this non-aqueous solvent system, even though the formation of bicarbonate is not possible in the absence of water.

An initial attempt to determine the exact reaction mechanism(s) responsible for the excess absorption of CO_2 was carried out using ^{1}H NMR spectroscopy, with associated spectra for the solvent mixture before and after uptake of CO_2 provided in the Supporting Information. ^{1}H NMR spectra were obtained in d_6-DMSO as well as with no deuterated solvent present in order to observe the CO_2-rich solvent in its actual state rather as a solute in DMSO. Proton signals associated with the N-H bonds in the CO_2-MEA complex originally in the range of 6.0-6.5 ppm when the solvent had absorbed less than 100% of its theoretical capacity were observed to shift downfield to the range of 6.5-7.0 ppm when the solvent had absorbed more than 100% of its theoretical CO_2 capacity. The stoichiometric excess of CO_2 and the relative downfield shift indicate that multiple species (i.e. MEA and 1-butylimidazole) are involved in the reaction(s) with CO_2 (Scheme 3). The chemical shifts for the reaction product(s) with CO_2 were also further downfield than were reported when CO_2 was captured by MEA in an IL, $[C_6mim][Tf_2N]$, which was limited to 0.50 mol CO_2 / mol MEA due the inability of the IL to participate with MEA to capture CO_2 and the subsequent precipitation of the MEA-carbamate product.[14] For the 1-butylimidazole-MEA solvent mixture, a large broad peak associated with the reaction product(s) from CO_2 uptake was observed even further downfield between 8.5-8.75 ppm, when no deuterated solvent was included in the NMR sample, which is likely indicative of H^+ exchange between 1-butylimidazole and MEA. A second, smaller broad peak associated with the reaction product(s) was observed in the range of 6.15 – 6.75 ppm in the CO_2 rich sample without deuterated solvent. The presence of two distinct peaks is in contrast to the spectra obtained in d_6-DMSO solvent where only a single broad peak with a shoulder was observed. This separation of peaks suggests that reaction products experience fundamentally different ^{1}H NMR behaviors in DMSO and in their neat state, and likely indicate that under these experimental conditions, 1-butylimidazole is not only a solvent but

has a participatory role in chemical reactions to capture CO_2 in the presence of MEA via the mechanisms shown in Scheme 3.

The viscosity of the CO_2-rich solvent was measured immediately after the experiment was completed and the liquid phase rapidly transferred to the viscometer. The viscosity of the CO_2-rich solution was initially measured as ~100 cP at 25°C, though the value drifted lower to 85 cP over several minutes, presumably due to loss of CO_2 from the reaction product(s).

The results for the 1-butylimidazole-MEA mixture indicate that the mixtures of 1-*n*-alkylimidazoles can be used as effective solvents/agents for low pressure CO_2 capture that provide high CO_2 capacity and relatively low viscosities for the CO_2-rich phase, especially when compared to TSIL compounds.[19, 20] Carbamate-imidazolium salts may be considered as IL analogues that exist as (reversible) products formed between CO_2, an amine and a 1-*n*-alkylimidazole.

2.6. Conclusions: Densities and viscosities were measured as a function of temperature for a series of ten 1-*n*-alkylimidazole compounds. Accurate models for the physical property behaviors were achieved using a dimensionless parameter, R', calculated from the ratio of the molecular weight of the *n*-alkyl chain relative to the molecular weight of the entire compound. All compounds except 1-methylimidazole were less dense than water over the entire temperature range, while viscosities for most 1-*n*-alkylimidazoles were below 10 cP, even at 298 K. Ideal CO_2 solubility data were measured at 298 K and low pressures for 1-*n*-alkylimidazoles. CO_2 solubility was observed to decrease with increasing chain length, which was correlated with decreasing solubility parameter (δ) as calculated from available vapor pressure data and a group contribution method.

A comparison of the physical properties of 1-*n*-alkylimidazoles to [$C_n$mim][X] ILs revealed that ILs are at least an order of magnitude more viscous than their neutral analogues. ILs are also denser than 1-*n*-alkylimidazoles, however, the differences are modest (10-50%). The solubility of CO_2 in both classes of compounds was quite similar from both a mole fraction and volumetric analysis, however 1-methylimidazole exhibits CO_2 solubility that is ~10% greater than the largest values observed in ILs at 298 K and low pressures. The solubility of CO_2 in both solvent types is physical in nature, and is less than most common organic solvents, but greater than that in polymers. Although 1-*n*-alkylimidazoles and [$C_n$mim][X] ILs can be tuned, structural tailoring does not increase CO_2 solubility as it does not increase FFV.

1-*n*-alkylimidazole can be used in combination with amines for low pressure CO_2 capture, and unlike [$C_n$mim][X] ILs, the 1-*n*-alkylimidazoles are able to participate in the CO_2 capture reaction. The available H^+ transfer mechanisms due to the Bronsted basicity of 1-*n*-alkylimidazoles enables more efficient use of

amines and overcomes stoichiometric limitations on amines in non-aqueous solvents by generating carbamate – imidazolium salts, which may be considered a type of reversible IL. It is likely that this approach can be applied to a wide variety of imidazole and amine compounds with opportunities to tailor chemical reactivity toward CO_2 as well as control over physical properties.

Indisputably, 1-*n*-alkylimidazoles are more volatile than their IL counterparts, though their high boiling points and low vapor pressures could make them valuable for many of the same engineering applications that have been proposed for ILs. Imidazoles offer the opportunity to engineer reactions wherein ILs are generated as products or intermediates that may be presently only transiently. Exploiting the H^+ accepting capabilities of the pyridine-like nitrogen within the imidazole ring may offer additional possibilities in separation applications such as highly selective removal of H_2S from CO_2.[59, 60]

Supporting Information Available (see 2.8 Appendix)

Plot of Figure 5 without overlaid regions, as well as associated references used to generate Figure 5; ^{1}H NMR spectra of 1-butylimidazole – MEA solvent mixtures with and without CO_2 (PDF). This material is available free of charge via the Internet at http://pubs.acs.org .

Acknowledgement

Partial support for this work provided by ION Engineering, LLC and The United States Department of Energy – National Energy Technology Laboratory (DE-FE00005799) is gratefully acknowledged. The expertise of Ken Belmore of the University of Alabama NMR Facility is greatly appreciated in obtaining ^{1}H NMR data. The authors wish to acknowledge James Hill and Ken Dunn of the University of Alabama for their assistance with laboratory construction, and Doug Cannon of the University of Alabama for his work on the electronic systems used for automated data acquisition.

2.7. References

1. Earle, M. J.; Esperanca, J.; Gilea, M. A.; Lopes, J. N. C.; Rebelo, L. P. N.; Magee, J. W.; Seddon, K. R.; Widegren, J. A. The distillation and volatility of ionic liquids. *Nature* 2006, *439*, 831-834.

2. Paulechka, Y. U.; Zaitsau, D. H.; Kabo, G. J.; Strechan, A. A. Vapor pressure and thermal stability of ionic liquid 1-butyl-3-methylimidazolium Bis(trifluoromethylsulfonyl)amide. *Thermochim. Acta* 2005, *439*, 158-160.

3. Holbrey, J. D.; Rogers, R. D.; Mantz, R. A.; Trulove, P. C.; Cocalia, V. A.; Visser, A. E.; Anderson, J. L.; Anthony, J. L.; Brennecke, J. F.; Maginn, E. J.; Welton, T. Physicochemical Properties. In *Ionic Liquids in Synthesis*, 2nd ed.; Wasserscheid, P.; Welton, T., Eds. Wiley-VCH: Weinheim, Germany, 2008.

4. Bara, J. E.; Camper, D. E.; Gin, D. L.; Noble, R. D. Room-Temperature Ionic Liquids and Composite Materials: Platform Technologies for CO_2 Capture. *Acc. Chem. Res.* 2010, *43*, 152-159.

5. Bara, J. E.; Carlisle, T. K.; Gabriel, C. J.; Camper, D.; Finotello, A.; Gin, D. L.; Noble, R. D. Guide to CO_2 Separations in Imidazolium-Based Room-Temperature Ionic Liquids. *Ind. Eng. Chem. Res.* 2009, *48*, 2739-2751.

6. Finotello, A.; Bara, J. E.; Camper, D.; Noble, R. D. Room-temperature ionic liquids: Temperature dependence of gas solubility selectivity. *Ind. Eng. Chem. Res.* 2008, *47*, 3453-3459.

7. Armand, M.; Endres, F.; MacFarlane, D. R.; Ohno, H.; Scrosati, B. Ionic-liquid materials for the electrochemical challenges of the future. *Nature Mater.* 2009, *8*, 621-629.

8. Seddon, K. R.; Stark, A.; Torres, M. J. Viscosity and density of 1-alkyl-3-methylimidazolium ionic liquids. In *Clean Solvents - Alternative Media for Chemical Reactions and Processing*, Abraham, M. A.; Moens, L., Eds. 2002; Vol. 819, pp 34-49.

9. Sharma, A.; Julcour, C.; Kelkar, A. A.; Deshpande, R. M.; Delmas, H. Mass Transfer and Solubility of CO and H_2 in Ionic Liquid. Case of Bmim PF_6 with Gas-Inducing Stirrer Reactor. *Ind. Eng. Chem. Res.* 2009, *48*, 4075-4082.

10. McCabe, W. L.; Smith, J. C.; Harriott, P. *Unit Operations of Chemical Engineering*. 6th ed.; McGraw-Hill: New York, 2001.

11. Gardas, R. L.; Coutinho, J. A. P. A group contribution method for viscosity estimation of ionic liquids. *Fluid Phase Equilibr.* 2008, *266*, 195-201.

12. NIST, Ionic Liquids Database (ILThermo) - NIST Standard Reference Database #147. http://ilthermo.boulder.nist.gov/ILThermo/mainmenu.uix (Accessed 31 May 2011)

13. NETL DOE/NETL Advanced Carbon Dioxide Capture R&D Program: Technology Update 9/2010. http://www.netl.doe.gov/technologies/coalpower/ewr/pubs/CO2%20Capture%20Tech%20Update%20Final.pdf (Accessed 31 May 2011)

14. Camper, D.; Bara, J. E.; Gin, D. L.; Noble, R. D. Room-Temperature Ionic Liquid-Amine Solutions: Tunable Solvents for Efficient and Reversible Capture Of CO_2. *Ind. Eng. Chem. Res.* 2008, *47*, 8496-8498.

15. Shiflett, M. B.; Drew, D. W.; Cantini, R. A.; Yokozeki, A. Carbon Dioxide Capture Using Ionic Liquid 1-Butyl-3-methylimidazolium Acetate. *Energy Fuels* 2010, *24*, 5781-5789.

16. Wang, G. N.; Hou, W. L.; Xiao, F.; Geng, J. A.; Wu, Y. T.; Zhang, Z. B. Low-Viscosity Triethylbutylammonium Acetate as a Task-Specific Ionic Liquid for Reversible CO_2 Absorption. *J. Chem. Eng. Data* 2011, *56*, 1125-1133.

17. Carvalho, P. J.; Alvarez, V. H.; Schroder, B.; Gil, A. M.; Marrucho, I. M.; Aznar, M.; Santos, L.; Coutinho, J. A. P. Specific Solvation Interactions of CO_2 on Acetate and Trifluoroacetate Imidazolium Based Ionic Liquids at High Pressures. *J. Phys. Chem. B* 2009, *113*, 6803-6812.

18. Shiflett, M. B.; Kasprzak, D. J.; Junk, C. P.; Yokozeki, A. Phase behavior of {carbon dioxide plus bmim Ac} mixtures. *J. Chem. Thermodyn.* 2008, *40*, 25-31.

19. Bates, E. D.; Mayton, R. D.; Ntai, I.; Davis, J. H. CO_2 capture by a task-specific ionic liquid. *J. Am. Chem. Soc.* 2002, *124*, 926-927.

20. Gutowski, K. E.; Maginn, E. J. Amine-Functionalized Task-Specific Ionic Liquids: A Mechanistic Explanation for the Dramatic Increase in Viscosity upon Complexation with CO_2 from Molecular Simulation. *J. Am. Chem. Soc.* 2008, *130*, 14690-14704.

21. Bara, J. E. A Versatile and Scalable Method for Producing *N*-functionalized Imidazoles. *Ind. Eng. Chem. Res.* (In Review).

22. Han, X.; Armstrong, D. W., Ionic liquids in separations. *Acc. Chem. Res.* 2007, *40*, 1079-1086.

23. Palleros, D. Heterocycles. www.chemistry.ucsc.edu/courses/palleros/Heterocycles.pdf (Accessed 31 May 2011)

24. Lin, H.; Freeman, B. D. Materials selection guidelines for membranes that remove CO_2 from gas mixtures. *J. Molec. Struct.* 2005, *739*, 57-74.

25. Bara, J. E.; Hatakeyama, E. S.; Noble, R. D.; Gin, D. L. Heteroaryl Salts and Methods For Producing and Using the Same. US Patent Application #20090171098.

26. Maddox, R. N.; Bhairi, A. H.; Diers, J. R.; Thomas, P. A. *Research Report RR-104: Equilibrium Solubility of Carbon Dioxide or Hydrogen Sulfide in Aqueous Solutions of Monoethanolamine, Diglycolamine, Diethanolamine and Methyldiethanolamine*; Gas Processors Association: Tulsa, OK, 1987.

27. Jou, F. Y.; Mather, A. E.; Otto, F. D. The solubility of CO_2 in a 30-mass-percent monoethanolamine solution. *Can. J. Chem. Eng.* 1995, *73*, 140-147.

28. Vrachnos, A.; Kontogeorgis, G.; Voutsas, E. Thermodynamic modeling of acidic gas solubility in aqueous solutions of MEA, MDEA and MEA-MDEA blends. *Ind. Eng. Chem. Res.* 2006, *45*, 5148-5154.

29. Green, D. W.; Perry, R. H. Perry's Chemical Engineers' Handbook (8th Edition). In McGraw-Hill: 2008.

30. Bara, J. E.; Gabriel, C. J.; Lessmann, S.; Carlisle, T. K.; Finotello, A.; Gin, D. L.; Noble, R. D. Enhanced CO_2 separation selectivity in oligo(ethylene glycol) functionalized room-temperature ionic liquids. *Ind. Eng. Chem. Res.* 2007, *46*, 5380-5386.

31. Finotello, A.; Bara, J. E.; Narayan, S.; Camper, D.; Noble, R. D. Ideal gas solubilities and solubility selectivities in a binary mixture of room-temperature ionic liquids. *J. Phys. Chem. B* 2008, *112*, 2335-2339.

32. Camper, D.; Bara, J.; Koval, C.; Noble, R. Bulk-fluid solubility and membrane feasibility of Rmim-based room-temperature ionic liquids. *Ind. Eng. Chem. Res.* 2006, 45, 6279-6283.

33. Carlisle, T. K.; Bara, J. E.; Gabriel, C. J.; Noble, R. D.; Gin, D. L. Interpretation of CO_2 solubility and selectivity in nitrile-functionalized room-temperature ionic liquids using a group contribution approach. *Ind. Eng. Chem. Res.* 2008, *47*, 7005-7012.

34. Blanchard, L. A.; Gu, Z. Y.; Brennecke, J. F. High-pressure phase behavior of ionic liquid/CO_2 systems. *J. Phys. Chem. B* 2001, *105*, 2437-2444.

35. Ye, C. F.; Shreeve, J. M., Rapid and accurate estimation of densities of room-temperature ionic liquids and salts. *J. Phys. Chem. A* 2007, *111*, 1456-1461.

36. Smith, G. D.; Borodin, O.; Li, L. Y.; Kim, H.; Liu, Q.; Bara, J. E.; Gin, D. L.; Nobel, R. A comparison of ether- and alkyl-derivatized imidazolium-based room-temperature ionic liquids: a molecular dynamics simulation study. *Phys. Chem. Chem. Phys.* 2008, *10*, 6301-6312.

37. Ghatee, M. H.; Zare, M.; Moosavi, F.; Zolghadr, A. R. Temperature-Dependent Density and Viscosity of the Ionic Liquids 1-Alkyl-3-methylimidazolium Iodides: Experiment and Molecular Dynamics Simulation. *J. Chem. Eng. Data* 2010, *55*, 3084-3088.

38. Barton, A. F. M. *CRC Handbook of Solubility Parameters and Other Cohesion Parameters*. 2nd ed.; CRC Press: Boca Raton, FL, 1991.

39. Liebner, F.; Patel, I.; Ebner, G.; Becker, E.; Horix, M.; Potthast, A.; Rosenau, T. Thermal aging of 1-alkyl-3-methylimidazolium ionic liquids and its effect on dissolved cellulose. *Holzforschung* 2010, *64*, 161-166.

40. Bowing, A. G.; Jess, A. Kinetics of single- and two-phase synthesis of the ionic liquid 1-butyl-3-methylimidazolium chloride. *Green Chem.* 2005, 7, 230-235.

41. Treble, R. G.; Johnson, K. E.; Tosh, E. The volatilities and conductivities of ionic liquids - GC-MS methodology and preliminary studies of acetic acid-base systems. *Can. J. Chem.* 2006, *84*, 915-924.

42. Bender, M. L.; Turnquest, B. W. General Basic Catalysis of Ester Hydrolysis and Its Relationship to Enzymatic Hydrolysis. *J. Am. Chem. Soc.* 1957, *79*, 1656-1662.

43. Katritzky, A. R.; Millet, G. H.; Noor, H. M.; Yates, F. S. Heterocycles in Organic Synthesis. 11. Reactions of Heteroaromatic N-oxides with Pyridine and Diazoles. *J. Org. Chem.* 1978, *43*, 3957-3960.

44. Cowgill, R. W.; Clark, W. M. Metalloporphyrins. *J. Biol. Chem.* 1952, *198*, 33-61.

45. Pernak, J.; Feder-Kubis, J.; Cieniecka-Roslonkiewicz, A.; Fischmeister, C.; Griffin, S. T.; Rogers, R. D. Synthesis and properties of chiral imidazolium ionic liquids with a (1R,2S,5R)-(-)-menthoxymethyl substituent. *New J. Chem.* 2007, *31*, 879-892.

46. Buchel, K.-H.; Falbe, J. F. A Process for Preparing an *n*-Alkyl or *n*-Alkenyl Imidazole. GB Patent 1,122,717, 1968.

47. Gasparini, J. P.; Gassend, R.; Maire, J. C.; Elguero, J. Study on Organosilyl Azole Series. 1. Action of Alkyl-halides, Acid-chlorides and Halogenated Ketones. *J. Organomet. Chem.* 1980, *188*, 141-150.

48. Tosoni, M.; Laschat, S.; Baro, A. Synthesis of novel chiral ionic liquids and their phase behavior in mixtures with smectic and nematic liquid crystals. *Helv. Chim. Acta* 2004, *87*, 2742-2749.

49. Hansen, C. M. *Hansen Solubility Parameters: A User's Handbook*. 2nd ed.; CRC Press: Boca Raton, FL, 2007.

50. Brandrup, J.; Immergut, E. H.; Grulke, E. A.; Abe, A.; Bloch, D. R. *Polymer Handbook*. 4th ed.; John Wiley & Sons: New York, 1999.

51. Ji, X. Y.; Adidharma, H. Thermodynamic modeling of ionic liquid density with heterosegmented statistical associating fluid theory. *Chem. Eng. Sci.* 2009, *64*, 1985-1992.

52. Jin, H.; O'Hare, B.; Dong, J.; Arzhantsev, S.; Baker, G. A.; Wishart, J. F.; Benesi, A. J.; Maroncelli, M. Physical properties of ionic liquids consisting of the 1-butyl-3-methylimidazolium cation with various anions and the bis(trifluoromethylsulfonyl)imide anion with various cations. *J. Phys. Chem. B.* 2008, *112*, 81-92.

53. Urry, W. H.; Eiszner, J. R.; Wilt, J. W. Free-Radical, Chain Reactions of Diazomethane with Polybromo- and Polyiodomethanes. *J. Am. Chem. Soc.* 1957, *79*, 918-922.

54. Anthony, J. L.; Anderson, J. L.; Maginn, E. J.; Brennecke, J. F., Anion effects on gas solubility in ionic liquids. *J. Phys. Chem. B* 2005, *109*, 6366-6374.

55. Cadena, C.; Anthony, J. L.; Shah, J. K.; Morrow, T. I.; Brennecke, J. F.; Maginn, E. J., Why is CO_2 so soluble in imidazolium-based ionic liquids? *J. Am. Chem. Soc.* 2004, *126*, 5300-5308.

56. Bara, J. E.; Gabriel, C. J.; Carlisle, T. K.; Camper, D. E.; Finotello, A.; Gin, D. L.; Noble, R. D. Gas separations in fluoroalkyl-functionalized room-temperature ionic liquids using supported liquid membranes. *Chem. Eng. J.* 2009, *147*, 43-50.

57. Gurkan, B. E.; de la Fuente, J. C.; Mindrup, E. M.; Ficke, L. E.; Goodrich, B. F.; Price, E. A.; Schneider, W. F.; Brennecke, J. F., Equimolar CO_2 Absorption by Anion-Functionalized Ionic Liquids. *J. Am. Chem. Soc.* 2010, *132*, 2116-2117.

58. Lee, W. M. Selection of Barrier Materials from Molecular Structure. *Polym. Eng. Sci.* 1980, *20*, 65-69.

59. Kidnay, A. J.; Parrish, W. R. *Fundamentals of Natural Gas Processing*. CRC Press: Taylor & Francis Group: Boca Raton, FL, 2006.

60. Astarita, G.; Savage, D. W.; Bisio, A. *Gas Treating with Chemical Solvents*. John Wiley & Sons: New York, 1983.

61. Karadas, F.; Atilhan, M.; Aparicio, S. Review on the Use of Ionic Liquids (ILs) as Alternative Fluids for CO_2 Capture and Natural Gas Sweetening. *Energ Fuel* 2010, *24*, 5817-5828.

62. Rochelle, G. T., Amine Scrubbing for CO_2 Capture. *Science* 2009, *325*, 1652-1654.

63. Zhou, S.; Chen, X.; Nguyen, T.; Voice, A. K.; Rochelle, G. T., Aqueous Ethylenediamine for CO_2 Capture. *Chemsuschem* 2010, *3*, 913-918.

64. Lenarcik, B.; Ojczenasz, P. The influence of the size and position of the alkyl groups in alkylimidazole molecules on their acid-base properties. *J. Heterocyclic Chem.* 2002, *39*, 287-290.

2.8. Appendix:

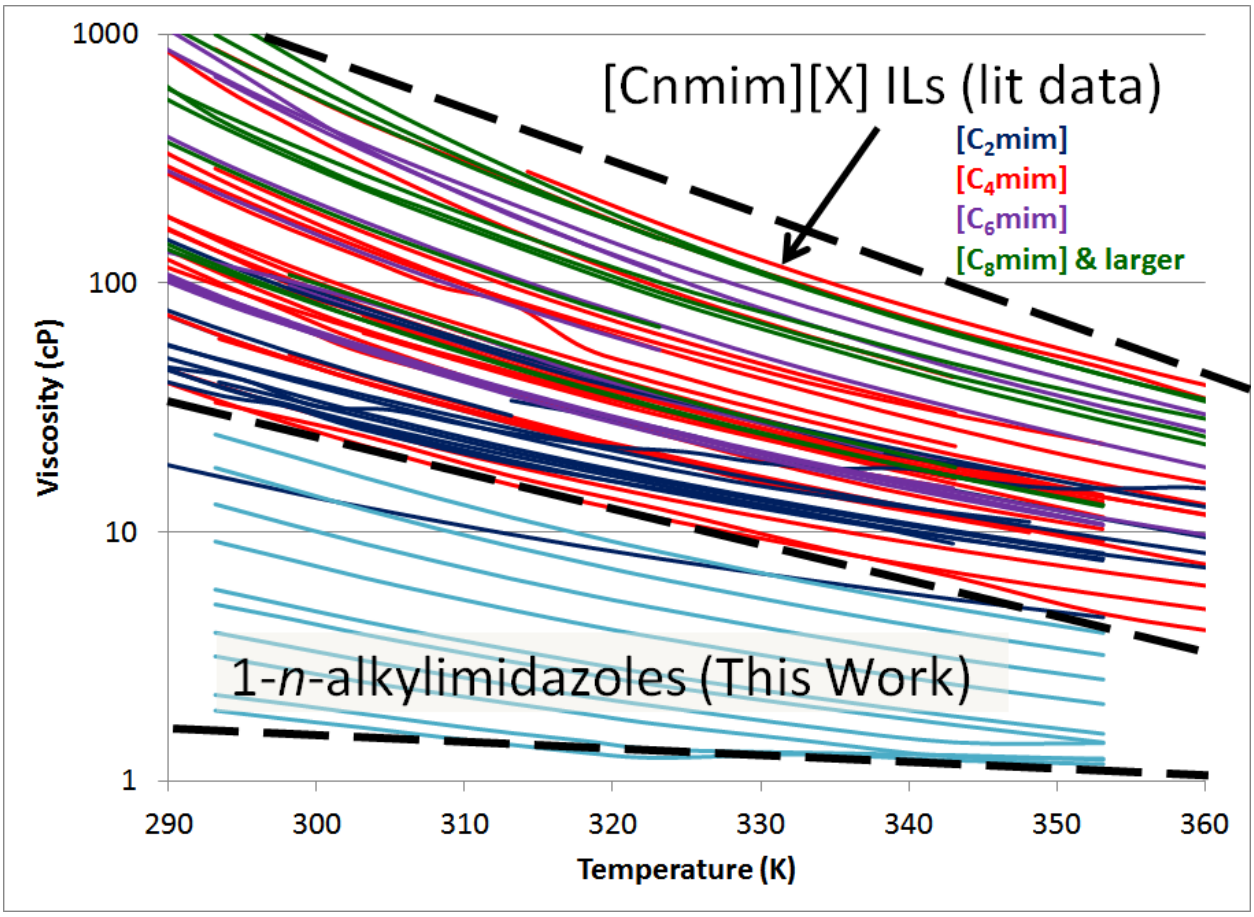

Figure S1: Figure 2.5 without overlaid regions.

References used to generate Figure S1:

1-butyl-3-methylimidazolium cation with various anions ([C_4mim][X] or "bmim" ILs):

[C_4mim][OAc] (acetate)

1. Crosthwaite, J. M.; Muldoon, M. J.; Dixon, J. K.; Anderson, J. L.; Brennecke, J. F. Phase Transition and Decomposition Temperatures, Heat Capacities and Viscosities of Pyridinium Ionic Liquids. *J. Chem. Thermodyn.* 2005, *37*, 559-568.

[C_4mim][dca] (dicyanamide)

2. Sanchez, L. G.; Espel, J. R.; Onink, F.; Meindersma, G. W.; De Haan, A. B. J. Density, Viscosity, and Surface Tension of Synthesis Grade Imidazolium, Pyridinium, and Pyrrolidinium Based Room Temperature Ionic Liquids. *Chem. Eng. Data* 2009, *54*, 2803-2812.

3. Carvalho, P. J.; Regueira, T.; Santos, L. M. N. B. F.; Fernandez, J.; Coutinho, J. A. P. Effect of Water on the Viscosities and Densities of 1-Butyl-3-methylimidazolium Dicyanamide and 1-Butyl-3-methylimidazolium Tricyanomethane at Atmospheric Pressure. *J. Chem. Eng. Data* 2010, *55*, 645-652.

[C_4mim][Tf2N] (bis(trifluoromethane)sulfonimide)
4. Tokuda, H.; Hayamizu, K.; Ishii, K.; Susan, M. A. B. H.; Watanabe, M. Physicochemical Properties and Structures of Room Temperature Ionic Liquids. 2. Variation of Alkyl Chain Length in Imidazolium Cation. *J. Phys. Chem. B* 2005, *109*, 6103-6110.
5. Jacquemin, J.; Husson, P.; Padua, A. A. H.; Majer, V. Density and Viscosity of Several Pure and Water-saturated Ionic Liquids. *Green Chem.* 2006, *8* , 172-180.
6. Tokuda, H.; Tsuzuki, S.; Susan, M. A. B. H.; Hayamizu, K.; Watanabe, M. How Ionic Are Room-Temperature Ionic Liquids? An Indicator of the Physicochemical Properties. *J. Phys. Chem. B* 2006, *110*, 19593-19600.

[C_4mim][beti] (bis(perfluoroethylsulfonyl)imide)
7. See reference 6

[C_4mim][$MeSO_4$] (methylsulfate)
8. Pereiro, A. B.; Verdia, P.; Tojo, E.; Rodriguez, A. J. Physical Properties of 1-Butyl-3-methylimidazolium Methyl Sulfate as a Function of Temperature. *Chem. Eng. Data* 2007, *52*, 377-380.

[C_4mim][NO_3] (nitrate)
9. Seddon, K. R.; Stark, A.; Torres, M.-J. Viscosity and Density of 1-Alkyl-3-methylimidazolium Ionic Liquids. *ACS Symp. Ser.* 2002, *819*, 34-49.
10. Mokhtarani, B.; Sharifi, A.; Mortaheb, H. R.; Mirzaei, M.; Mafi, M.; Sadeghian, F. Density and Viscosity of 1-butyl-3-methylimidazolium Nitrate with Ethanol, 1-propanol, or 1-butanol at Several Temperatures. *J. Chem. Thermodyn.* 2009, *41*, 1432-1438.

[C_4mim][$OcSO_4$] (octylsulfate)
11. Wasserscheid, P.; van Hal, R.; Bosmann, A. 1-n-butyl-3-methylimidazolium ([bmim]) octylsulfate: An Even Greener Ionic Liquid. *Green Chem.* 2002, *4*, 400-404.
12. Jacquemin, J.; Husson, P.; Majer, V.; Padua, A. A. H.; Gomes, M. F. C. Thermophysical Properties, Low Pressure Solubilities and Thermodynamics of Solvation of Carbon Dioxide and Hydrogen in Two Ionic Liquids Based on the Alkylsulfate Anion. *Green Chem.* 2008, *10*, 944-950.

[C_4mim][ClO_4] (perchlorate)
13. Mokhtarani, B.; Mojtahedi, M. M.; Mortaheb, H. R.; Mafi, M.; Yazdani, F.; Sadeghian, F. Densities, Refractive Indices, and Viscosities of the Ionic Liquids 1-Methyl-3-octylimidazolium Tetrafluoroborate and 1-Methyl-3-butylimidazolium Perchlorate and Their Binary Mixtures with Ethanol at Several Temperatures. *J. Chem. Eng. Data* 2008, *53*, 677-682.

[C_4mim][BF_4] (tetrafluoroborate)
14. See Reference 9
15. Zhou, Q.; Wang, L.-S. Densities and Viscosities of 1-Butyl-3-methylimidazolium Tetrafluoroborate + H_2O Binary Mixtures from (303.15 to 353.15) K. *J. Chem. Eng. Data* 2006, *51*, 905-908.
16. See Reference 5
17. See reference 6

18. Harris, K. R.; Kanakubo, M.; Woolf, L. A. Temperature and Pressure Dependence of the Viscosity of the Ionic Liquid 1-Butyl-3-methylimidazolium Tetrafluoroborate: Viscosity and Density Relationships in Ionic Liquids. *J. Chem. Eng. Data* 2007, *52*, 2425-2430.

[C_4mim][SCN] (thiocyanate)

19. Domanska, U.; Laskowska, M. Temperature and Composition Dependence of the Density and Viscosity of Binary Mixtures of {1-Butyl-3-methylimidazolium Thiocyanate + 1-Alcohols}. *J. Chem. Eng. Data* 2009, *54*, 2113-2119.

[C_4mim][$Me(CN)_3$] (tricyanomethane)

20. Carvalho, P. J.; Regueira, T.; Santos, L. M. N. B. F.; Fernandez, J.; Coutinho, J. A. P. Effect of Water on the Viscosities and Densities of 1-Butyl-3-methylimidazolium Dicyanamide and 1-Butyl-3-methylimidazolium Tricyanomethane at Atmospheric Pressure. *J. Chem. Eng. Data* 2010, *55*, 645-652.

[C_4mim][OTf] (triflate)

21. See reference 9
22. See reference 6
23. Ge, M.-L.; Zhao, R.-S.; Yi, Y.-F.; Zhang, Q.; Wang, L. -S. Densities and Viscosities of 1-Butyl-3-methylimidazolium Trifluoromethanesulfonate + H_2O Binary Mixtures at T) (303.15 to 343.15) K *J. Chem. Eng. Data* 2008, *53*, 2408-2411.

[C_4mim][TFA] (trifluoroacetate)

24. See reference 1
25. See reference 6

[C_{10}mim][Tf_2N] (1-decyl-3-methylimidazolium bis(trifluoromethane)sulfonimide)

26. Ahosseini, A.; Scurto, A. M. Viscosity of Imidazolium-Based Ionic Liquids at Elevated Pressures: Cation and Anion Effects. *Int. J. Thermophys.* 2008, *29*, 1222-1243

[C_{12}mim][PF_6] (1-dodecyl-3-methylimidazolium hexafluorophosphate)

27. See reference 9

1-ethyl-3-methylimidazolium cation with various anions ([C_2mim][X] or “emim” ILs):

[C_2mim][TF_2N] (bis(trifluoromethane)sulfonimide)

28. See reference 1
29. See reference 4
30. See reference 5
31. See reference 6

[C_2mim][dca] (dicyanamide)

32. Schreiner, C.; Zugmann, S.; Hartl, R.; Gores, H. J. Fractional Walden Rule for Ionic Liquids: Examples from Recent Measurements and a Critique of the So-Called Ideal KCl Line for the Walden Plot. *J. Chem. Eng. Data* 2010, *55*, 1784-1788.
33. Fletcher, S. I.; Sillars, F. B.; Hudson, N. E.; Hall, P. J. Physical Properties of Selected Ionic Liquids for Use as Electrolytes and Other Industrial Applications. *J. Chem. Eng. Data* 2010, *55*, 778-782.

[C_2mim][$EtSO_4$] (ethylsulfate)
34. Gomez, E.; Gonzalez, B.; Calvar, N.; Tojo, E.; Dominguez, A. Physical Properties of Pure 1-Ethyl-3-methylimidazolium Ethylsulfate and Its Binary Mixtures with Ethanol and Water at Several Temperatures. *J. Chem. Eng. Data* 2006, *51*, 2096-2102.
35. See reference 5
36. Rodriguez, H.; Brennecke, J. F. Temperature and Composition Dependence of the Density and Viscosity of Binary Mixtures of Water + Ionic Liquid. *J. Chem. Eng. Data* 2006, 51, 2145-2155.

[C_2mim][NO_3] (nitrate)
37. See reference 9

[C_2mim][BF_4] (tetrafluoroborate)
38. See reference 9
39. See reference 32
40. See reference 33

[C_2mim][OTf] (triflate)
41. See reference 9
42. See reference 36

1-hexyl-3-methylimidazolium cation with various anions ([C_6mim][X] or "hmim" ILs):

[C_6mim][TF_2N] (bis(trifluoromethane)sulfonimide)
43. See reference 1
44. See reference 4
45. See reference 6
46. Widegren, J. A.; Magee, J. W. Density, Viscosity, Speed of Sound, and Electrolytic Conductivity for the Ionic Liquid 1-Hexyl-3-methylimidazolium Bis(trifluoromethylsulfonyl)imide and Its Mixtures with Water. *J. Chem. Eng. Data* 2007, 52, 2331-2338.

[C_6mim][PF_6] (hexafluorophosphate)
47. See reference 9
48. Pereiro, A. B.; Legido, J. L.; Rodriguez, A. Physical Properties of Ionic Liquids Based on 1-alkyl-3-methylimidazolium Cation and Hexafluorophosphate as Anion and Temperature Dependence. *J. Chem. Thermodyn.* 2007, *39*, 1168-1175.
49. Muhammad, A.; Mutalib, M. I. A.; Wilfred, C. D.; Murugesan, T.; Shafeeq, A. Thermophysical Properties of 1-hexyl-3-methyl Imidazolium Based Ionic Liquids with Tetrafluoroborate, Hexafluorophosphate and bis(trifluoromethylsulfonyl)imide Anions. *J. Chem. Thermodyn.* 2008, 40, 1433-1438.

[C_6mim][NO_3] (nitrate)
50. See reference 9

[C_6mim][BF_4] (tetrafluoroborate)
51. See reference 9
52. Sanmamed, Y. A.; Gonzalez-Salagado, D.; Troncoso, J.; Cerdeirina, C. A.; Romani, L. Viscosity-induced errors in the density determination of room temperature ionic liquids using vibrating tube densitometry. *Fluid Phase Equilibr.* 2007, *252*, 96-102.

53. See reference 49

1-octyl-3-methylimidazolium cation with various anions ([C_8mim][X] or “hmim” ILs):

[C_8mim][PF_6] (hexafluorophosphate)
54. See reference 9
55. See reference 48

[C_8mim][NO_3] (nitrate)
56. See reference 9

[C_8mim][BF_4] (tetrafluoroborate)
57. See reference 9
58. See reference 9
59. See reference 13

[C_8mim][TF_2N] (bis(trifluoromethane)sulfonimide)
60. See reference 4
61. See reference 6

[C_8mim][OTf] (triflate)
62. See reference 9

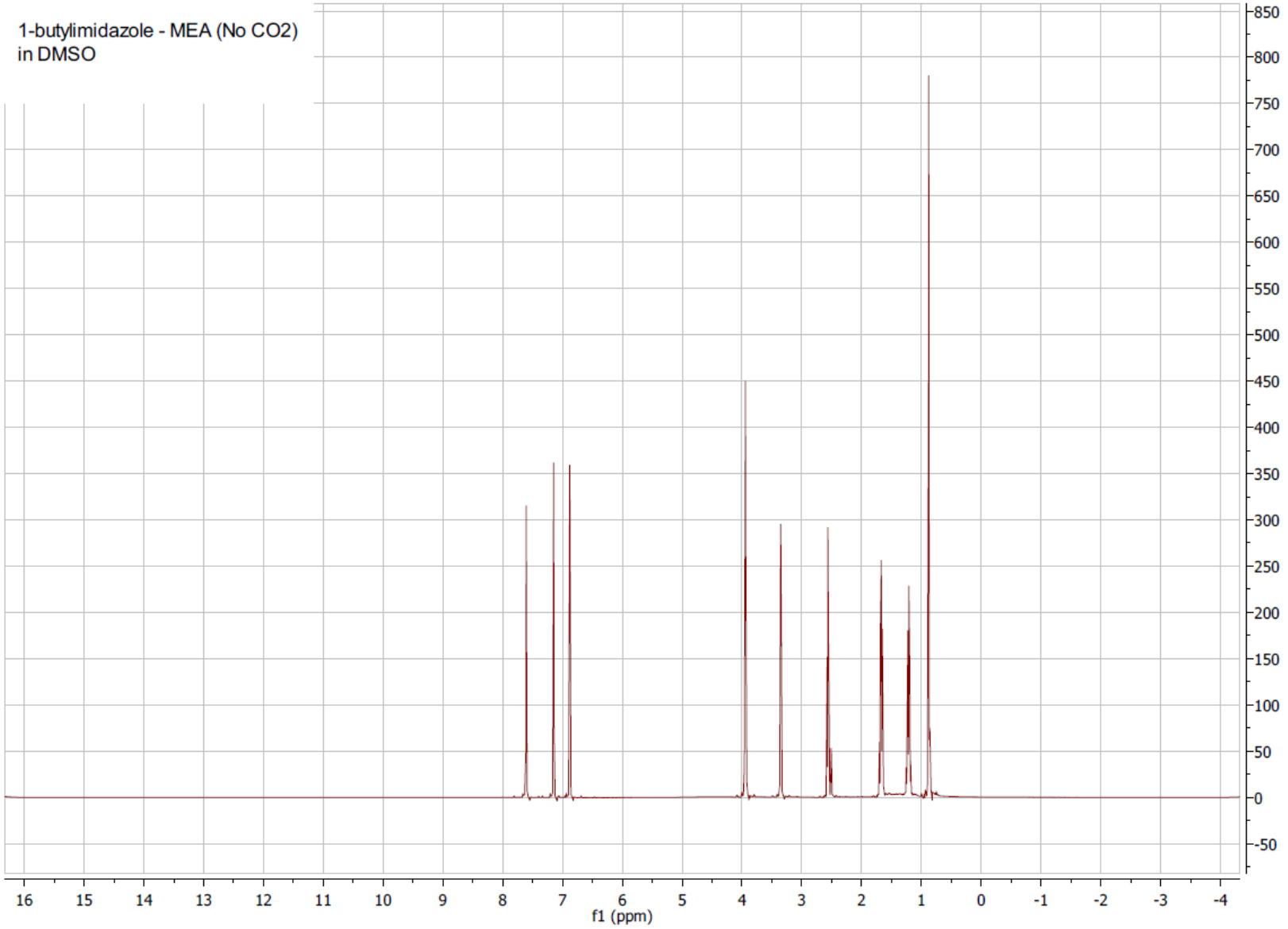
1-butylimidazole - MEA (No CO2)
in DMSO
850
800
750
700
650
600
550
500
450
400
350
300
250
200
150
100
50
0
-50
16
15
14
13
12
11
10
9
8
7
6
5
4
3
2
1
0
-1
-2
-3
-4
f1 (ppm)

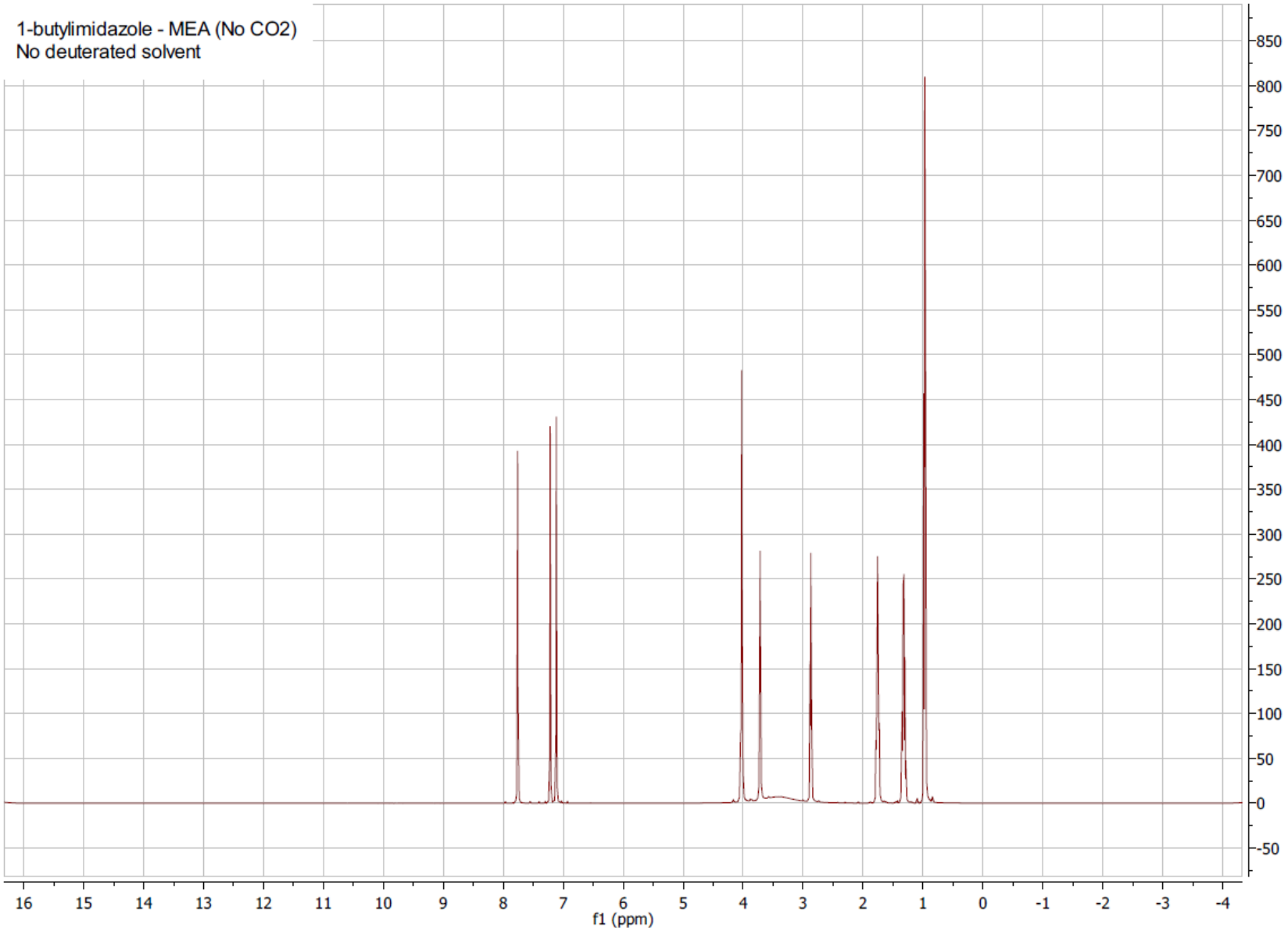
1-butylimidazole - MEA (No CO2)
No deuterated solvent
850
800
750
700
650
600
550
500
450
400
350
300
250
200
150
100
50
0
-50
16
15
14
13
12
11
10
9
8
7
6
5
4
3
2
1
0
-1
-2
-3
-4
f1 (ppm)

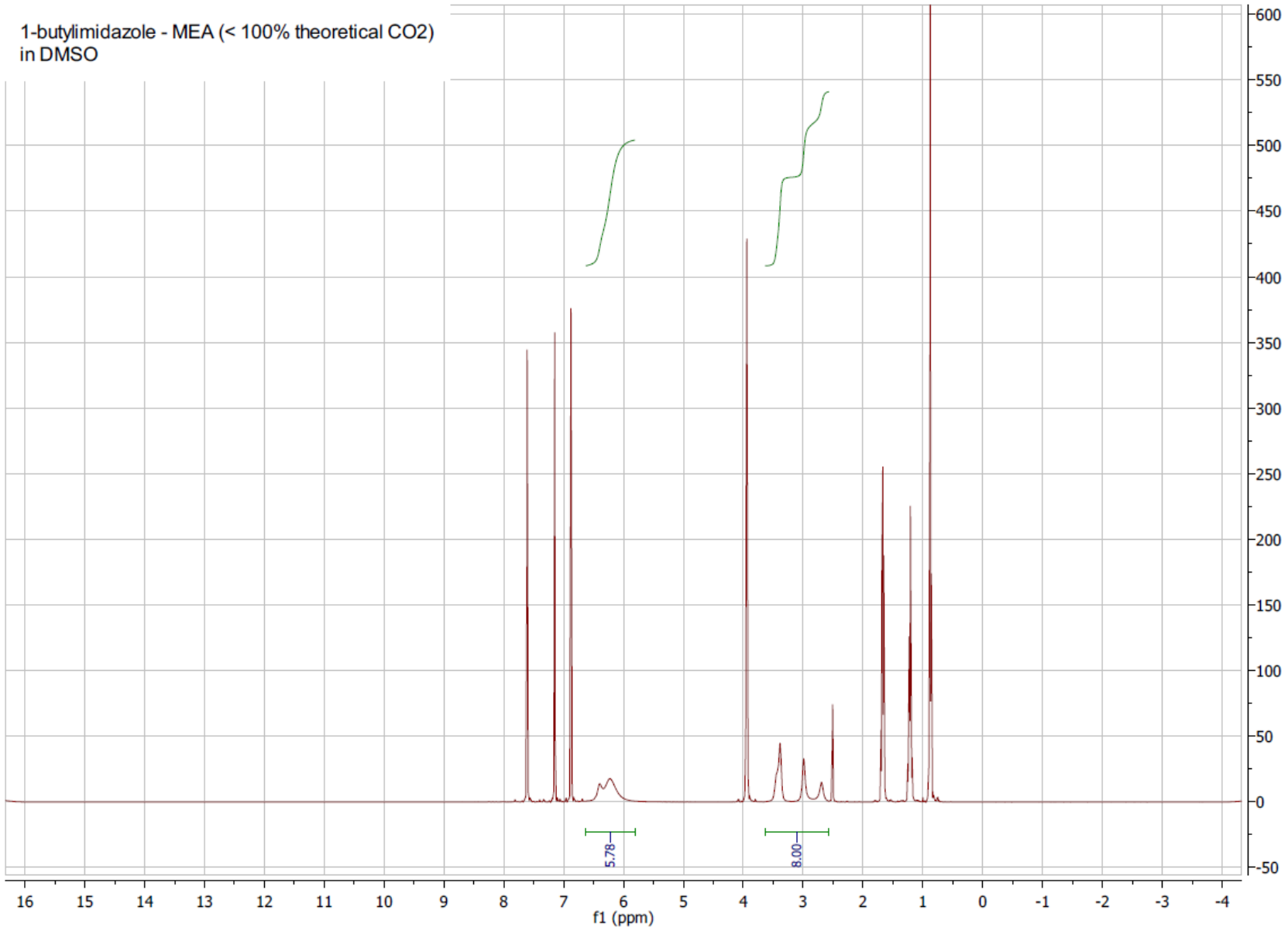
1-butylimidazole - MEA (< 100% theoretical CO2)
in DMSO
5.78
8.00
f1 (ppm)

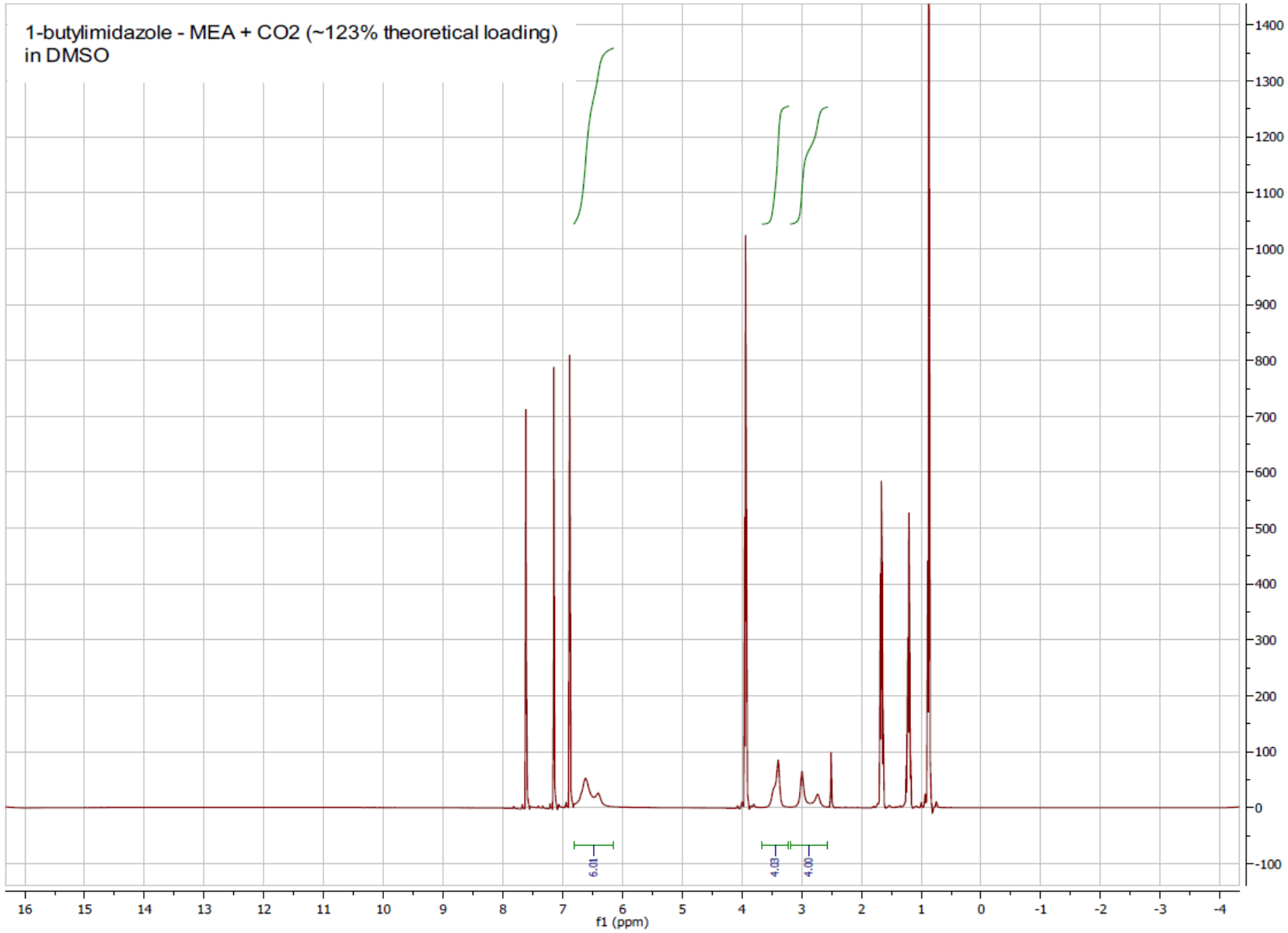
1-butylimidazole - MEA + CO2 (~123% theoretical loading)
in DMSO
6.01
4.03
4.00
f1 (ppm)

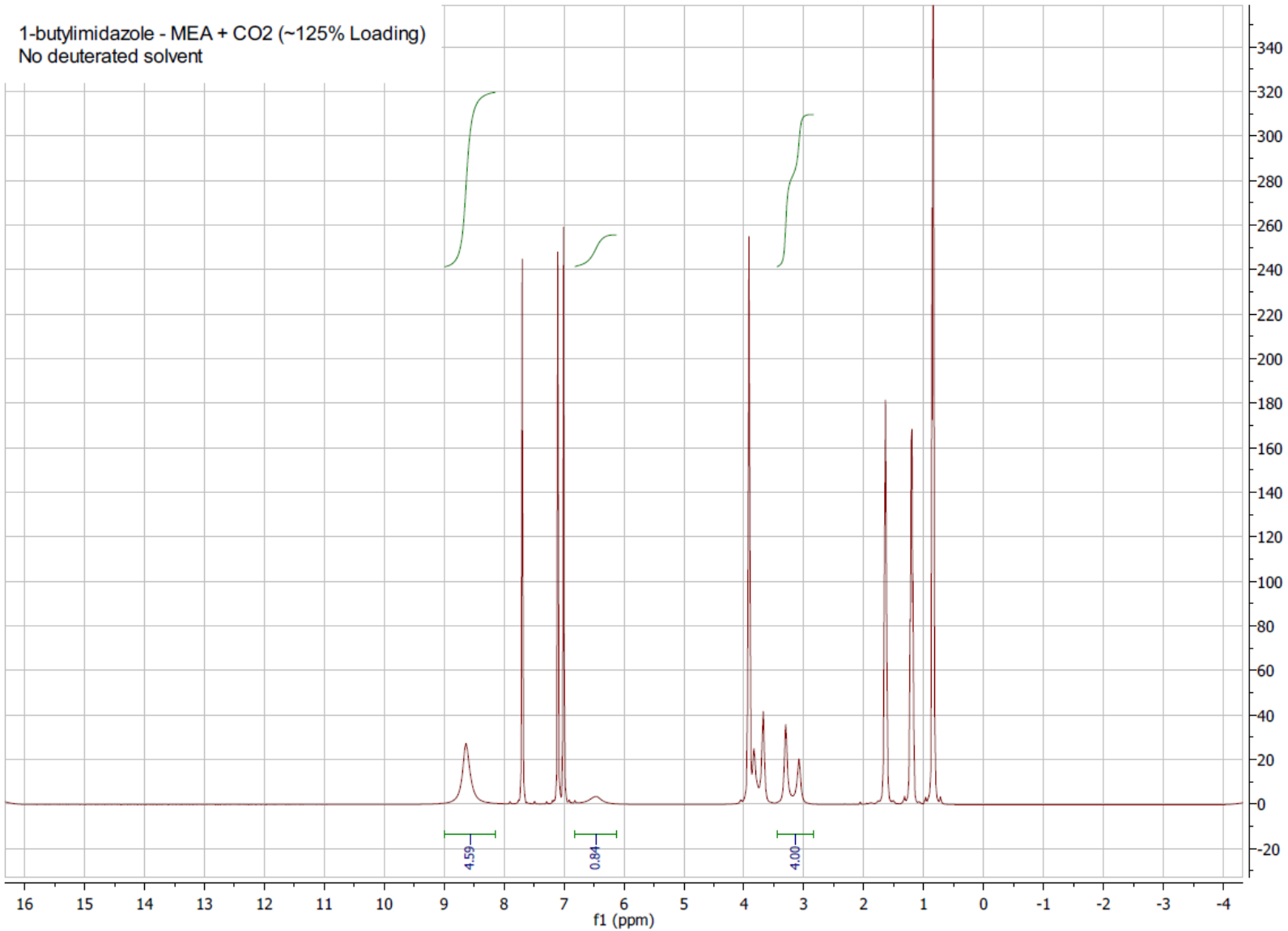
1-butylimidazole - MEA + CO2 (~125% Loading)
No deuterated solvent
4.59
0.84
4.00
f1 (ppm)

CHAPTER THREE

[†]Reactive & Reversible Ionic Liquids for CO_2 Capture and Acid Gas Removal

Matthew S. Shannon & Jason E. Bara*

Department of Chemical & Biological Engineering

The University of Alabama, Tuscaloosa, AL 35487-0203

Abstract

The use of ionic liquids (ILs) for CO_2 capture and the removal of acid gases from natural gas and other industrial processes has been one of the foremost research applications for this unique class of non-volatile solvents. However, most of the broadly studied ILs lack sufficient capacities for CO_2 and other acid gases such as H_2S, SO_2, etc. to be viewed as viable replacements for aqueous amine technologies which have been used industrially for acid gas removal for nearly a century. Furthermore, many of most well-known ILs are too viscous to be used within conventional process equipment and are likely too costly for use at large scales. As the negligible vapor pressure of ILs is an attractive property for gas separations, it is desirable to find new ILs with improved properties that can be synthesized from lower cost starting materials and/or natural products. Recently, new reactive and reversible IL solvents have emerged in efforts to improve upon the CO_2 capacity, physical properties and costs of IL-based gas separation technologies. In this review, we detail the differences between these novel approaches and the standard crop of ILs that have been reported in the literature. The various strategies that have been employed to develop these materials for energy-related separation applications will be examined, with an emphasis on how chemistry and physical properties relate to the demands of efficient chemical process engineering. Where applicable, comparisons to conventional (i.e. aqueous amine) solvents will be made so as provide baselines to commercial technologies. Finally, we introduce the concept of imidazoles and imidazole-amine hybrid solvents as another tunable platform for the removal of CO_2, SO_2 and H_2S.

Keywords

post-combustion carbon dioxide capture, reactive and reversible ionic liquids, chemical process engineering, imidazole compounds, separations for energy applications

[†]*Separation Science & Technology, 2012, 47, 178-188*.

3.1 Introduction: The massive chemical engineering and chemistry challenges associated with the generation and production of clean energy in the early 21st century have spurred the development new types of solvents to address the removal of CO_2, H_2S, SO_2 and other "acid" gases commonly found in processes that produce hydrocarbon fuels or generate electricity from coal or natural gas.[1-4]

Historically, the dominant technology for acid gas removal has been aqueous amine solvents used within absorber-stripper (also known as contactor-regenerator) processes.[2-4] Aqueous amine technologies have been commercially used for over 80 years in the natural gas industry and have been the subject of extensive research and development efforts.[2-9] Aqueous amine solvents rely on the use of reversible chemical reactions between an acid gas and an amine to separate contaminants from the desired product stream.[3, 4] While aqueous amine solutions are highly effective and reliable for the removal acid gases to the low levels required to meet industrial specifications,[1] they are energy intensive due to the evaporation of water during solvent regeneration, and suffer from other issues such as corrosiveness and volatility.[1]

Because of the drawbacks associated with conventional aqueous amine solvents, ionic liquids (ILs) have been proposed as an alternative solvent platform to aqueous amine solvents for applications such as the removal of CO_2 and SO_2 from the flue gas of coal-fired power plants[10-13] and the removal of CO_2 and/or H_2S from natural gas (i.e. CH_4), also known as "sweetening".[14] Within an optimized process, ILs may offer improved energy efficiency as they will not evaporate under the temperatures (up to 120 ^oC) that are typically employed in solvent regeneration.[1, 10] Imidazolium-based ILs have been among the most extensively studied due to their tunable structures and relatively low viscosities.[10, 15, 16] However, results to date indicate that most ILs lack the high acid gas capacities that are exhibited by aqueous amine solutions,[10, 17, 18] especially in applications where the acid gas partial pressures are low (i.e. post-combustion CO_2 capture). ILs might be better considered for use as alternative solvents in high pressure acid gas removal applications[10, 14, 18] where organic (physical) solvents such as methanol and oligomers of poly(ethylene glycol) find industrial application in the Rectisol® and Selexol® processes, respectively.

As these limitations have become apparent, recent work has focused on developing ILs that are capable of directly reacting with CO_2 or forming reversible ILs from neutral molecules that react with CO_2 (or other acid gases). This Review will thus focus on the various materials and methods that have been reported as capable of producing these types of ILs. Emphasis will be placed on performance in low partial pressure applications such as post-combustion CO_2 capture as this is where energy efficiency can be improved most dramatically compared to existing processes. Additional examples will examine reactive and reversible ILs as applied to the removal of H_2S, SO_2, and CS_2. Furthermore, we will present new data recently

developed in our laboratory on the use of imidazole and imidazole-amine hybrid solvents for CO_2 and SO_2 removal applications.

3.2 Reactive Ionic Liquids

The most-well known examples of reactive ILs reported for CO_2 capture and acid gas removal have been imidazolium-based amine-functionalized "task-specific" ILs (TSILs)[19, 20] and imidazolium-based ILs with acetate (OAc) anions (Figure 3.1).[12, 13, 21, 22]

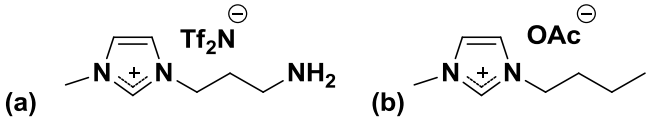

Figure 3.1: Examples of amine-functionalized TSILs and imidazolium acetate salts.

These ILs are unique in that they can form reversible complexes with CO_2 and SO_2, achieving large increases in CO_2 capacity at low pressures when compared to unfunctionalized ILs.[10, 19] However, drawbacks to these ILs include challenging synthetic methods and/or high viscosity in their CO_2-lean and CO_2-rich states.[19, 20] In addition to the ability of the solvent to absorb/desorb sufficient quantities of CO_2 under the appropriate process conditions, viscosity is an extremely important consideration in solvent selection for CO_2 capture and acid gas removal processes. As a benchmark, near ambient temperature, aqueous amine solvents typically have viscosities of < 20 cP in the CO_2 rich state,[2, 23, 24] with values as low as 2 cP possible.[8] Most common imidazolium-based ILs exhibit viscosities of at least 30 cP at ambient temperature, although many are at least an order of magnitude more viscous.[16, 25, 26] Efficient and economical acid gas removal processes require high rates of mass and heat transfer,[1, 2] which are negatively impacted by increased viscosity (i.e. decreased diffusion, reduced gas-liquid contact).[27]

As most ILs lack a sufficient CO_2 capacity at the low partial pressures found in post-combustion CO_2 capture and/or are too viscous for practical use, new research directions have emerged in the search for ILs with improved properties. Neutralized amino acid anions are one such approach that can incorporate various amine groups into ILs using natural products, while eliminating the need to synthetically tether amines to cations and/or anions. Imidazolium-based ILs featuring neutralized amino acid anions were first reported by Ohno and co-workers, though were not studied for use as CO_2 capture solvents.[28, 29] More recently, ILs based on trihexyltetradecylphosphonium ($[P_{6,6,6,14}]$) cations with several neutralized amino acid anions have been shown to exhibit a 1:1 mechanism in capturing CO_2 as after reaction with CO_2, the anion can exist as a stabilized carbamic acid.[30, 31] This 1:1 mechanism is unique as TSILs were only capable of a 1:2

(mol CO_2 / mol IL) mechanism.[19] Scheme 1 illustrates this reaction for the case of $[P_{6,6,6,14}]$ with a methioninate anion (($[P_{6,6,6,14}][Met]$).

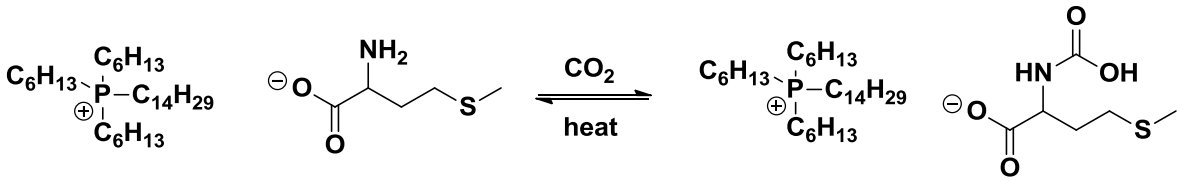

Scheme 1: 1:1 reaction between $[P_{6,6,6,14}][Met]$ and CO_2.

Stable $[P_{6,6,6,14}]$ cations have also been be paired with a series of basic anions reactive to CO_2 including different azolate species (Scheme 2).[32] For anions with pK_a values > 13, CO_2 capacities were observed to approach 1.00 mol CO_2 / mol anion under low CO_2 partial pressures (bubbling CO_2 in open container) and room temperature, while anions with pK_a values < 13 exhibited much lower CO_2 capacities (~0.20 mol CO_2/mol) under these experimental conditions.[32] Heat of reaction was observed to linearly correlate with pK_a, and the reactive ILs that absorbed more CO_2 exhibited much larger heats of reaction (i.e. more favorable to CO_2 absorption).[32] The authors demonstrated that absorption of CO_2 could be cycled (desorption of CO_2 via bubbling N_2 at 80°C) at least 25 times with no degradation to the cation or anion species.[32]

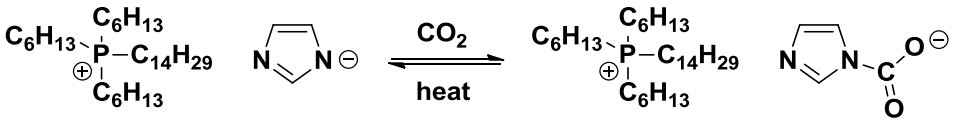

Scheme 2: Example of phosphonium IL with a reactive imidazolate anion for CO_2 capture.

[It is worth noting that many authors use bubbling N_2 with increased temperature as a means of desorbing CO_2. However, this does not imply that N_2 participates in the reaction, but is rather a means to promote mass transfer or desorption of CO_2 from the solvent. Desorption of CO_2 could also be achieved using steam or stirring the solvent under vacuum.]

A similar approach was also applied by Maginn and co-workers using $[P_{6,6,6,14}]$ with pyrrolide anions (Scheme 3), with an emphasis on molecular modeling as a guide to selecting anions with optimized combinations of properties.[33] The authors found that the reactive anions could complex with CO_2 in a 1:1 mechanism at low partial pressures, with 1:1 absorption occurring close to 1 bar and at temperatures

<40°C.[33] However, viscosity tended to increase to levels > 100 cP with increased CO_2 loading and lower temperatures.[33]

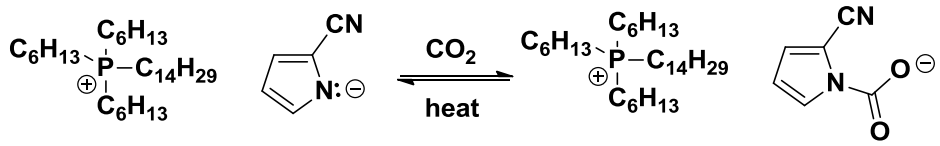

Scheme 3: Reaction of CO_2 with phosphonium pyrrolide ILs.

Hybrid solvents formulated by blending individual IL and amine components have also been demonstrated to dramatically improve CO_2 capacities by utilizing the chemical reactivity of the amine synergistically with the non-volatile properties of the IL component.[10, 17, 18] This approach offers flexibility in solvent design through the ability to choose both IL and amine components without the need to incorporate all of the desired functionality into a single molecule. The combination of amines such as monoethanolamine (MEA) and diethanolamine (DEA) with imidazolium-based ILs such as [C_6mim][Tf_2N] and [C_2OHmim][Tf_2N], respectively, has been shown to dramatically increase CO_2 capacity (up to 100x) at low pressures relatively to the physical solubility of CO_2 in the IL solvent alone.[17] This approach can offer tunability in solvent physical (e.g. viscosity), thermodynamic (e.g. heat of reaction and solution) and chemical (e.g. selectivity for H_2S) properties as a broad range of useful amines can be added directly to the IL.[10, 17, 18]

Increased CO_2 capacity in imidazolium-based ILs has also been achieved by using the intrinsic carbene chemistry available within imidazolium cations[34] to promote CO_2 capture. Dai and co-workers have reported on the use of amidine, guanidine and phosphazene superbases to demonstrate equimolar CO_2 capture at low pressure (i.e. bubbling CO_2 at ambient temperature) at the deprotonated the C(2) position within the imidazolium ring.[35] This approach results in the formation of a dicationic-dianionic complex containing zwitterionic imidazolium salt as detailed in Scheme 4 for the example of [C_4mim][Tf_2N] and 1,8-diazabicyclo-[5.4.0]-undec-7-ene (DBU).[35]

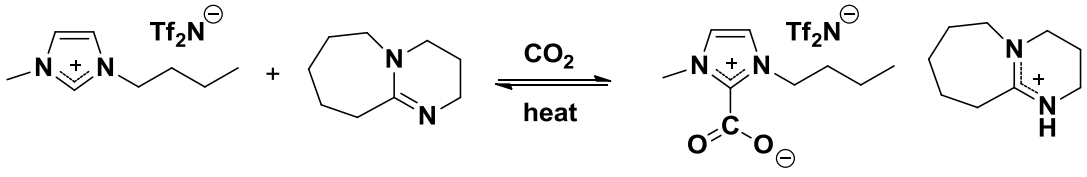

Scheme 4: Combination of [C_4mim][Tf_2N] with DBU promote chemical reaction with CO_2 at imidazolium C(2) position.

However, ILs with a "blocking" group (e.g. $-CH_3$) present at the C(2) position will not experience the reaction in Scheme 4. An alternative approach is to use DBU in combination with an IL containing a pendant hydroxyl group, where it has been shown that a carbonate mechanism is favored for reaction with CO_2 (Scheme 5).

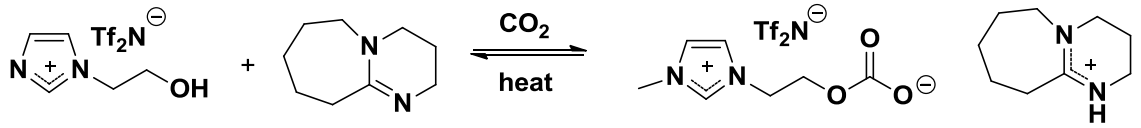

Scheme 5: Formation of carbonate between CO_2 and $[C_2OHmim][Tf_2N]$ in the presence of DBU.

CO_2-reactive, protic ILs with anions analogous to those shown in Schemes 2,3 have also been studied.[36] 7-methyl-1,5,7-triazabicyclo[4.4.0]dec-5-ene (MTBD) or 1-ethyl-2,2,4,4,4-pentakis(dimethylamino)-2λ5,4λ5-catenadi(phosphazene), also known as P_2-Et, were used as substrates in combination with several weak acids, whose conjugate anions showed strong affinities for CO_2. Many of these systems resulted in near equimolar CO_2 capacities based on the anion.[36] For the case of a diol, 2 equivalents of CO_2 could be absorbed.[36] Most systems remained as liquids after reaction with CO_2. In addition, the authors point out that these superbase-derived protic ILs have lower viscosities than amine-functionalized TSILs and ILs with amino acid-based anions.[36] Scheme 6 outlines a selected example of the formation of a superbase-derived protic IL and subsequent reaction with CO_2.

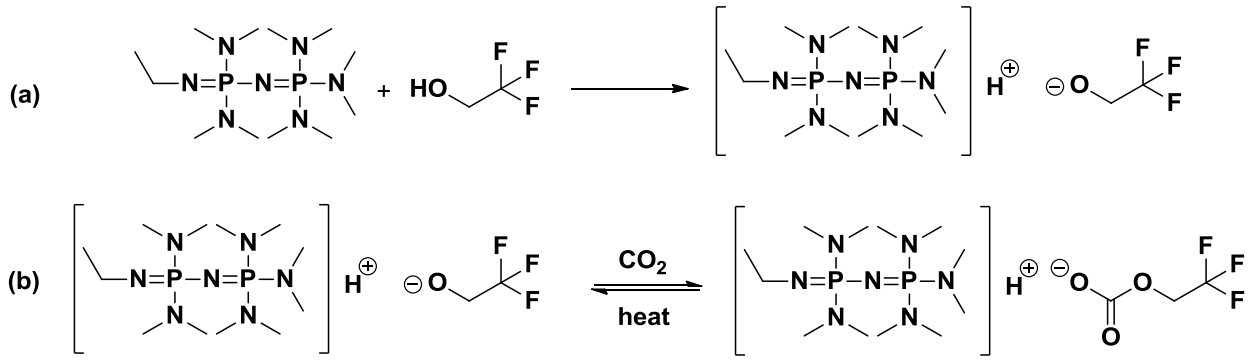

Scheme 6: (a) Formation of a superbase-derived protic IL from phosphazene (P_2-Et) and 2,2,2-trifluoroethanol and (b) reaction of anion with CO_2.

Certainly other approaches to reactive ILs for CO_2 capture will emerge in the near future. While reversible ILs can offer benefits through improving the capacity of ILs to absorb CO_2, all require that an IL first be synthesized/manufactured. For research purposes, much can be learned at the benchscale through the study of designer IL molecules in relatively small volumes (mL to L scales). However, industrial applications will require solvent volumes many orders of magnitude larger.[1] A single post-combustion CO_2 capture process designed to remove at least 90% of the CO_2 emissions from a 500 MW power plant will likely require solvent flowrates on the order of 10,000 gallons per minute (gpm).[1] Thus, selection of the lowest cost solvents with the required physical and chemical properties, as well as synthetic strategies that minimize cost of IL manufacture are highly desirable.

3.3 Reversible Ionic Liquids

An alternative approach to take advantage of the properties of ILs for CO_2 capture and acid gas removal, while perhaps reducing solvent cost, is to start with one or more neutral organic molecules that can react with acid gas in order to form an IL (or IL-like product) *in situ*. These "reversible" ILs will be presently only transiently while CO_2 or another acid gas is present, and upon regeneration, revert back to the neutral starting material(s). An advantage of this approach is that solvents can be developed directly from readily available and commodity starting materials. By tuning the chemical structures of these molecules, some degree of control may be achievable over physical (e.g. viscosity), thermodynamic (e.g. acid gas capacity and heat of absorption) and chemical (e.g. stability and selective reactivity) properties most relevant to acid gas removal processes.

3.3.1 Amines

The conventional approach to CO_2 and H_2S removal from gas streams has been the use of aqueous solutions of organic amines.[1-4] 1^o, 2^o and 3^o alkanolamines, including monoethanolamine (MEA), diethanolamine (DEA) and N-methyldiethanolamine (MDEA) are among the most widely used chemical agents.[3, 4] While water is not necessary for 1^o or 2^o amines to react with CO_2 (carbamate formation) (Scheme 7a,b) or 1^o, 2^o or 3^o amines to react with H_2S and bisulfide (HS^-) anion (an acid-base reaction) (Scheme 8), it does play an important role in the process. Primarily, water is responsible for lowering the overall viscosity of the solution, enabling maximum mass and heat transfer rates to be achieved.[3, 4] Furthermore, the relatively high heat capacity of water (4.18 J g^{-1} $^oC^{-1}$) helps limit the increase in solvent temperature as the reactions between amines and CO_2 or H_2S are exothermic.[3, 4] Lower solvent

temperatures favor increased uptake of CO_2 and H_2S, which in turn enables greater solution working capacity (i.e. the amount of CO_2 and/or H_2S captured and released per solution volume). Additionally, water can impart additional mechanisms for amine reactivity with CO_2 through the neutralization of carbonic acid (Scheme 7c).

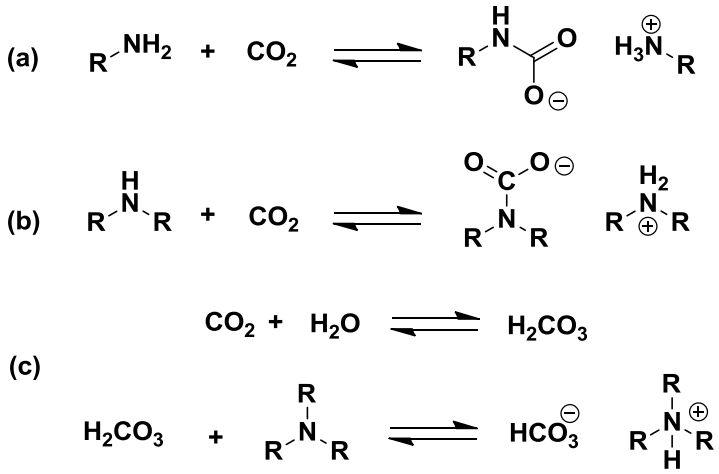

Scheme 7: Reaction of CO_2 with (a) 1° and (b) 2° amines to form carbamate ammonium salts, and (c) neutralization of carbonic acid by 3° amines.

Scheme 8: Reaction of (a) H_2S and (b) bisulfide anion with 1°, 2° or 3° amines to form ammonium salts.

Thus, while capable of reacting with acid gases without water, amines are typically not used as neat solvents for acid gas removal due to the high temperatures that would result from the exothermic reactions and the large increase in viscosity (or transition to solid or gel states) that occurs upon reaction with CO_2 or H_2S.[3, 4] While known for many years, the reactions between CO_2 or H_2S with amines in the absence of water are in fact early examples of reversible ILs.

The aforementioned issues associated with using common alkanolamines as neat solvents, in addition to problems such as corrosion and the tendency to degrade in the presence of species such as SO_2, necessitates a more targeted approach to molecular design in order to achieve reactive capture of CO_2 and/or H_2S while eliminating water from the process. Ideally, the carbamate-ammonium salt formed would

have a viscosity similar to that of CO_2-rich aqueous amine solvents (typically <20 cP or less)[23, 24] so that process equipment (e.g. absorption columns, heat exchangers, etc.) could be operated under similar conditions without loss of mass or heat transfer efficiencies.

To this goal, Eckert, Liotta and co-workers have examined 1^o trialkylsilylamines[37] and trialkoxysilylamines[38] (Figure 3.2) both of which capture low pressure CO_2 through carbamate formation via the 1:2 mechanism outlined Scheme 1a, with additional CO_2 physically absorbed at increasing pressures.[37-40]

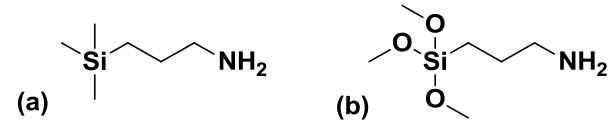

Figure 3.2: Examples of (a) trialkylsilylamines and (b) trialkoxysilylamines used for CO_2 capture.

While both classes of amines are functional for reversible complexation of CO_2, trialkylsilylamines were reported to be more stable in the presence of water.[37] The viscosities of the trialkoxysilylamines and trialkylsilylamines were reported to be < 5 cP before complexation with CO_2.[37] However, in both cases, the viscosity of the resultant reversible IL products containing CO_2 were ~1000 cP or greater, with the trialkyoxysilylamine products less viscous than the trialkylsilylamines.[37]

An alternative approach to using amines to capture CO_2, is to disallow carbamate and carbonate formation (Scheme 7) with an anhydrous 3^o alkanolamine, forcing CO_2 to react with the –OH group . Such an approach could offer much lower heat of reaction, but would require high pressures. Recently, Heldebrant and co-workers reported that anhydrous 3^o alkanolamines such as N,N-Dimethylethanolamine (DMEA), N,N-Diethylethanolamine (DEEA), N,N-Diisopropylethanolamine (DIPEA) and 2-(dimethylamino)-2-methyl-1-propanol (2-DMAM-PrOH) can form alkycarbonates in the presence of CO_2 at partial pressures > 100 psi.[41] An example of this reaction mechanism with DMEA is shown in Scheme 9.

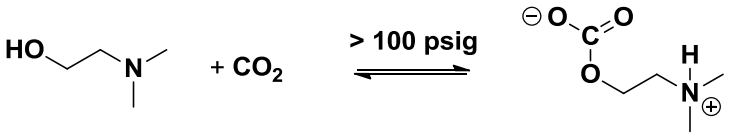

DMEA

Scheme 9: Reaction between CO_2 and anhydrous 3^o amine at elevated partial pressures to form zwitterionic ammonium alkyl carbonate.

CO_2 mass fractions as large as 0.20 were achievable at room temperature under 300 psig partial pressure. While a dry, concentrated and compressed gas stream is required for this approach to be

industrially applicable, the amine can be regenerated via pressure swings alone and without the use of thermal input, potentially creating energy savings.

This same research group has also applied anhydrous amine chemistry to both SO_2 and H_2S removal.[42, 43] Flue gas streams at coal-fired power plants often contain SO_2, which can irreversibly degrade amines such as MEA and reduce solvent capacity for CO_2, and create compounds that cause issues such as corrosion and foaming.[1] As such, CO_2 capture technologies employed at coal-fired power plants will likely rely upon advanced SO_2 control technologies or use materials that can reversibly remove SO_2 from the flue gas stream without degrading.

In the presence of, or when tethered to an alcohol, bulky 3° amines have been shown able to reversibly complex SO_2 as ammonium alkylsulfites without undergoing degradation.[42] Scheme 10 illustrates examples of the bimolecular (amine + alcohol) and unimolecular (alkanolamine) mechanisms.[42]

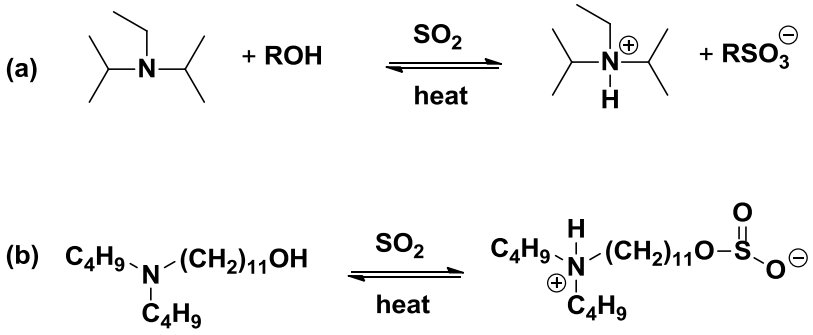

Scheme 10: Reversible formation of ammonium alkylsulfites between SO_2 and (a) amine + alcohol and (b) alkanolamine.

In natural gas processing, H_2S is often present alongside CO_2, and must be removed to very low levels (4 ppm_v), as H_2S is both corrosive to pipelines and highly toxic.[3, 4] Conventionally, aqueous 3° alkanolamines such as MDEA or sterically hindered 2° alkanolamines such as diisopropanolamine (DIPA) have been used to selectively separate H_2S from CO_2, as CO_2 is unable to form carbamates with these species (Scheme 7c), and the acid-base reactions between H_2S and amines (Scheme 8) are much faster than neutralization of carbonic acid (Scheme 7c).[3, 4] It has also recently been shown that anhydrous amines are capable of forming ammonium bisulfide salts (Scheme 11) with H_2S, and that the amine can be regenerated at ambient temperature via the introduction of a selected non-polar solvent that may be either miscible or immiscible with the amine, in a technique called “antisolvent stripping”.[43]

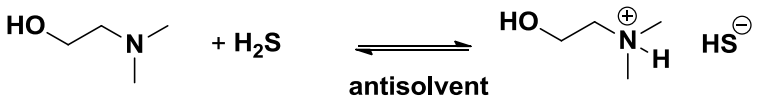

Scheme 11: Reaction of H_2S with an anhydrous 3^o amine to form ammonium bisulfide salt.

As with the CO_2-based chemistry shown in Scheme 9, this methodology will require a relatively dry stream of natural gas in order to be most efficient. As the authors point out, this technique is most applicable at CH_4 partial pressures < 500 psia, or the hydrocarbons in the stream will behave as antisolvents themselves, preventing separation of H_2S from the product gas.[43] Furthermore, given the complex and variable composition of raw natural gas streams, competition between CO_2 and H_2S within the reactions shown in Schemes 3 and 5 will certainly be of interest,[3, 4] but other species such as carbonyl sulfide (COS) and carbon disulfide (CS_2) may also play a role in determining the reaction selectivity.[3, 4]

3.3.2 Amidines & Guanidines

Amidines and guanidines are classes of strong bases, containing two or three nitrogen atoms in close proximity with one C=N double bond, and are capable of acting as H^+ acceptors. These properties enable the formation of reversible amidinium-based ILs in the presence of amines or alcohols with acid gases such as CO_2[42, 44-47] and CS_2.[48] General structures of amidines and guanidines are shown in Figure 3.3.

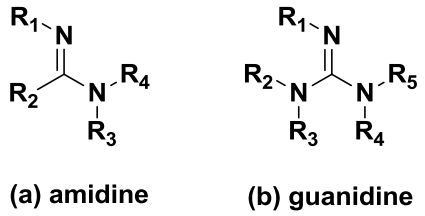

Figure 3.3: General structures of (a) amidines and (b) guanidines.

DBU was first demonstrated to promote formation of alkyl carbonates in the presence of an alcohol according to the mechanism Scheme 12.[44]

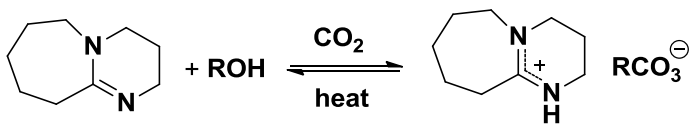

Scheme 12: Reaction between DBU and alcohols in the presence of CO_2.

An analogous reaction between a guanidine (tetramethylbutylguanidine (TMBG)) and an alcohol in the presence of CO_2 is shown in Scheme 13.[40]

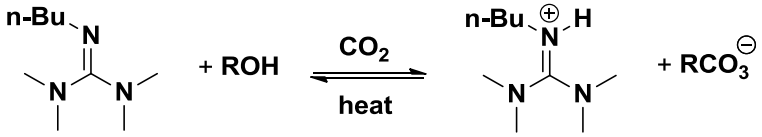

Scheme 13: Reaction of TMBG with an alcohol in the presence of CO_2.[40]

Weiss and co-workers demonstrated that 1:1 (mol:mol) mixtures of amidines and chiral alkanolamines based on amino acids could reversibly capture CO_2 as outlined in Scheme 14 for the case of N'-butyl-N,N-dimethylacetamidine and ValOH (a valine derivative).[47]

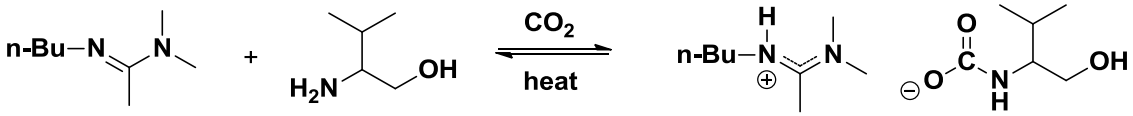

Scheme 14: Example reaction between an amidine and amino-acid derived alkanolamine in the presence of CO_2.

This research group has also applied the same general approach to the use of amidines and guanidines for CO_2 capture with amino acid esters[46] and aliphatic 1° amines[45] with similar results. While amidinium and guanidinium carbamate salts were observed to readily form with various amine species, the resultant reversible ILs decomposed rapidly at 50°C.[45-48] This temperature is near that of post-combustion flue gas streams,[1] which may present challenges for applying this approach within an industrial CO_2 capture process.

The pairing of amidines and guanidines with amines is also applicable to CS_2 removal.[48] CS_2 is often found alongside CO_2 and H_2S in raw natural gas streams.[3, 4] The combination of DBU, tetramethylguanidine (TMG) or other amidines with various amines in the presence of CS_2 results in the irreversible formation of amidiniun dithiocarbamates.[48] Scheme 15 illustrates the reaction with CS_2 for the combination of DBU and cyclohexylamine.

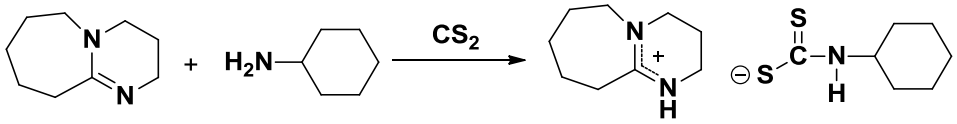

Scheme 15: Reaction between DBU and cyclohexylamine in the presence of CS_2.

In contrast to CO_2-based systems, the amidinium dithiocarbamates were more thermally stable and did not thermally revert to the neutral state (i.e. loss of CS_2), but rather underwent thermolysis at ~80°C.[48] However, CS_2 could be released upon addition of a carboxylic acid (e.g. CH_3COOH) to protonate both the amidine/guanidine and amine species.[48] While the protonated forms would then ultimately need to be neutralized to completely regenerate the solvent for CS_2 removal, this unique behavior might enable selective removal of CS_2 from CO_2 in certain natural gas processing applications.

Amidines featuring tethered hydroxyl groups could be used to capture CO_2 through a unimolecular mechanism.[42] Scheme 16 details these reactions for dihydroimidazole and DBU cores.

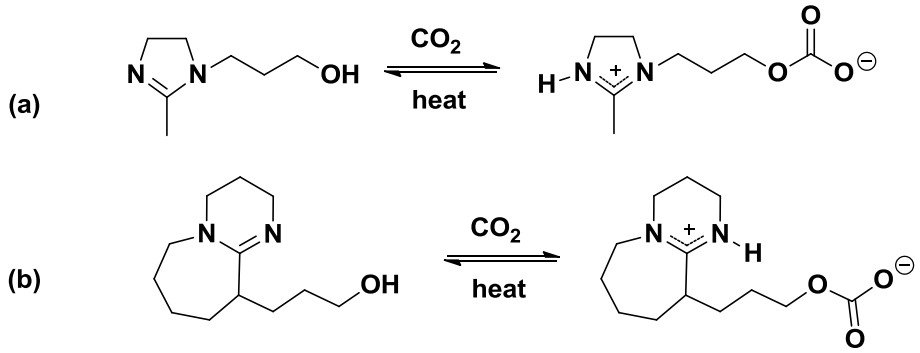

Scheme 16: Reaction with between CO_2 and (a) dihydroimidazole and (b) DBU cores tethered to hydroxyl groups.

It is clear that many options exist to develop reversible ILs from a variety of common amines, and other organic bases and heterocycles. Ideally, components of reversible ILs will have high CO_2 capacities, low volatility and low viscosity. Reversible ILs may be advantageous in that most appear to require little or no synthetic work in order to produce solvents reactive to CO_2 and other acid gases.

3.4 Can Imidazoles Be Used as a Substrate for Reversible ILs?

Although imidazoles are integral starting materials for the synthesis of imidazolium-based ILs, their utility as agents for CO_2 capture and acid gas removal applications has been virtually unexplored. Imidazoles are a highly tunable class of organic bases with respect to both physical and chemical properties. *N*-

functionalized Imidazoles (Figure 3.4) are structurally similar to the various platforms detailed here. Imidazoles are weaker bases than amines, amidines, etc.,[49] but exhibit low volatilities (T_b > 200°C), and much lower viscosities than conventional imidazolium-based ILs and reactive ILs.[25] Imidazoles feature a basic nitrogen center which is capable of acting as a base or nucleophile, and may be exploitable for reactions involving acid gases.[50] This reactive center can be key to forming reversible ILs for acid gas removal.

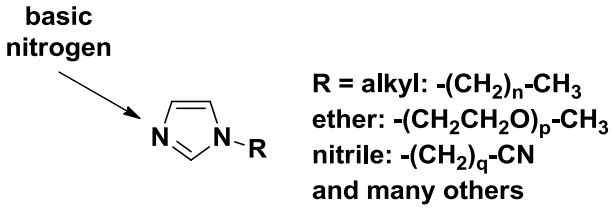

Figure 3.4: Examples of *N*-functionalized imidazoles.

3.4.1 CO_2 Capture by Imidazoles and Amines

We recently reported on the physical properties and CO_2 solubility in 1-*n*-alkylimidazoles with chain lengths ranging from methyl to tetradecyl and compared these properties to analogous imidazolium-based ILs.[25] 1-*n*-alkylimidazoles were shown to have viscosities as low as 2 cP at ambient temperature, which translates to ~1-2 orders of magnitude less than their corresponding [$C_n$mim][X] ILs.[25] We also reported that a mixture of 1-butylimidazole and MEA absorbed 145% of the theoretical CO_2 based on MEA stoichiometry, indicating a synergistic effect between imidazoles and amines for CO_2 capture.[25] A possible mechanism for this reaction is shown in Scheme 17.

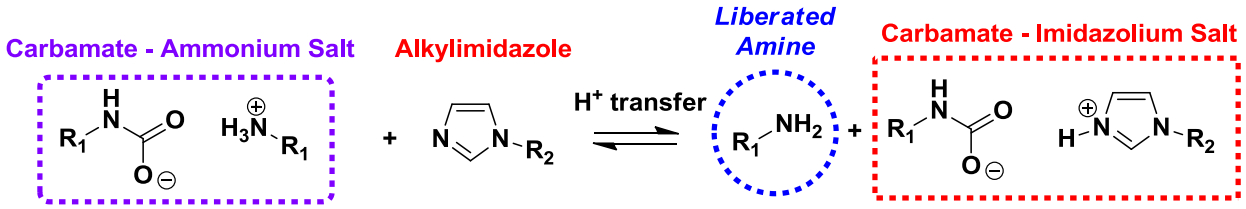

Scheme 17: Potential H^+ transfer from carbamate-ammonium salt to imidazoles in CO_2 capture reactions.[25]

While aqueous MEA is a widely used convenient baseline for assessing new CO_2 capture solvents,[1] other amines may present advantages in terms of energy input, volatility and/or stability.[2] To further examine the utility of imidazoles for CO_2 capture applications, we have applied this approach to mixtures of 1-butylimidazole with other amine-based compounds. Chemical structures of 1-butylimidazole and some amines of interest are shown in Figure 3.5. Experiments were carried out according to our previously published procedure[25] at ambient temperature (25°C) and at CO_2 partial pressures between 5-225 kPa. The

relationships between CO_2 absorbed and pressure for various 1-butylimidazole + amine combinations are presented in Figure 3.6.

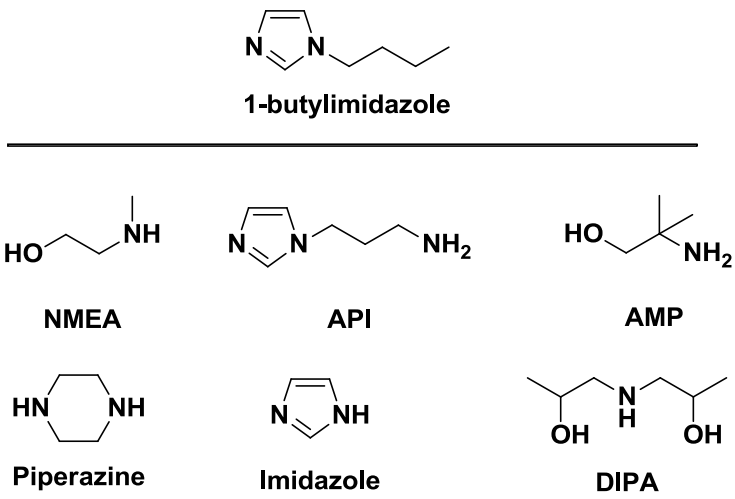

Figure 3.5: Chemical structures of 1-butylimidazole and amines used in mixtures for CO_2 capture.

With the exception of 1-buytlimidazole + imidazole, all combinations exhibited chemical reactions with CO_2 as evidenced by a sharp increase in loading of CO_2 at partial pressures ~10 kPa. In the case of piperazine, which was only sparingly soluble in 1-butylimidazole, high levels of CO_2 uptake were still achieved via rapid CO_2 reaction with the well-mixed slurry. Piperazine was nearly stoichiometrically saturated with CO_2 in a 1:1 ratio prior to any appreciable pressure measurement could be obtained from the equipment. The slope of the line presented (nearly parallel to that of the mixture containing imidazole, which experienced no chemical reaction at all) is thus indicative of CO_2 physical solubility in 1-butylimidazole, as all of the piperazine has already been reacted with CO_2.

At loadings below ~0.35 mol CO_2 / mol amine, 2-amino-2-methylpropanol (AMP) remained soluble in 1-butylimidazole and displayed a sharp increase in CO_2 absorbed at partial pressures ~10 kPa. However, above this loading, AMP-carbamate precipitated from solution and the relationship between loading and pressure became more representative of a physical solvent. Precipitation of AMP upon reaction with CO_2 is commonly observed in organic solvents where carbamate formation is favored (Scheme 7a), but not in aqueous solutions where carbonate formation is the preferred mechanism (Scheme 7c).[9]

NMEA did not precipitate from solution upon absorption of CO_2, and exhibited the most favorable loading profile. At a partial pressure of 50 kPa, the 1-butylimidazole + NMEA mixture achieved a loading of 0.75 mol CO_2 / mol NMEA. In a non-aqueous solvent containing 2^o amines, it would be expected that a level of 0.50 mol CO_2 / mol amine could be achieved, with additional physical solubility occurring at increasing

pressure. However, as we previously reported, physical solubility in the 1-butylimidazole solvent at these relatively low CO_2 partial pressures could only account for a fraction (< 20%) of the CO_2 absorbed in excess of the 0.50 mol CO_2 / mol NMEA stoichiometric chemical reaction limit. By comparison of the slope of the data for 1-butylimidazole + imidazole, it appears that the combination of 1-butylimidazole + NMEA creates a synergistic effect on CO_2 uptake.

DIPA, a bulky, hindered 2° amine also exhibited absorption behavior similar to NMEA, but with less overall loading as the amine group is less accessible to CO_2 to form the carbamate.

Interestingly, API (an amine-imidazole hybrid) achieved a loading of 0.50 mol CO_2 / mol $-NH_2$ group below 10 kPa, yet exhibited only physical solubility for CO_2 at increasing pressures. Based on possible H^+ transfer mechanism (Scheme 17), this behavior suggests that the carbamate formed between 2 molecules of API may not be accessible to 1-butylimidazole to promote levels of CO_2 uptake similar to solvents containing NMEA, or as in the case of AMP, 1° amines with bulky side groups are less likely candidates to readily achieve loadings > 0.50 per molecule of amine. With the exception of piperazine, which was a heterogeneous mixture, it appears that small alkanolamines, such as NMEA and MEA, can achieve the greatest CO_2 uptake in imidazole-based solvents.

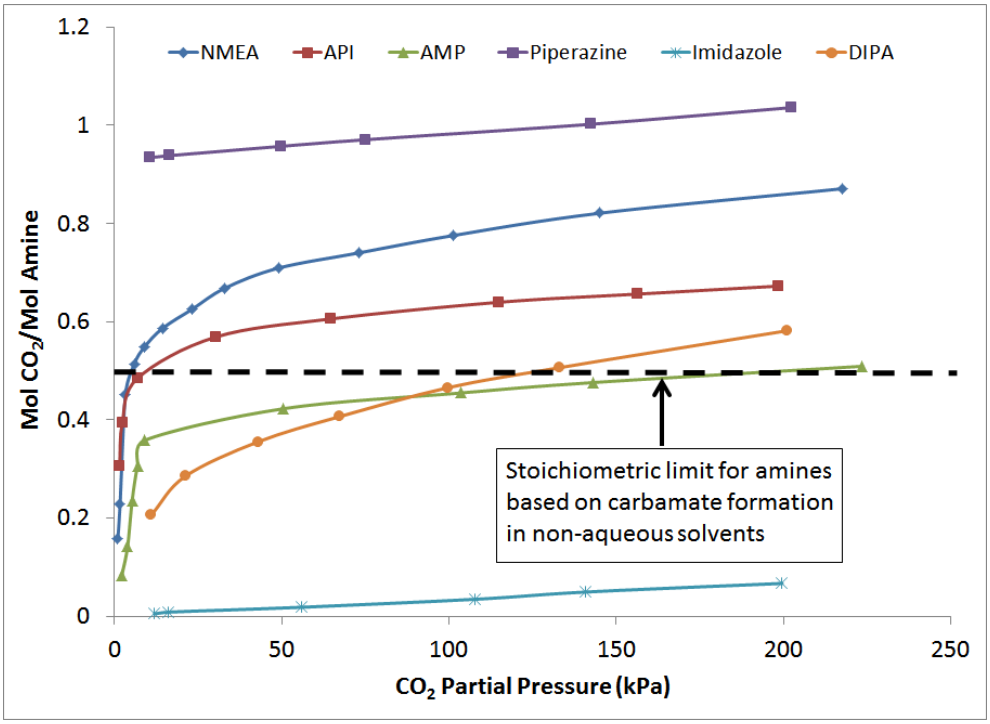

Figure 3.6: Relationship between CO_2 partial pressure and loading per initial amine molecule in 80:20 (vol:vol) 1-butylimidazole-amine mixtures at 25°C.

For NMEA, API, and DIPA viscosities of the CO_2-rich mixtures at the maximum CO_2 loading were measured immediately after the experiments were completed in compliance with our previously detailed procedures.[25] The results are summarized in Table 3.1. Interestingly, all of the CO_2-rich solvents had viscosities in the range of 30-40 cP, which represents an 8-10x increase from the viscosity of neat 1-butylimidazole at 25°C.[25] The 1-butylimidazole + NMEA viscosity in the highly CO_2-rich state was only ~1/3 that of a mixture containing 1-butylimidazole + MEA at a similar loading.[25] It is also worth noting that although viscosity increases with CO_2 absorption, the values observed are still less than most conventional ILs which cannot achieve high levels of CO_2 loading under these partial pressures and other reactive & reversible ILs.[10, 16, 26] Additionally, this viscosity range is approaching that of some aqueous amine solvents proposed for post-combustion CO_2 capture applications as well as solutions already commercially applied in the natural gas industry.[2-4, 8, 23, 24] Initial results in our lab indicate that further reductions in viscosity can be achieved with *N*-functionalized imidazoles with shorten pendant alkyl chains (e.g. 1-methylimidazole, 1,2-dimethylimidazole, etc.).

Table 3.1: Viscosity data for 1-butylimidazole + amine solvents in their final CO_2-rich states at 25°C.

Compound	*Type*	*Viscosity (cP) of CO_2-rich Solution (25 °C)*
N-methylethanolamine (NMEA)	2° alkanolamine	*28-31*
1-(3-aminopropyl)-imidazole (API)	Imidazole - 1° amine hybrid	*41*
Diisopropanolamine (DIPA)	Hindered 2° alkanolamine	*27-32*

Based on the performance of the 1-butylimidazole + NMEA mixture at ambient temperature, we sought to characterize the temperature dependence of loading in order to generate baseline data for both absorption and desorption in imidazole + amine mixtures. Figure 3.7 presents these data across the range of 25-80°C at pressures > 10 kPa. For typical flue gas conditions (40°C, 2 psia CO_2), the 1-butylimidazole + NMEA solvent achieves loadings approaching 0.50 mol CO_2 / mol amine. As can be seen in Figure 3.7, CO_2 solubility decreases with increasing temperature for a given pressure, which is typical characteristic of amine solutions.[7] The 1-butylimidazole + NMEA mixture exhibits a working capacity of ~0.40 mol CO_2 / mol NMEA at a constant pressure when the temperature is increased from 40°C to 80°C. These data, combined with the relatively low viscosity in the CO_2-rich state, indicate that imidazole + amine solvents are capable of both the capture and release of CO_2 within a conventional absorber-stripper process.

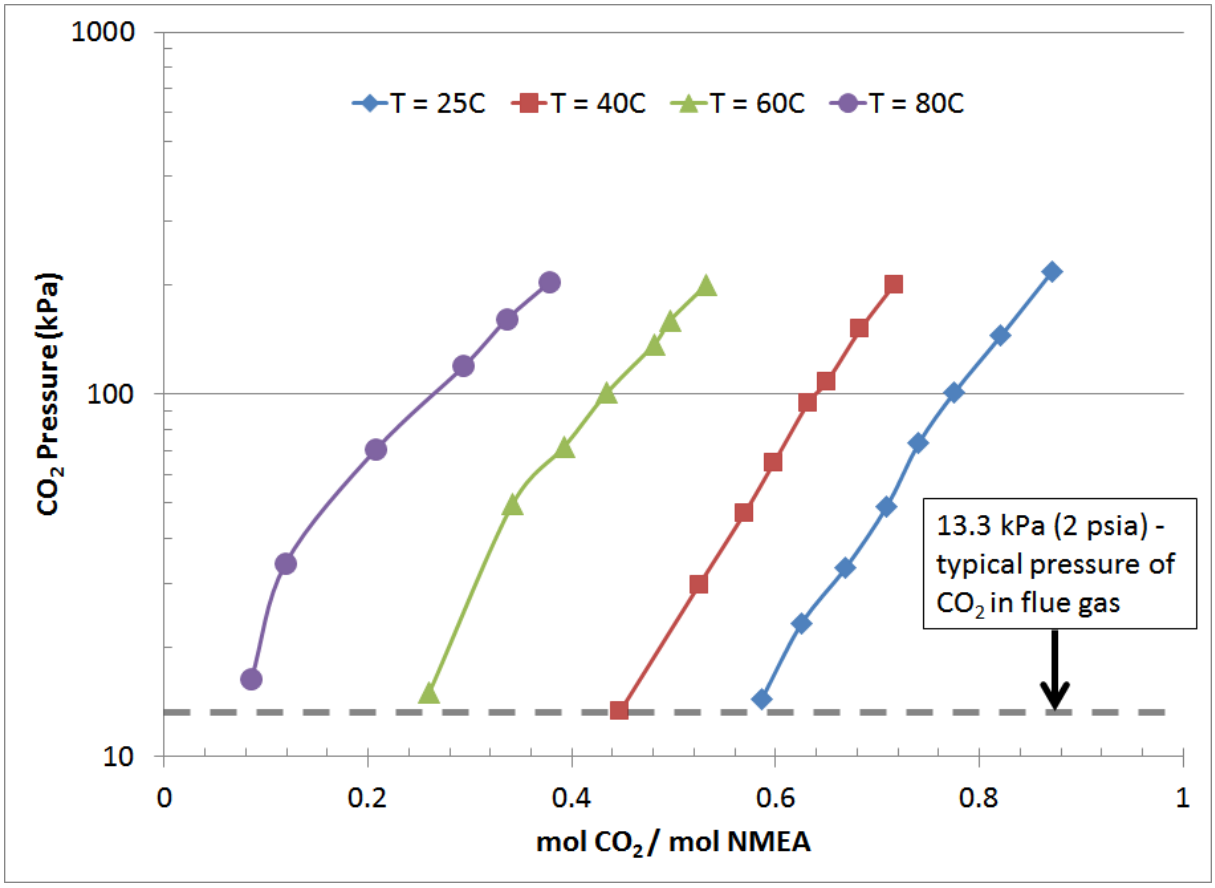

Figure 3.7: Relationship between CO_2 partial pressure and loading in 80:20 (vol:vol) 1-buytlimidazole + NMEA mixtures at temperatures between 25-80°C.

As a wide variety of imidazole and amine derivatives might be used in various concentrations to formulate solvent mixtures CO_2 capture, this particular combination of 1-butylimidazole + NMEA (80:20 vol:vol) is only a representative example. Both the structures of the imidazole and amine components are likely to influence both physical and chemical properties of the resultant solvent mixture.

3.4.2 Imidazoles as Agents for SO_2 Removal

While amines are necessary for imidazoles to participate in the CO_2 capture reactions in a non-aqueous environment,[25] we have also recently explored the use of alkylimidazoles to reversibly absorb SO_2 via both physical and chemical interactions. This feature presents interesting possibilities as alkylimidazoles could be used as both a chemical and physical solvent to recover SO_2 from flue gas.

To demonstrate absorption of SO_2 in an alkylimidazole solvent, a straightforward experiment was carried out in a well-ventilated fume hood. A handheld SO_2 sensor was also employed to ensure

exposure of personnel to SO_2 was minimized. 1-hexylimidazole (5.00 g, 32.8 mmol) was stirred in a 50 mL round bottom flask contained within a room-temperature water bath. Low pressure SO_2 (~1 psig) was bubbled into the solvent, and the total solution volume was observed to expand rapidly with a single liquid phase present. After 5 minutes exposure to the bubbling SO_2 stream, the mass of the flask contents was observed to increase by 2.46 g, indicating that 38.4 mmol or 1.17 mol SO_2 / mol 1-hexylimidazole were present in the flask. After the flow of the SO_2 stream ceased, the contents of the flask were swept with a stream of N_2 for several hours at room temperature. After this time, the liquid phase had transformed to a transparent, viscous gel, containing ~0.5 mol SO_2 / mol 1-hexylimidazole as determined by the residual mass of the flask contents. The SO_2 lost is likely the portion that was physically dissolved, thus indicating that SO_2 reacts with alkylimidazoles in a 1:2 ratio (Scheme 18). The chemically-bound SO_2 could be released by heating the sample at >100°C while under N_2 sweep. No irreversible degradation of the 1-hexylimidazole was observed via ^{1}H NMR.

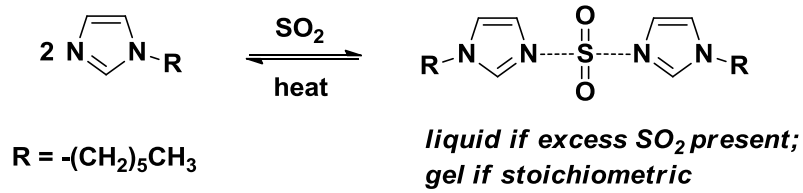

Scheme 18: Reaction of SO_2 with 2 equivalents of 1-hexylimidazole.

While 1-hexylimidazole was chosen for convenience of its very low volatility, this reaction could have been carried out with any alkylimidazole compound. Thus it is likely that the properties of the reaction product (i.e. viscosity and solid/liquid/gel state) between SO_2 and imidazoles will likely depend on the length of the alkyl chain ('R' in Scheme 18) as well as any additional functionalization at the C(2), C(4) and/or C(5) positions. Functionalization of the carbon positions may also provide opportunities to tune the equilibrium of the chemical reaction or control desorption temperature.

As with the 1-butylimidazole + NMEA mixture for CO_2 capture, the example of 1-hexylimidazole is not optimized. However, *N*-functionalized imidazoles may present new opportunities for reversible SO_2 capture from flue gas in the electric power industry. Reversible SO_2 capture is of interest as current "scrubbing" technologies most often rely on the reaction of SO_2 + CaSO3 → $CaSO_3$, with $CaSO_3$ then oxidized to $CaSO_4$ and commonly sold for use as drywall. Direct recovery of SO_2 could eliminate process engineering

issues with the handling of solids in flue gas desulfurization, while simultaneously allowing for the production of higher value sulfur products such as H_2SO_4.

Additional opportunities may exist in applying imidazoles for H_2S removal through an acid-base reaction similar to that exhibited by anhydrous amines. As the pK_a of the first proton dissociation for H_2S is ~7.0, 1,2-dialkylimidazoles and 1,2,4-triaklyimidazoles certainly appear to be capable of near quantitative deprotonation of H_2S to form an imidazolium bisulfide salt (Scheme 19), similar to the mechanism described for anhydrous 3° amines (Scheme 11).

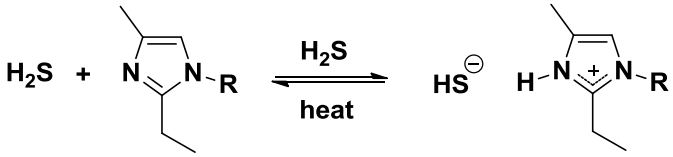

Scheme 19: Potential formation of imidazolium bisfulfide salts as reversible ILs.

3.5 Conclusions & Outlook

Reactive and reversible ILs have evolved from conventional ILs in CO_2 capture and other acid gas removal applications. Although amine-functionalized ILs with intrinsic chemical affinity to CO_2 have been known for nearly a decade,[19] recent development of new reactive ILs from amino acids, superbases and aprotic heterocyclic anions provide more straightforward synthesis options with a wider array of possible chemistries and improved physical properties. Reversible ILs are an alternative, highly promising approach, in that they also exhibit tunable properties and chemistries, but do not require that an IL be synthesized. The use of "off-the-shelf" chemistry can help reduce the cost of advanced solvents for CO_2 capture.

We have also reported that imidazoles can be used in combination with various amines for CO_2 capture, and can also complex directly with SO_2, without the need for a co-solvent. As imidazoles have low volatilities, low viscosities and tunable chemistries, we will continue to pursue them as solvents for CO_2 capture and acid gas removal.

The viability of IL-based or other alternative solvents to industrial gas processing applications such as CO_2 capture or natural gas sweetening will depend on the compatibility of the solvent with chemical engineering process technologies. As researchers continue to demonstrate that there are a seemingly infinite number of solvents that can be developed to capture CO_2, focus is needed on identifying solvents with physical properties that are good matches for conventional chemical engineering unit operations. Specifically, viscosity (in both the CO_2-lean and CO_2-rich states) is almost certain to be one of the most

important factors of solvent success. Low viscosity solvents will provide more rapid mass transfer rates, which in turn will allow for lower solvent circulation rates, which enables a smaller process footprint, which is one of a major driver of process cost.

Emphasis should also be placed on maximizing CO_2 capacity per mass or volume of solvent. Solvents with very large molecular weights that capture CO_2 in a 1:1 mechanism will ultimately be at a disadvantage when compared to conventional solvents that absorb CO_2 via a 1:2 mechanism.

Finally, water will be an inevitable part of any post-combustion CO_2 capture process and will also likely be present in most raw natural gas streams. While much can be learned through research under relatively dry or anhydrous conditions, researchers must give more focus on the anticipated effects of water on solvent performance, as dehydrating gas streams for CO_2 capture will likely be impractical and uneconomical.

Acknowledgment

Partial support for this work provided by ION Engineering, LLC and The United States Department of Energy – National Energy Technology Laboratory (DE-FE00005799) is gratefully acknowledged. Additional support from the University of Alabama Research Grants Committee is also gratefully acknowledged.

3.6 References

1. NETL DOE/NETL Advanced Carbon Dioxide Capture R&D Program: Technology Update 9/2010. www.netl.doe.gov/technologies/coalpower/ewr/pubs/CO2%20Capture%20Tech%20Update%20Final.pdf (Accessed 14 June 2011)

2. Rochelle, G. T. Amine Scrubbing for CO_2 Capture. *Science* 2009, 325, 1652-1654.

3. Astarita, G.; Savage, D. W.; Bisio, A. *Gas Treating with Chemical Solvents*. John Wiley & Sons: New York, 1983.

4. Kidnay, A. J.; Parrish, W. R. *Fundamentals of Natural Gas Processing*. CRC Press: Taylor & Francis Group: Boca Raton, FL, 2006.

5. Jou, F. Y.; Mather, A. E.; Otto, F. D. The solubility of CO_2 in a 30-Mass-Percent Monoethanolamine Solution. *Can J. Chem. Eng.* 1995, *73*, 140-147.

6. Teng, T. T.; Maham, Y.; Hepler, L. G.; Mather, A. E. Viscosity of Aqueous-solutions of N-Methyldiethanolamine and of Diethanolamine. *J. Chem. Eng. Data* 1994, *39*, 290-293.

7. Vrachnos, A.; Kontogeorgis, G.; Voutsas, E. Thermodynamic modeling of acidic gas solubility in aqueous solutions of MEA, MDEA and MEA-MDEA blends. *Ind. Eng. Chem. Res.* 2006, *45*, 5148-5154.

8. Weiland, R. H.; Dingman, J. C.; Cronin, D. B.; Browning, G. J. Density and viscosity of some partially carbonated aqueous alkanolamine solutions and their blends. *J. Chem. Eng. Data* 1998, *43*, 378-382.

9. Xu, S.; Wang, Y.-W.; Otto, F. D.; Mather, A. E. Kinetics of the reaction of carbon dioxide with 2-amino-2-methyl-1-propanol solutions. *Chem. Eng. Sci.* 1996, *51*, 841-850.

10. Bara, J. E.; Carlisle, T. K.; Gabriel, C. J.; Camper, D.; Finotello, A.; Gin, D. L.; Noble, R. D. Guide to CO_2 Separations in Imidazolium-Based Room-Temperature Ionic Liquids. *Ind. Eng. Chem. Res.* 2009, *48*, 2739-2751.

11. Anderson, J. L.; Dixon, J. K.; Maginn, E. J.; Brennecke, J. F. Measurement of SO_2 solubility in ionic liquids. *J. Phys. Chem. B* 2006, *110*, 15059-15062.

12. Shiflett, M. B.; Drew, D. W.; Cantini, R. A.; Yokozeki, A. Carbon Dioxide Capture Using Ionic Liquid 1-Butyl-3-methylimidazolium Acetate. *Energy Fuels* 2010, *24*, 5781-5789.

13. Shiflett, M. B.; Yokozeki, A. Chemical Absorption of Sulfur Dioxide in Room-Temperature Ionic Liquids. *Ind. Eng. Chem. Res.* 2010, *49*, 1370-1377.

14. Karadas, F.; Atilhan, M.; Aparicio, S. Review on the Use of Ionic Liquids (ILs) as Alternative Fluids for CO_2 Capture and Natural Gas Sweetening. *Energy Fuels* 2010, *24*, 5817-5828.

15. Holbrey, J. D.; Rogers, R. D.; Mantz, R. A.; Trulove, P. C.; Cocalia, V. A.; Visser, A. E.; Anderson, J. L.; Anthony, J. L.; Brennecke, J. F.; Maginn, E. J.; Welton, T. Physicochemical Properties. In *Ionic Liquids in Synthesis*, 2nd ed.; Wasserscheid, P.; Welton, T., Eds. Wiley-VCH: Weinheim, Germany, 2008.

16. Gardas, R. L.; Coutinho, J. A. P., A group contribution method for viscosity estimation of ionic liquids. *Fluid Phase Equilibr.* 2008, *266*, 195-201.

17. Camper, D.; Bara, J. E.; Gin, D. L.; Noble, R. D. Room-Temperature Ionic Liquid-Amine Solutions: Tunable Solvents for Efficient and Reversible Capture Of CO_2. *Ind. Eng. Chem. Res.* 2008, *47*, 8496-8498.

18. Bara, J. E.; Camper, D. E.; Gin, D. L.; Noble, R. D. Room-Temperature Ionic Liquids and Composite Materials: Platform Technologies for CO_2 Capture. *Acc. Chem. Res.* 2010, *43*, 152-159.

19. Bates, E. D.; Mayton, R. D.; Ntai, I.; Davis, J. H. CO_2 capture by a task-specific ionic liquid. *J. Am. Chem. Soc.* 2002, *124*, 926-927.

20. Gutowski, K. E.; Maginn, E. J. Amine-Functionalized Task-Specific Ionic Liquids: A Mechanistic Explanation for the Dramatic Increase in Viscosity upon Complexation with CO_2 from Molecular Simulation. *J. Am. Chem. Soc.* 2008, *130*, 14690-14704.

21. Shiflett, M. B.; Kasprzak, D. J.; Junk, C. P.; Yokozeki, A. Phase behavior of {carbon dioxide plus bmim Ac } mixtures. *J. Chem. Thermodyn.* 2008, *40*, 25-31.

22. Carvalho, P. J.; Alvarez, V. H.; Schroder, B.; Gil, A. M.; Marrucho, I. M.; Aznar, M.; Santos, L.; Coutinho, J. A. P. Specific Solvation Interactions of CO_2 on Acetate and Trifluoroacetate Imidazolium Based Ionic Liquids at High Pressures. *J. Phys. Chem. B* 2009, *113*, 6803-6812.

23. Zhou, S.; Chen, X.; Nguyen, T.; Voice, A. K.; Rochelle, G. T. Aqueous Ethylenediamine for CO_2 Capture. *Chemsuschem* 2010, *3*, 913-918.

24. Freeman, S. A.; Dugas, R.; Van Wagener, D. H.; Nguyen, T.; Rochelle, G. T. Carbon dioxide capture with concentrated, aqueous piperazine. *Int. J. Greenh. Gas Con.* 2010, *4*, 119-124.

25. Shannon, M. S.; Bara, J. E. Properties of Alkylimidazoles as Solvents for CO_2 Capture and Comparisons to Imidazolium-based Ionic Liquids. *Ind. Eng. Chem. Res.* 2011, *50*, 8665-8677.

26. NIST, Ionic Liquids Database (ILThermo) - NIST Standard Reference Database #147. http://ilthermo.boulder.nist.gov/ILThermo/mainmenu.uix (Accessed 14 June 2011)

27. McCabe, W. L.; Smith, J. C.; Harriott, P. *Unit Operations of Chemical Engineering*. 6th ed.; McGraw-Hill: New York, 2001.

28. Ohno, H.; Fukumoto, K. Amino acid ionic liquids. *Acc. Chem. Res.* 2007, *40*, 1122-1129.

29. Fukumoto, K.; Yoshizawa, M.; Ohno, H. Room Temperature Ionic Liquids from 20 Natural Amino Acids. *J. Am. Chem. Soc.* 2005, *127*, 2398-2399.

30. Gurkan, B. E.; de la Fuente, J. C.; Mindrup, E. M.; Ficke, L. E.; Goodrich, B. F.; Price, E. A.; Schneider, W. F.; Brennecke, J. F. Equimolar CO_2 Absorption by Anion-Functionalized Ionic Liquids. *J. Am. Chem. Soc.* 2010, 132, 2116-2117.

31. Goodrich, B. F.; de la Fuente, J. C.; Gurkan, B. E.; Zadigian, D. J.; Price, E. A.; Huang, Y.; Brennecke, J. F. Experimental Measurements of Amine-Functionalized Anion-Tethered Ionic Liquids with Carbon Dioxide. *Ind. Eng. Chem. Res.* 2010, *50*, 111-118.

32. Wang, C. M.; Luo, X. Y.; Luo, H. M.; Jiang, D. E.; Li, H. R.; Dai, S., Tuning the Basicity of Ionic Liquids for Equimolar CO_2 Capture. *Angew. Chem. Int. Edit.* 2011, *50*, 4918-4922.

33. Gurkan, B.; Goodrich, B. F.; Mindrup, E. M.; Ficke, L. E.; Massel, M.; Seo, S.; Senftle, T. P.; Wu, H.; Glaser, M. F.; Shah, J. K.; Maginn, E. J.; Brennecke, J. F.; Schneider, W. F. Molecular Design of High Capacity, Low Viscosity, Chemically Tunable Ionic Liquids for CO_2 Capture. *J. Phys. Chem. Lett.* 2010, *1*, 3494-3499.

34. McGuinness, D. S.; Cavell, K. J.; Yates, B. F.; Skelton, B. W.; White, A. H. Oxidative Addition of the Imidazolium Cation to Zerovalent Ni, Pd, and Pt: A Combined Density Functional and Experimental Study. *J. Am. Chem. Soc.* 2001, *123*, 8317-8328.

35. Wang, C.; Luo, H.; Luo, X.; Li, H.; Dai, S. Equimolar CO_2 capture by imidazolium-based ionic liquids and superbase systems. *Green Chem.* 2010, *12*, 2019-2023.

36. Wang, C. M.; Luo, H. M.; Jiang, D. E.; Li, H. R.; Dai, S. Carbon Dioxide Capture by Superbase-Derived Protic Ionic Liquids. *Angew. Chem. Int. Edit.* 2010, *49*, 5978-5981.

37. Blasucci, V.; Hart, R.; Mestre, V. L.; Hahne, D. J.; Burlager, M.; Huttenhower, H.; Thio, B. J. R.; Pollet, P.; Liotta, C. L.; Eckert, C. A. Single component, reversible ionic liquids for energy applications. *Fuel* 2010, *89*, 1315-1319.

38. Blasucci, V.; Dilek, C.; Huttenhower, H.; John, E.; Llopis-Mestre, V.; Pollet, P.; Eckert, C. A.; Liotta, C. L. One-component, switchable ionic liquids derived from siloxylated amines. *Chem. Commun.* 2009, 116-118.

39. Blasucci, V. M.; Hart, R.; Pollet, P.; Liotta, C. L.; Eckert, C. A. Reversible ionic liquids designed for facile separations. *Fluid Phase Equilibr.* 2010, *294*, 1-6.

40. Hart, R.; Pollet, P.; Hahne, D. J.; John, E.; Llopis-Mestre, V.; Blasucci, V.; Huttenhower, H.; Leitner, W.; Eckert, C. A.; Liotta, C. L. Benign coupling of reactions and separations with reversible ionic liquids. *Tetrahedron* 2010, *66*, 1082-1090.

41. Rainbolt, J. E.; Koech, P. K.; Yonker, C. R.; Zheng, F.; Main, D.; Weaver, M. L.; Linehan, J. C.; Heldebrant, D. J., Anhydrous tertiary alkanolamines as hybrid chemical and physical CO_2 capture reagents with pressure-swing regeneration. *Energ. Environ. Sci.* 2011, *4*, 480-484.

42. Heldebrant, D. J.; Koech, P. K.; Rainbolt, J. E.; Zheng, F. CO_2 -binding organic liquids, an integrated acid gas capture system. *Energy Procedia* 2011, *4*, 216-223.

43. Koech, P. K.; Rainbolt, J. E.; Bearden, M. D.; Zheng, F.; Heldebrant, D. J. Chemically selective gas sweetening without thermal-swing regeneration. *Energ. Environ. Sci.* 2011, *4*, 1385-1390.

44. Jessop, P. G.; Heldebrant, D. J.; Li, X.; Eckert, C. A.; Liotta, C. L. Green chemistry: Reversible nonpolar-to-polar solvent. *Nature* 2005, *436*, 1102.

45. Yamada, T.; Lukac, P. J.; George, M.; Weiss, R. G. Reversible, Room-Temperature Ionic Liquids. Amidinium Carbamates Derived from Amidines and Aliphatic Primary Amines with Carbon Dioxide. *Chem. Mater.* 2007, *19*, 967-969.

46. Yamada, T.; Lukac, P. J.; Yu, T.; Weiss, R. G. Reversible, Room-Temperature, Chiral Ionic Liquids. Amidinium Carbamates Derived from Amidines and Amino-Acid Esters with Carbon Dioxide. *Chem. Mater.* 2007, *19*, 4761-4768.

47. Yu, T.; Yamada, T.; Gaviola, G. C.; Weiss, R. G. Carbon Dioxide and Molecular Nitrogen as Switches between Ionic and Uncharged Room-Temperature Liquids Comprised of Amidines and Chiral Amino Alcohols. *Chem. Mater.* 2008, *20*, 5337-5344.

48. Yu, T.; Yamada, T.; Weiss, R. G. In situ Formation of Thermally Stable, Room-Temperature Ionic Liquids from CS_2 and Amidine/Amine Mixtures. *Chem. Mater.* 2010, *22*, 5492-5499.

49. Lenarcik, B.; Ojczenasz, P. The influence of the size and position of the alkyl groups in alkylimidazole molecules on their acid-base properties. *J. Heterocyclic Chem.* 2002, *39*, 287-290.

50. Palleros, D. Heterocycles. www.chemistry.ucsc.edu/courses/palleros/Heterocycles.pdf (Accessed 31 May 2011)

CHAPTER FOUR

[†]Evaluation of Alkylimidazoles as Physical Solvents for CO_2/CH_4 Separation

Matthew S. Shannon, Jason M. Tedstone, Scott P. O. Danielsen & Jason E. Bara*

Department of Chemical & Biological Engineering

The University of Alabama, Tuscaloosa AL USA 35487-0203

Abstract

1-*n*-alkylimidazoles are a class of tunable solvents with low volatility and low viscosities. Although imidazoles have been known for some time in the pharmaceutical industry, and as convenient precursors for synthesizing imidazolium-based ionic liquids (ILs), only recently have they been given consideration in some of the same solvent-based separations applications that ILs have been studied for, such as post-combustion CO_2 capture and natural gas treating. "Sweetening", the removal of CO_2, H_2S and other "acid" gases from natural gas (CH_4), is an existing industrial application where low volatility, low viscosity physical solvents are already applied successfully and economically at large scale. Physical solvents are also used for syngas clean-up and are in the emerging application of pre-combustion CO_2 capture. Given the similarities in physical properties between 1-*n*-alkylimidazoles, and physical solvents currently used in industrial gas treating, the 1-*n*-alkylimidazole class of solvents warrants further investigation.

Solubilities of CO_2 and CH_4 in a series of 1-*n*-alkylimidazoles were measured under conditions relevant to the use of physical solvents for natural gas treating: ~5 atm partial pressure of CO_2 and temperatures of 30-75^{o}C. Solubility of CO_2 and CH_4 were found to be strongly dependent on temperature, with solubility of each gas in all solvents diminishing with increasing temperature, although the CO_2 exhibited a stronger temperature dependence than CH_4. Ideal CO_2/CH_4 solubility selectivities were also more favorable at lower temperatures in 1-*n*-alkylimidazole solvents with shorter chain lengths. CO_2 solubility decreased with increasing chain length, while CH_4 solubility exhibited a maximum in 1-hexylimidazole. The observed solubility trends observed with temperature and chain length can be explained through calculation of solution enthalpies and solvent fractional free volume as approximated from van der Waals' volumes as calculated via atomic contributions. Of the solvents examined, 1-methylimidazole displays the most favorable CO_2 solubility, CO_2/CH_4 selectivity, and has the lowest viscosity. A comparison of 1-methylimidazole to commercially used solvents reveals similar physical properties and the potential for use in industrial gas processing. Imidazolium-based ILs are also compared, although appear less favorable for use within established process schemes given their higher viscosities and reduced capacity for CO_2.

Keywords

Natural gas sweetening, imidazole compounds, carbon capture, ionic liquids, carbon dioxide (CO_2) and hydrogen sulfide (H_2S)

[†]*Industrial & Engineering Chemistry Research, 2012, 51, 515-522*.

4.1. Introduction: Physical (i.e. non-chemically reacting) solvents are used industrially for the removal of CO_2, H_2S and other contaminants from natural gas (CH_4) in "sweetening" processes.[1, 2] The use of physical solvents is advantageous for bulk removal of CO_2 when the partial pressure(s) and concentration(s) of the acid gas(es) are high.[1, 2] Physical solvent processes are economically favorable under these conditions as high acid gas loadings in the solvent can be achieved in the absorber while regeneration is much less energy intensive than for chemical (reactive) solvents (i.e. aqueous amines).[1, 2] Selexol® and Rectisol® are examples of commercial processes that utilize physical solvents composed of dimethyl ethers of poly(ethylene glycol) (DMPEG) and chilled MeOH, respectively.[3, 4] Physical solvent processes can also be run to selectively recover separate H_2S and CO_2 streams when both gases are present, so as to convert H_2S to elemental sulfur via the Claus Process,[1, 2] and then compress a relatively pure CO_2 stream for applications such as enhanced oil recovery (EOR) or geologic sequestration.[5] Physical solvents are also used for pre-combustion CO_2 capture in the integrated gasification combined cycled (IGCC) process and syngas clean-up (CO_2/H_2 separation).[5, 6] Figure 4.1 presents useful guidelines for selecting the appropriate solvent type based on feed conditions and requisite product purity.[2, 7] As a point of reference, process conditions for post-combustion CO_2 capture[6, 8] have been appended to the lower left corner of the chart.

Recently, ionic liquids (ILs) have emerged as a new class of physical solvents that may have utility for the separation of CO_2 from CH_4 in natural gas sweetening,[9, 10] as certain ILs have been shown exhibit selectivities for CO_2/CH_4 that rank among the most selective organic solvents.[9, 11] Furthermore, additional applications involving the removal of H_2S may also be applicable to the use of IL solvents.[6, 12-15] Solubilities of CO_2 and CH_4, and CO_2/CH_4 selectivity have been shown to be controlled by the chemical structure of the IL cation and anion,[9, 11, 16-19] as well as temperature.[20] Although ILs typically exhibit ~10x higher viscosities[21, 22] and ~60% of the CO_2 capacity of MeOH and other organic solvents,[3, 4, 9, 23, 24] ILs appear similar to the DMPEG molecules (e.g. tetraethylene glycol dimethyl ether and larger oligomers), as both lack an appreciable vapor pressure,[3, 4, 25] which helps to minimize solvent regeneration energy and eliminate fugitive losses due to evaporation.[3, 4, 9]

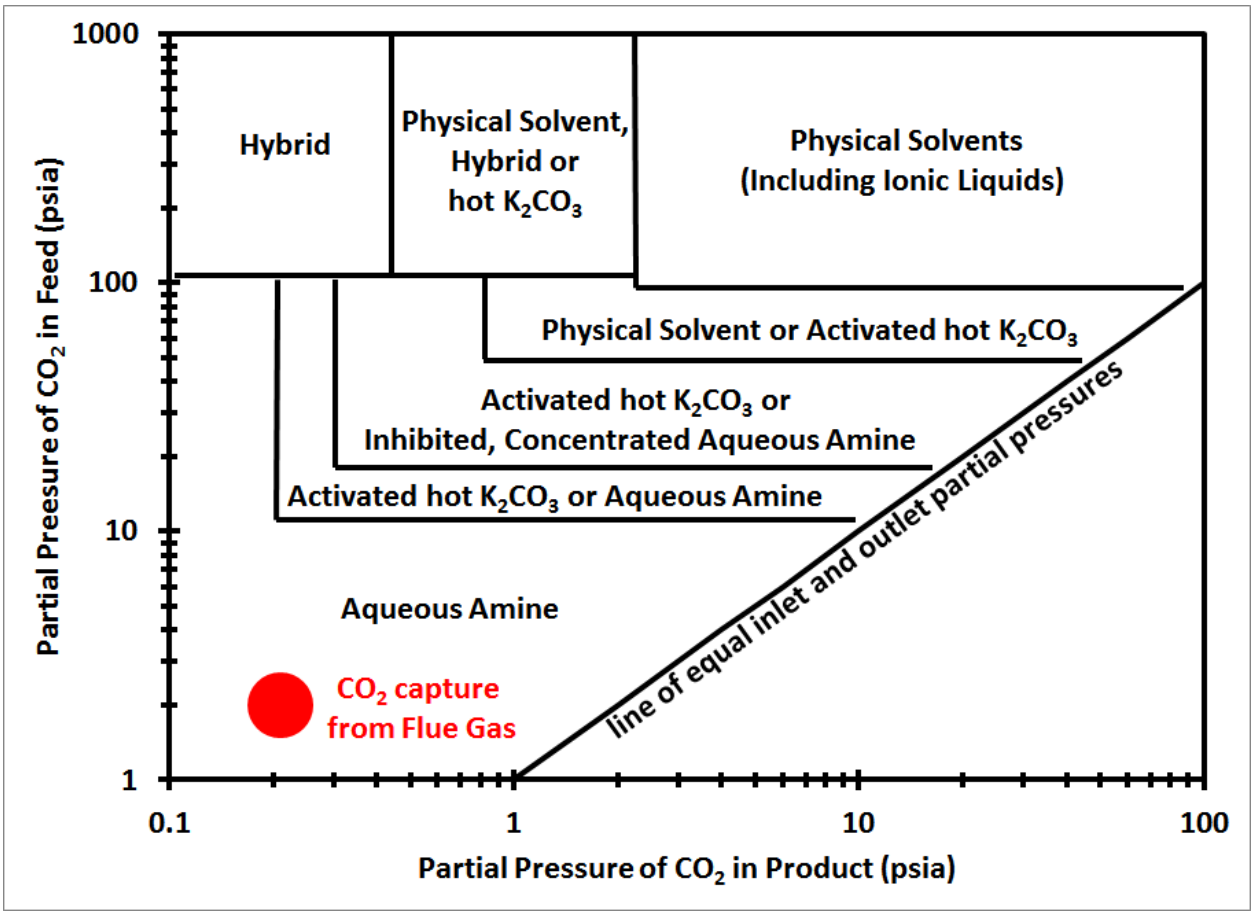

Figure 4.1: Process selection guidelines for the removal of CO_2 from CH_4 using absorptive (solvent-based) processes. Adapted from References 2 & 7.

While imidazolium-based ILs (Figure 4.2a) have been at forefront of research into new solvents for gas processing,[9, 10] little attention has been given to the *N*-functionalized imidazoles (Figure 4.2b) from which they are typically produced, even though 1-methylimidazole and others are readily available and at lower cost than ILs. Recently, we examined the properties of the 1-*n*-alkylimidazole series with chain lengths ranging from methyl (C_1) to tetradecyl (C_{14}).[21] At 25°C, 1-*n*-alkylimidazoles were found to be ~90% less viscous than their 1-*n*-alkyl-3-methylimidazolium-based IL analogues,[21] while CO_2 exhibited greater levels of physical solubility in 1-*n*-alkylimidazoles than in imidazolium-based ILs.[21, 26] Other recent work on 1-*n*-alkylimidazoles has confirmed that they are relatively non-volatile solvents, exhibiting vapor pressures < 1 torr and heats of vaporization (ΔH_{vap}) > 55 kJ/mol at ambient temperature, with normal boiling points >200°C.[27, 28]

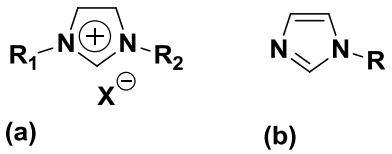

Figure 4.2: General structures of (a) imidazolium-based ILs and (b) *N*-functionalized imidazoles.

The similarities in viscosity, volatility and CO_2 capacities between 1-*n*-alkylimidazoles and commercial solvents make them interesting candidates for study in the application of physical solvents for CO_2/CH_4 separation. This report characterizes the structure-property relationships for six 1-*n*-alkylimidazoles (methyl, ethyl, butyl, hexyl, octyl and decyl) arising from *n*-alkyl chain length and the temperature dependence of ideal (i.e. single gas) CO_2 and CH_4 solubilities at a partial pressure of 5 atm (~75 psia), a condition relevant to the industrial use of physical solvents for CO_2 removal (Figure 4.1). Solubilities for both gases in each 1-*n*-alkylimidazole were measured at 30, 45, 60 and 75^{o}C. Heats of solution for CO_2 and CH_4, as calculated from the van't Hoff Equation, were shown to be exothermic for both gases, with dissolution of CO_2 more thermodynamically driven. Both CO_2 solubility and CO_2/CH_4 selectivity were most favorable in 1-methylimidazole, the smallest molecule in the series, while 1-hexylimidazole exhibited the maximum CH_4 solubility among the six compounds. Gas solubility and selectivity trends can be explained in terms of 1-*n*-alkylimidazole solubility parameters as well as fractional free volumes (FFV). Solubility parameters that we have previously calculated for 1-*n*-alkylimidazoles via group contribution methods[21] have been refined to reflect recently published data for ΔH_{vap} of 1-*n*-alkylimidazoles.[27, 28] FFV as calculated via an atomic contribution approach[29] to calculating the van der Waals' volumes (V_{vdW}) of 1-*n*-alkylimidazoles helps to provide insight into the solubility and selectivity trends observed. Finally, a comparison of physical properties of commercially used physical solvents, 1-methylimidazole and ILs is provided. Using the data developed in this and other works, 1-methylimidazole is revealed to exhibit several favorable properties for use in existing process configurations. Examination of ILs shows that while they exhibit the lowest vapor pressures of any physical solvents, their relatively large viscosities may be a hindrance to use within conventional process schemes.

4.2. Experimental

4.2.1 Materials : 1-Methylimidazole (1) and 1-ethylimidazole (2) were obtained from Sigma-Aldrich (Milwaukee, WI, USA) and used without further purification. Other 1-*n*-alkylimidazoles (3-6) were

synthesized in our laboratory from sodium imidazolate and a corresponding alkyl bromide, according to a previously outlined procedure.[30] Research grades of CO_2 and CH_4 were purchased from AirGas (Radnor, PA, USA).

4.2.2 CO_2 and CH_4 Solubility Measurements: Solubilities of CO_2 and CH_4 in each 1-*n*-alkylimidazole were measured using the same apparatus with a similar methodology as described in our previous work.[21, 31] Experiments were conducted at temperatures of 30, 45, 60, and 75°C (as controlled by an oil bath) for both CO_2 and CH_4 measurements. An initial charge of gas was fed at 30°C until the pressure equilibrated at ~5 atm, which was selected as the target pressure based on Figure 4.1, which suggested that 5 atm (75 psia) would be a pressure where physical solvents would first be considered for use in CO_2 removal. Solubility values for all temperatures were then calculated from this known mass of gas in the system and the change in pressure upon heating, similar to the methodologies outlined by Finotello.[20] Based on published data,[27, 28] the vapor pressure of the 1-*n*-alkylimidazole compound can be assumed as negligible under the experimental temperature and pressure conditions, as it is low (~5 mm Hg maximum and typically < 1 torr) and very small (~0.1%) compared to the partial pressure of the gas. The respective errors associated with H and S were calculated based upon propagation of error of the experimental parameters (i.e. pressure, temperature, volumes, mass, etc.), in which all errors associated with the instrumentation were quantified. In this method, both the moles of gas dissolved in the liquid and molecular weight of the gas are the most significant factors determining the magnitude of the uncertainty. As CO_2 is both more soluble and of a greater molecular weight than CH_4, measurements for CO_2 exhibit an order of magnitude smaller error than those for CH_4, with typical experimental errors of 1-2% and 10-15%, respectively. The errors for CO_2 solubility are consistent with those observed in our previous work.[21]

4.3. Results & Discussion

4.3.1 Ideal Gas Solubility and Selectivity: Henry's constants (H_j *(atm)*) and volumetric solubilities (S_j) of CO_2 and CH_4 in 1-*n*-alkylimidazoles at temperatures between 30-75°C are presented in Table 4.1, while Table 4.2 presents ideal CO_2/CH_4 separation selectivities for each compound within this temperature range.

Table 4.1: Solubilities of CO_2 and CH_4 in 1-*n*-alkylimidazoles (1-6) at a partial pressures ~5 atm and temperatures between 30-75°C expressed as Henry's constants (H_j (atm)) and volumetric solubilities (S_j).

		CO_2				CH_4			
1-*n*-alkylimidazole	Temp. (°C)	H_{CO2} (atm)	±	S_{CO2} [a]	±	H_{CH4} (atm)	±	S_{CH4} [a]	±
1 – Methyl	30	121	2	2.45	0.04	1920	270	0.14	0.02
	45	180	3	1.61	0.03	2140	300	0.13	0.02
	60	221	4	1.24	0.02	2300	340	0.12	0.02
	75	254	5	1.08	0.02	2420	380	0.11	0.02
2 – Ethyl	30	114	1	2.14	0.03	1240	150	0.19	0.02
	45	153	2	1.52	0.02	1470	210	0.16	0.02
	60	180	3	1.24	0.02	1630	240	0.14	0.02
	75	201	3	1.12	0.02	1760	280	0.13	0.02
3 – Butyl	30	86.3	0.9	2.07	0.03	584	39	0.27	0.02
	45	123	1	1.45	0.02	616	42	0.25	0.02
	60	150	2	1.15	0.02	638	43	0.24	0.02
	75	170	2	1.01	0.02	656	43	0.23	0.02
4 – Hexyl	30	69.8	0.7	2.08	0.03	462	27	0.30	0.02
	45	98.3	1.1	1.46	0.02	511	32	0.26	0.02
	60	118	2	1.16	0.02	545	35	0.24	0.02
	75	134	2	1.02	0.02	572	37	0.23	0.02
5 – Octyl	30	68.3	1.0	1.78	0.02	571	57	0.20	0.02
	45	91.5	1.0	1.32	0.02	704	79	0.16	0.02
	60	108	1	1.09	0.01	798	99	0.14	0.02
	75	121	1	0.96	0.01	871	118	0.13	0.02
6 – Decyl	30	63.3	1.0	1.61	0.03	501	55	0.19	0.02
	45	91.3	1.6	1.14	0.02	624	77	0.16	0.02
	60	111	2	0.90	0.02	712	100	0.14	0.02
	75	127	3	0.77	0.02	779	120	0.12	0.02

a: S [=] (cm^3 gas (STP)) (cm^3 solvent)$^{-1}$ atm^{-1}

Error represents one standard deviation

Table 4.1 reveals that at any given temperature, 1-methylimidazole exhibited the highest solubility of CO_2 and lowest solubility of CH_4 per volume. 1-hexylimidazole displayed the greatest volumetric solubility of CH_4 under the same conditions. Solubility of both gases in each of the 1-*n*-alkylimidazoles decreased with increasing temperature. As a point of reference, molar solubility data are also presented in Table 4.1 as Henry's constants, and would seem to indicate that CO_2 is most

soluble in 1-octylimidazole and 1-decylimidazole, while still indicating that CH_4 is most soluble in 1-hexylimidazole. However, the greater CO_2 solubility indicated by the smaller Henry's constants for larger 1-*n*-alkylimidazoles is primarily due to the > 2x increase in molecular weight between 1-methylimidazole and 1-octylimidazole (i.e. larger molar volume). Thus, the volumetric solubility data are more useful in forming direct comparisons to conventional solvents, ILs, and polymers.[9, 24]

The solubility data in Table 4.1 indicate that 1-methylimidazole also has the greatest working capacity of the 1-*n*-alkylimidazole solvents in terms of an absorption-regeneration process for CO_2 removal from CH_4 using a physical solvent. The ~60% decrease in CO_2 solubility between 30-75^{o}C indicates that CO_2 can easily be desorbed from the solvent under moderate heating and/or mild vacuum. As physical solvents can also be chilled to sub-ambient temperatures in the absorption stage to maximize CO_2 uptake,[1, 2] a larger working capacity could be achieved in practice. Of course, the increased dissolution of CO_2 can also enhance the solubility of CH_4 when both gases are present, and this should be considered in future applied research.

Figure 4.3 illustrates the trends in CO_2 and CH_4 volumetric solubility (S) as a function of *n*-alkyl chain length at the four temperature intervals considered. A roughly linear relationship between CO_2 solubility and *n*-alkyl chain length is apparent, while a more complex relationship exists for CH_4. The trends presented suggest that increasing solvent hydrocarbon content (i.e. reducing solvent polarity and reducing free volume) disfavors CO_2 dissolution, while a balance between hydrocarbon content and free volume plays a role in determining CH_4 solubility. A more detailed discussion on fractional free volume (FFV) and an approach to its quantification in 1-*n*-alkylimidazoles will be presented in Section 4.3.2. CO_2 solubility exhibits stronger temperature dependence than CH_4 as evidenced by larger spacings between the solubility isotherms with respect to *n*-alkyl chain length (Figure 4.3). At 60^{o}C and above, CO_2 solubility in 1-*n*-alkylimidazoles other than 1-decylimidazole appears to become roughly equivalent. In contrast, the maxima observed for CH_4 solubility in 1-hexylimidazole are obvious at all temperatures, though CH_4 exhibits similar solubility in 1-butylimidazole and 1-hexylimidazole with increasing temperature, presenting a less distinct maximum.

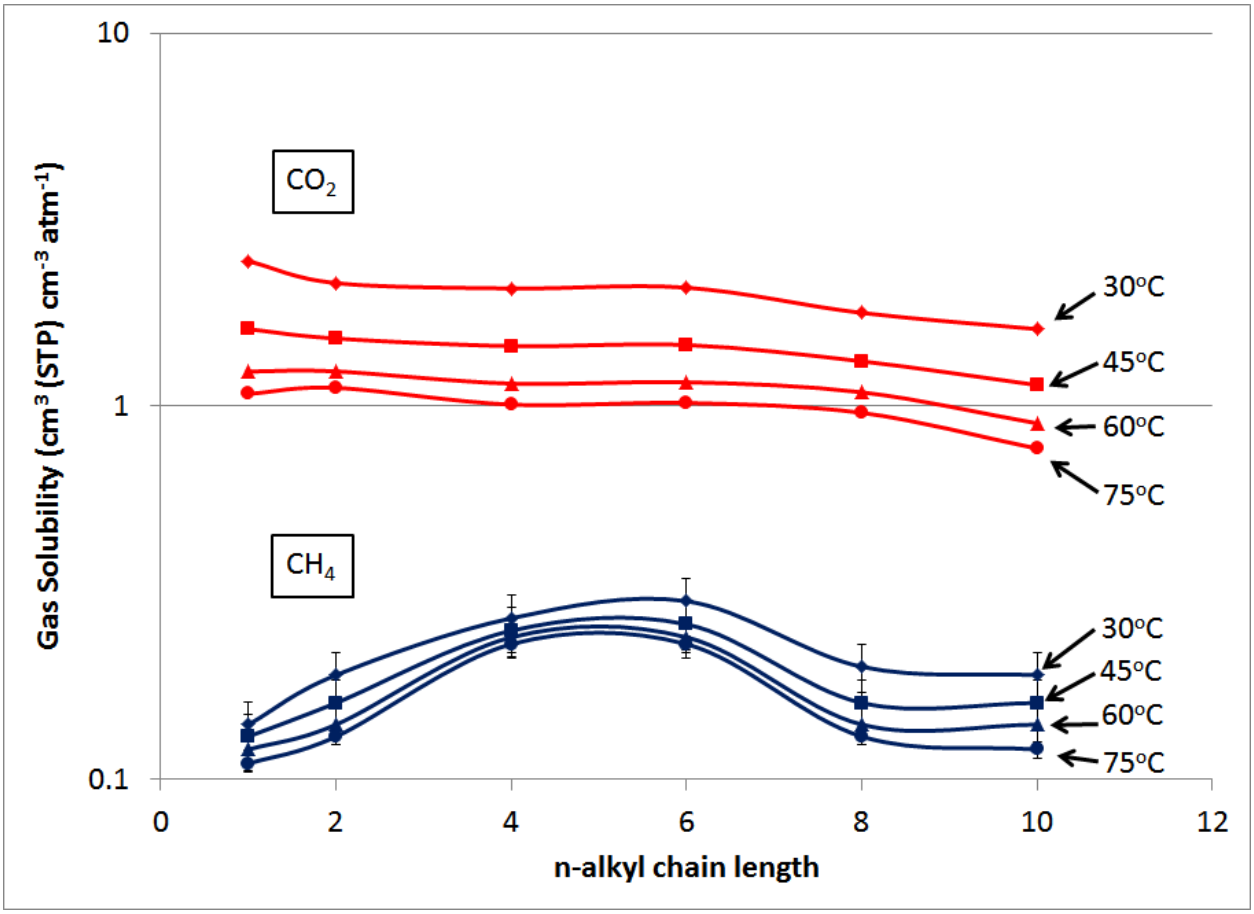

Figure 4.3: Plot of volumetric solubility of CO_2 (red) and CH_4 (blue) in 1-*n*-alkylimidazoles at temperatures between 30-75°C as a function of *n*-alkyl chain length. (Error bars for CO_2 are within symbol.)

Table 4.2 presents ideal CO_2/CH_4 solubility selectivity, calculated as the ratio of the volumetric solubilities of the two gases in each solvent at each temperature (S_{CO2}/S_{CH4}). 1-methylimidazole exhibited the greatest solubility selectivity at each temperature, with a maximum separation factor of 17 at 30°C. All solvents displayed decreasing selectivity for CO_2 with increasing temperature, with the lowest separation factors observed in 1-butylimidazole and 1-hexylimidazole, as these two solvents had the greatest capacity for CH_4. The ideal values presented in Table 4.2 suggest that only 1-methylimidazole would compare favorably with other commercial physical solvents for CO_2/CH_4 separation.[3, 4] Detailed comparisons of various physical solvent processes to 1-methylimidazole and ILs will be provided in Section 4.4.

Table 4.2: Ideal CO_2/CH_4 solubility selectivities in 1-*n*-alkylimidazoles (1-6) at temperatures between 30-75°C.

T (°C)	Ideal CO_2/CH_4 Solubility Selectivity					
	1 – Methyl	2 – Ethyl	3 – Butyl	4 – Hexyl	5 – Octyl	6 – Decyl
30	17	11	7.6	6.9	8.8	8.4
45	12	9.8	5.8	5.6	8.1	7.3
60	10	9.0	4.8	4.8	7.7	6.7
75	9.6	8.8	4.3	4.4	7.4	6.4

The decrease in solubility with temperature can be explained via determination of solution enthalpy (ΔH_{soln}) for each 1-*n*-alkylimidazole/gas pair using the integrated form of the van't Hoff Equation (Eqn. 1). Finotello previously applied the van't Hoff Equation to calculate enthalpies of solution for CO_2, CH_4 and other gases in imidazolium-based ILs.[20]

$$\ln(x_{gas})_P = -\frac{\Delta H_{so\ln}}{R}\left(\frac{1}{T(K)}\right) + B \qquad (1)$$

Mole fractions of each gas in each 1-*n*-alkylimidazole were calculated for a partial pressure of 5 atm at each temperature. The slope of the natural log of gas mole fraction ($\ln(x_{gas})$) vs. 1/T(K) was used to determine ΔH_{soln} for each 1-*n*-alkylimidazole – gas pair, with the values obtained presented in Table 4.3. The 'B' term (y-intercept) becomes a limiting value for $\ln(x_{gas})$ as 1/T approaches zero (i.e. very high temperatures), but has no bearing on the calculation of ΔH_{soln}. Reported errors were determined via the uncertainty associated with calculating the slope based on uncertainty in mole fraction data, with errors for enthalpies of solution for CH_4 an order of magnitude larger than those for CO_2. Example data used for these calculations are presented as Supporting Information.

Table 4.3: Calculated enthalpies of solution for 1-*n*-alkylimidazoles (1-6) with CO_2 and CH_4.

	CO_2		CH_4	
1-*n*-alkylimidazole	ΔH_{soln} (kJ/mol)	±	ΔH_{soln} (kJ/mol)	±
1 – Methyl	-16.3	0.5	-4.9	5.5
2 – Ethyl	-13.1	0.5	-7.6	5.2
3 – Butyl	-12.8	0.5	-2.5	2.4
4 – Hexyl	-13.6	0.5	-4.6	2.3
5 – Octyl	-11.6	0.3	-8.1	4.3
6 – Decyl	-13.4	0.7	-9.0	4.9

Table 4.3 shows that all of the calculated values for enthalpy of solution are negative, indicating that the dissolution of both gases in 1-*n*-alkylimidazoles is exothermic and thus, thermodynamically favorable. For both CO_2 and CH_4, enthalpies of solution can be viewed as roughly equivalent in each 1-*n*-alkylimidazole, with respective values and signs typical of physical solvents.[32] The larger error associated with CH_4 dissolution in 1-methylimidazole suggests the possibility of a slightly endothermic, and less thermodynamically favorable, solvation. While the values for CH_4 are consistent between molecules, the certainty of the calculations for CH_4 could be improved through the use of a larger solvent volume (> 100 mL) in the experiment and/or conducting experiments at higher pressures, which would result in a greater mass of CH_4 absorbed in the liquid phase.

4.3.2 Influence of Solvent Structure on Gas Solubility and Selectivity: With increasing chain lengths in 1-*n*-alkylimidazoles, it was observed that CH_4 solubility (S_{CH4}) increased from 1-methylimidazole to 1-hexylimidazole, yet declined in 1-octylimidazole and 1-decylimidazole. The profile presented in Figure 4.3 suggests that although the overall solvent environments are much less polar in 1-octylimidazole and 1-decylimidazole than in 1-ethylimidazole, these solvents exhibit similar levels of CH_4 uptake. These trends indicate that greater hydrocarbon content does not necessarily favor CH_4 dissolution in this family of molecules, as increasing chain length must eventually limit the available space for CH_4 to dissolve.

To attempt to quantify this occurrence, the concept of FFV can be employed as a means of estimating the amount of void space in a liquid or solid material in which gases may dissolve. FFV values have been tabulated for a number of organic solvents and polymers of interest to CO_2/CH_4

separations.[24] Liquids typically possess much larger FFV values than polymers, which can be correlated to the much greater levels of gas solubility observed in liquids than in polymers.[24] FFV can be calculated from the molar volume (V_m) and van der Waals volume (V_{vdW}) of a given molecule, according to Eqn. 2.[33]

$$FFV = \frac{V_m - 1.3V_{vdW}}{V_m} \quad (2)$$

It has been shown that for a wide variety of organic molecules, including those containing heterocyclic structures such as 1-*n*-alkylimidazoles, V_{vdW} (units of Å^3 molecule^{-1}) can be rapidly calculated with very good accuracy according to Equation 3,[29]

$$V_{vdW} = \sum AAC - 5.92N_B - 14.7_{RA} - 3.8R_{NR} \quad (3)$$

where AAC (all atom contributions) is the sum of all atoms' V_{vdW} (tabulated in References 29, 34), N_B is the number of total bonds, R_A is the number of aromatic rings (1 in the case of compounds 1-6), and R_{NR} is the number of nonaromatic rings (0 for compounds 1-6). N_B was determined as the number of atoms minus one plus the total number of ring structures (i.e. 1). Equation 3 is a correlation solely based on atomic and bond contributions and is related to 677 organic compounds (440 general organic compounds and 237 drug compounds), including imidazole.[29] In the original work,[29] values from this correlation were compared to values calculated using the TSAR program (Oxford Molecular, Ltd.), and had a regression value of 0.992 with 8.6 being the standard error. Eqn. 3 can prove to be quite useful in that it provides a fast, simplistic calculation for the van der Waals volumes using only spreadsheets.[29]

The calculated V_{vdW} values (Å^3 molecule^{-1}) from Eqn. 3 were then converted to the appropriate units of cm^3 mol^{-1} to calculate the FFV of each 1-*n*-alkylimidazole using Equation 2, with V_m (cm^3 mol^{-1}) values at 25°C taken from our prior work.[21] Calculated FFV values for 1-n-alkylimidazoles (1-6) and others are reported in Table 4.4. This approach provided FFV values for other organic solvents similar to those estimated by Lin using a Bondi group contribution method.[24]

Table 4.4: Calculated FFV values for 1-*n*-alkylimidazoles

1-*n*-alkylimidazole	FFV
1 – methyl	0.300
2 – ethyl	0.286
propyl	0.272
3 – butyl	0.265
pentyl	0.257
4 – hexyl	0.249
5 – octyl	0.242
6 – decyl	0.235
dodecyl	0.228
tetradecyl	0.224

As seen from Table 4.4, there is an appreciable (~25%) decrease in FFV as the *n*-alkyl chain length increases from methyl to tetradecyl, declining more rapidly in the smaller 1-*n*-alkylimidazoles. At the longer chain lengths, the incremental increase in hydrocarbon contents result in smaller changes in FFV, implying that the molecule is taking on much more of the character of an alkane than an imidazole. While these values in Table 4.4 directly account for the decreasing CO_2 solubility trend in larger 1-*n*-alkylimidazoles, no dramatic change in FFV is calculated between 1-hexylimidazole and 1-octylimidazole that might account for the maximum in CH_4 solubility observed. However, the viscosity data previously obtained for 1-*n*-alkylimidazoles shows a steep increase beginning with 1-octylimidazole, suggesting significant interdigitation of the *n*-alkyl chains and localized phase separation between the polar imidazole headgroups and non-polar hydrocarbon chains.[21] The steep increase in viscosity corresponds with a loss of free volume within the non-polar regions in which the larger CH_4 molecules prefer to dissolve, thus reducing the solubility of CH_4 in the solvent despite increased hydrocarbon content. Models demonstrating increasing viscosity with decreasing FFV in a series of *n*-alkanes were first put forth by Doolittle,[35, 36] and are also widely applicable to polymers.[37] Similar trends to these 1-*n*-alkylimidazoles are observed for hexane and larger *n*-alkanes, as the solubility of CH_4 (S_{CH4}) has also been shown to decrease with incrementally larger chain lengths, even though the mole fraction of CH_4 appears to slightly increase.[38]

Previously, we used vapor pressure data for 1-methylimidazole obtained from several sources to estimate solubility parameters of 1-*n*-alkylimidazoles via a group contribution approach.[9, 17, 21] Recently, extensive data have been reported on the vapor pressure and enthalpies of vaporization for 1-*n*-alkylimidazoles.[27, 28] The value for heat of vaporization of 1-methylimidazole at 298K (55.3 kJ/mol) that we previously calculated from the Clausius-Clapyeron Equation[21] using several different data sources was in excellent agreement with the experimental value of 55.14 kJ/mol reported by Verevkin and co-workers. Vapor pressures reported by this group for 1-*n*-alkylimidazoles at 298K decrease from 49.58 Pa (0.3719 mmHg) to 0.02 Pa (1.5×10^{-4} mmHg) for 1-methylimidazole and 1-dodecylimidazole, respectively.

The experimental data for ΔH_{vap} of 1-*n*-alkylimidazoles were used to calculate the solubility parameter (δ) as the square root of the cohesive energy density (Eqn. 4) to verify the solubility parameters we previously calculated via group contributions.[21]

$$\delta = \sqrt{\frac{\Delta H_{vap} - RT}{V_m}} \tag{4}$$

The results obtained confirm that the "high" estimate values we calculated using 1-methylimidazole in a group contribution approach are within 0.1 $MPa^{1/2}$ of those directly calculated via Eqn. 4.[21] Furthermore, for 1-*n*-alkylimidazoles, a direct correlation appears to exist between solubility parameter and FFV, as illustrated in Figure 4.4. Both curves can be fit as power functions ($y=Ax^B$) with R^2 values of 0.99, with nearly identical exponents for solubility parameter and FFV, respectively (B = -0.127 and -0.117), indicating very similar behavior for each property with extension of *n*-alkyl chain length. Pre-exponential coefficients of 'A' were found to be 25.91 and 0.307 for the solubility parameter and FFV functions, respectively. While the trend of both metrics with increasing chain length is nearly identical, the use of FFV may be more straightforward as no experimental data other than density are needed for its calculation when the van der Waals' volumes of the atoms comprising the molecule are known.[29, 34, 39]

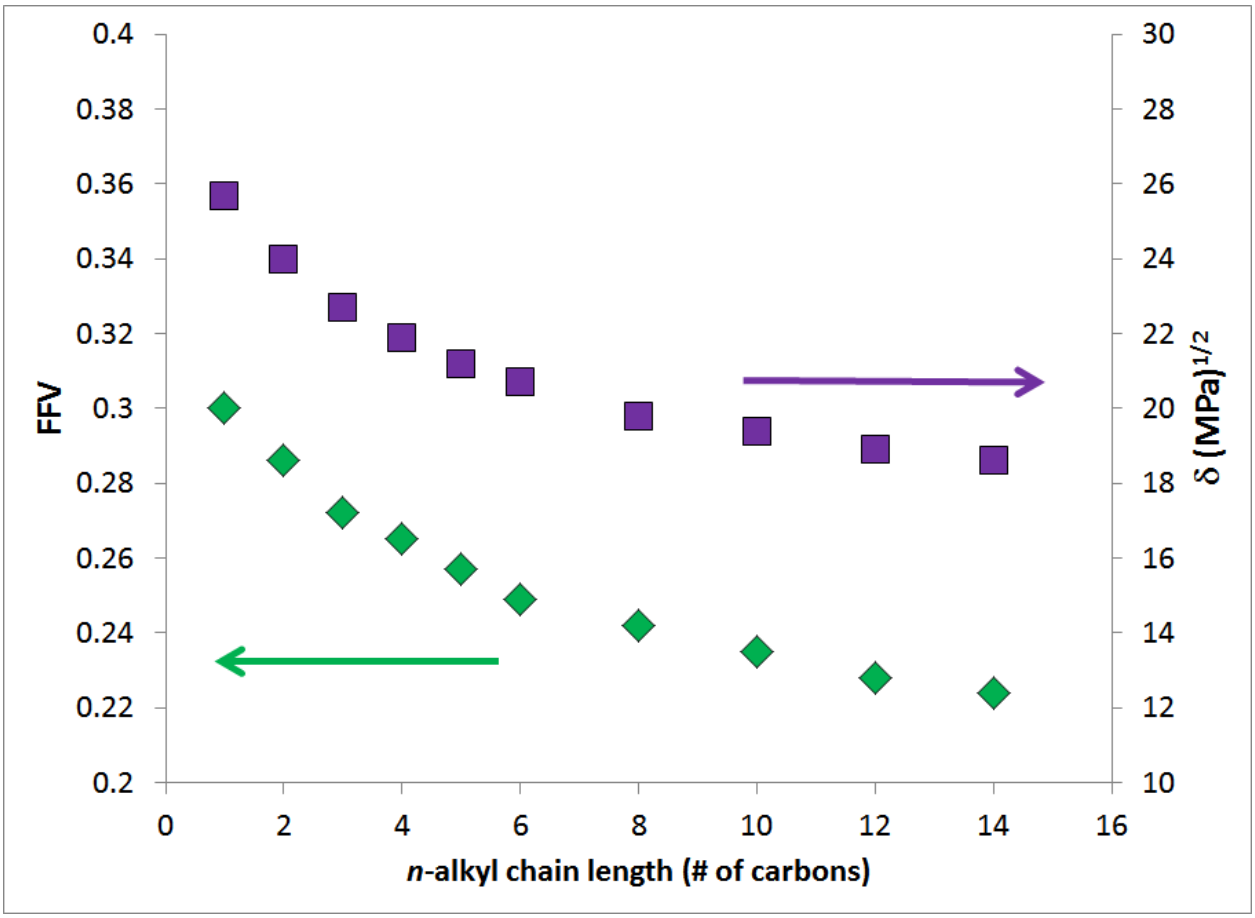

Figure 4.4: Dependence of solubility parameter and FFV in 1-*n*-alkylimidazoles on *n*-alkyl chain length.

4.4. Comparison of 1-Methylimidazole to Commercial Physical Solvent Processes and ILs: A general principle applied to selecting solvents for acid gas removal is that polar groups (ethers, nitriles, etc.) favor CO_2 dissolution and CO_2/CH_4 separation.[9, 24] Thus, polar organic solvents (DMPEG, MeOH, etc.) are typically used for natural gas sweetening and other acid gas removal applications.[2, 24] However, a variety of factors are critical for a physical solvent to be used in a commercially viable process, including low volatility, low viscosity, stability and availability in bulk at favorable costs.[3, 4, 7] Furthermore, no one physical solvent is appropriate for every gas treating application, due to the differences in the gas streams to be treated and/or the requisite purity of the product gas.[1-4, 7] Four of the most utilized physical solvents are: dimethyl ethers of poly(ethylene glycol) (DMPEG), propylene carbonate (PC), *N*-methyl-2-pyrrolidone (NMP), and methanol (MeOH), each with its own capabilities and limitations.[3, 4] A

number of factors relating to solvent properties and the composition of the gas to be treated also play roles in determining solvent selection.

For example, DMPEG is effective at achieving selective separation of H_2S from CO_2, but has a higher viscosity than other physical solvents which reduces mass transfer rates, especially if operated below 25°C.[3, 4] PC is not typically recommended for use when high concentrations of H_2S are present, as it becomes unstable during regeneration (~93°C).[3, 4] Of the solvents considered here, NMP has the highest selectivity for H_2S/CO_2, but is more volatile than DMPEG or PC.[3, 4] At ambient conditions, MeOH is quite volatile, but when chilled to sub-zero temperatures (as low as -70.5°C), MeOH becomes effective at near complete removal of CO_2, H_2S and other contaminants.[3, 4] Chilling MeOH (or any physical solvent) increases acid gas loadings, but does so at the cost of the power supply for refrigeration, and potential increases in solvent viscosity.[3, 4] However, these operating expenses can be offset via reduced solvent circulation rates (process footprint), which results in lower capital expenses.[3, 4] Also, as the solubility of CH_4 changes much less with temperature than does CO_2 (or other acid gases) selectivity enhancements can be achieved through chilling.[3, 4, 20]

While CO_2 and/or H_2S are typically the impurities present in the greatest proportions, other minor species such as carbonyl sulfide (COS), carbon disulfide (CS_2) and mercaptans (RSH) must also be removed.[1, 2] Another consideration in solvent selection and process design is the absorption and loss of larger hydrocarbons, which may accumulate in the solvent.[3, 4] Thus, process designs can be quite different for each of these solvents depending on both solvent physical properties and the number of unit operations required.[3, 4]

Table 4.5 presents physical properties most relevant to process operation for the four physical solvents discussed, as well as 1-methylimidazole. ILs have also been included in this comparison, as although recent reviews on the use of ILs for CO_2 removal and natural gas processing have focused on comparisons between different ILs or ILs and certain organic solvents,[10, 19] emphasis was primarily placed on CO_2 solubility and CO_2/CH_4 selectivity, with less discussion devoted to process operation.[9, 10] Units of the physical properties listed in Table 4.5 are reflective of those most commonly used within the industrial literature.[1-4]

Table 4.5: Comparison of physical properties of commercially used physical solvents, 1-methylimidazole and ILs.

	DMPEG	PC	NMP	MeOH	1-methylimidazole	Ionic Liquids
Commercial Process Name	Selexol	Fluor Solvent	Purisol	Rectisol/ Ifpexol	N/A	N/A
Viscosity (cP)	5.8	3.0	1.65	0.6	1.77	~25-1000
Specific Gravity ($kg\ m^{-3}$)	1030	1195	1027	785	1031	1000-1500
Molecular Weight ($g\ mol^{-1}$)	280	102	99	32	82	~200-500
Vapor Pressure (mm Hg)	0.00073	0.085	0.40	125	0.37	.000001
Freezing Point	-28	-48	-24	-92	-6	variable
Boiling Point (760 mm Hg)	275	240	202	65	198	N/A
Maximum Operating Temperature (^oC)	175	65	Boiling Point	Boiling Point	*Boiling Point*	Depends on stability
CO_2 Solubility (ft^3 U.S. $gallon^{-1}$)	0.485	0.455	0.477	0.425	0.377	≥ 0.335
CO_2/CH_4	15	26	14	20**	> 17	8-18
H_2S/CO_2	8.82	3.29	10.2	7.06**	*TBD (≥ NMP)*	2-4
H_2O miscible?	Yes	Partial	Yes	Yes	Yes	varies

*All physical Properties at 25^{o}C, except otherwise noted.

**Solubility selectivity data at -25^{o}C for MeOH.

Italics indicate authors' estimates

Table 4.5 illustrates that 1-methylimidazole is most similar to NMP in terms of physical properties. Both NMP and 1-methylimidazole are ~50% less viscous than PC and ~70% less viscous than DMPEG. While 1-methylimidazole has about 20% lower CO_2 solubility than NMP and DMPEG,[32] it has a higher CO_2/CH_4 selectivity than DMPEG and NMP. The potential for higher H_2S/CO_2 selectivity also exists in 1-methylimidazole based on analogy to the CO_2/CH_4 and H_2S/CO_2 ratios observed for NMP,[32] and the presence of a basic, nitrogen center which has enabled its use as an acid scavenger,[40, 41] and might

enable reversible acid-base interactions with the acidic proton(s) of H_2S. As NMP would appear to be best-suited for IGCC or pre-combustion CO_2 capture based on its selectivity for H_2S/CO_2,[3] 1-methylimidazole could also be useful for that application. Table 4.5 assumes that 1-methylimidazole can be used up to its boiling point as the compound is readily distillable without degradation.[28, 42-45] An ideal CO_2/CH_4 solubility of at least 17 is expected at 25°C from the measurements made in this work and the observed trend of increasing selectivity with decreasing temperature in 1-*n*-alkylimidazoles and other physical solvents.[20]

While 1-*n*-alkylimidazoles with longer side chains would exhibit reduced volatility, CO_2 solubility and selectivity would suffer. However, introduction of an ether group within the imidazole side chain might have multiple beneficial effects: reduction of volatility and increased CO_2/CH_4 selectivity while maintaining relatively low viscosity (3 - 5 cP) at 25°C. Such ether-functionalized imidazoles have already been prepared as precursors for ILs.[11, 46]

ILs compare less favorably to commercial solvents, especially with respect to viscosity. Commonly used ILs are at least 4.5x more viscous than DMPEG (the most viscous solvent listed in Table 4.5), although most are 10x more viscous.[21, 22] Near-zero volatility has been touted as one of the major advantages of ILs,[47] as solvent losses can be minimized due to vaporization, although the importance of near zero volatility may be overstated. For example, the vapor pressure of DMPEG is 730x greater than ILs, yet solvent losses due to DMPEG volatility are not viewed as problematic in acid gas removal processes.[3] Furthermore, efficient process engineering designs employ solvent recovery operations for the more volatile PC, NMP and MeOH solvents.[3, 4] Although ILs exhibit almost a negligible volatility,[47] focusing solely on this property at the expense of viscosity may be counterproductive to achieving an process with optimal mass and heat transfer rates. However, this may enable certain ILs (with requisite thermal stability) to be regenerated at higher temperatures that other organic solvents cannot achieve. This feature could be beneficial to achieve essentially zero acid gas loadings in the lean solvent and reduce solvent circulation rates. Conversely, chilling ILs might cause exceedingly high viscosities or solidification. A relatively straightforward approach to pilot testing ILs could be in mixtures with other commercially available solvents.[48] A blending approach can reduce overall solvent costs and keep viscosity relatively low, while reducing overall solvent volatility and enabling use of existing process equipment. It is our experience that most imidazolium-based ILs will blend completely with DMPEG, MeOH and 1-methylimidazole. Although we cannot comment on miscibility with PC or NMP, it is likely that at least some ILs should be freely miscible with these solvents.

4.5 Conclusions: Ideal solubilities of CO_2 and CH_4 and ideal CO_2/CH_4 selectivities were determined as a function of temperature for a series of six 1-*n*-alkylimidazoles with increasing lengths of alkyl substituents. CO_2 was shown to be most soluble in 1-methylimidazole, which also exhibited the greatest selectivity for CO_2/CH_4. CO_2 solubility decreased with increasing chain length, while CH_4 solubility exhibited a maximum in 1-hexylimidazole. Solubility of each gas in all solvents was observed to decrease with increasing temperature. Enthalpies of solution for each gas-solvent combination were determined via the van't Hoff equation, and the dissolution found to be thermodynamically favorable, with CO_2 more exothermic than CH_4. Solubility and selectivity trends were explained in terms of FFV and solubility parameters, which are directly and highly correlated.

Of the 1-*n*-alkylimidazoles examined, only 1-methylimidazole appears to possess characteristics favorable to use within a larger scale acid gas removal process, via analogy to its commonalities with NMP. While a promising solvent candidate for natural gas sweetening and pre-combustion CO_2 capture, additional research is needed to determine the performance of 1-methylimidazole in the presence of H_2S, other acid gases and hydrocarbons. Future research will also focus on the characterization of imidazole solvents with various polar substituents and multiple substitutions. Tailored derivatives could increase CO_2 solubility, improve selectivity, reduce vapor pressure while maintaining a useful viscosity range. Ultimately, development of process simulations (e.g. ASPEN®, ProMax®, ProTreat®, ChemCad® etc.) using imidazole-based solvents for various gas treating applications will be highly valuable in determining the best application fit(s), as well as developing comparative energy and economic analyses to the currently employed processes.

Acknowledgments

Partial support for this work was provided by ION Engineering, LLC; United States Department of Energy – National Energy Technology Laboratory (DE-FE00005799); and the National Science Foundation Research Experiences for Undergraduates Program (EEC-1062705) is gratefully acknowledged. J.E.B. also wishes to thank Johnny E. Johnson and Barry Friedman of URS/Washington Group for many helpful discussions on industrial gas treating.

Supporting Information Available (*See Section 4.7*)

Example plots used for calculating heats of solutions for CO_2 and CH_4 in 1-methylimidazole. This material is available free of charge via the Internet at http://pubs.acs.org.

4.6 References:

1. Astarita, G.; Savage, D. W.; Bisio, A., *Gas Treating with Chemical Solvents*. John Wiley & Sons: New York, 1983.
2. Kidnay, A. J.; Parrish, W. R., *Fundamentals of Natural Gas Processing*. CRC Press: Taylor & Francis Group: Boca Raton, FL, 2006.
3. Burr, B.; Lyddon, L., A Comparison of Physical Solvents for Acid Gas Removal. In *Gas Processors' Association Convention*, Grapevine, TX, 2008.
4. Bucklin, R. W.; Schendel, R. L., Physical Solvent Processes Can Be Very Useful for Acid Gas Removal Applications. *Energy Prog.* 1984, *4*, 137-142.
5. Heintz, Y. J.; Sehabiague, L.; Morsi, B. I.; Jones, K. L.; Luebke, D. R.; Pennline, H. W., Hydrogen Sulfide and Carbon Dioxide Removal from Dry Fuel Gas Streams Using an Ionic Liquid as a Physical Solvent†‡. *Energy Fuels* 2009, *23*, 4822-4830.
6. NETL DOE/NETL Advanced Carbon Dioxide Capture R&D Program: Technology Update May 2011. http://www.netl.doe.gov/technologies/coalpower/ewr/pubs/CO2CaptureTechUpdate051711.pdf (Accessed 14 September 2011)
7. Tennyson, R. N.; Schaaf, R. P., Guidelines can help choose proper process for gas-treating plants. *Oil Gas J.* 1977, *75*, 78-86.
8. Rochelle, G. T., Amine Scrubbing for CO_2 Capture. *Science* 2009, *325*, 1652-1654.
9. Bara, J. E.; Carlisle, T. K.; Gabriel, C. J.; Camper, D.; Finotello, A.; Gin, D. L.; Noble, R. D., Guide to CO_2 Separations in Imidazolium-Based Room-Temperature Ionic Liquids. *Ind. Eng. Chem. Res.* 2009, *48*, 2739-2751.
10. Karadas, F.; Atilhan, M.; Aparicio, S., Review on the Use of Ionic Liquids (ILs) as Alternative Fluids for CO_2 Capture and Natural Gas Sweetening. *Energy Fuels* 2010, *24*, 5817-5828.
11. Bara, J. E.; Gabriel, C. J.; Lessmann, S.; Carlisle, T. K.; Finotello, A.; Gin, D. L.; Noble, R. D., Enhanced CO_2 separation selectivity in oligo(ethylene glycol) functionalized room-temperature ionic liquids. *Ind. Eng. Chem. Res.* 2007, *46*, 5380-5386.
12. Jalili, A. H.; Rahmati-Rostami, M.; Ghotbi, C.; Hosseini-Jenab, M.; Ahmadi, A. N., Solubility of H_2S in Ionic Liquids [bmim][PF_6], [bmim][BF_4], and [bmim][Tf_2N]. *J. Chem. Eng. Data* 2009, *54*, 1844-1849.
13. Shiflett, M. B.; Niehaus, A. M. S.; Yokozeki, A., Separation of CO_2 and H_2S Using Room-Temperature Ionic Liquid [bmim][$MeSO_4$]. *J. Chem. Eng. Data* 2010, *55*, 4785-4793.
14. Jou, F. Y.; Mather, A. E., Solubility of hydrogen sulfide in bmim PF_6. *Int. J. Thermophys.* 2007, *28*, 490-495.
15. Pomelli, C. S.; Chiappe, C.; Vidis, A.; Laurenczy, G.; Dyson, P. J., Influence of the Interaction between Hydrogen Sulfide and Ionic Liquids on Solubility: Experimental and Theoretical Investigation. *J. Phys. Chem. B* 2007, *111*, 13014-13019.
16. Camper, D.; Bara, J.; Koval, C.; Noble, R., Bulk-fluid solubility and membrane feasibility of Rmim-based room-temperature ionic liquids. *Ind. Eng. Chem. Res.* 2006, *45*, 6279-6283.
17. Carlisle, T. K.; Bara, J. E.; Gabriel, C. J.; Noble, R. D.; Gin, D. L., Interpretation of CO_2 solubility and selectivity in nitrile-functionalized room-temperature ionic liquids using a group contribution approach. *Ind. Eng. Chem. Res.* 2008, *47*, 7005-7012.

18. Finotello, A.; Bara, J. E.; Narayan, S.; Camper, D.; Noble, R. D., Ideal gas solubilities and solubility selectivities in a binary mixture of room-temperature ionic liquids. *J. Phys. Chem. B* 2008, *112*, 2335-2339.
19. Bara, J. E.; Gabriel, C. J.; Carlisle, T. K.; Camper, D. E.; Finotello, A.; Gin, D. L.; Noble, R. D., Gas separations in fluoroalkyl-functionalized room-temperature ionic liquids using supported liquid membranes. *Chem. Eng. J.* 2009, *147*, 43-50.
20. Finotello, A.; Bara, J. E.; Camper, D.; Noble, R. D., Room-temperature ionic liquids: Temperature dependence of gas solubility selectivity. *Ind. Eng. Chem. Res.* 2008, *47*, 3453-3459.
21. Shannon, M. S.; Bara, J. E., Properties of Alkylimidazoles as Solvents for CO_2 Capture and Comparisons to Imidazolium-Based Ionic Liquids. *Ind. Eng. Chem. Res.* 2011, 50, 8665-8677.
22. Gardas, R. L.; Coutinho, J. A. P., A group contribution method for viscosity estimation of ionic liquids. *Fluid Phase Equilibr.* 2008, *266*, 195-201.
23. Bara, J. E.; Camper, D. E.; Gin, D. L.; Noble, R. D., Room-Temperature Ionic Liquids and Composite Materials: Platform Technologies for CO_2 Capture. *Acc. Chem. Res.* 2010, *43*, 152-159.
24. Lin, H. Q.; Freeman, B. D., Materials selection guidelines for membranes that remove CO_2 from gas mixtures. *J. Molec. Struct.* 2005, *739*, 57-74.
25. Li, J.; Mundhwa, M.; Henni, A., Volumetric Properties, Viscosities, Refractive Indices, and Surface Tensions for Aqueous Genosorb 1753 Solutions. *J. Chem. Eng. Data* 2007, *52*, 955-958.
26. Henni, A.; Tontiwachwuthikul, P.; Chakma, A., Solubilities of carbon dioxide in polyethylene glycol ethers. *Can. J. Chem. Eng.* 2005, *83*, 358-361.
27. Emel'yanenko, V. N.; Portnova, S. V.; Verevkin, S. P.; Skrzypczak, A.; Schubert, T., Building blocks for ionic liquids: Vapor pressures and vaporization enthalpies of 1-(n-alkyl)-imidazoles. *J. Chem. Thermodyn.* 2011, *43*, 1500-1505.
28. Verevkin, S. P. V. S. P.; Zaitsau, D. H.; Emel'yanenko, V. N.; Paulechka, Y. U.; Blokhin, A. V.; Bazyleva, A. B.; Kabo, G. J., Thermodynamics of Ionic Liquids Precursors: 1-Methylimidazole. *J. Phys. Chem. B* 2011, 115, 4404-4411.
29. Zhao, Y. H.; Abraham, M. H.; Zissimos, A. M., Fast calculation of van der Waals volume as a sum of atomic and bond contributions and its application to drug compounds. *J. Org. Chem.* 2003, *68*, 7368-7373.
30. Bara, J. E., Versatile and Scalable Method for Producing N-Functionalized Imidazoles. *Industrial & Engineering Chemistry Research* 2011 ACS ASAP, doi: 10.1021/ie102535c.
31. Maddox, R. N.; Bhairi, A. H.; Diers, J. R.; Thomas, P. A. *Research Report RR-104: Equilibrium Solubility of Carbon Dioxide or Hydrogen Sulfide in Aqueous Solutions of Monoethanolamine, Diglycolamine, Diethanolamine and Methyldiethanolamine*; Tulsa, OK, 1987.
32. Murrieta-Guevara, F.; Romero-Martinez, A.; Trejo, A., Solubilities of carbon dioxide and hydrogen sulfide in propylene carbonate, N-methylpyrrolidone and sulfolane. *Fluid Phase Equilibr.* 1988, *44*, 105-115.
33. Lee, W. M., Selection of Barrier Materials from Molecular Structure. *Polym. Eng. Sci.* 1980, 20, (1), 65-69.
34. Bondi, A., van der Waals Volumes and Radii. *J. Phys. Chem.* 1964, *68*, 441-451.
35. Miller, A. A., Free Volume and Viscosity of Liquids: Effects of Temperature. *J. Phys. Chem.* 1963, *67*, 1031-1035.
36. Doolittle, A. K., Newtonian flow. II. The dependence of the viscosity of liquids on free space. *J. Appl. Phys.* 1951, *22*, 1471-1475.
37. Williams, M. L.; Landel, R. F.; Ferry, J. D., The Temperature Dependence of Relaxation Mechanisms in Amorphous Polymers and Other Glass-forming Liquids. *J. Am. Chem. Soc.* 1955, *77*, 3701-3707.

38. Ghosh, A.; Chapman, W. G.; French, R. N., Gas solubility in hydrocarbons--a SAFT-based approach. *Fluid Phase Equilibr.* 2003, *209*, 229-243.
39. Mantina, M.; Chamberlin, A. C.; Valero, R.; Cramer, C. J.; Truhlar, D. G., Consistent van der Waals Radii for the Whole Main Group. *J. Phys. Chem. A* 2009, *113*, 5806-5812.
40. Plechkova, N. V.; Seddon, K. R., Applications of ionic liquids in the chemical industry. *Chem. Soc. Rev.* 2008, *37*, 123-150.
41. Lenarcik, B.; Ojczenasz, P., The influence of the size and position of the alkyl groups in alkylimidazole molecules on their acid-base properties. *J. Heterocycl. Chem.* 2002, *39*, 287-290.
42. Liebner, F.; Patel, I.; Ebner, G.; Becker, E.; Horix, M.; Potthast, A.; Rosenau, T., Thermal aging of 1-alkyl-3-methylimidazolium ionic liquids and its effect on dissolved cellulose. *Holzforsch.* 2010, *64*, 161-166.
43. Bowing, A. G.; Jess, A., Kinetics of single- and two-phase synthesis of the ionic liquid 1-butyl-3-methylimidazolium chloride. *Green Chem.* 2005, 7, 230-235.
44. Treble, R. G.; Johnson, K. E.; Tosh, E., The volatilities and conductivities of ionic liquids - GC-MS methodology and preliminary studies of acetic acid-base systems. *Can. J. Chem.* 2006, *84*, 915-924.
45. Bender, M. L.; Turnquest, B. W., General Basic Catalysis of Ester Hydrolysis and Its Relationship to Enzymatic Hydrolysis. *J. Chem. Soc.* 1957, *79*, 1656-1662.
46. Smith, G. D.; Borodin, O.; Li, L. Y.; Kim, H.; Liu, Q.; Bara, J. E.; Gin, D. L.; Nobel, R., A comparison of ether- and alkyl-derivatized imidazolium-based room-temperature ionic liquids: a molecular dynamics simulation study. *Phys. Chem. Chem. Phys.* 2008, *10*, 6301-6312.
47. Earle, M. J.; Esperanca, J.; Gilea, M. A.; Lopes, J. N. C.; Rebelo, L. P. N.; Magee, J. W.; Seddon, K. R.; Widegren, J. A., The distillation and volatility of ionic liquids. *Nature* 2006, 439, 831-834.
48. Camper, D.; Bara, J. E.; Gin, D. L.; Noble, R. D., Room-Temperature Ionic Liquid-Amine Solutions: Tunable Solvents for Efficient and Reversible Capture Of CO_2. *Ind. Eng. Chem. Res.* 2008, *47*, 8496-8498.

4.7 Appendix:

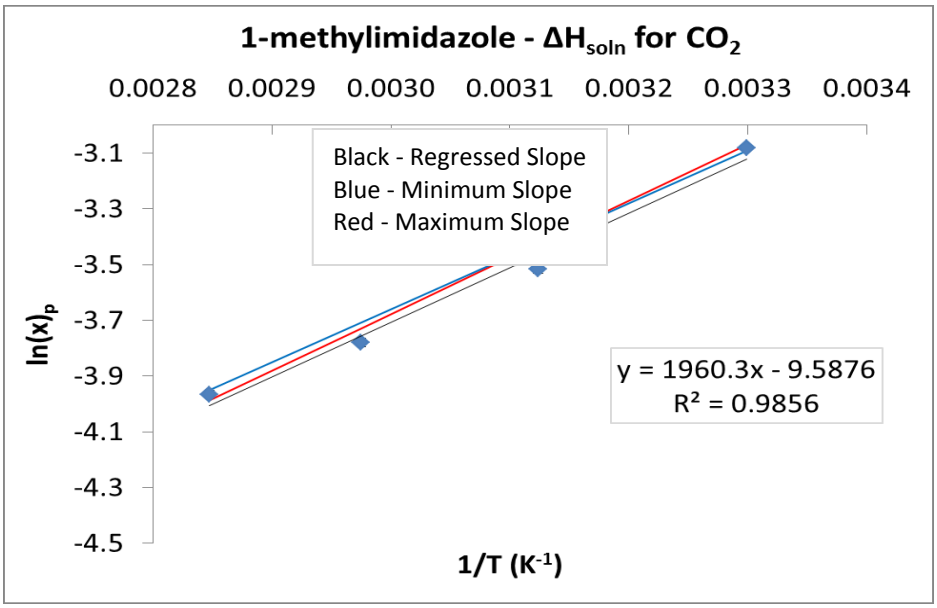

Figure S1: Enthalpy of solution for dissolution of CO_2 in 1-methylimidazole. Chart annotated with regression fit and min-max slopes from standard error of solubility data with regressed slope.

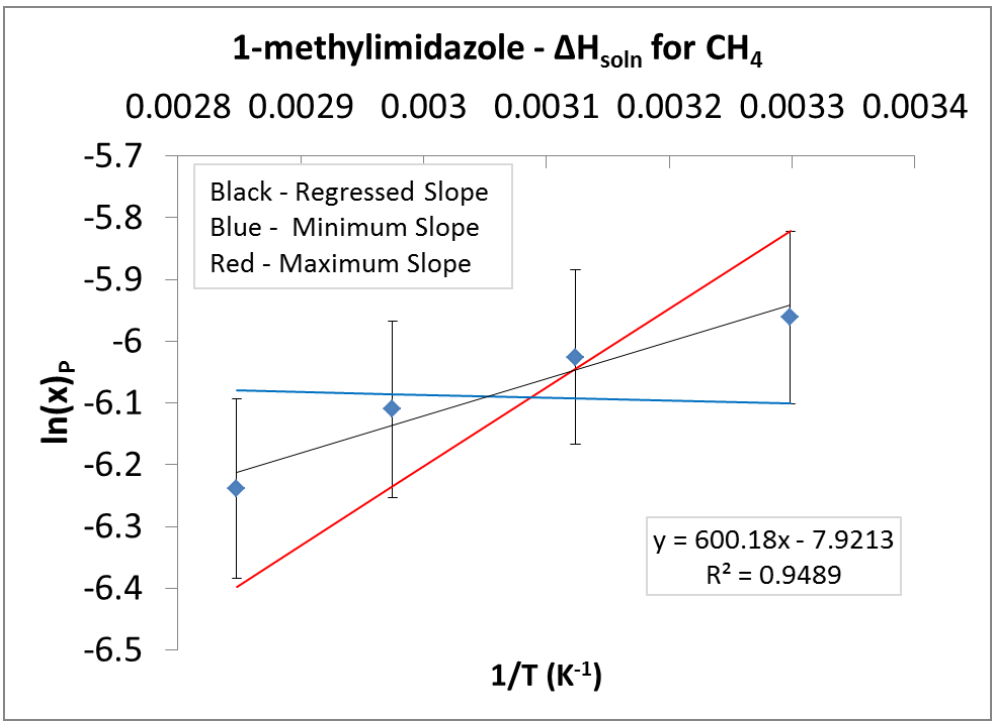

Figure S2: Enthalpy of solution for dissolution of CH_4 in 1-methylimidazole. Chart annotated with regression fit and min-max slopes from standard error of solubility data with regressed slope.

CHAPTER FIVE

[†]Free Volume as the Basis of Gas Solubility & Selectivity in Imidazolium-based Ionic Liquids

Matthew S. Shannon,[1] Jason M. Tedstone,[2,3] Scott P. O. Danielsen[2,4] Michelle S. Hindman,[1] A. Christopher Irvin[1] & Jason E. Bara[1]*

1. Department of Chemical & Biological Engineering, University of Alabama, Tuscaloosa AL USA 35487-0203
2. NSF-REU Site: Engineering Solutions for Clean Energy Generation, Storage and Consumption, Department of Chemical & Biological Engineering, University of Alabama, Tuscaloosa AL USA 35487-0203
3. Department of Chemical & Biomolecular Engineering, Clemson University, Clemson, SC USA 29634
4. Department of Chemical & Biomolecular Engineering, University of Pennsylvania, Philadelphia, PA USA 19104-6315

Abstract

While molar volume-based models for gas solubility in ionic liquids (ILs) have been proposed, free volume within the IL can be shown to be the underlying property driving gas solubility and selecitivity. Previously published observations as to the distinct differences in solubility trends for gases such as CH_4 and N_2 relative to CO_2 in systematically varied ILs can be attributed to positive and negative effects arising from increasing free volume with increasing alkyl chain length. Through the use of COSMOtherm as a powerful and rapid tool to calculate free volumes in 165 existing and theoretical 1-*n*-alkyl-3-methylimidazolium ([$C_n$mim][X]) ILs, a previously unreported, yet speculated, critical underlying relationship between gas solubility in ILs is herein described. These results build upon previous assertions that Regular Solution Theory is applicable to imidazolium-based ILs, which appeared to indicate that a global maximum had already been observed for CO_2 solubility in imidazolium-based ILs. However, the findings of this computational study indicate that the perceived maximum in CO_2 solubility might be exceeded through rational design of ILs. We observe that although Henry's constants in ILs are dependent on the inverse of molar volume and free volume, the volume-normalized solubility of CH_4 and N_2 are proportional to free volume, while CO_2 is inversely proportional to the square root of free volume. Our free volume model is compared to experimental data for CO_2/CH_4 and CO_2/N_2 selectivity, and a nearly identical plot of selectivity relative to IL molar volume can be generated from the computational method alone. The overall implication is that large, highly delocalized anions paired with imidazolium cations that have minimally sized alkyl chains may hold the key to achieving greater CO_2 solubility and selectivity in ILs.

[†]*Industrial & Engineering Chemistry Research, 2012, 51, 5565-5576*.

5.1 Introduction: In 2006, Camper et al. introduced a model for low pressure CO_2 solubility and selectivity in imidazolium-based ionic liquids (ILs) that, at 25°C, 40°C and 50°C, displayed distinct maxima coinciding with the widely-studied 1-ethyl-3-methylimidazolium bis(triflamide), [C_2mim][Tf_2N] (Figure 5.1).[1]

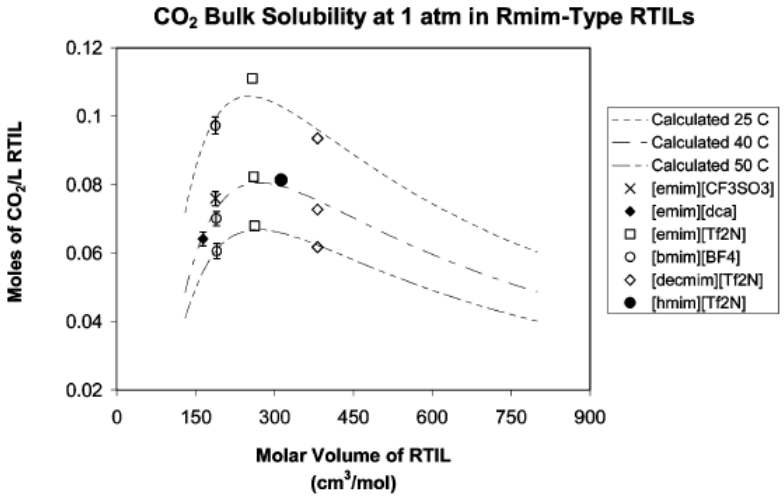

Figure 5.1: Camper's model for CO_2 solubility in ILs (moles CO_2 per liter) at 1 atmosphere partial pressure as a function of IL molar volume. Reprinted with permission from: Camper, D.; Bara, J.; Koval, C.; Noble, R., Bulk-fluid solubility and membrane feasibility of Rmim-based room-temperature ionic liquids. *Ind. Eng. Chem. Res.* 2006, 45, (18), 6279-6283. Copyright 2006 American Chemical Society.

As regular solution theory (RST) was reported to be applicable to imidazolium-based ILs,[1-4] a simplified two constant model in Figure 5.1 was proposed by which to relate CO_2 solubility to the IL molar volume (V_m) (Eqn. 1).

$$S_{CO_2}(mol \cdot L^{-1}) = \frac{1}{V_m \cdot \exp\left(\frac{\alpha}{V_m^{4/3}} + \beta\right)} \qquad (1)$$

The dependence on the molar volume to the 4/3 power in Eqn. 1 originates from the use of the Kapustinskii Equation,[1, 2, 5] which has been shown to reliably calculate lattice energies of ionic crystals, and from which solubility parameters can be estimated for inorganic salts with high melting points (e.g. NaCl, KBr, etc.).[5] Takamatsu applied the Kapustinskii equation to demonstrate that RST could be applied to the

phase behaviors of aqueous and organic solutions of alkali metal salts.[6-8] However, inorganic alkali metal salts composed of spherical, atomic ions are fundamentally very different species than organic, imidazolium-based ILs composed of molecular ions. Thus, the use of the Kapustinskii Equation as a means of estimating IL solubility parameters should be further scrutinized. Experimental data,[9] group contribution methods,[10] atomistic simulations[11, 12] and direct measurements of IL vaporization enthalpies[13] show that the Kapustinskii Equation can overestimate IL solubility parameters by at least 20%.[2, 10] Interestingly, despite the discrepancies in the values of the solubility parameters calculated from these methods and Kapustinskii's Equation, Camper's model has still provided a useful approximation for predicting CO_2 solubility and selectivity trends for many 1-*n*-alkyl-3-methylimidazolium, or [$C_n$mim][X], ILs.

However, the agreement between Eqn. 1 and experimental data might be attributable to the form of Eqn. 1 itself (a type of sigmoid function), rather than presenting a global trend of gas solubility in ILs. A regression analysis of Eqn. 1 fit to the data points in Figure 5.1 reveals that the combined RST-Kapustinskii model has R^2 values of 0.7851 (25°C), 0.8471 (40°C) and 0.9485 (50°C), while the absolute errors between the experimental data and the model at of the experimental data point were within 5%. The less than optimal correlation could be attributed to the quality of the experimental data used in formulating the model, the limited number of data points around which the model was fit, and/or the fact that a single curve cannot accurately model the solubility of CO_2 across all [$C_n$mim][X] ILs, especially at lower temperatures. Finotello later confirmed that the molar volume dependence of CO_2 solubility in ILs is less pronounced at higher temperatures, as solubility tends to decrease and converge within a narrower range.[14] In fact, improved fits of Eqn. 1 to the experimental data in Figure 5.1 can be achieved by relaxing the model such that the 4/3 exponent is an optimizable constant. In this case, higher correlations can be achieved with exponents other than 4/3 (i.e. replace the 4/3 exponent with γ (gamma) in Eqn. 1) along with the new corresponding α and β values, which would not match those obtained from a linear fit of experimental data. For example, changing the exponent from 4/3 (1.333) to 5/2 (2.500) yields an R^2 value of 0.9979 for the 25°C data. However, this does not mean that gas solubility is inherently dependent on $V_m^{5/2}$, rather it is the form of Eqn. 1 that lends itself to fitting a variety of datasets arising from other functions.

A re-examination of the RST model in ILs is needed, as gas solubility might be more appropriately related to some underlying property associated with molar volume. The systematically variable nature of [$C_n$mim][X] ILs allows for incremental changes in structure to be correlated with physical properties. Such structure-property relationships have been confirmed for IL density,[15, 16] viscosity,[17] heat capacity[18] and other thermophysical properties[19, 20] that can measured with great accuracy for a large sample set of systematically varied ILs. These properties are typically rationalized through ILs with progressively larger

'C_n' groups (e.g. increasing viscosity from $[C_2mim][BF_4]$ to $[C_4mim][BF_4]$ to $[C_6mim][BF_4]$…). However, for gas solubility data, such structure-property relationships have not been fully elucidated. Due to the lack of a sufficiently thorough experimental study that not only spans the molar volume range of Camper model (Figure 5.1) but also includes a sufficient number of cation and anion species, the solubilities of CO_2 in series of $[C_nmim]$ ILs with a common anion are not available to determine the confidence intervals or bandwidth in which ILs can lie above and below the calculated lines in Figure 5.1. Deviations from the model that have been observed have been either attributed to experimental error or are due to modifying the imidazolium cation with polar groups such as ethers[21, 22] and nitriles,[10] as well as fluoroalkyls,[23, 24] siloxanes[25] and others.[26]

Work by Finotello et al. later displayed the analogous RST-based models for CH_4 and N_2 solubility for $[C_nmim][X]$ ILs that exhibited somewhat broader maxima over IL molar volumes of 400-450 cm^3 mol^{-1} (Figure 5.2).[27]

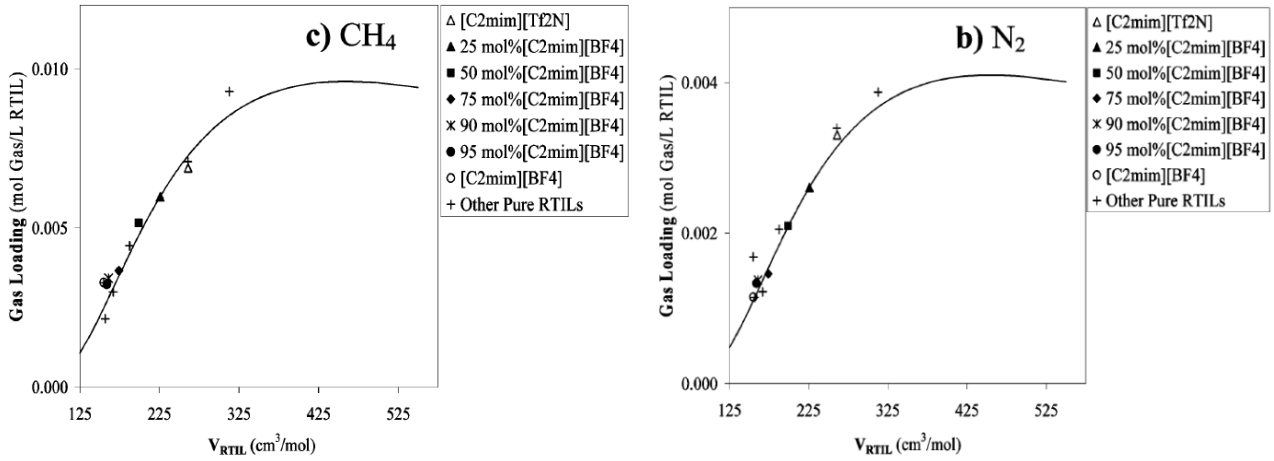

Figure 5.2: Experimental solubility data and RST model (line) for CH_4 (left) and N_2 (right) for $[C_nmim][X]$ ILs. Reprinted with permission from: Finotello, A.; Bara, J. E.; Narayan, S.; Camper, D.; Noble, R. D., Ideal gas solubilities and solubility selectivities in a binary mixture of room-temperature ionic liquids. *J. Phys. Chem. B* 2008, 112, (8), 2335-2339. Copyright 2008 American Chemical Society.

In Figure 5.2, the function relating CH_4 solubility to IL molar volume can be directly scaled from that for N_2. A similarly scalable function for carbon monoxide (CO) was also presented by Camper.[1] A regression analysis shows that the N_2 and CH_4 data reported in that work are well-described by Eqn. 1, with R^2 values >0.98 for each gas, although for reasons mentioned earlier, this does not necessarily validate Eqn. 1 as the most appropriate description. An examination of CH_4 and N_2 solubility trends in $[C_nmim][X]$ ILs reveal that those gases continue to increase in solubility while CO_2 begins to gradually decrease at molar volumes >275

$cm^3\ mol^{-1}$. While Figure 5.2 suggests that maxima for the solubility of CH_4 and N_2 would be expected in the range of 400-450 $cm^3\ mol^{-1}$, few [$C_n$mim][X] ILs this large have been synthesized which could test the limits of the model. From the standpoint of industrial practicality, those that would be found in this range would likely be too viscous for use as solvents for gas removal, and would resemble long hydrocarbon molecules much more than ILs.[28]

While only weak, apolar van der Waals interactions exist between the IL and N_2 or CH_4, the solubilities of these gases increase 2-3x with increasing molar volume (Figure 5.2). Rather than attempt to rationalize why molar volume (i.e. a larger molecule) would drive this increase, it may be more reasonable to attribute these increased solubilities to a growing void space (free volume) that might be present as molar volume increases. The ratio of empty space to occupied space in a material is known as fractional free volume (FFV).[29-31] Thus, it can be inferred that with increasing *n*-alkyl chain length, free volume increases, providing more free space for CH_4 and N_2 to dissolve. It should also seem that increasing free volume could also favor increased CO_2 dissolution, yet this is not observed. Camper's model explicitly shows that for a pair of ILs that differ only in the length of the *n*-alkyl chain, specifically [C_2mim][Tf_2N] and [C_{10}mim][Tf_2N], CO_2 solubility diminishes (Figure 5.1). Given the different behaviors between CO_2 and these gases, competing effects must exist within ILs. Gas solubility can thus be attributed to the bulk free volume, in which any gas can dissolve, and a portion of that volume which more strongly favors dissolution of CO_2. Increasing chain length tends to dilute the concentration of ions within the IL, decreasing the volume fraction of the ionic and polar components and disfavoring dissolution of gases such as CO_2.[30]

Simulations by Maginn and Cadena for [$C_n$mim] ILs with [PF_6] and [Tf_2N] anions revealed that CO_2 prefers to organize around the anion.[11, 32] However, the exact role of the anion dependence on CO_2 solubility is still somewhat ambiguous, as almost all simple anions that have been studied (perhaps with the exception of acetate anion, [OAc])[33-37] are very weak nucleophiles and should not be chemically reactive toward CO_2. Furthermore, CO_2-anion interactions would suggest that ILs with the smallest molar volumes would experience the greatest CO_2 solubility since there would be more anions present in a given volume. To the contrary, it has been shown that ILs with larger anions experience greater CO_2 solubility on basis of moles CO_2 per volume of IL.[38, 39] Furthermore, the [C_2mim][Tf_2N] and [C_{10}mim][Tf_2N] points in the Camper model implicitly suggests a balance between anion and cation sizes determines CO_2 solubility.[1, 25]

While much work has focused on tailoring the imidazolium cation to control CO_2 physical solubility,[10, 21, 23, 25, 26, 40] less work has been devoted to developing new anions, with the exception of very large perfluorinated species,[41] by which to accomplish this goal. This is presumably due to the fact that tailored imidazolium cations are much more straightforward to synthesize than novel, predominantly

inorganic anion species. Because of this, studies on gas solubility in ILs have typically focused on relatively narrow set of anions,[32, 42] and the development of ILs with increased CO_2 capacity per volume relative to Camper's model have not been reported until very recently.

Mahurin observed that the solubility of CO_2 at 25°C and 1 atm partial pressure in 1-ethyl-3-methyl tetracyanoborate ($[C_2mim][B(CN)_4]$) exceeded that in $[C_2mim][Tf_2N]$ by 30%, thus significantly exceeding the apparent upper limit of the Camper model (Figure 5.1).[39] Babarao further validated this result by computationally demonstrated that the $[B(CN)_4]$ anion plays a key role in this improved performance.[38] As the solubility level of CO_2 in $[C_2mim][B(CN)_4]$ at 1 atm was 0.13 mol CO_2 $(L\ IL)^{-1}$, this is still likely indicative of a physical solvent,[30] rather than a strong chemical reaction between CO_2 and the $[B(CN)_4]$ anion.

The recent findings related to the $[B(CN)_4]$ anion justify a reconsideration in the approach by which imidazolium-based ILs are studied for CO_2 separations, as other anions not yet studied – or even synthesized – could give rise to even higher CO_2 solubilities in ILs, which in turn could translate into breakthroughs in the performances of IL-based membranes.[1, 40, 43-47] If this is the case, it would appear that gas solubility in imidazolium-based ILs is strongly dependent on some not yet accounted for property. Across a single $[C_n mim][X]$ family of ILs, a trade-off exists between CO_2 solubility and selectivity that correlates to increasing the alkyl chain length. We recently reported this chain length effect on CO_2 solubility and selectivity across a group of 1-*n*-alkylimidazoles, neutral analogues and starting materials for imidazolium-based ILs.[28, 48] Therefore, we hypothesize that for ILs, both properties can be optimized when the cation size is minimized (e.g. short alkyl chains) and when the anion is fully delocalized and its size maximized. In other terms, ILs should be as "ionic" (or polar) as possible.

FFV is only weakly correlated to CO_2 solubility and selectivity across a wide range of molecular solvents such as methanol, acetonitrile, *n*-hexane and others.[30] However, the much higher solubility of CO_2 in these organic solvents, when compared to polymer materials, is clearly delineated by much larger FFV values in the former.[30] Lin points out that most polymers have FFV values < 0.21, while most organic solvents have FFV values >> 0.21.[30] Increased FFV can also produce exponential gains in gas permeability (diffusivity) in polymer membranes.[30, 49] For ILs, which have CO_2 solubilities between that of small organic molecules and polymers,[25] FFV values for ILs might be expected to fall between these two classes of materials.[25, 30] However, no systematic analysis of FFV in ILs has yet been reported. As this property may be key to understanding CO_2 solubility in ILs and guide the design of new ILs with improved properties, relationships between IL anion, cation and FFV must be developed.

Fundamentally, FFV appears to be a relatively simple property to calculate, requiring only a compound's molar volume (V_m) (i.e. molecular weight and density) and its van der Waals volume (V_{vdW}), according to Eqn. 2.[30, 49]

$$FFV = \frac{V_m - 1.3 \cdot V_{vdW}}{V_m} \quad (2)$$

Conventionally, V_{vdW} values are calculated from van der Waals radii (r_{vdW}), using the methods and values set forth by Bondi.[50, 51] Accurate determination of FFV in ILs can be challenging as the calculation of V_{vdW} for an IL using group contribution methods[52] requires accounting for a number of complex and charged functional groups with double and triple bonds, and perhaps relatively uncommon elements. Historically, van der Waals radii had not been established for some of the main group elements that can be included in ILs (e.g. boron, antimony).[53]

In the only report of which we are aware wherein the FFV of an IL was calculated by Bondi's methods, Li determined an FFV = 0.1145 for [C_4mim][Tf_2N].[51] However, the authors did not provide any further details or assumptions as to their approach to handling the various functional groups in calculating V_{vdW} for this IL. While there are no other comparative data available, Li's value does not appear unreasonable as ILs should be expected to have FFV in between small molecules and polymers.[25] Other works have discussed the concept of free volume in ILs and its correlation to CO_2 solubility, but there has been no dedicated effort to determine these values.[54-58] Hu presented molar volumes and van der Waals volumes of ILs, and simply reported free volume as the difference between the two quantities.[59] Application of Eqn. 2 to the reference data provided in Hu, et al.,[59] resulted in an FFV value for [C_4mim][Tf_2N] that is somewhat larger (0.1869) than Li's calculation.

A potentially very powerful and rapid approach to calculating FFV of ILs is through the use of the COSMOtherm software package, which is becoming a commonly used tool for rapidly and accurately estimating IL thermophysical properties, including gas solubilities.[60-66] In addition to very accurate calculation of IL molar volumes (i.e. densities),[66] COSMOtherm calculates a "COSMO Volume" which is the volume enclosed by the COSMO surface, or the solvent accessible area. Example COSMO structures for an IL cation and anion are shown in Figure 5.3, where blue areas and orange/red areas represent electron-sparse and electron-dense regions, respectively.

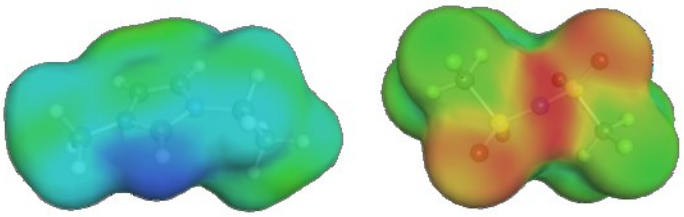

Figure 5.3: COSMO surfaces of the [C_2mim] cation (left) and [Tf_2N] anion (right).

COSMO radii for most main group elements have been shown to be *approximately* equal to 1.17 times r_{vdW},[67] although this does not necessarily mean that the COSMO volume is 1.60 times (i.e. $(1.17)^3$) the V_{vdW}. As shown in the Supporting Information, when comparing COSMO Volumes to those calculated from Bondi group contributions, we have found that for some organic molecules, the COSMO Volume is very close (± 5%) to 1.3*V_{vdW}, when V_{vdW} has been calculated from Bondi's increments. For others, the COSMO Volume can somewhat larger *or* smaller than the calculated value of 1.3*V_{vdW}. As will also be shown later, for [C_4mim][Tf_2N] we calculated an FFV of 0.1281, which is within 10% of the value of 0.1145 calculated by Li from Bondi's methods.

As the COSMO Volume can be rapidly calculated for complex molecules such as ILs, and that it may be directly applicable for calculating FFV and free volume, we have employed COSMOtherm in this task for 165 existing and theoretical [$C_n$mim][X] ILs. In each of the 15 families of ILs examined, the FFV of the IL (FFV_{IL}) is shown to increase with increasing *n*-alkyl chain length toward an apparent asymptote of FFV = 0.22, as the volume fraction of the *n*-alkyl chain approaches unity and the volume occupied by the ions approaches zero. The function relating FFV_{IL} to IL molar volume can then be incorporated within RST to produce an equation for gas-specific Henry's Constants in each [$C_n$mim][X] family where free volume, rather than molar volume, is the independent variable. Furthermore, by utilizing computation results and experimental decreases in CO_2 solubility with increasing free volume can be rationalized. Solubility selectivity for CO_2 can be approximated as inversely proportional to IL free volume to the 3/2 power, showing a very similar trend to experimental data. The results present a new dimension by which to consider the design of [$C_n$mim][X] ILs for CO_2 removal.

5.2 Revisiting the Application of Regular Solution Theory to ILs: First, the application of RST to imidazolium-based ILs must be revisited in order to develop a more complete and rigorous approach to gas solubility in ILs. Eqn. 3 presents a correlation to RST, where $H_{2,1}$ is the Henry's Law Constant, where the subscripts 1 and 2, respectively indicate the IL and the gas.[68, 69]

$$\ln(H_{2,1}) = a + b(\delta_1 - \delta_2)^2 \tag{3}$$

Rather than applying any simplifications or assumptions to Eqn 3., the fundamental definition of the IL solubility parameter will be applied, i.e. the square root of the cohesive energy density (Eqn. 4). In Eqn. 4, δ_i is the solubility parameter, H_{vap} is the enthalpy of vaporization, R is the gas constant and T is absolute temperature.

$$\delta_i = \sqrt{\frac{H_{vap} - RT}{V_m}} \tag{4}$$

H_{vap} for a given series of ILs with common anions (e.g. $[C_n mim][Tf_2N]$) can be well-represented as a linear function of molar volume[70] according to Eqn. 5:

$$H_{vap} = A \cdot V_m + B \tag{5}$$

Thus, substitution of Eqn. 5 for H_{vap} in Eqn. 4 yields the following result (Eqn. 6).

$$\delta_i = \sqrt{\frac{A \cdot V_m + B - RT}{V_m}} \tag{6}$$

At a constant temperature (e.g. 298 K), Eqn. 6 reduces to Eqn. 7, where B* = B-RT.

$$\delta_i = \sqrt{\frac{A \cdot V_m + B^*}{V_m}} \tag{7}$$

For convenience, Equation 7 is further simplified to Eqn. 8.

$$\delta_i = \sqrt{A + \frac{B^*}{V_m}} \tag{8}$$

The expression for the solubility parameter for a [$C_n$mim][X] series of IL given by Eqn. 8 is thereby substituted for δ_1 in Eqn. 3, resulting in Eqn. 9, which describes the solubility of a gas in a series of ILs with common anions as a function of molar volume.

$$\ln(H_{2,1}) = a + b\left(\sqrt{A + \frac{B^*}{V_m}} - \delta_2\right)^2 \tag{9}$$

Expansion of Eqn. 9 yields Eqn. 10, a full expression of RST relationship for Henry's Constants in ILs.

$$\ln(H_{2,1}) = a + b\left[A + \frac{B^*}{V_m} - 2\delta_2\sqrt{A + \frac{B^*}{V_m}} + \delta_2{}^2\right] \tag{10}$$

Combining the constants in Eqn. 10, results in a simplified form of the RST equation (Eqn. 11).

$$\ln(H_{2,1}) = d + \frac{c}{V_m} - \left[a' + \frac{b'}{V_m}\right]^{0.5} \tag{11}$$

Through a regression analysis (see Supporting Information), it can be shown that the form of Eqn. 11 is very-well approximated by Eqn. 12 ($R^2 > 0.99$), which can then be written explicitly for the Henry's Constant in terms of the molar volume (Eqn. 13).

$$\ln(H_{2,1}) = d' + \frac{c'}{V_m} \tag{12}$$

$$H_{2,1} = D\exp\left(\frac{c'}{V_m}\right) \tag{13}$$

Eqn. 13 is useful for describing Henry's constants, or mole fraction-based solubility across a [$C_n$mim][X] IL family. Eqn. 13 also serves to confirm that there is no inherent dependence relating gas solubility to a molar volume term with a 4/3 exponent. To examine the validity of Eqn. 13, experimentally determined Henry's constants data for selected [$C_n$mim][Tf_2N] ILs were applied, as summarized in Table 5.1.[25]

Table 5.1: Data for selected [$C_n$mim][Tf_2N]] ILs relating Henry's constants to molar volume.

Cation	Anion	H CO_2 (atm)	V_m (cm^3 mol^{-1})/100
C_2mim	Tf_2N	37	2.561
C_4mim		35	2.901
C_6mim		33	3.240
C_{10}mim		29	3.916

A fit of the data in Table 5.1 to Eqn. 13 yielded coefficients of D = 18.87 atm, and c' = 1.756 (cm^3 mol^{-1}/100), with an R^2 value of 0.9714, indicating Eqn. 13 is valid for [$C_n$mim][X] ILs with incrementally larger alkyl chains. The D coefficient has a rational physical basis, in that D represents the asymptotic value of the Henry's constant at large molar volumes. Although the physical implications of c' is not entirely clear at this time, it may represent a transition or "tipping point" between cation-anion and alkyl chain interactions with the gas.

As researchers and engineers should be ultimately interested in the solubility of a gas in a given volume of IL,[25, 39, 40] solubility of gases in liquids should also be reported on a basis of moles of gas per volume of solvent. Volume-based solubility data provide more convenient engineering guidance than mole fraction solubility in terms of designing solvent and membrane-based processes for industrial gas treating, CO_2 capture, etc., as the amount of CO_2 that can be absorbed in a given volume is one of the most critical considerations in process scale and cost. Calculation of both Henry's constants and volume-based solubility from experimental data is trivial.[25] Camper applied Eqn. 14 to convert Henry's constants to volume-based solubility (mol gas (L IL)$^{-1}$ atm^{-1}), where V_m is the IL molar volume (L mol^{-1}).[1]

$$S_{2,1} \approx \frac{1}{H_{2,1} \cdot V_m} \tag{14}$$

Eqn. 14 more accurately approximates sparingly soluble gases (e.g. N_2, CH_4 and H_2) than moderately soluble gases such as CO_2. At a given temperature and pressure, the mole fraction of CO_2 in ILs is 1-2 orders of magnitude greater than these other gases, and one of the assumptions applied to Eqn. 14 is that the term for moles of gas in the denominator of the mole fraction term in the Henry's constant can be neglected. This assumption may result in disagreements between experimentally determined and calculated values, even at low pressures (e.g. 1 – 5 atm). For example, in our prior work with 1-*n*-alkylimidazoles, we reported a Henry's constant for CO_2 in 1-methylimidazole of 109 (+/- 2) atm, with a corresponding CO_2 solubility per volume of 2.71 (+/- 0.04) cm^3 (STP) (cm^3 solvent)$^{-1}$ atm^{-1}, as calculated from a mole balance.[28] If this Henry's constant were used as the input for Eqn. 14, a value of 2.58 cm^3 (STP) (cm^3 solvent)$^{-1}$ atm^{-1} would be calculated, or a ~4% difference from the mole balance value. While 4% is a seemingly small error, the larger V_m values of ILs will multiply the effects of this assumption. Thus, it may be preferable to calculate CO_2 solubility per unit volume directly from a mole balance.[28, 48]

Having discussed and examined the solubility of gases in ILs with respect to molar volume, an underlying relationship to free volume must be determined. If free volume governs gas solubility in [$C_n$mim][X] ILs, as has been deduced from the solubilities of N_2 and CH_4 with respect to IL molar volume (Figure 5.2), then a function to relate IL molar volume to FFV_{IL} must be developed. Thus, we propose that to better understand the solubilities of CO_2, N_2 and CH_4 in [$C_n$mim][X] ILs, all which is needed is a means of

accurately modeling free volume and FFV_{IL}. COSMOtherm is a powerful and versatile tool that can be employed in this task.

5.3 Computational Methods: A set of eleven systematically varied [$C_n$mim] cations (Figure 5.4) and fifteen anions (Table 5.1) were selected for use within COSMOtherm. Densities, molar volumes and COSMO volumes were obtained for each of the 165 cation-anion combinations considered. When available, cation and anion species were used from the COSMObase library obtained from the software provider (COSMOlogic GmbH, Leverkusen, Germany). For those cation and anion species not available within COSMObase, COSMO files were developed by our group. Optimized structures of cations and anions were developed with TURBOMOLE,[71] using the triple-zeta valence potential (TZVP) basis set[72] with the Becke and Perdew (b-p)[73, 74] functional at the density functional theory (DFT) level. All COSMO calculations were performed at the TZVP level of theory, consistent with other published works on ILs that have utilized COSMOtherm.[60-62, 64, 65]

methyl (C_1); ethyl (C_2); propyl (C_3); butyl (C_4)**;**
pentyl (C_5); hexyl (C_6)**; heptyl (C_7)**; octyl (C_8)**;**
decyl (C_{10}); dodecyl (C_{12}); tetradecyl (C_{14})

***included within COSMOBase Library*

Figure 5.4: Structures of [$C_n$mim] cations examined.

Table 5.2: Anion species examined.

Tetrafluoroborate (BF_4)**		Fluorosulfonimide (FSI)	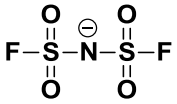
Hexafluorophosphate (PF_6)**	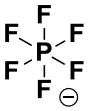	Bis(triflluoromethyl sulfonyl)imide (Tf_2N)**	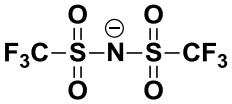
Hexafluoroantimonate (SbF_6)	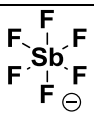	bis(perfluoroethyl sulfonyl)imide (beti)	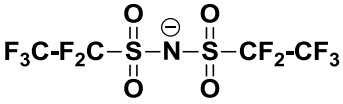
Methanesulfonate (OMs)	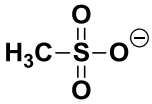	Dicyanamide ($N(CN)_2$)	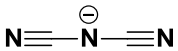
Methylsulfate ($MeSO_4$)	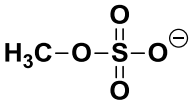	Tricyanomethane ($C(CN)_3$)	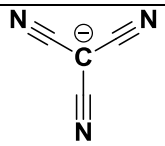
Ethylsulfate ($EtSO_4$)**	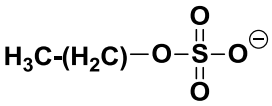	Tetracyanoborate ($B(CN)_4$)	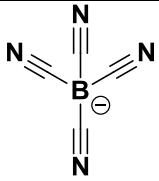
Trfilate (OTf)	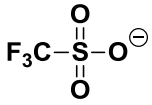	Hexacyanophosphate ($P(CN)_6$)	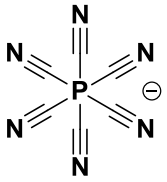
		Hexacyanoantimonate ($Sb(CN)_6$)	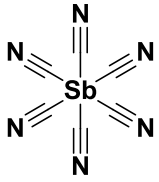

*Cells with bold outlines indicate theoretical species.

** Species included within COSMOBase library.

Using the density application within COSMOtherm, IL molar volumes (V_m) were calculated at 25°C, and were found to be within ± 1-2% of experimental values (for those species where experimental data is

available). FFV_{IL} was then calculated as described earlier, according to Eqn. 15, where the term ($V_m - V_{COSMO}$) is taken to be the molar free volume, V_f ($cm^3\ mol^{-1}$).

$$FFV_{IL} = \frac{V_m - V_{COSMO}}{V_m} \tag{15}$$

5.4 Experimental Section

5.4.1 Materials: All chemicals were obtained from Sigma-Aldrich (Milwaukee, WI USA) and were used without further purification. [$C_n$mim][BF_4] ILs (n = 2, 4, 6, 8) were synthesized in our laboratory using established procedures.[14, 27]

5.4.2 CO_2 Solubility Measurements: Solubility of CO_2 in each of the [$C_n$mim][BF_4] ILs at low pressure (~5 atm) and ambient temperature (25°C) was measured using the same apparatus and similar methodology as described in our previous work.[28, 48, 75]

5.5 Results & Discussion: Although ILs with *n*-alkyl chain lengths ranging from methyl (C_1) to tetradecyl (C_{14}) were examined computationally, it cannot be certain that all of these imidazolium salts are in fact liquids at room temperature, nor we did not attempt to exclude any ILs based on this criteria. Additionally, we do recognize that many [$C_n$mim][X] ILs with chain lengths > decyl (C_{10}) will tend to have melting points greater than 25°C.[76] We also advise the reader that all of the ILs we have considered here may not yet have been synthesized and characterized in the literature. Furthermore, the [$P(CN)_6$] and [$Sb(CN)_6$] anions are logical extensions of the cyano series, but are currently hypothetical constructs, as no synthetic report of either anion has yet to appear in the literature.

Figure 5.5 displays calculated FFV_{IL} values (as data points) with respect to IL molar volume in each [$C_n$mim][X] series. For simplicity, the IL molar volumes are presented in units of cubic centimeters per mole of IL divided by 100 (i.e. $cm^3\ mol^{-1}/100$). Recognizing from Figure 5.5 that FFV_{IL} increases with increasing IL molar volume via introduction of incremental -CH_2- groups, ultimately, FFV_{IL} should asymptote to the value associated with the -CH_2- group, as sufficiently large [$C_n$mim][X] ILs will far more resemble long alkanes or polyethylene than the small cations from which they were extended. We propose Eqn. 16 as a simple

function that can relate FFV_{IL} to IL molar volume for the range of compounds studied and will approach an asymptote as the alkyl chain becomes very large.

$$FFV_{IL} = Q + \frac{Z}{V_m} \tag{16}$$

Also presented in Figure 5.5 is the fitted function to each [$C_n$mim][X] data set (as solid lines) obtained via the curve fitting tool in Matlab.

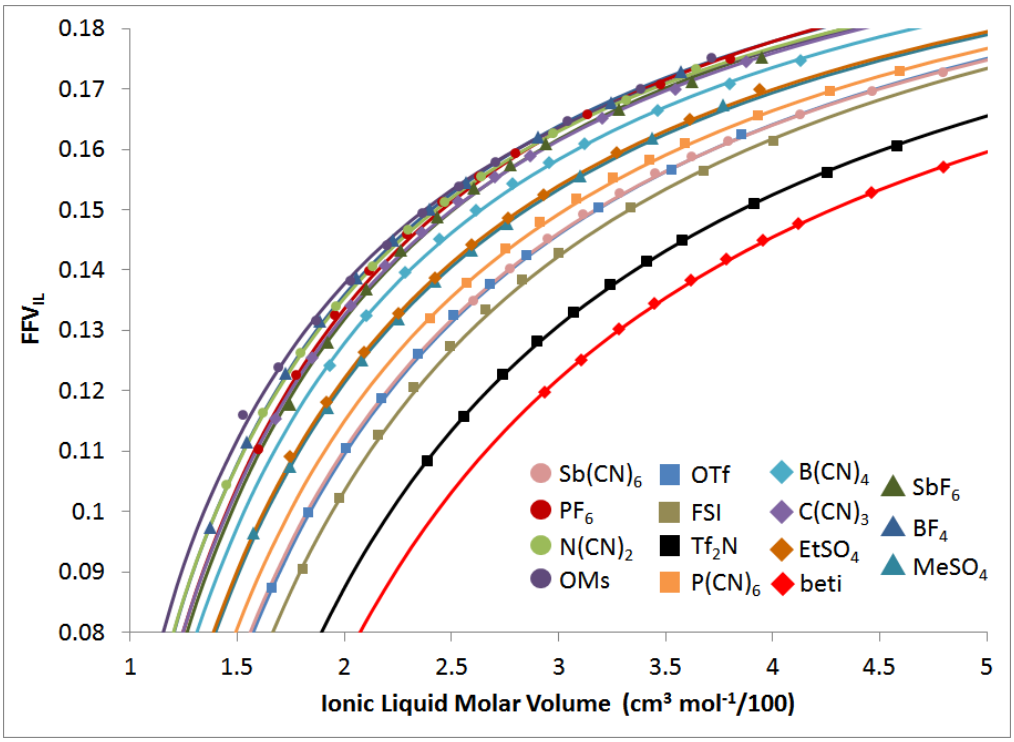

Figure 5.5: Calculated data points and fitted functions (lines) for FFV_{IL} with respect to IL molar volume at 25°C.

Figure 5.5 illustrates that FFV_{IL} increases with increasing IL molar volume and the models tend toward asymptotes. It should be noted that these points include ILs with cation substituents as large as tetradecyl ([C_{14}mim]), although in many of these [$C_n$mim][X] families, [C_{10}mim] and larger cations may not actually exist in the molten state at 25°C,[76] so some cation-anion combinations would not be considered 'ILs' under this condition. Figure 5.5 also shows that for any given molar volume, almost all [$C_n$mim][X] ILs fall

within a narrow range of FFV_{IL}. The $[C_n mim][Tf_2N]$ and $[C_n mim][beti]$ series are the only IL families that fall slightly outside the general cluster, though this may be due to the fact that these highly fluorinated anions are much bulkier and of a larger molecular weight than the other species of interest, or some correction may be need to be applied to the COSMOTherm data when handling fluoroalkyl-containing species. We will certainly consider this as a potential refinement to the model in future work. As an aside, Figure 5.5 suggests that although Figures 5.1 and 5.2 present models for imidazolium-based ILs with molar volumes as large as 900 $cm^3\ mol^{-1}$, few ILs will actually possess molar volumes larger than 400 $cm^3\ mol^{-1}$.

It is apparent from Figure 5.5 that Eqn. 16 presents an accurate model of FFV_{IL}. Table 5.3 reports the fitted constants Q and Z with the respective functions for each anion species in Eqn. 16, where Q can be considered as the asymptotic value of FFV_{IL} as the alkyl chain becomes exceedingly long and Z is the contribution of the cation-anion pair to FFV_{IL}. As a validation of the asymptotic behavior of ILs with large alkyl chains, FFV values of *n*-alkanes calculated from the COSMO volume are also observed to asymptote toward a value of ~0.20, and these data are provided as Supporting Information.

Table 5.3: Fitted Q and Z coefficients and overall quality of fit for each $[C_n mim][X]$ series for FFV_{IL} in Eqn. 16.

Anion (X^-)	Q [-]	Z (cm^3/mol)/100)	R^2
BF_4	0.2199	-0.1680	0.9998
PF_6	0.2222	-0.1772	0.9983
SbF_6	0.2213	-0.1788	0.9982
OMs	0.2154	-0.1553	0.9976
$MeSO_4$	0.2175	-0.1923	0.9997
$EtSO_4$	0.2178	-0.1914	0.9997
OTf	0.2188	-0.2186	0.9999
FSI	0.2201	-0.2333	0.9993
Tf_2N	0.2177	-0.2607	0.9998
beti	0.2160	-0.2820	0.9998
$N(CN)_2$	0.2183	-0.1658	0.9999
$C(CN)_3$	0.2194	-0.1737	0.9996
$B(CN)_4$	0.2193	-0.1828	0.9994
$P(CN)_6$	0.2179	-0.2058	0.9993
$Sb(CN)_6$	0.2179	-0.2153	0.9995

FFV_{IL} as a function of molar volume is thus shown to be well-described by Eqn. 16, such that it can then be rearranged to calculate free volume (V_f) as a function of molar volume (V_m). Substituting V_f/V_m for FFV_{IL} results in Eqn. 17.

$$\frac{V_f}{V_m} = Q + \frac{Z}{V_m} \tag{17}$$

Eqn. 17 is simplified to Eqn. 18, an explicit function for V_f in terms of V_m.

$$V_f = Q \cdot V_m + Z \tag{18}$$

A plot of V_f against V_m verifies this linear relationship (Figure 5.6), and also illustrates that at a given molar volume, [$C_n$mim][X] ILs tend to exhibit very similar free volumes (+/- 10 cm^3 mol^{-1}).

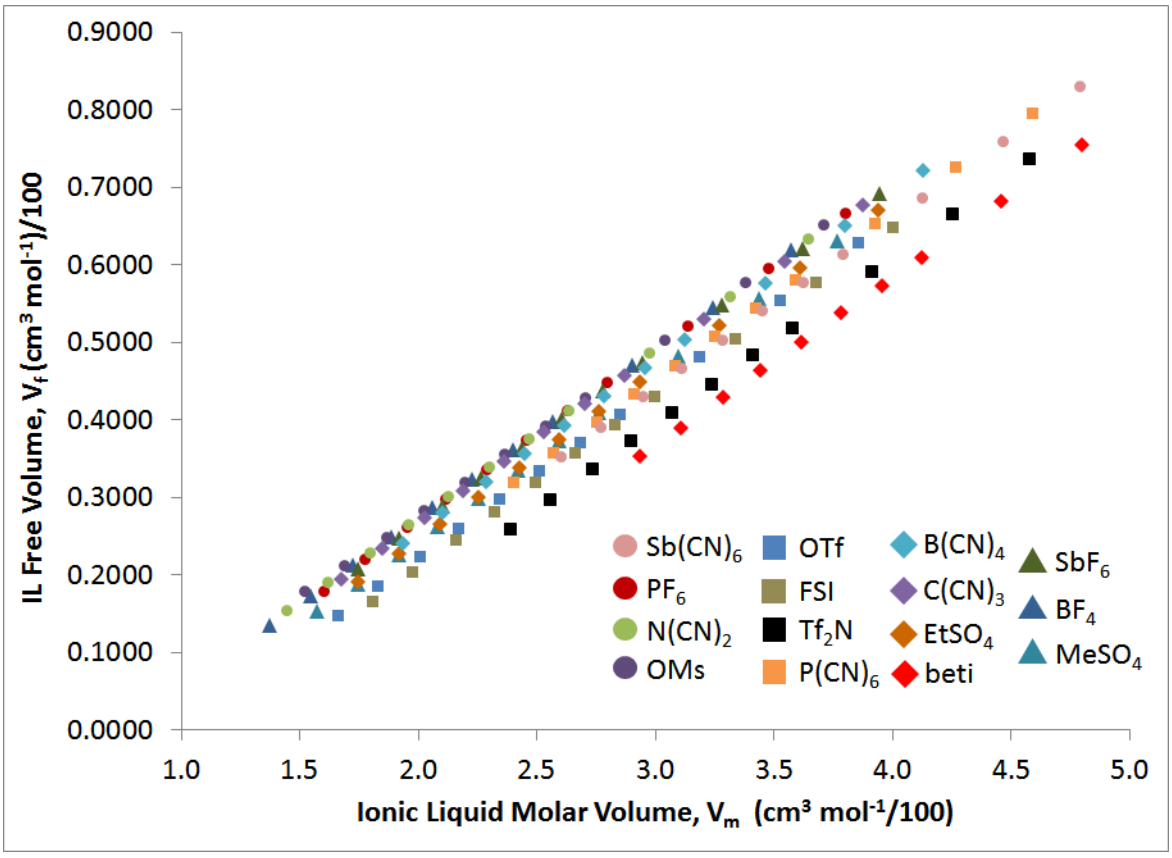

Figure 5.6: Plot of calculated IL free volume (V_f) against IL molar volume (V_m).

A rearrangement of Eqn. 18 results in Eqn. 19, where V_m is a function of V_f.

$$V_m = \frac{V_f}{Q} - Z \tag{19}$$

Eqn. 19 can now be used as a means to re-write Eqn. 13 in terms of IL free volume (V_f) rather than molar volume (V_m), as the independent variable determining gas solubility in ILs. First, substitution of Eqn. 19 into Eqn. 14 results in Eqn. 20, which relates the Henry's Constant to IL free volume.

$$H_{2,1} = D \cdot \exp\left(\frac{c'}{\frac{V_f}{Q} - Z} \right) \tag{20}$$

Although many ILs have been studied in the context of CO_2 solubility, there have been few studies dedicated to a systematic analysis of CO_2 solubility in a series of ILs with common anions. As many reports still present somewhat different values of Henry's Constants for the same ILs, sufficient and consistent data are not conveniently available to validate Eqn. 20 across most of the [$C_n$mim][X] ILs presented within Figure 5.4 and Table 5.2. Furthermore, focus is often given only to CO_2, so even fewer consistent and reliable N_2 and CH_4 data are available; and the solubilities of these gases are often more difficult to accurately quantify. We have previously described the inherent challenges associated with measuring the solubilities of CH_4 and N_2 (and by extension, the especial difficulties with H_2) in organic solvents via pressure decay or combined pressure decay/gravimetric techniques.[28, 48] Thus, we had focused on the literature data for the [$C_n$mim][Tf_2N] series earlier in the discussion and now to our own experimental work for the [$C_n$mim][BF_4] series as a means to confirm the link between free volume and CO_2 solubility. Table 5.4 presents CO_2 solubility measurements for [$C_n$mim][BF_4] ILs obtained in our laboratory at near-ambient temperature and low pressure. We employed a relatively large volume of solvent (40-50 mL) in order to minimize experimental error by absorbing > 1.00 g of CO_2 in the ILs. This required a CO_2 partial pressure of ~5 atm and the Henry's constants obtained were assumed to be independent of pressure under this condition.

Table 5.4: Experimental data for CO_2 solubility in selected $[C_n mim][BF_4]$ ILs at 298K and low pressure.

IL	V_m [a]	FFV_{IL}	V_f [a]	V_f* [b]	H CO_2 (atm)		S CO_2 [c]		S CO_2 [d]	
$[C_2mim][BF_4]$	1.549	0.1115	0.1728	1.1149	79.0	±1.1	1.96	±0.03	0.088	±0.001
$[C_4mim][BF_4]$	1.874	0.1314	0.2462	1.3138	52.7	±0.6	2.48	±0.04	0.111	±0.001
$[C_6mim][BF_4]$	2.209	0.1450	0.3203	1.4496	47.8	±0.7	2.35	±0.03	0.105	±0.001
$[C_8mim][BF_4]$	2.542	0.1545	0.3927	1.5451	42.9	±0.5	2.32	±0.03	0.103	±0.001

a: $(cm^3\ mol^{-1})/100$

b: $(cm^3\ L^{-1})/100$

c: $(cm^3\ (STP)\ (cm^3\ IL)^{-1}\ atm^{-1})$

d: $(mol\ (L\ IL)^{-1}\ atm^{-1})$

Our experimentally determined Henry's Constant for CO_2 in $[C_4mim][BF_4]$ is comparable to that reported by Cadena (56.5 ± 1.4 bar)[32] and those for CO_2 in $[C_6mim][BF_4]$ and $[C_8mim][BF_4]$ are consistent with recent data by Moganty (57 ± 4 atm & 43 ± 5 atm, respectively) .[77] While the value of 79.0 atm for $[C_2mim][BF_4]$ appears to be significantly higher than the other members of this series, our measurements are in line with the values reported by Finotello (80 ± 4 atm)[14] and Kim (77 atm).[78]

Using the Q and Z values for $[C_n mim][BF_4]$ ILs (Table 5.3), a fit of the Henry's constants in Table 5.4 to Eqn. 20 yielded coefficients of D = 22.59 atm and c' = 1.179 ($cm^3\ mol^{-1}/100$) with $R^2 = 0.9752$. The utility of Eqn. 20 for relating Henry's Constants to the free volume within an IL is thus shown to be consistent and compatible with experimental results.

Table 5.4 clearly shows that although Henry's constants decrease, implying an increase in CO_2 solubility in terms of mole fraction for $[C_4mim][BF_4]$ – $[C_8mim][BF_4]$, the moles of CO_2 that can be absorbed in a given volume actually decrease with increasing chain length. The data in the two rightmost columns verify that a negative impact on CO_2 solubility is associated with extension of the alkyl group. CO_2 exhibits a much lower solubility in $[C_2mim][BF_4]$ per unit volume than the rest of this series, which was also observed by Finotello. It has been proposed that the strong hydrogen-bonding interactions between cation and anion in this IL result in a fundamentally different arrangement of cations and anions at the molecular level,[79] which may inhibit CO_2-ion interactions and thus significantly reduce the capacity of the IL for CO_2.

For $[C_4mim][BF_4]$ – $[C_8mim][BF_4]$, CO_2 solubility is observed to decrease with increasing chain length or increasing free volume. To relate the S_{CO2} data (mol CO_2 $(L\ IL)^{-1}$ atm^{-1}) to the free volume in a liter of the IL (V_f*), the data in Table 5.4 were fit to Eqn. 21.

$$S_{CO_2} = \frac{m}{\left(V_f^*\right)^n} \tag{21}$$

Applying Eqn. 21 to the [C_4mim]-[C_8mim][BF_4] series yielded coefficient values of m = 0.1245 and n = 0.449 with R^2 = 0.9809. In accounting for the error of the experimental data, fits of the data yield values of the exponent that vary between 0.400-0.500. This experimental data for CO_2, along with the data in Figures 5.1 and 5.2, confirm that solubility of CO_2 in a given volume of IL has a fundamentally different dependence on free volume than the solubilities of gases such as N_2 and CH_4, which appear to exhibit a linear relationship (Eqn. 22).

$$S_j \propto V_f^* \tag{22}$$

Thus, if Eqns. 21 and 22 are valid, then the quotient of S_{CO2}/S_j will represent the solubility selectivity and display a similar trend to experimentally determined data. As the solubility of CO_2 is approximately dependent on V_f* to the -0.5 power, the solubility selectivity should be proportional to V_f* to the -1.5 power (Eqn. 23).

$$\frac{S_{CO_2}}{S_j} \propto \frac{\left(V_f^*\right)^{-0.5}}{V_f^*} = \left(V_f^*\right)^{-1.5} \tag{23}$$

Figure 5.7 presents a plot of calculated $(V_f)^{-1.5}$ values for the 15 series examined against the IL molar volume, and shows an asymptotic increase as the molar volume approaches ~150 $cm^3\ mol^{-1}$. Figure 5.10 has been reproduced from the literature to show other models and experimental data points for CO_2/CH_4 and CO_2/N_2 selectivities in [$C_n$mim][X] ILs. It should be noted that in Figure 5.8, Scovazzo's Universal Model is based on gas permeability, which is largely comprised of solubility selectivity but includes minor contributions for diffusion selectivity. We do acknowledge that values of m and n in Eqn. 21 may not be the

same for all IL families, but given the tremendous experimental effort required to determine that dependence, we base our model on the convenient value of n = 0.500 at this time.

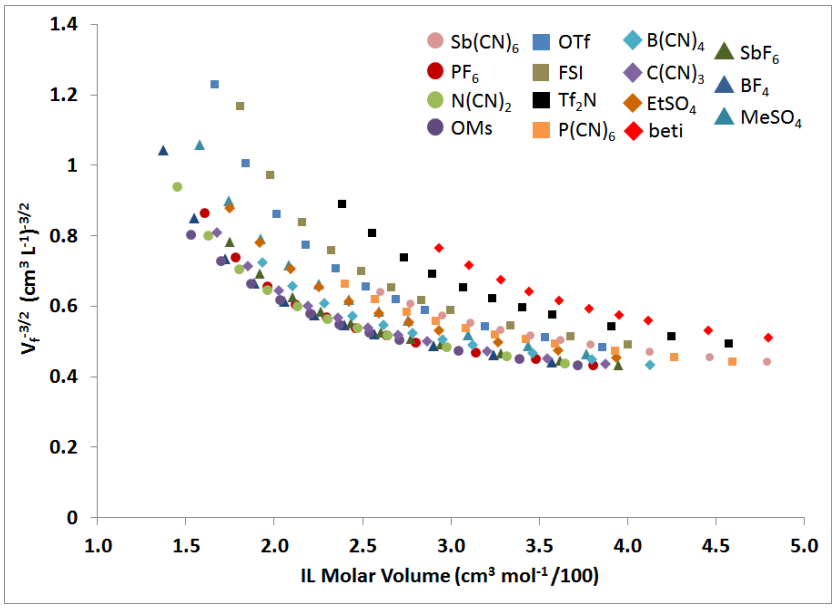

Figure 5.7: Plot of $(V_f^*)^{-3/2}$ for $[C_n mim][X]$ ILs relative to IL molar volume ($cm^3\ mol^{-1}$ / 100).

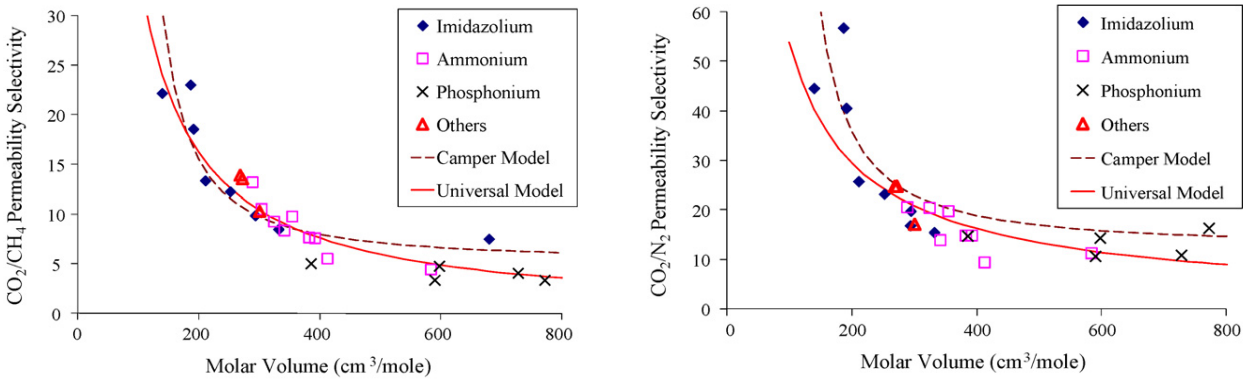

Figure 5.8: CO_2/CH_4 (left) and CO_2/N_2 (right) solubility selectivities in imidazolium-based and other ILs as put forth by the Camper and Universal Models. Reprinted from *Journal of Membrane Science*, 343, Scovazzo, P. Determination of the upper limits, benchmarks, and critical properties for gas separations using stabilized room temperature ionic liquid membranes (SILMs) for the purpose of guiding future research, Pages 199-211, 2009, with permission from Elsevier.

Figure 5.7 exhibits striking similarities to the Camper Model and Scovazzo's Universal Model, (Figure 5.8), both in terms of shape of the data cluster and the relative span of the y-axis. In all cases, selectivity is observed to rapidly increase at molar volumes below 200 $cm^3\ mol^{-1}$, while almost all ILs begin to converge

into a relatively tight cluster above 300 cm^3 mol^{-1}. Similar to Figures 5.5 and 5.6, the relative positions of certain IL families, such as [Tf_2N] and [beti], on the y-axis may slightly overstated as these ILs would be expected to fall closer to the general cluster based on experimental data. However, Figures 5.7 and 5.8 clearly suggest that CO_2 selectivity is governed by how much larger a given IL is relative to the smallest members of its group. Ideal combinations of high CO_2 solubility and selectivity could be achievable if free volume is increased while the molar volume is minimized. In other terms, the ILs should be as "ionic" as possible with small cations and large, delocalized anions. Ultimately, new anion species are likely to be required to determine if a breakthrough in performance of imidazolium-based ILs can be achieved.

5.6 Conclusions: A re-examination of prior RST-based models for CO_2 solubility and selectivity in imidazolium-based ILs revealed that dependence of these properties on the IL molar volume to the 4/3 power does not necessarily exist. Furthermore, a critical examination at reported experimental data for solubility of CO_2, N_2 and CH_4 with respect to IL structure indicated that free volume can serve as the basis of gas solubility and selectivity. Through examination of 165 actual and theoretical combinations of cations and anions using COSMOtherm to calculate only the molar volumes and COSMO volumes of these ILs, in combination with the revised RST model and experimental data, we have confirmed a link between free volume and gas solubility and selectivity in ILs. FFV as calculated by COSMOTherm can provide new insights into gas solubility and selectivity in imidazolium-based ILs. The results of this study suggest that hydrocarbon bulk on the anion must be minimized while anions should be large and fully delocalized in order to achieve optimal combinations of CO_2 solubility and selectivity.

[$C_n$mim] cations and various anions explored in this work encompass but a small fraction of possible IL species. Future work utilizing COSMOtherm will consider the effects of groups such as ethers, nitriles, fluoroalkyls, aromatics and cycloalkyls and their effects on FFV_{IL}, gas solubility and selectivity. Furthermore, this approach can also likely be applied to understanding the performances of and developing new design criteria of other IL-based materials for CO_2 separations including IL and poly(IL) membranes[47, 80, 81] and sorbents,[82, 83] as well as perhaps in other IL-based applications.[84-86]

Acknowledgments

Support for this work provided by ION Engineering, LLC; United States Department of Energy – National Energy Technology Laboratory (DE-FE00005799); and the National Science Foundation Research Experiences

for Undergraduates Program (EEC-1062705) is gratefully acknowledged. J.E.B. also wishes to thank David Gallagher of CACheResearch, LLC and Frank Eckert of COSMOLogic GmbH for their helpful discussions on COSMOtherm and the COSMO Volume.

Supporting Information Available (*See Section 5.8*)

Comparison of FFV calculated from Bondi values to COSMO FFV for selected organic solvents. Tables of molecular weight, density, molar volume, COSMO volume, fractional free volume and related values for each of the 15 [$C_n$mim][X] IL series. Images of COSMO surfaces for the 11 cations and 15 anion species examined. Examples of approximations for Eqn. 11. An analysis of FFV as calculated by COSMOTherm for *n*-alkanes. This material is available free of charge via the Internet at http://pubs.acs.org.

5.7 References:

1. Camper, D.; Bara, J.; Koval, C.; Noble, R., Bulk-fluid solubility and membrane feasibility of Rmim-based room-temperature ionic liquids. *Ind. Eng. Chem. Res.* 2006, *45*, 6279-6283.
2. Camper, D.; Becker, C.; Koval, C.; Noble, R., Low pressure hydrocarbon solubility in room temperature ionic liquids containing imidazolium rings interpreted using regular solution theory. *Ind. Eng. Chem. Res.* 2005, *44*, 1928-1933.
3. Camper, D.; Scovazzo, P.; Koval, C.; Noble, R., Gas solubilities in room-temperature ionic liquids. *Ind. Eng. Chem. Res.* 2004, *43*, 3049-3054.
4. Scovazzo, P.; Camper, D.; Kieft, J.; Poshusta, J.; Koval, C.; Noble, R., Regular solution theory and CO_2 gas solubility in room-temperature ionic liquids. *Ind. Eng. Chem. Res.* 2004, *43*, 6855-6860.
5. Kapustinskii, A. F., Lattice energy of ionic crystals. *Q. Rev. Chem. Soc,* 1956, *10*, 283-294.
6. Takamatsu, T., Application of the regular solution theory to the ion-pair systems. *Bull. Chem. Soc. Jap.* 1974, *47*, 1287-1288.
7. Takamatsu, T., Solubility studies of ion-pairs in organic solvents. *Bull. Chem. Soc. Jap.* 1974, 47, 1285-1286.
8. Takamatsu, T., Solubility study of ion pairs in organic solvents. *Bull. Chem. Soc. Jpn.* 1974, 47, 2647-2649.
9. Lee, S. H.; Lee, S. B., The Hildebrand solubility parameters, cohesive energy densities and internal energies of 1-alkyl-3-methylimidazolium-based room temperature ionic liquids. *Chem. Commun.* 2005, *27*, 3469-3471.
10. Carlisle, T. K.; Bara, J. E.; Gabriel, C. J.; Noble, R. D.; Gin, D. L., Interpretation of CO_2 solubility and selectivity in nitrile-functionalized room-temperature ionic liquids using a group contribution approach. *Ind. Eng. Chem. Res.* 2008, *47*, 7005-7012.
11. Maginn, E. J., Molecular simulation of ionic liquids: current status and future opportunities. *J. Phys.-Condens. Mat.* 2009, *21*, 17.
12. Morrow, T. I.; Maginn, E. J., Molecular Dynamics Study of the Ionic Liquid 1-*n*-Butyl-3-methylimidazolium Hexafluorophosphate. *J. Phys. Chem. B* 2002, *106*, 12807-12813.
13. Emel'yanenko, V. N.; Zaitsau, D. H.; Verevkin, S. P.; Heintz, A.; Voss, K.; Schulz, A., Vaporization and Formation Enthalpies of 1-Alkyl-3-methylimidazolium Tricyanomethanides. *J. Phys. Chem. B* 2011, *115*, 11712-11717.

14. Finotello, A.; Bara, J. E.; Camper, D.; Noble, R. D., Room-temperature ionic liquids: Temperature dependence of gas solubility selectivity. *Ind. Eng. Chem. Res.* 2008, *47*, 3453-3459.
15. Gardas, R. L.; Coutinho, J. A. P., Extension of the Ye and Shreeve group contribution method for density estimation of ionic liquids in a wide range of temperatures and pressures. *Fluid Phase Equilibr.* 2008, *263*, 26-32.
16. Ye, C. F.; Shreeve, J. M., Rapid and accurate estimation of densities of room-temperature ionic liquids and salts. *J. Phys. Chem. A* 2007, *111*, 1456-1461.
17. Gardas, R. L.; Coutinho, J. A. P., A group contribution method for viscosity estimation of ionic liquids. *Fluid Phase Equilibr.* 2008, 266, (1-2), 195-201.
18. Paulechka, Y. U., Heat Capacity of Room-Temperature Ionic Liquids: A Critical Review. *J. Phys. Chem. Ref. Data* 2010, 39, 033108-23.
19. Aparicio, S.; Atilhan, M.; Karadas, F., Thermophysical Properties of Pure Ionic Liquids: Review of Present Situation. *Ind. Eng. Chem. Res.* 2010, 49, (20), 9580-9595.
20. Rooney, D.; Jacquemin, J.; Gardas, R., Thermophysical Properties of Ionic Liquids. In *Ionic Liquids*, Kirchner, B., Ed. Springer Berlin / Heidelberg: 2010; Vol. 290, pp 185-212.
21. Bara, J. E.; Gabriel, C. J.; Lessmann, S.; Carlisle, T. K.; Finotello, A.; Gin, D. L.; Noble, R. D., Enhanced CO_2 separation selectivity in oligo(ethylene glycol) functionalized room-temperature ionic liquids. *Ind. Eng. Chem. Res.* 2007, *46*, 5380-5386.
22. Smith, G. D.; Borodin, O.; Li, L. Y.; Kim, H.; Liu, Q.; Bara, J. E.; Gin, D. L.; Nobel, R., A comparison of ether- and alkyl-derivatized imidazolium-based room-temperature ionic liquids: a molecular dynamics simulation study. *Phys. Chem. Chem. Phys.* 2008, *10*, 6301-6312.
23. Bara, J. E.; Gabriel, C. J.; Carlisle, T. K.; Camper, D. E.; Finotello, A.; Gin, D. L.; Noble, R. D., Gas separations in fluoroalkyl-functionalized room-temperature ionic liquids using supported liquid membranes. *Chem. Eng. J.* 2009, *147*, 43-50.
24. Smith, G. D.; Borodin, O.; Magda, J. J.; Boyd, R. H.; Wang, Y. S.; Bara, J. E.; Miller, S.; Gin, D. L.; Noble, R. D., A comparison of fluoroalkyl-derivatized imidazolium:TFSI and alkyl-derivatized imidazolium:TFSI ionic liquids: a molecular dynamics simulation study. *Phys. Chem. Chem. Phys.* 2010, *12*, 7064-7076.
25. Bara, J. E.; Carlisle, T. K.; Gabriel, C. J.; Camper, D.; Finotello, A.; Gin, D. L.; Noble, R. D., Guide to CO_2 Separations in Imidazolium-Based Room-Temperature Ionic Liquids. *Ind. Eng. Chem. Res.* 2009, *48*, 2739-2751.
26. Mahurin, S. M.; Dai, T.; Yeary, J.; Luo, H.; Dai, S., Benzyl-Functionalized Room Temperature Ionic Liquids for CO_2/N_2 Separation. *Ind. Eng. Chem. Res.* 2011, *50*, 14061-14069.
27. Finotello, A.; Bara, J. E.; Narayan, S.; Camper, D.; Noble, R. D., Ideal gas solubilities and solubility selectivities in a binary mixture of room-temperature ionic liquids. *J. Phys. Chem. B* 2008, *112*, 2335-2339.
28. Shannon, M. S.; Bara, J. E., Properties of Alkylimidazoles as Solvents for CO_2 Capture and Comparisons to Imidazolium-Based Ionic Liquids. *Ind. Eng. Chem. Res.* 2011, 50, 8665-8677.
29. Miller, A. A., FREE VOLUME AND VISCOSITY OF LIQUIDS: EFFECTS OF TEMPERATURE. *J. Phys. Chem.* 1963, 67, (5), 1031-1035.
30. Lin, H. Q.; Freeman, B. D., Materials selection guidelines for membranes that remove CO2 from gas mixtures. *J. Molec. Struct.* 2005, 739, 57-74.
31. Doolittle, A. K., Newtonian flow. II. The dependence of the viscosity of liquids on free space. *J. Appl. Phys.* 1951, 22, 1471-1475.
32. Cadena, C.; Anthony, J. L.; Shah, J. K.; Morrow, T. I.; Brennecke, J. F.; Maginn, E. J., Why is CO_2 so soluble in imidazolium-based ionic liquids? *J. Am. Chem. Soc.* 2004, *126*, 5300-5308.
33. Wang, G. N.; Hou, W. L.; Xiao, F.; Geng, J. A.; Wu, Y. T.; Zhang, Z. B., Low-Viscosity Triethylbutylammonium Acetate as a Task-Specific Ionic Liquid for Reversible CO_2 Absorption. *J. Chem. Eng. Data* 2011, *56*, 1125-1133.

34. Shiflett, M. B.; Drew, D. W.; Cantini, R. A.; Yokozeki, A., Carbon Dioxide Capture Using Ionic Liquid 1-Butyl-3-methylimidazolium Acetate. *Energy Fuel* 2010, *24*, 5781-5789.
35. Shiflett, M. B.; Yokozeki, A., Chemical Absorption of Sulfur Dioxide in Room-Temperature Ionic Liquids. *Ind. Eng. Chem. Res.* 2010, *49*, 1370-1377.
36. Carvalho, P. J.; Alvarez, V. H.; Schroder, B.; Gil, A. M.; Marrucho, I. M.; Aznar, M.; Santos, L.; Coutinho, J. A. P., Specific Solvation Interactions of CO_2 on Acetate and Trifluoroacetate Imidazolium Based Ionic Liquids at High Pressures. *J. Phys. Chem. B* 2009, *113*, 6803-6812.
37. Shiflett, M. B.; Kasprzak, D. J.; Junk, C. P.; Yokozeki, A., Phase behavior of {carbon dioxide plus bmim Ac } mixtures. *J. Chem. Thermodyn.* 2008, *40*, 25-31.
38. Babarao, R.; Dai, S.; Jiang, D. E., Understanding the High Solubility of CO_2 in an Ionic Liquid with the Tetracyanoborate Anion. *J. Phys. Chem. B* 2011, *115*, 9789-9794.
39. Mahurin, S. M.; Lee, J. S.; Baker, G. A.; Luo, H. M.; Dai, S., Performance of nitrile-containing anions in task-specific ionic liquids for improved CO_2/N_2 separation. *J. Membr. Sci.* 2010, *353*, 177-183.
40. Bara, J. E.; Camper, D. E.; Gin, D. L.; Noble, R. D., Room-Temperature Ionic Liquids and Composite Materials: Platform Technologies for CO_2 Capture. *Acc. Chem. Res.* 2010, 43, 152-159.
41. Muldoon, M. J.; Aki, S. N. V. K.; Anderson, J. L.; Dixon, J. K.; Brennecke, J. F., Improving Carbon Dioxide Solubility in Ionic Liquids. *J. Phys. Chem. B* 2007, 111, 9001-9009.
42. Anthony, J. L.; Anderson, J. L.; Maginn, E. J.; Brennecke, J. F., Anion effects on gas solubility in ionic liquids. *J. Phys. Chem. B* 2005, 109, (13), 6366-6374.
43. Bara, J. E.; Gin, D. L.; Noble, R. D., Effect of Anion on Gas Separation Performance of Polymer-Room-Temperature Ionic Liquid Composite Membranes. *Ind. Eng. Chem. Res.* 2008, 47, 9919-9924.
44. Bara, J. E.; Lessmann, S.; Gabriel, C. J.; Hatakeyama, E. S.; Noble, R. D.; Gin, D. L., Synthesis and performance of polymerizable room-temperature ionic liquids as gas separation membranes. *Ind. Eng. Chem. Res.* 2007, 46, 5397-5404.
45. Scovazzo, P., Determination of the upper limits, benchmarks, and critical properties for gas separations using stabilized room temperature ionic liquid membranes (SILMs) for the purpose of guiding future research. *J. Membr. Sci.* 2009, 343, 199-211.
46. Scovazzo, P.; Kieft, J.; Finan, D. A.; Koval, C.; DuBois, D.; Noble, R., Gas separations using non-hexafluorophosphate PF_6(-) anion supported ionic liquid membranes. *J. Membr. Sci.* 2004, 238, (1-2), 57-63.
47. Lodge, T. P., Materials science - A unique platform for materials design. *Science* 2008, 321, 50-51.
48. Shannon, M. S.; Tedstone, J. M.; Danielsen, S. P. O.; Bara, J. E., Evaluation of Alkylimidazoles as Physical Solvents for CO_2/CH_4 Separation. *Ind. Eng. Chem. Res.* 2011, *51*, 515-522.
49. Lee, W. M., Selection of Barrier Materials from Molecular Structure. *Polym. Eng. Sci.* 1980, 20, 65-69.
50. Bondi, A., van der Waals Volumes and Radii. *J. Phys. Chem.* 1964, 68, 441-451.
51. Bondi, A. A., *Physical Properties of Molecular Crystals, Liquids, and Glasses*. Wiley: New York, 1968.
52. Zhao, Y. H.; Abraham, M. H.; Zissimos, A. M., Fast calculation of van der Waals volume as a sum of atomic and bond contributions and its application to drug compounds. *J. Org. Chem.* 2003, *68*, 7368-7373.
53. Mantina, M.; Chamberlin, A. C.; Valero, R.; Cramer, C. J.; Truhlar, D. G., Consistent van der Waals Radii for the Whole Main Group. *J. Phys. Chem. A* 2009, *113*, 5806-5812.
54. Chen, Y.; Han, J.; Wang, T.; Mu, T., Determination of Absorption Rate and Capacity of CO_2 in Ionic Liquids at Atmospheric Pressure by Thermogravimetric Analysis. *Energy Fuel.* 2011, *55,* 5810-5815.
55. Koval, C.; Camper, D.; Finotello, A.; Noble, R., Properties of imidazolium-based room temperature ionic liquids that effect CO_2 solubility and selectivity for CO_2/N_2 and CO_2/CH_4 gas separations. *PMSE Prepr.* 2006, *95*, 266.
56. Blanchard, L. A.; Gu, Z. Y.; Brennecke, J. F., High-pressure phase behavior of ionic liquid/CO_2 systems. *J. Phys. Chem. B* 2001, *105*, 2437-2444.
57. Palgunadi, J.; Kang, J. E.; Nguyen, D. Q.; Kim, J. H.; Min, B. K.; Lee, S. D.; Kim, H.; Kim, H. S., Solubility of CO_2 in dialkylimidazolium dialkylphosphate ionic liquids. *Thermochim. Acta* 2009, *494*, 94-98.

58. Deschamps, J.; Costa Gomes, M. F.; Pádua, A. A. H., Molecular Simulation Study of Interactions of Carbon Dioxide and Water with Ionic Liquids. *Chem. Phys. Chem.* 2004, *5*, 1049-1052.
59. Hu, Y. F.; Liu, Z. C.; Xu, C. M.; Zhang, X. M., The molecular characteristics dominating the solubility of gases in ionic liquids. *Chem. Soc. Rev.* 2011, *40*, 3802-3823.
60. Palomar, J.; Gonzalez-Miquel, M.; Polo, A.; Rodriguez, F., Understanding the Physical Absorption of CO_2 in Ionic Liquids Using the COSMO-RS Method. *Ind. Eng. Chem. Res.* 2011, *50*, 3452-3463.
61. Sistla, Y. S.; Khanna, A., Validation and Prediction of the Temperature-Dependent Henry's Constant for CO_2–Ionic Liquid Systems Using the Conductor-like Screening Model for Realistic Solvation (COSMO-RS). *J. Chem. Eng. Data* 2011, *56*, 4045-4060.
62. Sumon, K. Z.; Henni, A., Ionic liquids for CO_2 capture using COSMO-RS: Effect of structure, properties and molecular interactions on solubility and selectivity. *Fluid Phase Equilibr.* 2011, *310*, 39-55.
63. Diedenhofen, M.; Klamt, A., COSMO-RS as a tool for property prediction of IL mixtures-A review. *Fluid Phase Equilibr.* 2010, *294*, 31-38.
64. Shimoyama, Y.; Ito, A., Predictions of cation and anion effects on solubilities, selectivities and permeabilities for CO_2 in ionic liquid using COSMO based activity coefficient model. *Fluid Phase Equilibr.* 2010, *297*, 178-182.
65. Zhang, X. C.; Liu, Z. P.; Wang, W. C., Screening of ionic liquids to capture CO_2 by COSMO-RS and experiments. *AIChE J.* 2008, 54, (10), 2717-2728.
66. Palomar, J.; Ferro, V. R.; Torrecilla, J. S.; Rodríguez, F., Density and Molar Volume Predictions Using COSMO-RS for Ionic Liquids. An Approach to Solvent Design. *Industrial & Engineering Chemistry Research* 2007, 46, (18), 6041-6048.
67. Klamt, A., Chapter 7 - Refinements, parameterization, and the complete COSMO-RS. In *COSMO-RS: From Quantum Chemistry to Fluid Phase Thermodynamics and Drug Design*, Elsevier: Amsterdam, 2005; pp 109-125.
68. Barton, A. F. M., *CRC Handbook of Solubility Parameters and Other Cohesion Parameters*. 2nd ed.; CRC Press: Boca Raton, FL, 1991.
69. Prausnitz, J. M.; Lichtenthaler, R. N.; Gomes de Azevedo, E., *Molecular Thermodynamics of Fluid-Phase Equilibria*. 3rd ed.; Prentice-Hall: Upper Saddle River, NJ, 1999.
70. Verevkin, S. P., Predicting enthalpy of vaporization of ionic liquids: A simple rule for a complex property. *Angew. Chem. Int. Edit.* 2008, *47*, 5071-5074.
71. Ahlrichs, R.; Bär, M.; Häser, M.; Horn, H.; Kölmel, C., Electronic structure calculations on workstation computers: The program system turbomole. *Chem. Phys. Lett.* 1989, *162*, 165-169.
72. Schafer, A.; Huber, C.; Ahlrichs, R., Fully optimized contracted Gaussian basis sets of triple zeta valence quality for atoms Li to Kr. *J. Chem. Phys.* 1994, *100*, 5829-5835.
73. Becke, A. D., Density-functional exchange-energy approximation with correct asymptotic behavior. *Phys. Rev. A* 1988, *38*, 3098-3100.
74. Perdew, J. P., Density-functional approximation for the correlation energy of the inhomogeneous electron gas. *Phys. Rev. B* 1986, *33*, 8822-8824.
75. Shannon, M. S.; Bara, J. E., Reactive and Reversible Ionic Liquids for CO_2 Capture and Acid Gas Removal. *Sep. Sci. Technol.* 2012, *47*, 178-188.
76. Binnemans, K., Ionic liquid crystals. *Chem. Rev.* 2005, *105*, 4148-4204
77. Moganty, S. S.; Baltus, R. E., Regular Solution Theory for Low Pressure Carbon Dioxide Solubility in Room Temperature Ionic Liquids: Ionic Liquid Solubility Parameter from Activation Energy of Viscosity. *Ind. Eng. Chem. Res.* 2010, *49*, 5846-5853.
78. Kim, Y. S.; Choi, W. Y.; Jang, J. H.; Yoo, K. P.; Lee, C. S., Solubility measurement and prediction of carbon dioxide in ionic liquids. *Fluid Phase Equilibr.* 2005, *228–229*, 439-445.
79. Huang, J.-F.; Chen, P.-Y.; Sun, I. W.; Wang, S. P., NMR evidence of hydrogen bonding in 1-ethyl-3-methylimidazolium-tetrafluoroborate room temperature ionic liquid. *Inorg. Chim. Acta* 2001, *320*, 7-11.

80. Bara, J. E.; Noble, R. D.; Gin, D. L., Effect of "Free" Cation Substituent on Gas Separation Performance of Polymer-Room-Temperature Ionic Liquid Composite Membranes. *Ind. Eng. Chem. Res.* 2009, *48*, 4607-4610.
81. Voss, B. A.; Bara, J. E.; Gin, D. L.; Noble, R. D., Physically Gelled Ionic Liquids: Solid Membrane Materials with Liquidlike CO_2 Gas Transport. *Chem. Mater.* 2009, *21*, 3027-3029.
82. Tang, J.; Shen, Y.; Radosz, M.; Sun, W., Isothermal Carbon Dioxide Sorption in Poly(ionic liquid)s. *Ind. Eng. Chem. Res.* 2009, *48*, 9113-9118.
83. Tang, J.; Tang, H.; Sun, W.; Radosz, M.; Shen, Y., Poly(ionic liquid)s as new materials for CO2 absorption. *J. Polym. Sci., Part A: Polym. Chem.* 2005, *43*, 5477-5489.
84. Armand, M.; Endres, F.; MacFarlane, D. R.; Ohno, H.; Scrosati, B., Ionic-liquid materials for the electrochemical challenges of the future. *Nature Mater.* 2009, *8*, 621-629.
85. Ohno, H., Design of ion conductive polymers based on ionic liquids. *Macromol. Symp.* 2007, *249/250*, 551-556.
86. Mecerreyes, D., Polymeric ionic liquids: Broadening the properties and applications of polyelectrolytes. *Prog. Polym. Sci.* 2011, *36*, 1629-1648.

5.8 Appendix:

Table S1: Comparison of FFV for selected organic solvents and water calculated from Bondi and COSMOtherm.

Solvent	FFV		% Difference
	Bondi	COSMO	
Chloroform	0.328	0.211	36%
Acetone	0.312	0.301	4%
n-Hexane	0.324	0.337	-4%
Propylene Carbonate (PC)	0.244	0.155	36%
Dimethyl Sulfoxide (DMSO)	N/A	0.173	N/A
Methanol (MeOH)	0.306	0.304	1%
N,N-dimethylformamide (DMF)	0.214	0.262	-22%
Water	0.179	0.147	18%
Tetrahydrofuran (THF)	0.263	0.273	-4%
Methyl Acetate (MeOAc)	0.307	0.273	11%
Acetonitrile (ACN)	0.302	0.325	-7%

% Difference = 100*((Bondi-COSMO) /Bondi)

Bondi FFV data taken from: Lin, H. Q.; Freeman, B. D., Materials selection guidelines for membranes that remove CO_2 from gas mixtures. *Journal of Molecular Structure,* 2005, *739*, 57-74.

Figure S1: [C_1mim] cation	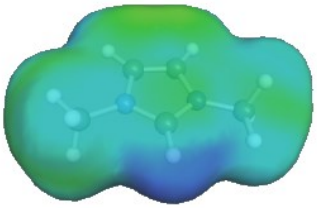
Figure S2: [C_2mim] cation	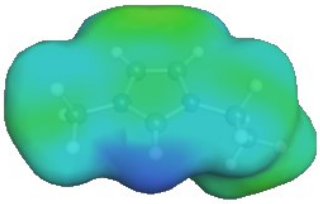
Figure S3: [C_3mim] cation	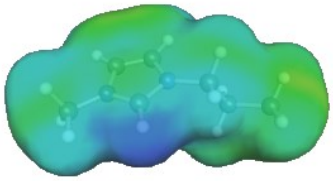
Figure S4: [C_4mim] cation	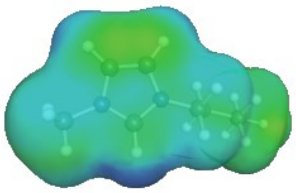

Figure S5: [C_5mim] cation	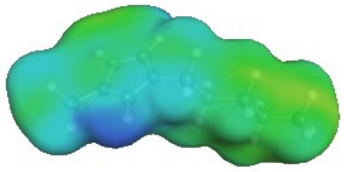
Figure S6: [C_6mim] cation	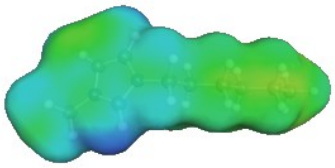
Figure S7: [C_7mim] cation	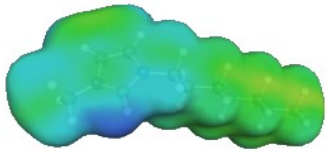
Figure S8: [C_8mim] cation	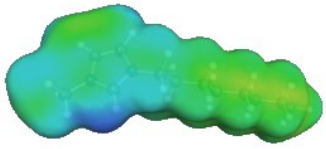

Figure S9: [C_{10}mim] cation	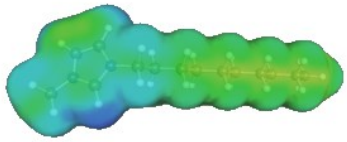
Figure S10: [C_{12}mim] cation	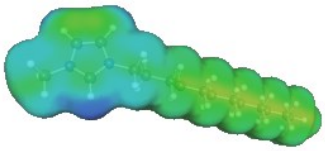
Figure S11: [C_{14}mim] cation	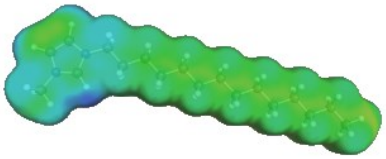
Figure S12: [BF_4] anion	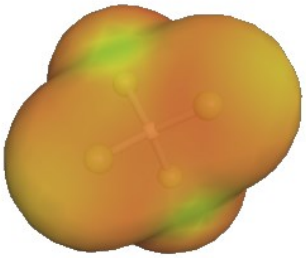

Figure S13: $[PF_6]$ anion	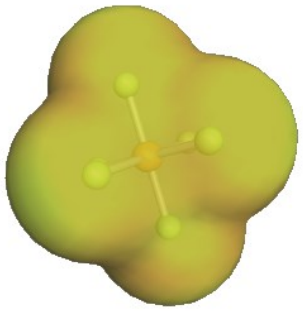
Figure S14: $[SbF_6]$ anion	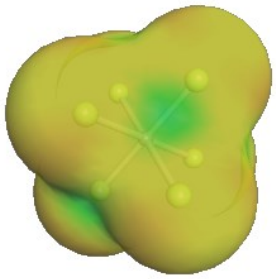
Figure S15: [OMs] anion	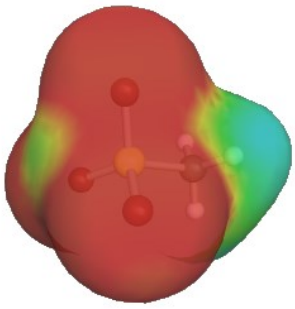
Figure S16: $[MeSO_4]$ anion	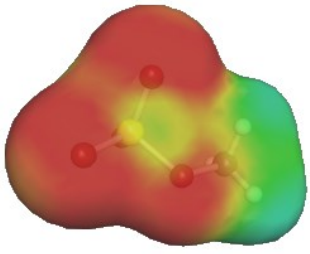

Figure S17: [$EtSO_4$] anion	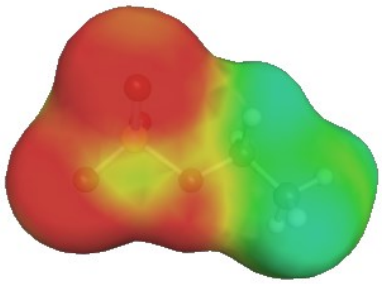
Figure S18: [OTf] anion	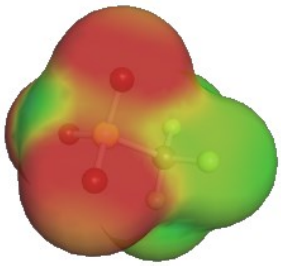
Figure S19: [FSI] anion	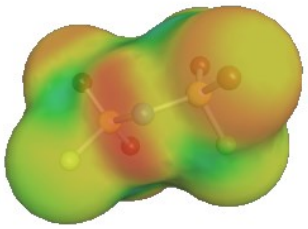
Figure S20: [Tf_2N] anion	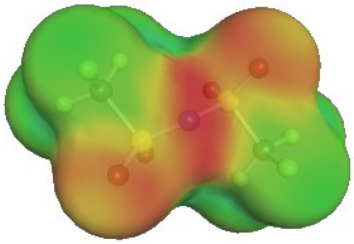

Figure S21: [beti] anion	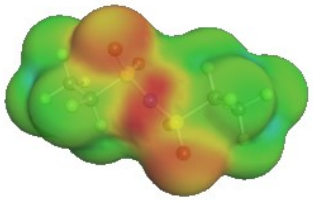
Figure S22: $[N(CN)_2]$ anion	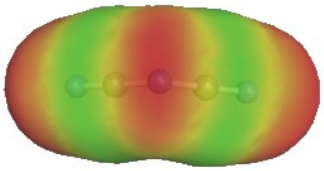
Figure S23: $[C(CN)_3]$ anion	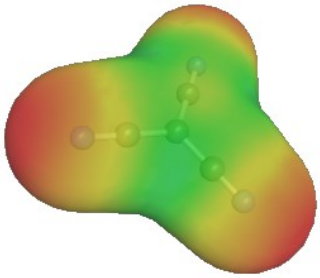
Figure S24: $[B(CN)_4]$ anion	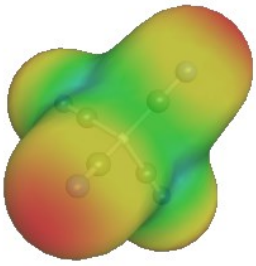

Figure S25: $[P(CN)_6]$ anion	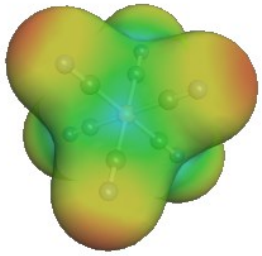
Figure S26: $[Sb(CN)_6]$ anion	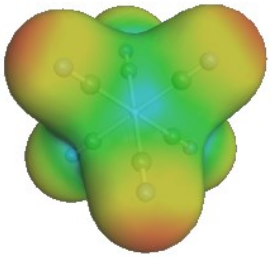

Table S2: Comparison of 4-constant RST Equation to 2-constant fit; first example.

x	y	y'	a'	b'	c	d
1	0.585786	0.575457	1	1	1	1
2	0.275255	0.284507	c'	d'	R^2	
3	0.178633	0.187524	0.5819	-0.00644	0.9987	
4	0.131966	0.139032				
5	0.104555	0.109937				
6	0.086543	0.09054				
7	0.073812	0.076686				
8	0.06434	0.066295				
9	0.057019	0.058213				
10	0.051191	0.051747				
11	0.046443	0.046457				
12	0.0425	0.042049				
13	0.039174	0.038319				
14	0.03633	0.035121				
15	0.033871	0.03235				
16	0.031724	0.029926				
17	0.029832	0.027786				
18	0.028153	0.025885				
19	0.026653	0.024183				
20	0.025305	0.022652				
21	0.024086	0.021267				
22	0.02298	0.020007				
23	0.02197	0.018857				
24	0.021046	0.017803				
25	0.020196	0.016833				

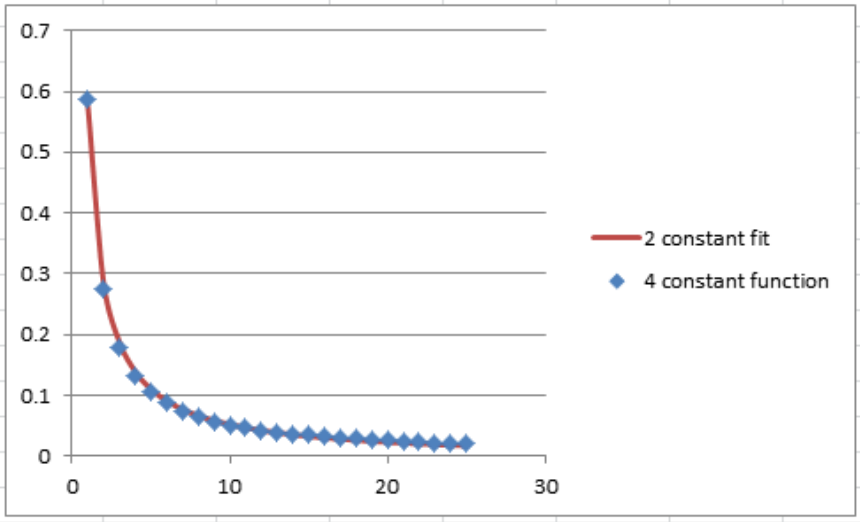

Table S3: Comparison of 4-constant RST Equation to 2-constant fit; second example.

x	y	y'	a'	b'	c	d
1	0.051191	0.051	1	0.1	1	0.1
2	-0.4247	-0.42455	c'	d'	R^2	
3	-0.5832	-0.58307	0.9511	-0.9001	1.000	
4	-0.66242	-0.66233				
5	-0.70995	-0.70988				
6	-0.74163	-0.74158				
7	-0.76426	-0.76423				
8	-0.78123	-0.78121				
9	-0.79443	-0.79442				
10	-0.80499	-0.80499				
11	-0.81363	-0.81364				
12	-0.82082	-0.82084				
13	-0.82692	-0.82694				
14	-0.83214	-0.83216				
15	-0.83666	-0.83669				
16	-0.84062	-0.84066				
17	-0.84411	-0.84415				
18	-0.84722	-0.84726				
19	-0.85	-0.85004				
20	-0.8525	-0.85255				
21	-0.85476	-0.85481				
22	-0.85682	-0.85687				
23	-0.85869	-0.85875				
24	-0.86041	-0.86047				
25	-0.862	-0.86206				

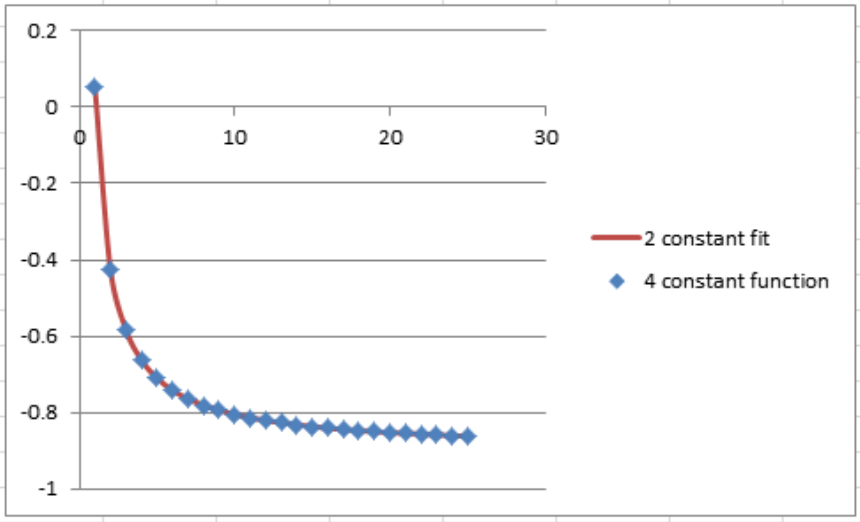

Table S4: Comparison of 4-constant RST Equation to 2-constant fit; third example.

x	y	y'	a'	b'	c	d
1	0.051191	-0.0026	0.1	1	0.1	1
2	0.275403	0.31505	c'	d'	R^2	
3	0.375053	0.420933	-0.6353	0.6327	0.967	
4	0.433392	0.473875				
5	0.472277	0.50564				
6	0.500269	0.526817				
7	0.52148	0.541943				
8	0.538158	0.553288				
9	0.551643	0.562111				
10	0.562786	0.56917				
11	0.572159	0.574945				
12	0.580159	0.579758				
13	0.58707	0.583831				
14	0.593104	0.587321				
15	0.598418	0.590347				
16	0.603137	0.592994				
17	0.607356	0.595329				
18	0.61115	0.597406				
19	0.614582	0.599263				
20	0.617702	0.600935				
21	0.62055	0.602448				
22	0.62316	0.603823				
23	0.625563	0.605078				
24	0.62778	0.606229				
25	0.629834	0.607288				

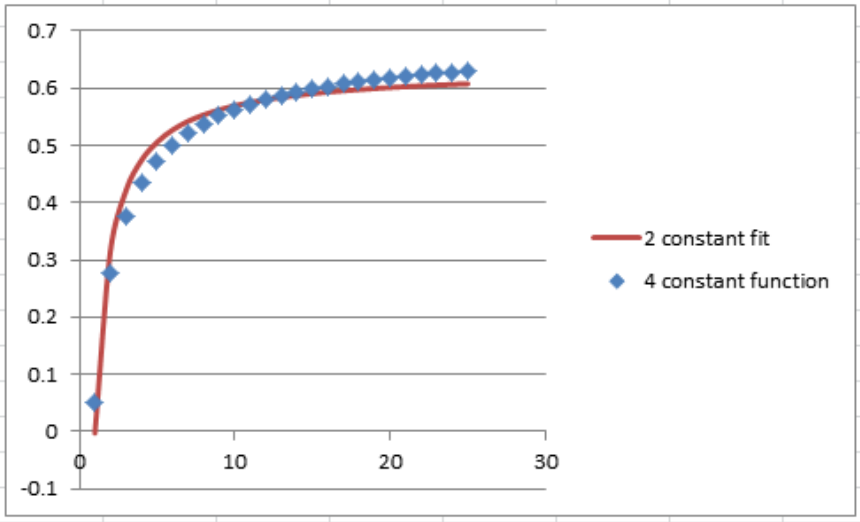

Table S5: Comparison of 4-constant RST Equation to 2-constant fit; fourth example.

x	y	y'	a'	b'	c	d
1	0	-0.11	1	-1	1	-1
2	-1.20711	-1.076	c'	d'	R^2	
3	-1.48316	-1.398	1.932	-2.042	0.987	
4	-1.61603	-1.559				
5	-1.69443	-1.6556				
6	-1.7462	-1.72				
7	-1.78296	-1.766				
8	-1.81041	-1.8005				
9	-1.8317	-1.82733				
10	-1.84868	-1.8488				
11	-1.86255	-1.86636				
12	-1.87409	-1.881				
13	-1.88385	-1.89338				
14	-1.8922	-1.904				
15	-1.89943	-1.9132				
16	-1.90575	-1.92125				
17	-1.91132	-1.92835				
18	-1.91627	-1.93467				
19	-1.9207	-1.94032				
20	-1.92468	-1.9454				
21	-1.92828	-1.95				
22	-1.93155	-1.95418				
23	-1.93454	-1.958				
24	-1.93728	-1.9615				
25	-1.9398	-1.96472				

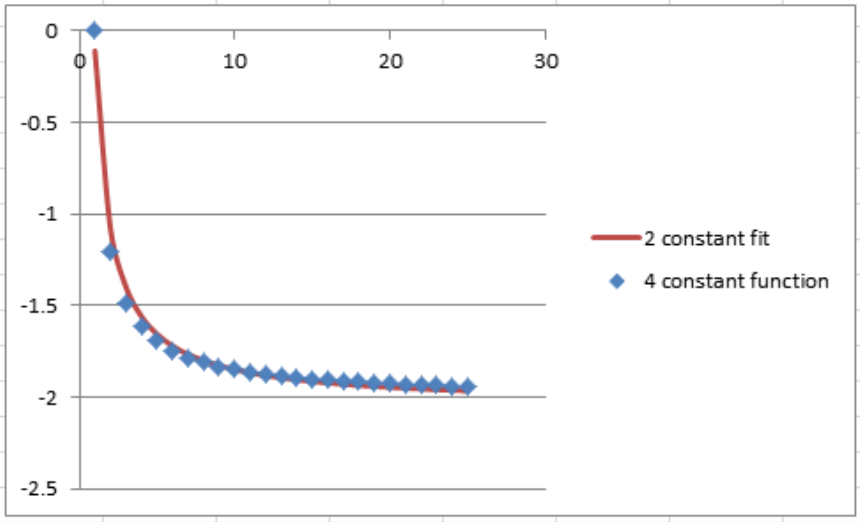

Table S6: Comparison of 4-constant RST Equation to 2-constant fit; fifth example.

x	y	y'	a'	b'	c	d
1	-1.31662	-1.3176	10	1	1	1
2	-1.74037	-1.7403	c'	d'	R^2	
3	-1.88122	-1.8812	0.8454	-2.163	1.000	
4	-1.95156	-1.95165				
5	-1.99374	-1.99392				
6	-2.02185	-2.0221				
7	-2.04193	-2.04223				
8	-2.05698	-2.05733				
9	-2.06869	-2.06907				
10	-2.07805	-2.07846				
11	-2.08571	-2.08615				
12	-2.09209	-2.09255				
13	-2.09749	-2.09797				
14	-2.10212	-2.10261				
15	-2.10613	-2.10664				
16	-2.10964	-2.11016				
17	-2.11274	-2.11327				
18	-2.11549	-2.11603				
19	-2.11796	-2.11851				
20	-2.12017	-2.12073				
21	-2.12218	-2.12274				
22	-2.124	-2.12457				
23	-2.12567	-2.12624				
24	-2.12719	-2.12778				
25	-2.1286	-2.12918				

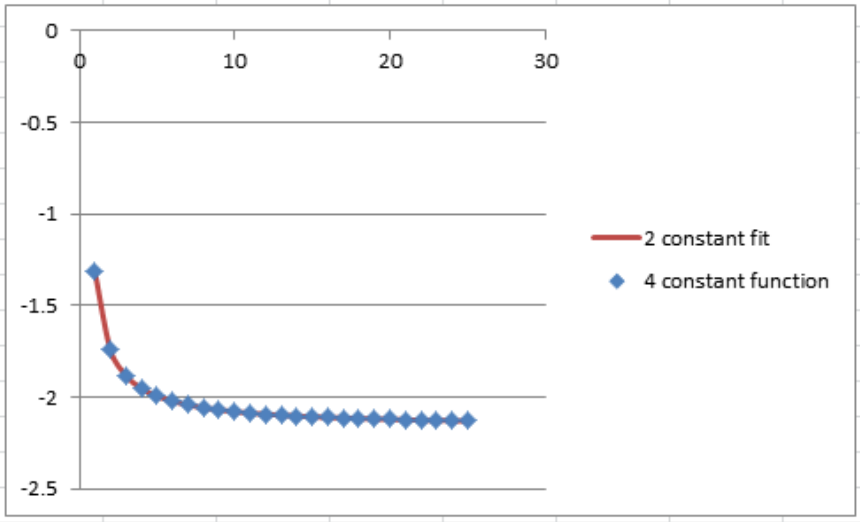

Table S7: Comparison of 4-constant RST Equation to 2-constant fit; sixth example.

x	y	y'	a'	b'	c	d
1	0	-0.35	10	-10	10	-10
2	-7.23607	-6.825	c'	d'	R^2	
3	-9.24866	-8.98333	12.95	-13.3	0.997	
4	-10.2386	-10.0625				
5	-10.8284	-10.71				
6	-11.2201	-11.1417				
7	-11.4991	-11.45				
8	-11.708	-11.6813				
9	-11.8703	-11.8611				
10	-12	-12.005				
11	-12.106	-12.1227				
12	-12.1943	-12.2208				
13	-12.269	-12.3038				
14	-12.333	-12.375				
15	-12.3884	-12.4367				
16	-12.4369	-12.4906				
17	-12.4796	-12.5382				
18	-12.5176	-12.5806				
19	-12.5516	-12.6184				
20	-12.5822	-12.6525				
21	-12.6099	-12.6833				
22	-12.635	-12.7114				
23	-12.658	-12.737				
24	-12.679	-12.7604				
25	-12.6984	-12.782				

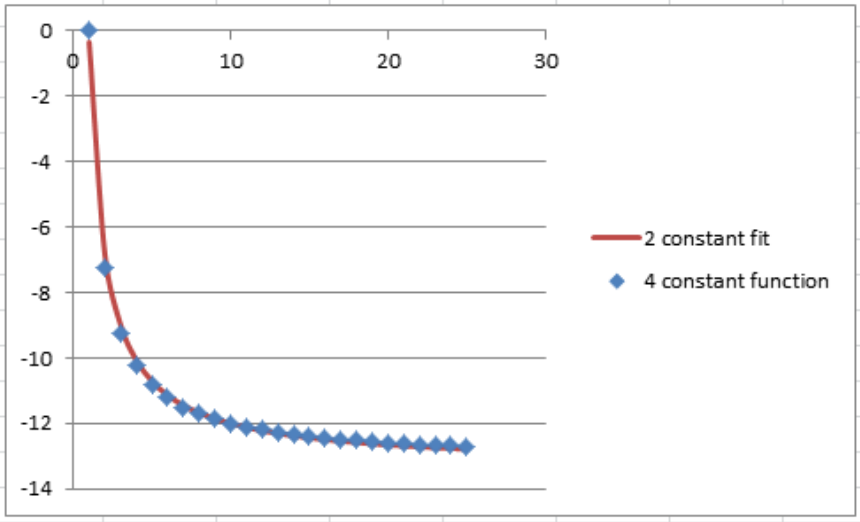

Table S8: Comparison of 4-constant RST Equation to 2-constant fit; seventh example.

x	y	y'	a'	b'	c	d
1	-0.1005	-0.1	100	0.01	10	-0.1
2	-5.10025	-5.1	c'	d'	R^2	
3	-6.76683	-6.76667	10	-10.1	1.000	
4	-7.60012	-7.6				
5	-8.1001	-8.1				
6	-8.43342	-8.43333				
7	-8.6715	-8.67143				
8	-8.85006	-8.85				
9	-8.98894	-8.98889				
10	-9.10005	-9.1				
11	-9.19095	-9.19091				
12	-9.26671	-9.26667				
13	-9.33081	-9.33077				
14	-9.38575	-9.38571				
15	-9.43337	-9.43333				
16	-9.47503	-9.475				
17	-9.51179	-9.51176				
18	-9.54447	-9.54444				
19	-9.57371	-9.57368				
20	-9.60002	-9.6				
21	-9.62383	-9.62381				
22	-9.64548	-9.64545				
23	-9.66524	-9.66522				
24	-9.68335	-9.68333				
25	-9.70002	-9.7				

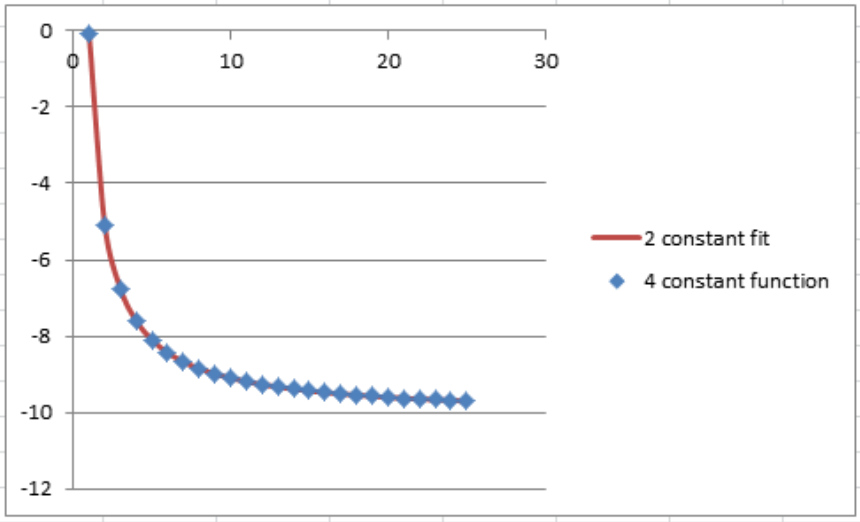

Table S9: Comparison of 4-constant RST Equation to 2-constant fit; eighth example.

x	y	y'	a'	b'	c	d
1	-60.0509	-60.05	100	1	-50	-0.001
2	-35.026	-35.025	c'	d'	R^2	
3	-26.6843	-26.6833	-50.05	-10	1.000	
4	-22.5135	-22.5125				
5	-20.011	-20.01				
6	-18.3427	-18.3417				
7	-17.151	-17.15				
8	-16.2572	-16.2563				
9	-15.5621	-15.5611				
10	-15.006	-15.005				
11	-14.551	-14.55				
12	-14.1718	-14.1708				
13	-13.851	-13.85				
14	-13.576	-13.575				
15	-13.3377	-13.3367				
16	-13.1291	-13.1281				
17	-12.9451	-12.9441				
18	-12.7816	-12.7806				
19	-12.6352	-12.6342				
20	-12.5035	-12.5025				
21	-12.3843	-12.3833				
22	-12.276	-12.275				
23	-12.1771	-12.1761				
24	-12.0864	-12.0854				
25	-12.003	-12.002				

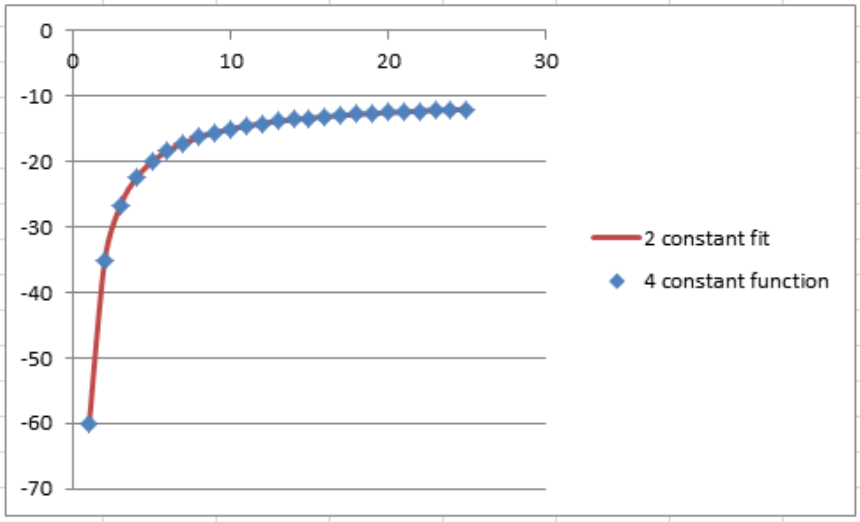

Table S10: COSMOtherm calculations for density, molar volume and FFV in *n*-alkanes at 298K.

Compound	Density (g cm^{-3})	Volume (A^3 molec.$^{-1}$)	MW (g mol^{-1})	VCOSMO (A^3 molec.$^{-1}$)	V_m (cm^3 mol^{-1})/100	FFV
hexane	0.65169	219.58291	86.1759	145.6834	1.3223	0.3365
n-heptane	0.67362	247.01335	100.2026	167.634	1.4875	0.3214
octane	0.69123	274.41759	114.2293	189.5431	1.6526	0.3093
n-nonane	0.70608	301.63505	128.256	211.3144	1.8165	0.2994
n-decane	0.71783	329.14399	142.2826	233.3154	1.9821	0.2911
n-undecane	0.72625	357.39801	156.3093	255.9728	2.1523	0.2838
dodecane	0.73742	383.57346	170.336	276.8313	2.3099	0.2783
tetradecane	0.75186	438.16624	198.3893	320.4391	2.6387	0.2687
tridecane	0.74342	411.80717	184.3627	299.468	2.4799	0.2728
pentadecane	0.75602	466.56215	212.416	343.264	2.8097	0.2643
n-hexadecane	0.75916	495.31298	226.4427	366.4031	2.9828	0.2603
heptadecane	0.76603	521.27992	240.4694	387.0185	3.1392	0.2576
octadecane	0.77024	548.67219	254.496	408.9217	3.3041	0.2547
nonadecane	0.77405	576.06157	268.5227	430.822	3.4691	0.2521
eicosane	0.77752	603.44384	282.5494	452.7133	3.634	0.2498

Liquid density and volume at T = 298.15 K - density is in g/ml - volume is in A^3 - area is in A^2

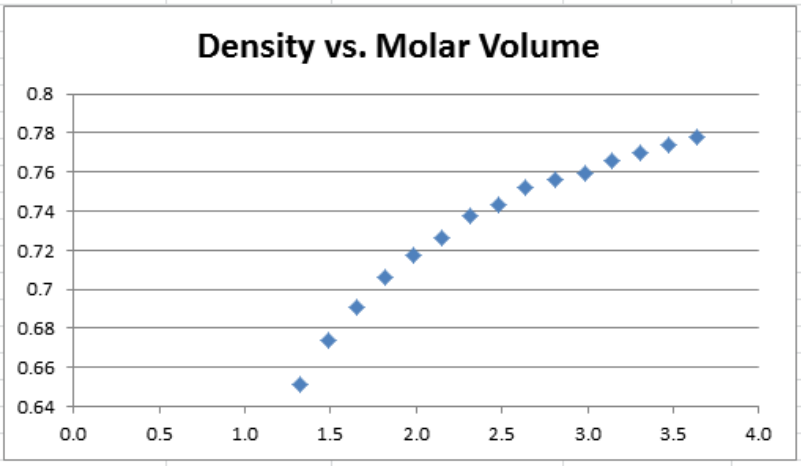

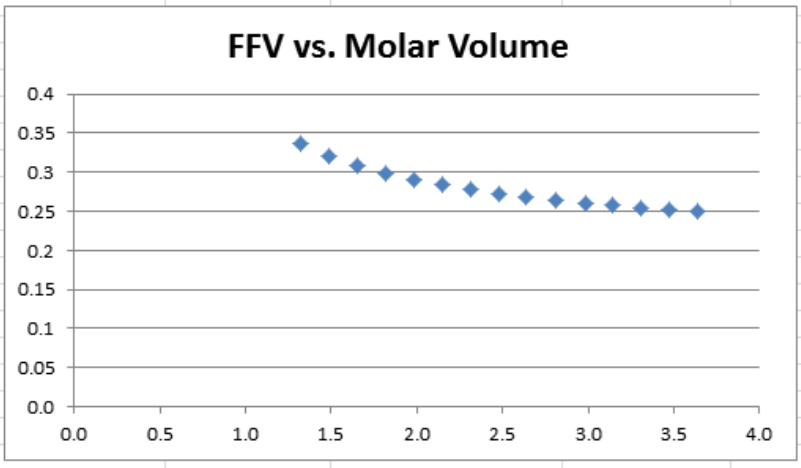

Alkane FFV as a function of molar volume:

FFV = $0.1805/V_m$ +0.2001 (R^2 = 1.00)

CHAPTER SIX

[†]Properties of Alkylbenzimidazoles for CO_2 and SO_2 Capture and Comparisons to Ionic Liquids

Matthew S. SHANNON,[1] Michelle S. HINDMAN,[1] Scott. P.O. DANIELSEN,[2,3]
Jason M. TEDSTONE,[2,4] Ricky D. GILMORE & Jason E. BARA[,*]

1. Department of Chemical & Biological Engineering, University of Alabama, Tuscaloosa AL USA 35487-0203
2. NSF-REU Site: Engineering Solutions for Clean Energy Generation, Storage and Consumption, Department of Chemical & Biological Engineering, University of Alabama, Tuscaloosa AL USA 35487-0203
3. Department of Chemical & Biomolecular Engineering, University of Pennsylvania, Philadelphia, PA USA 19104-6315
4. Department of Chemical & Biomolecular Engineering, Clemson University, Clemson, SC USA 29634

Abstract

To date, few reports have been concerned with the physical properties of the liquid phases of imidazoles and benzimidazoles – potential starting materials for a great number of ionic liquids. Prior research has indicated that alkylimidazole solvents exhibit different, and potentially advantageous physical properties, when compared to corresponding imidazolium-based ionic liquids. Given that even the most fundamental physical properties of alkylimidazole solvents have only recently been reported, there is still a lack of data for other relevant imidazole derivatives, including benzimidazoles. In this work, we have synthesized a series of eight 1-*n*-alkylbenzimidazoles, with chain lengths ranging from ethyl to dodecyl, all of which exist as neat liquids at ambient temperature. Their densities and viscosities have been determined as functions of both temperature and molecular weight. Alkylbenzimidazoles have been found to exhibit viscosities that are more similar to imidazolium-based ILs than alkylimidazoles, owed to a large contribution to viscosity from the presence of a fused ring system. Solubilities of CO_2 and SO_2, two species of concern in the emission of coal-fired power generation, were determined for selected alkylbenzimidazoles to understand what effects a fused ring system might have on gas solubility. For both gases, alkylbenzimidazoles were determined to experience physical, non-chemically reactive, interactions. The solubility of CO_2 in alkylbenzimidazoles is 10-30% less than observed for corresponding ILs and alkylimidazoles. 1-butylbenzimidazole was found to readily absorb at least 0.333 gram SO_2 per gram at low pressure and ambient temperature, which could be readily desorbed under an N_2 flush, a behavior more similar to imidazolium-based ILs than alkylimidazoles. Thus, we find that as solvents for gas separations, benzimidazoles share characteristics with both ILs and alkylimidazoles.

Keywords
benzimidazole, imidazole, ionic liquids, carbon dioxide (CO_2) capture, sulfur dioxide (SO_2)

[†]*Science China: Chemistry, 2012, 55, 1638-1647*.

6.1 Introduction: Imidazolium salts (Figure 6.1a) have been the dominant motif for the development of ionic liquids (ILs) and have been explored in a diverse and ever-growing number of applications, including CO_2 capture,[1, 2] electrochemistry,[3-5] energetic materials,[6-8] cellulose processing[9] and polymer science,[10-16] to name but a few. Benzimidazolium salts (Figure 6.1b), while possessing the same modularity as their imidazolium counterparts, have rarely been explored for the same applications that have been proposed for imidazolium-based ILs. This might be attributable to the much higher melting points of benzimidazolium salts than imidazolium salts.[17] However, benzimidazolium salts have found great utility as frameworks for *N*-heterocyclic carbenes (NHCs) for catalysis,[18-20] as liquid crystals (LCs)[21] and antimicrobials.[22] Benzobis(imidazolium) or "Janus" benzimidazolium salts (Figure 6.1c) have also been of interest for their unique fluorescence and as sensors.[23, 24] Poly(benzimidazolium) salts can be formed form the alkylation of poly(benzimidazole) and used as anion conductors.[25] However, to our knowledge, there are no reports on the use of benzimidazolium ILs (e.g. 1-ethyl-3-methylbenzimidazolium tetrafluoroborate) as bulk liquids, even as related to characterizations of physical properties such as density or viscosity. Thus, although an important building block in many applications,[26] the impact of the versatile and readily available benzimidazole moiety on physical and thermodynamic properties has not been quantified.

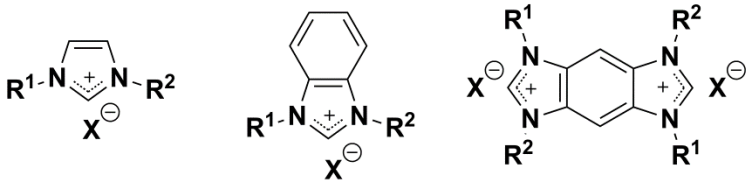

Figure 6.1: General structures of (a) imidazolium salts, (b) benzimidazolium salts and (c) benzobis(imidazolium) salts.

Although the characterization of physical properties for imidazolium-based ILs has now been a priority of many research efforts for more than a decade,[27] there has only recently been an interest in developing a similar understanding of the physical properties of the starting materials for imidazolium-based ionic liquids (ILs), such as alkylimidazoles (Figure 6.2a).[28-32] Fundamentally, alkylimidazoles can be functionalized in similar manners to ILs to control their physical[28-30, 32, 33] and/or chemical[34] and/or biological[35] properties. As there are likely quadrillions (10^{15}) if not quintillions (10^{18}) of possible ILs,[36]

encompassing a number of different species, it may be safely assumed that the number of possible imidazole derivatives could easily exceed 10^6 (if not orders of magnitude greater).

Imidazoles and benzimidazoles (Figure 6.2b) are known for their antimicrobial, antifungal, and medicinal properties and thus have numerous applications in the pharmaceutical industry.[26, 35, 37, 38] In addition to these vital uses, imidazoles are an important class of building blocks for synthetic organic chemistry.[10, 39] Furthermore, virtually all imidazolium salts originate from imidazoles, and the properties of ILs are better understood via comparisons to imidazoles.[30, 40] Imidazoles have also found industrial utility in separations, as the BASIL™ (*biphasic acid scavenging using ionic liquids*) process directly used 1-methylimidazole as an acid (H^+) scavenger to form 1-methylimidazolium chloride and enabled significant improvements in the manufacture of alkoxyphenylphosphines.[41, 42]

Developing understandings of neutral, imidazole-based molecules can be keys to advancing IL-based technologies. To further this area of research, we have explored the properties of some relatively simple benzimidazole derivatives. Herein, we report on density, viscosity and solubilities of carbon dioxide (CO_2) and sulfur dioxide (SO_2) in 1-*n*-alkylbenzimidazoles (Figure 6.2b) and provide comparisons to alkylimidazoles and imidazolium-based ILs. Density and viscosity were found to be strongly related to the length of the alkyl chain and temperature, and highly correlated functions were developed as a means of modeling these properties. Solubility of CO_2 was also found to be correlated to alkyl chain length and temperature, although the 1-*n*-alkylbenzimidazole solvents appear to have somewhat less of an affinity for CO_2 than alkylimidazoles or ILs. Interestingly, although 0.33 grams of SO_2 could be absorbed per gram of 1-butylbenzimidazole, this was not attributable to a chemical reaction that was previously observed for alkylimidazoles.[28] The properties and behaviors of 1-*n*-alkylbenzimidazoles thus appear to have commonalities with both alkylimidazoles and imidazolium-based ILs.

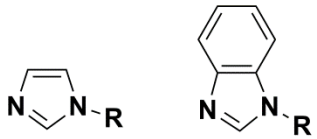

(a) (b)

Figure 6.2: Structures of (a) imidazoles and (b) benzimidazoles.

6.2 Materials and Method

6.2.1 Materials : All chemicals were purchased from Sigma-Aldrich (Milwaukee, WI USA) and were used as received without further purification. CO_2 and anhydrous SO_2 were purchased from AirGas (Radnor, PA USA) at a minimum of 99.98% purity.

6.2.2 Synthesis of 1-n-alkylbenzimidazoles: Sodium benzimidazolate (NaBenz) was first produced via the neutralization of benzimidazole with NaOH in THF (Scheme 1a) and subsequent drying. NaBenz was then used to produce a series of 1-*n*-alkylbenzimidazoles (1 – 8) via reaction with a corresponding 1-bromoalkane (Scheme 1b). This synthetic method is based on our prior work with a variety of *N*-functionalized imidazoles.[43]

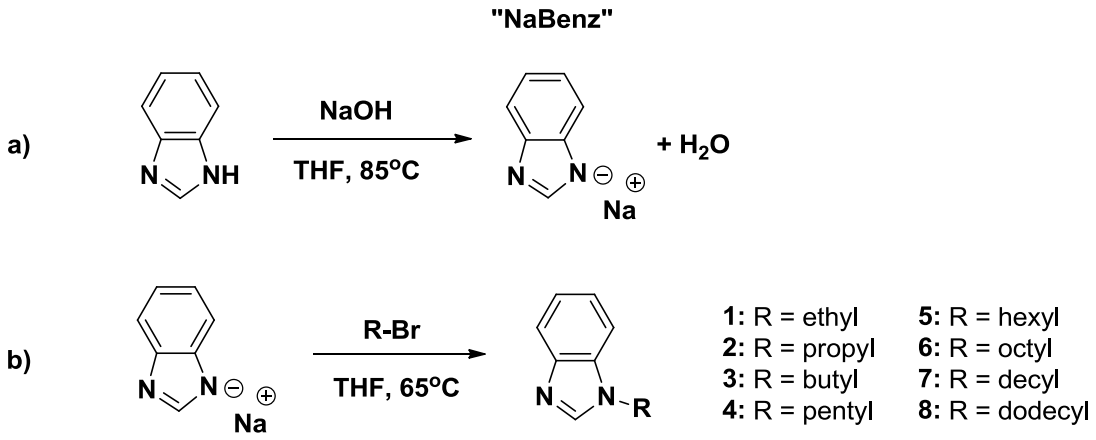

Scheme 1: Synthesis of (a) NaBenz precursor and (b) subsequent formation of 1-*n*-alkylimidazoles (1-8)

6.2.2.1 Procedure for preparing sodium benzimidazolate (NaBenz): Benzimidazole (200.00 g, 1.693 mol) was dissolved in refluxing THF (500 mL). NaOH (74.49 g, 1.862 mol) was added and observed to gradually disappear as the reaction was stirred for 16 hours at 65°C. The reaction was stopped, and while warm (~40°C), filtered through a thin layer of basic Al_2O_3 to remove the small amount of insoluble material present. The solvent was removed via rotary evaporation until a viscous oil remained, which was then spread onto a large area Pyrex® glass tray and placed in a vacuum oven set to 80°C. After several minutes, the viscous oil underwent a transition to an off-white solid. At this time, the product was briefly removed from the oven and the solid crushed to produce a fine powder. The powdered product was returned to the vacuum oven for 16 hours at 120°C. 207.633 g of the product containing NaBenz and residual THF and NaOH were collected. By ^{1}H NMR analysis, about 4 mol% THF remained in

the NaBenz product based on the expected chemical shifts of THF in DMSO-d6 (multiplets at δ 3.60 and δ 1.76).[44] The NaBenz product was used without further purification. An image of this ^{1}H NMR spectra is provided as Supporting Information. ^{1}H NMR (500 MHz, DMSO-d6) δ 7.93 – 7.69 (m, 1H), 7.38 (ddt, *J* = 6.1, 3.2, 1.7 Hz, 2H), 6.80 (ddt, *J* = 5.9, 3.0, 1.4 Hz, 2H), 2.54 – 2.47 (m, 1H).

6.2.2.2 Synthesis of 1-n-alkylbenzimidazoles (1-8)

6.2.2.2.1 Synthesis of 1-ethylbenzimidazole (1): NaBenz (50.00 g, 357 mmol) was dissolved in 500 mL THF in a 1000 mL round bottom flask. Bromoethane (35.01 g, 23.98 mL, 321 mmol) was added and a solid precipitate was observed soon thereafter. A reflux condenser was attached and the reaction allowed to proceed overnight at 65^{o}C while stirring. After this time, the reaction was cooled, the solids filtered and the THF removed via rotary evaporation. The product was extracted into 400 mL of a 50:50 (vol:vol) mixture of EtOAc and hexanes. The solution was then dried over $MgSO_4$, mixed with activated carbon and filtered through a plug of basic Al_2O_3, which was then washed with an additional 200 mL of a the EtOAc/hexanes mixture. The filtrate was reduced via rotary evaporation and the product dried under vacuum lines to produce 1 as a pale yellow oil. Yield = 25.885 g (55.1%). ^{1}H NMR (500 MHz, DMSO) δ 8.24 (s, 1H), 7.62 (dd, *J* = 28.1, 7.9 Hz, 2H), 7.22 (dt, *J* = 27.7, 7.4 Hz, 2H), 4.27 (q, *J* = 7.3 Hz, 2H), 1.41 (t, *J* = 7.3 Hz, 3H). ^{1}H NMR consistent with published data.[45]

6.2.2.2.2 Synthesis of 1-n-propylbenzimidazole (2): Compound 2 was produced from NaBenz (30.00 g, 214 mmol) and 1-bromopropane (23.79 g, 17.60 mL, 193 mmol) in a manner similar to that employed for 1. Yield = 21.81 g (79.4%). ^{1}H NMR (500 MHz, DMSO) δ 8.22 (s, 1H), 7.62 (dd, *J* = 24.2, 7.9 Hz, 2H), 7.36 – 7.09 (m, 2H), 4.20 (t, *J* = 7.0 Hz, 2H), 1.91 – 1.66 (m, 2H), 0.84 (t, *J* = 7.4 Hz, 3H). ^{1}H NMR consistent with published data.[46, 47]

6.2.2.2.3 Synthesis of 1-butylbenzimidazole (3): Compound 3 was produced from NaBenz (50.00 g, 357 mmol) and 1-bromobutane (44.01 g, 34.57 mL, 321 mmol) in a manner similar to that employed for 1. ^{1}H NMR (500 MHz, DMSO) δ 8.22 (s, 1H), 7.62 (dd, *J* = 28.1, 7.9 Hz, 2H), 7.36 – 7.02 (m, 2H), 4.23 (t, *J* = 7.1 Hz, 2H), 1.91 – 1.62 (m, 2H), 1.40 – 1.08 (m, 2H), 0.88 (t, *J* = 7.4 Hz, 3H). ^{1}H NMR consistent with published data.[48, 49]

6.2.2.2.4 Synthesis of 1-pentylbenzimidazole (4): Compound 4 was produced from NaBenz (30.00 g, 214 mmol) and 1-bromopentane (29.22 g, 23.93 mL, 193 mmol) in a manner similar to that employed for 1. Yield = 24.72 g (76.6%). ^{1}H NMR (500 MHz, DMSO) δ 8.22 (s, 1H), 7.61 (dd, *J* = 27.0, 7.9 Hz, 2H), 7.22 (dt, *J* = 28.0, 7.4 Hz, 2H), 4.23 (t, *J* = 7.1 Hz, 2H), 1.91 – 1.62 (m, 2H), 1.47 – 1.03 (m, 4H), 0.83 (t, *J* = 7.2 Hz, 3H). ^{1}H NMR consistent with published data.[50]

*6.2.2.2.5 Synthesis of 1-hexylbenzimidazole (5): C*ompound 5 was produced from NaBenz (50.00 g, 357 mmol) and 1-bromohexane (53.06 g, 45.12 mL, 321 mmol) in a manner similar to that employed for 1. Yield = 51.33 g (78.9%). ^{1}H NMR (500 MHz, DMSO) δ 8.22 (s, 1H), 7.64 (d, *J* = 7.9 Hz, 1H), 7.58 (d, *J* = 7.9 Hz, 1H), 7.28 – 7.12 (m, 2H), 4.23 (t, *J* = 7.1 Hz, 2H), 1.83 – 1.69 (m, 2H), 1.41 – 1.08 (m, 6H), 0.82 (t, *J* = 6.9 Hz, 3H). ^{1}H NMR consistent with published data.[51]

6.2.2.2.6 Synthesis of 1-octylbenzimidazole (6): Compound 6 was produced from NaBenz (50.00 g, 357 mmol) and 1-bromooctane (62.05 g, 55.9 mL, 321 mmol) in a manner similar to that employed for 1. Yield = 53.44 g (72.2%). ^{1}H NMR (500 MHz, DMSO) δ 8.21 (s, 1H), 7.61 (dd, *J* = 31.0, 7.9 Hz, 2H), 7.32 – 7.15 (m, 2H), 4.22 (t, *J* = 7.1 Hz, 2H), 1.85 – 1.70 (m, 2H), 1.51 – 1.01 (m, 10H), 0.82 (t, *J* = 6.9 Hz, 3H).

6.2.2.2.7 Synthesis of 1-decylbenzimidazole (7): Compound 7 was produced from NaBenz (50.00 g, 357 mmol) and 1-bromodecane (71.07 g, 66.48 mL, 321 mmol) in a manner similar to that employed for 1. Yield = 56.64 g (68.2%). ^{1}H NMR (500 MHz, DMSO) δ 8.21 (s, 1H), 7.61 (dd, *J* = 28.9, 7.9 Hz, 2H), 7.36 – 7.09 (m, 2H), 4.22 (t, *J* = 7.1 Hz, 2H), 1.87 – 1.66 (m, 2H), 1.42 – 1.03 (m, 14H), 0.84 (t, *J* = 6.9 Hz, 3H). ^{1}H NMR consistent with published data.[50, 52]

6.2.2.2.8 Synthesis of 1-dodecylbenzimidazole (8): Compound 8 was produced from NaBenz (50.00 g, 357 mmol) and 1-bromododecane (77.86 g, 74.87 mL, 321 mmol) in a manner similar to that employed for 1. Yield = 64.52 g (70.1%). ^{1}H NMR (500 MHz, DMSO) δ 8.21 (s, 1H), 7.61 (dd, *J* = 33.0, 7.9 Hz, 2H), 7.36 – 7.07 (m, 2H), 4.22 (t, *J* = 7.1 Hz, 2H), 1.87 – 1.64 (m, 2H), 1.46 – 0.99 (m, 18H), 0.84 (t, *J* = 6.9 Hz, 3H). ^{1}H NMR consistent with published data.[49]

6.2.3 Density Measurements: Density values for each 1-*n*-alkylbenzimidazole were obtained over the range of 20.00-80.00^{o}C at 10.00^{o}C increments using a Mettler Toledo DM45 DeltaRange density meter,

using the same methodology as in our previous work.[30] The uncertainty associated with this measurement is ± 0.00005 g cm^{-3}.

6.2.4 Viscosity Measurements: Viscosity data were obtained for each 1-*n*-alkylbenzimidazole using a Brookfield DV-II+ Pro viscometer, under the same methodology as in our previous work, with the appropriate sized spindle (i.e. ULA) for relatively low viscosity liquids.[28, 30] Measurements were taken over the range of 20.00-80.00°C, with 5.00°C increments from 20.00-50.00°C and 10.00°C increments from 50.00-80.00°C. The temperature of the jacketed sample chamber was controlled via the Brookfield TC-602P circulating bath. The viscometer accuracy is ±1% of the reading for torque measurement with a repeatability of ±0.2% of the reading.

6.2.5 CO_2 Solubility Measurements: Solubilities of CO_2 in each 1-*n*-alkylbenzimidazole were measured gravimetrically using equipment and methodologies described in our previous works.[28-30] Experiments were conducted at temperatures of 30, 45, 60, and 75°C (as controlled by an oil bath). An initial charge of gas was fed at 30°C until the pressure equilibrated at ~5 atm. The respective errors associated with H and S were calculated based upon propagation of error of the experimental parameters (i.e. pressure, temperature, volumes, mass, etc.), in which all errors associated with our instrumentation are known. In this method, both the solubility and molecular weight of the gas are factors that influence the overall error. Measurements for CO_2 solubility exhibit typical experimental errors of ~4%, similar to our previous results for 1-n-alkylimidazoles. Based on published vapor pressure data and our previous measurements for 1-*n*-alkylimidazoles,[28-32] the vapor pressure of the 1-*n*-alkylbenzimidazole compounds can be assumed as negligible under the experimental temperature and pressure conditions, as it is low (~5 mm Hg maximum and typically < 1 torr) and very small (~0.1%) compared to the partial pressure of the gas.

6.2.6 SO_2 Solubility Measurements: Solubility of SO_2 in 1-butylbenzimidazole was measured in a different manner than that of CO_2. 1-butylbenzimidazole (5.00 g, 28.7 mmol) was added to a 50 mL round bottom flask with a stir bar. The flask was secured with a clamp, suspended over a stir-plate, and stirring initiated. SO_2 gas at ~1 psig was bubbled via a 1/16" outside diameter stainless steel tube into the stirring mixture. The mass of the flask and its contents, as well as the color of the liquid were recorded at several time intervals over a period of 20 minutes. After this time, SO_2 was desorbed from the liquid via a flush with N_2 for 40 minutes, and the mass of the flask contents and color of the liquid

were observed to return to their original value/state. The error associated with the measurement of the mass of the flask and its contents is ±0.0005 g, which is the uncertainty associated with the resolution of the balance used.

6.3. Results & Discussion

6.3.1. Densities of 1-n-Alkylbenzimidazoles: The measured density values for 1-*n*-alkylbenzmidazoles over the temperature range of 20-80 ^{o}C are presented in Table 6.1. For each compound, density was observed to decrease linearly with increasing temperature. Also, across the entire group of 1-*n*-alkylbenzimidazoles, density decreased as the *n*-alkyl substituent length increased, which is similar to observations across families of [$C_n$mim][X] ILs as the length of the "C_n" chain increases. Decreased density can be rationalized as the dilution of the polar imidazole ring (or ions in the case of ILs) within the bulk by increasing the volume fraction of the less dense hydrocarbon chains. A surface plot of density against temperature and the contribution of the alkyl chain for the 1-*n*-alkylbenzimidazoles is shown in Figure 6.1. As in our previous work, the "molecular weight parameter" (R'), a dimensionless value relating the molecular weight of the side chain to the molecular weight of the entire molecule, was used as means of quantifying the impact of the *n*-alkyl substituent. R' is calculated according to Eqn. 1 and values for each compound are presented in Table 6.1.

$$R' = \frac{MW(alkylchain)}{MW(molecule)} \quad (1)$$

Table 6.1: Densities of 1-*n*-alkylbenzimidazoles (1-8).

Compound			density (g cm^{-3}) at given temperature						
	MW(g mol^{-1})	R'	20 ^{o}C	30 ^{o}C	40 ^{o}C	50 ^{o}C	60 ^{o}C	70 ^{o}C	80 ^{o}C
1, ethyl	146.19	0.199	1.09399	1.08626	1.07859	1.07093	1.06327	1.0556	1.04792
2, propyl	160.22	0.269	1.06565	1.05799	1.05039	1.04282	1.03525	1.02769	1.02009
3, butyl	174.24	0.328	1.04381	1.03630	1.02884	1.02141	1.01401	1.00660	0.99918
4, pentyl	188.27	0.378	1.02438	1.01694	1.00936	1.00221	0.99485	0.98750	0.98012
5, hexyl	202.30	0.421	1.00943	1.00210	0.99484	0.98760	0.98037	0.97315	0.96589
6, octyl	230.35	0.492	0.98502	0.97794	0.97092	0.96391	0.95693	0.94996	0.94300
7, decyl	258.40	0.547	0.96606	0.95911	0.95221	0.94534	0.93849	0.93163	0.92477
8, dodecyl	286.45	0.591	0.95587	0.94913	0.94243	0.93569	0.92885	0.92183	0.91483

Similar to the results obtained for our characterizations of 1-*n*-alkylimidazoles,[30] a surface plot of density is approximately planar with respect to temperature and R' (Figure 6.3). However, a 7-10% increase in density is observed when comparing 1-*n*-alkylbenzimidazoles to 1-*n*-alkylimidazoles over the same temperature range. 1-*n*-alkylbenzimidazoles are less dense than many ILs, although this is likely to due to the absence of elements other than C, H and N and/or fluorinated groups.[27, 53-56]

The data presented in Table 6.1 and Figure X could be fit with a high degree of accuracy to the same form of equation we applied to our density measurements of 1-*n*-alkylimidazoles (Eqn. 2). A surface regression of the data in Figure 6.3 performed with Matlab provides an excellent fit (R^2 = 0.9968) to Eqn. 2, with constants A = -7.253x10^{-4} g cm^{-3} K^{-1}, B = -0.3479 g cm^{-3}, and C = 1.3710 g cm^{-3}, where T is temperature in Kelvin and R' is the dimensionless molecular weight parameter for a given molecule (Table 6.1). Thus, this relatively simple model provides the ability to accurately describe density at a given temperature for 1-*n*-alkylbenzimidazoles with side chains as large as dodecyl.

$$\rho(T, R') = AT + BR' + C \qquad (2)$$

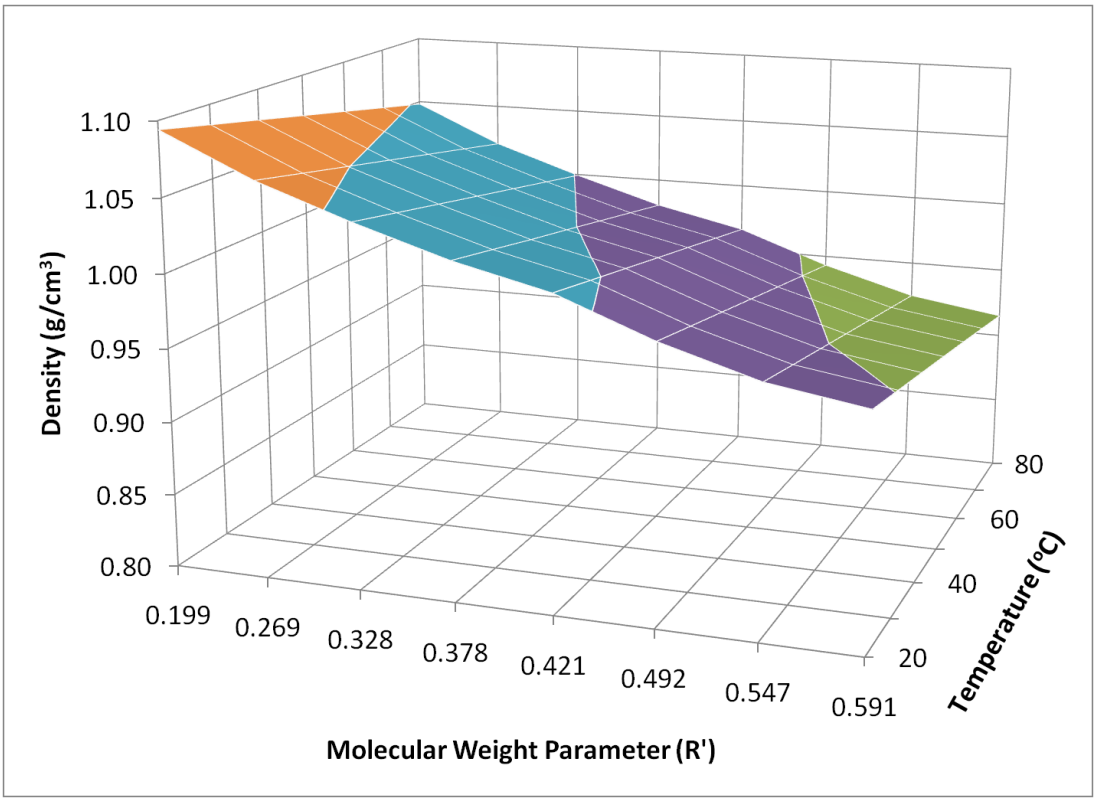

Figure 6.3: Three-dimensional plot of 1-*n*-alkylbenzimidazole densities as related to temperature and R'.

6.3.2. Viscosities of 1-n-alkylbenzimidazoles: The measured viscosity values for 1-*n*-alkylbenzimidazoles over the temperature range of 20-80 °C are presented in Table 6.2. Viscosities of the eight 1-*n*-benzalkylimidazole compounds examined were < 100 cP. For each compound, viscosity was observed to decrease in a nonlinear fashion with increasing temperature. Viscosity was strongly correlated to the length of the *n*-alkyl substituent, with 1-dodecylbenzimidazole observed to be ~3.5x more viscous between than 1-ethylbenzimidazole at 20 °C, although the magnitude of this difference reduced to ~2x at 80°C.

Table 6.2: Viscosities of 1-*n*-alkylbenzimidazoles (1-8).

	viscosity (cP) at given temperature									
Compound	20 °C	25 °C	30 °C	35 °C	40 °C	45 °C	50 °C	60 °C	70 °C	80 °C
1 ethyl	27.09	20.67	16.03	12.73	10.32	8.50	7.18	5.31	4.13	3.29
2, propyl	49.01	35.82	26.51	20.06	15.62	12.37	10.05	7.01	5.15	3.99
3, butyl	49.49	38.34	28.19	21.50	16.71	13.23	10.77	7.47	5.45	4.15
4, pentyl	52.79	40.91	30.35	23.25	18.00	14.36	11.60	8.05	5.91	4.54
5, hexyl	60.44	45.37	33.89	25.72	19.98	15.86	13.87	8.85	6.64	4.91
6, octyl	68.10	50.51	38.04	29.25	23.00	18.20	14.83	10.26	7.46	5.67
7, decyl	71.13	54.12	41.02	31.71	24.97	19.95	16.24	11.22	8.17	6.20
8, dodecyl	96.34	70.19	52.55	40.07	31.06	24.54	19.75	13.36	9.54	7.14

The temperature dependence of viscosity for each compound can be shown to follow the Litovitz Model (Eqn. 3), which we have shown provides a very accurate model of the viscosities of 1-*n*-alkylimidazoles, and has also been successfully applied to imidazolium-based ILs.[53] Using the data in Table 6.2, we obtained A and B coefficients for compounds 1-8 via regression using Matlab, which are presented along with goodness of fit values (R^2) in Table 6.3.

$$\mu(T) = A\exp\left(\frac{B}{T^3}\right) \qquad (3)$$

Table 6.3: Empirical constants and quality of fit for Eqn. 3 as applied to viscosities of 1-*n*-alkylbenzimidazoles (1-8).

Compound	A (cP)	B x 10^{-8} (K^3)	R^2
1 ethyl	0.188	1.24	0.9977
2, propyl	0.129	1.48	0.9979
3, butyl	0.139	1.48	0.9989
4, pentyl	0.155	1.47	0.9989
5, hexyl	0.168	1.48	0.9988
6, octyl	0.195	1.47	0.9994
7, decyl	0.227	1.45	0.9997
8, dodecyl	0.212	1.54	0.9996

Figure 6.4 presents a surface plot of the viscosity data in Table 6.2 with respect to temperature and R'. As can be seen in Figure 6.4 a relatively smooth surface exists between R' values of 0.269 – 0.547, which corresponds to the range encompassed by 1-propylbenzimidazole and 1-decylbenzimidazole. Sharper changes in viscosity occur at the edges of the plot, corresponding to 1-ethylbenzimidazole and 1-dodecylbenzimidazole. Attempts to fit the entire surface to a 2-parameter (T, R') Litovitz Model, although successfully applied in our previous work with 1-*n*-alkylimidazoles, were unsuccessful for 1-*n*-alkylbenzimidazoles. Thus, a single equation for viscosity cannot be applied across the entire series.

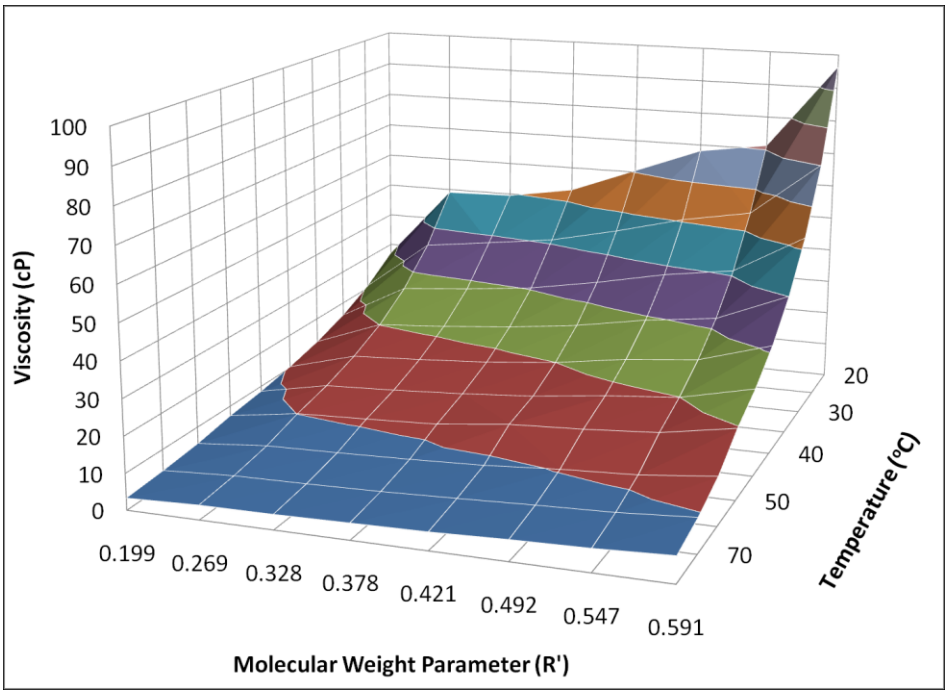

Figure 6.4: Three-dimensional plot of 1-*n*-alkylbenzimidazole viscosities as related to temperature and R'.

However, in examination of Table 6.3, it appears that for the range of compounds that fall between 1-propylbenzimidazole (2) and 1-decylbenzimidazole (7), a single model can be developed, as the constant 'A' is correlated R' and B is virtually independent of R', as its value is 1.47×10^8 K^3 for each of the compounds. We have found that the relationship between A and R' is well-described ($R^2 = 0.9896$) by Eqn. 4, with coefficients of 0.722 cP and 2.0445 (dimensionless).

$$A = 0.0722 \cdot \exp(2.0445 \cdot R') \tag{4}$$

The substitution of Eqn. 4 into Eqn. 3 yields Eqn. 5, which can be used to describe the viscosity (cP) of 1-*n*-alkylbenzimidazoles ranging from 1-propylbenzimidazole to 1-decylbenzimidazole, with an $R^2 = 0.9934$.

$$\mu(T,R) = 0.0722 \cdot \exp\left(2.0445 \cdot R' + \frac{1.47 \times 10^8}{T^3}\right) \tag{5}$$

Eqn. 5 thus presents a useful and accurate model for estimating the viscosity of a range of 1-*n*-alkylbenzimidazoles as a function of temperature and the contribution of the alkyl chain. This model is

somewhat more simplistic than that found for describing the viscosity of 1-*n*-alkylimidazoles, although the 1-*n*-alkylimidazoles were much less viscous. This may be due to the fact that viscosities of the 1-*n*-alkylbenzimidazoles span a relatively smaller range of magnitudes than 1-*n*-alkylimidazoles, where the large fused ring system in the former plays a much more influential role in governing molecular motion, while the viscosities of the latter are much more sensitive to the influence of alkyl chain length. This effect of increasing viscosity with increasing chain length is also observed for homologous series of ILs that vary only in the length of the alkyl chain.[27, 53, 57-60]

Figure 6.5 presents a graphical illustration of the relative viscosity ranges exhibited by ILs, 1-*n*-alkylimidazoles and 1-*n*-alkylbenzimidazoles. As is apparent, 1-*n*-alkylbenzimidazoles possess viscosities that mostly exceed those exhibited by 1-*n*-alkylimidazoles, yet fall near the lower range of those exhibited by 1-*n*-alkyl-3-methylimidazolium ILs. As a point of reference, 1-*n*-alkylbenzimidazoles tend to overlap the region occupied by 1-ethyl-3-methylimidazolium salts (e.g. $[C_2mim][Tf_2N]$, $[C_2mim][dca]$, etc.). The underlying data points used to form this graph can be viewed in the Supporting Information from our prior work.[30]

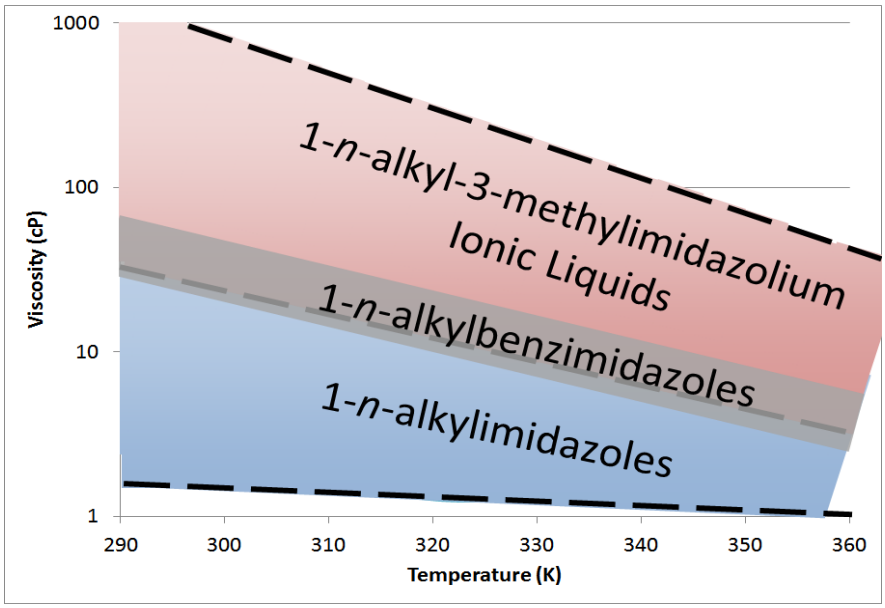

Figure 6.5: Graphical comparison of reported viscosity ranges of 1-*n*-alkylimidazoles (lower, blue); 1-*n*-alkylbenzimidazoles (this work)(middle, grey); and 1-*n*-alkyl-3-methylimidazolium ILs (upper, red). Modified with permission from Shanonn, M.S.; Bara, J. E. Properties of Alkylimidazoles as Solvents for CO_2 Capture and Comparisons to Imidazolium-Based Ionic Liquids. *Ind. Eng. Chem. Res.* 2011, *50* (14), 8665-8677. Copyright 2011 American Chemical Society.

6.3.3 Solubility of CO_2: Henry's constants (*H*) and volumetric solubilities (*S*) of CO_2 in 1-*n*-alkylbenzimidazoles at temperatures between 30-75°C are presented in Table 6.4.

Table 6.4: Solubility of CO_2 in several 1-*n*-alkylbenzimidazoles at partial pressures of ~5 atm and temperatures between 30-75°C expressed as both Henry's constants (H(atm)) and volumetric solubilities (S).

Compound	Temp. (°C)	H (atm)	+/-	S[a]	+/-
1, ethyl	30	96	2	1.80	0.05
	45	126	4	1.36	0.04
	60	160	5	1.03	0.03
	75	202	7	0.82	0.03
3, butyl	30	88	2	1.60	0.04
	45	123	4	1.14	0.04
	60	160	6	0.83	0.03
	75	200	8	0.70	0.03
5, hexyl	30	89	3	1.30	0.05
	45	133	6	0.86	0.04
	60	203	12	0.55	0.03
	75	298	22	0.38	0.03

a: S [=] (cm^3 gas (STP)) (cm^3 solvent)$^{-1}$ atm^{-1}

Uncertainty represents +/- one standard deviation

The data presented are largely indicative of physical solubility behavior, rather than any type of chemical reaction between CO_2 and the benzimidazole molecules. This behavior is consistent with what has been observed for alkylimidazoles and most ILs, indicating that each of these classes of compounds would be most useful under high pressures or high concentrations of CO_2, rather than in low pressure applications (i.e. post-combustion CO_2 capture).

At any given temperature, 1-ethylbenzimidazole showed the highest CO_2 solubility per volume, as extension of the alkyl chain serves to diminish CO_2 solubility, as has been observed for alkylimidazoles and imidazolium-based ILs.[2, 29, 30, 61] The values reported are lower than those reported for alkylimidazoles and imidazolium-based ILs,[2, 29, 30] indicating that the six-membered aromatic ring

present within benzimidazoles has a negative effect on CO_2 affinity. A similar effect has been observed for benzyl-functionalized imidazolium-based ILs,[2, 62] although interactions between CO_2 and the □-electrons were expected to increase CO_2 solubility. One possible explanation is that the benzimidazole solvent (and by extension, ILs with benzyl groups) possess less free volume in which CO_2 can dissolve. This is supported by the fact that improved separation of CO_2/N_2 has been observed in ionic liquid-based membranes where these groups are present.[1, 62, 63] We have not measured comparative data for CO_2 solubility in 1-benzylimidazole due to the fact it is a crystalline solid with a melting point of ~70°C.[43, 47, 64]

Also shown in Table 6.4, for the convenience of the reader, are Henry's constants, which describe the solubility of CO_2 in terms of mole fraction at a given temperature. However, as with the same discussion in our previous work, this observation and assessment of using Henry's constants (i.e. mole basis) for gas solubility comparisons among varying substituent chain lengths is not appropriate. It can be seen that although the Henry's constants (i.e. mole fraction of CO_2) are similar for each molecule at a given temperature, this is primarily due to an increase in solvent molecular weight (i.e. fewer moles of solvent) rather than increased affinity of CO_2 for the solvent.

6.3.4 Solubility of SO_2: Experimental results for SO_2 absorption in 1-butylbenzimidazole are presented below in Table 6.5, with Figure 6.6 also provided as visual evidence to support our observations of the color change associated with SO_2 absorption. A larger version of Figure 6.6 is provided as Supporting Information. The choice of 1-butylbenzimidazole was based on its relatively low viscosity amongst this group of compounds and the expectation that its vapor pressure is lower than that of 1-ethylbenzimidazole. It is likely that any of the 1-*n*-alkylbenzimidazole compounds would produce similar results. It should be noted that the small difference in mass recorded between the initial and final readings is slightly less than zero. This is almost certainly due to the loss of small quantities of 1-butylbenzimidazole on the stainless steel tubing that was submerged into the liquid to introduce SO_2.

Table 6.5: Experimental data for absorption of SO_2 in 5.00 g (28.7 mmol) 1-butylbenzimidazole at 25°C (3).

Time (min)	Flask Mass (g)	Δm (g SO_2 absorbed)	mol SO_2 absorbed	mol SO_2 (mol 1-butylbenzimidazole)$^{-1}$	Observation
0 (start SO_2)	98.865	0.000	0.00000	0.00000	pale yellow
5	99.208	0.343	0.00536	0.18676	bright yellow
10	99.851	0.986	0.01541	0.53688	yellow-orange
20 (stop SO_2, start N_2 flush)	100.641	1.776	0.02775	0.96703	dark orange, more viscous
60 (stop N_2 flush)	98.847	-0.018	-0.00028	-0.009801	pale yellow

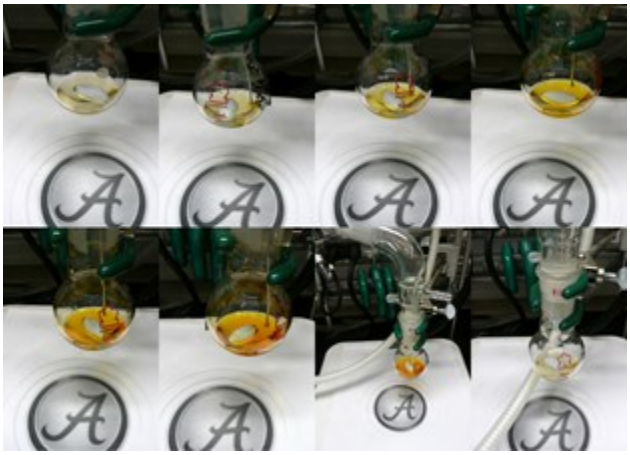

Figure 6.6: Progressive darkening from essentially colorless to pale yellow to orange in 1-butylbenzimidazole (3) upon exposure to SO_2 and subsequent return to an essentially colorless liquid upon flushing with N_2 (bottom left).

The data in Table 6.5 indicate that SO_2 can be readily and rapidly absorbed at room temperature and low pressure (~1 psig) to at least a 1:1 (mol:mol) ratio with 1-butylbenzimidazole. Furthermore, SO_2 can be easily desorbed at room temperature using only an N_2 flush. While we previously observed that 1-hexylimidazole was also capable of absorbing at least 1 mole of SO_2 per mole 1-hexylimidazole under similar conditions, a portion of that SO_2 was not readily desorbed from 1-hexylimidazole. SO_2 and 1-

hexylimidazole formed a relatively stable 1:2 adduct, and higher temperatures (> 80°C) and vacuum were required to remove SO_2. However, while SO_2 has been shown to undergo reversible chemical reaction with alkylimidazoles, alkylbenzimidazoles do not undergo a similar chemical reaction as the reactive nitrogen is likely de-activated by the fused ring system. This behavior is similar to that observed for many imidazolium-based ILs where there is no nucleophilic or basic site to react with SO_2,[65] with exceptions observed when the anion is chemically reactive.[66, 67] Although the interactions between SO_2 and the 1-butylbenzimidazole molecule are weak, the fact that a significant color change is observed at relatively low concentrations could make these molecules useful as visual indicators of the presence of SO_2.

6.4 Conclusions: A series of eight 1-*n*-alkylbenzimidazoles was synthesized and their densities and viscosities characterized as functions of temperature and alkyl chain length. Each property was found to be strongly dependent on both variables. A highly-correlated model for density was developed that encompassed all of the compounds of interest, while a similarly accurate viscosity model could be applied from 1-propylbenzimidazole through 1-decylbenzimidazole. Density and viscosity profiles for 1-*n*-alkylbenzimidazoles were noted to possess similar characteristics to 1-*n*-alkylimidazoles and imidazolium-based ILs. CO_2 solubility, however, is somewhat negatively impacted by the presence of the benzimidazole moiety, as measured values were less than those obtained for 1-*n*-alkylimidazoles and many imidazolium-based ILs. Further research is needed as to why the presence of benzene rings in both neutral and charged (i.e. ILs) molecules hinders CO_2 dissolution. Finally, 1-butylbenzimidazole was demonstrated to exhibit physical, rather than chemical interactions with SO_2, a property more in line with imidazolium-based ILs than alkylimidazoles.

1-*n*-alkylbenzimidazoles can be viewed to have hybrid properties of ILs and alkylimidazoles. It is our hope that this initial study on the properties of benzimidazoles in the liquid state will bring greater attention to this versatile class of molecules in identifying applications and gain a more thorough understanding of imidazolium/benzimidazolium ILs.

Acknowledgments

Support for this work provided by ION Engineering, LLC; United States Department of Energy – National Energy Technology Laboratory (DE-FE00005799); and the National Science Foundation Research Experiences for Undergraduates Program (EEC-1062705) is gratefully acknowledged. Additional support from the University of Alabama Research Grants Committee is also gratefully

acknowledged. The authors thank Ken Belmore of the University of Alabama for acquisition of ^{1}H NMR spectra.

6.5 References:

[1] BARA JE, CAMPER DE, GIN DL, et al. Room-Temperature Ionic Liquids and Composite Materials: Platform Technologies for CO_2 Capture. *Acc Chem Res*, 2010, 43: 152-159.
[2] BARA JE, CARLISLE TK, GABRIEL CJ, et al. Guide to CO2 Separations in Imidazolium-Based Room-Temperature Ionic Liquids. *Ind Eng Chem Res,* 2009, 48: 2739-2751.
[3] ARMAND M, ENDRES F, MACFARLANE DR, et al. Ionic-liquid materials for the electrochemical challenges of the future. *Nature Mater*, 2009, 8: 621-629.
[4] KATO T. From Nanostructured Liquid Crystals to Polymer-Based Electrolytes. *Angew Chem Int Ed*, 2010, 49: 7847-7848.
[5] ICHIKAWA T, YOSHIO M, HAMASAKI A, et al. 3D Interconnected Ionic Nano-Channels Formed in Polymer Films: Self-Organization and Polymerization of Thermotropic Bicontinuous Cubic Liquid Crystals. *J Am Chem Soc*, 2011, 133: 2163-2169.
[6] GUTOWSKI KE, HOLBREY JD, ROGERS RD, et al. Prediction of the formation and stabilities of energetic salts and ionic liquids based on ab initio electronic structure calculations. *J Phys Chem B*, 2005, 109: 23196-23208.
[7] DRAB D M, SMIGLAK M, SHAMSHINA J L, et al. Synthesis of N-cyanoalkyl-functionalized imidazolium nitrate and dicyanamide ionic liquids with a comparison of their thermal properties for energetic applications. *New J Chem*, 2011, 35: 1701-1717.
[8] POGODINA NV, METWALLI E, MULLER-BUSCHBAUM P, et al. Peculiar Behavior of Azolium Azolate Energetic Ionic Liquids. *J Phys Chem Lett*, 2011, 2: 2571-2576.
[9] WANG H, GURAU G, ROGERS RD. Ionic liquid processing of cellulose. *Chem Soc Rev*, 2012, 41: 1519-1537
[10] ANDERSON EB, LONG TE. Imidazole- and imidazolium-containing polymers for biology and material science applications. *Polymer*, 2010, 51: 2447-2454.
[11] OHNO H, YOSHIZAWA M, OGIHARA W. Development of new class of ion conductive polymers based on ionic liquids. *Electrochim Acta*, 2004, 50: 255-261.
[12] GU YY, LODGE TP. Synthesis and Gas Separation Performance of Triblock Copolymer Ion Gels with a Polymerized Ionic Liquid Mid-Block. *Macromolecules*, 2011, 44: 1732-1736.
[13] LODGE T P. Materials science - A unique platform for materials design. *Science*, 2008, 321: 50-51.
[14] BARA JE, GIN DL, NOBLE RD. Effect of Anion on Gas Separation Performance of Polymer-Room-Temperature Ionic Liquid Composite Membranes. *Ind Eng Chem Res*, 2008, 47: 9919-9924.
[15] BARA JE, HATAKEYAMA ES, GIN DL, et al. Improving CO_2 permeability in polymerized room-temperature ionic liquid gas separation membranes through the formation of a solid composite with a room-temperature ionic liquid. *Polym Advan Technol*, 2008, 19: 1415-1420.
[16] MECERREYES D. Polymeric ionic liquids: Broadening the properties and applications of polyelectrolytes. *Prog Polym Sci*, 2011, 36: 1629-1648.
[17] KATRITZKY AR, JAIN R, LOMAKA A, et al. Correlation of the Melting Points of Potential Ionic Liquids (Imidazolium Bromides and Benzimidazolium Bromides) Using the CODESSA Program. *J Chem Inf Comp Sci*, 2002, 42: 225-231.
[18] LIN IJB, VASAM CS. Preparation and application of N-heterocyclic carbene complexes of Ag(I). *Coord Chem Rev*, 2007, 251: 642-670.

[19] AMYES T L, DIVER ST, RICHARD JP, et al. Formation and Stability of N-Heterocyclic Carbenes in Water: The Carbon Acid pKa of Imidazolium Cations in Aqueous Solution. *J Am Chem Soc*, 2004, 126: 4366-4374.
[20] CHAN A, SCHEIDT KA. Conversion of α,β-Unsaturated Aldehydes into Saturated Esters: An Umpolung Reaction Catalyzed by Nucleophilic Carbenes. *Org Lett*, 2005, 7: 905-908.
[21] BINNEMANS K. Ionic liquid crystals. *Chem Rev*, 2005, 105: 4148-4204.
[22] PERNAK J, ROGOŻA J, MIRSKA I. Synthesis and antimicrobial activities of new pyridinium and benzimidazolium chlorides. *Eur J Med Chem*, 2001, 36: 313-320.
[23] BOYDSTON AJ, VU PD, DYKHNO OL, et al. Modular Fluorescent Benzobis(imidazolium) Salts: Syntheses, Photophysical Analyses, and Applications. *J Am Chem Soc*, 2008, 130: 3143-3156.
[24] BOYDSTON AJ, PECINOVSKY CS, CHAO ST, et al. Phase-Tunable Fluorophores Based upon Benzobis(imidazolium) Salts. *J Am Chem Soc*, 2007, 129: 14550-14551.
[25] THOMAS OD, SOO KJWY, PECKHAM TJ, et al. Anion conducting poly(dialkyl benzimidazolium) salts. *Polym Chem*, 2011, 2: 1641-1643.
[26] PRESTON PN. Synthesis, reactions, and spectroscopic properties of benzimidazoles. *Chem Rev*, 1974, 74: 279-314.
[27] SEDDON KR, STARK A, TORRES MJ. Viscosity and density of 1-alkyl-3-methylimidazolium ionic liquids; in ABRAHAM MA, MOENS L. Clean Solvents - Alternative Media for Chemical Reactions and Processing. ACS Symposisum Series, 2002: 34-49.
[28] SHANNON MS, BARA JE. Reactive and Reversible Ionic Liquids for CO_2 Capture and Acid Gas Removal. *Sep Sci Technol*, 2012, 47: 178-188.
[29] SHANNON MS, TEDSTONE JM, DANIELSEN SPO, et al. Evaluation of Alkylimidazoles as Physical Solvents for CO_2/CH_4 Separation. *Ind Eng Chem Res*, 2011, 51: 515-522.
[30] SHANNON MS, BARA JE. Properties of Alkylimidazoles as Solvents for CO2 Capture and Comparisons to Imidazolium-Based Ionic Liquids. *Ind Eng Chem Res*, 2011, 50: 8665-8677.
[31] EMEL'YANENKO VN, PORTNOVA SV, VEREVKIN SP, et al. Building blocks for ionic liquids: Vapor pressures and vaporization enthalpies of 1-(n-alkyl)-imidazoles. *J Chem Thermodyn*, 2011, 43: 1500-1505.
[32] VEREVKIN SP, ZAITSAU DH, EMEL'YANENKO VN, et al. Thermodynamics of Ionic Liquids Precursors: 1-Methylimidazole. *J Phys Chem B*, 2011, 115: 4404-4411.
[33] EMEL'YANENKO V N, ZAITSAU D H, VEREVKIN S P, et al. Vaporization and Formation Enthalpies of 1-Alkyl-3-methylimidazolium Tricyanomethanides. *J Phys Chem B*, 2011, 115: 11712-11717.
[34] LENARCIK B, OJCZENASZ P. The influence of the size and position of the alkyl groups in alkylimidazole molecules on their acid-base properties. *J Heterocyclic Chem*, 2002, 39: 287-90.
[35] DE LUCA L. Naturally occurring and synthetic imidazoles: Their chemistry and their biological activities. *Curr Med Chem*, 2006, 13: 1-23.
[36] ROGERS RD, SEDDON KR. Ionic Liquids--Solvents of the Future?. *Science*, 2003, 302: 792-793.
[37] BONAZZI D, CAVRINI V, GATTI R, et al. Determination of imidazole antimycotics in creams by supercritical fluid extraction and derivative UV spectroscop. *J Pharm Biomed Anal*, 1998, 18: 235-240.
[38] BOIANI M, GONZALEZ M. Imidazole and benzimidazole derivatives as chemotherapeutic agents. *Mini-Rev Med Chem*, 2005, 5: 409-24.
[39] GREEN MD, ALLEN MH, DENNIS JM, et al. Tailoring macromolecular architecture with imidazole functionality: A perspective for controlled polymerization processes. *Eur Polym J*, 2011, 47: 486-496.
[40] STURLAUGSON AL, FRUCHEY KS, FAYER MD. Orientational Dynamics of Room Temperature Ionic Liquid/Water Mixtures: Water-Induced Structure. *J Phys Chem B*, 2012, In Press. DOI: 10.1021/jp209942r
[41] PLECHKOVA NV, SEDDON KR. Applications of ionic liquids in the chemical industry. *Chem Soc Rev*, 2008, 37: 123-150.
[42] SEDDON KR. Ionic liquids: A taste of the future. *Nat Mater*, 2003, 2: 363-5.

[43] BARA J E. Versatile and Scalable Method for Producing N-Functionalized Imidazoles. *Ind En Chem Res*, 2011, 50: 13614-13619.
[44] GOTTLIEB HE, KOTLYAR V, NUDELMAN A. NMR chemical shifts of common laboratory solvents as trace impurities. *J Org Chem*, 1997, 62: 7512-7515.
[45] HANAN EJ, CHAN BK, ESTRADA AA, et al. Mild and General One-Pot Reduction and Cyclization of Aromatic and Heteroaromatic 2-Nitroamines to Bicyclic 2H-Imidazoles. Synlett, 2010, 2010: 2759-2764.
[46] LYGIN AV, DE MEIJERE A. Synthesis of 1-Substituted Benzimidazoles from o-Bromophenyl Isocyanide and Amines. *Eur J Org Chem*, 2009, 30: 5138-5141.
[47] MILEN M, GRUN A, BALINT E, et al. Solid-Liquid Phase Alkylation of N-Heterocycles: Microwave-Assisted Synthesis as an Environmentally Friendly Alternative. *Synthetic Commun,* 2010, 40: 2291-2301.
[48] KUANG DB, KLEIN C, ITO S, et al. High-efficiency and stable mesoscopic dye-sensitized solar cells based on a high molar extinction coefficient ruthenium sensitizer and nonvolatile electrolyte. *Advan Mater*, 2007, 19(8): 1133-7.
[49] KOSE O, SAITO S. Cross-coupling reaction of alcohols for carbon-carbon bond formation using pincer-type NHC/palladium catalysts. *Org Biomol Chem*, 2010, 8: 896-900.
[50] BOGDAL D, PIELICHOWSKI J, JASKOT K. Remarkable fast N-alkylation of azaheterocycles under microwave irradiation in dry media. *Heterocycles*, 1997, 45: 715-722.
[51] WANNALERSE B, TUNTULANI T, TOMAPATANAGET B. Synthesis, optical and electrochemical properties of new receptors and sensors containing anthraquinone and benzimidazole units. *Tetrahedron*, 2008, 64: 10619-10624.
[52] DU PREEZ JGH, MATTHEUS C, SUMTER N, et al. Nitrogen reagents in metal ion separation. Part VIII. Substituted imidazoles as extractants for Cu^{2+}. *Solvent Extr Ion Exc*, 1998, 16: 565-586.
[53] GHATEE MH, ZARE M, MOOSAVI F, et al. Temperature-Dependent Density and Viscosity of the Ionic Liquids 1-Alkyl-3-methylimidazolium Iodides: Experiment and Molecular Dynamics Simulation. *J Chem Eng Dat*, 2010, 55: 3084-3088.
[54] SMITH GD, BORODIN O, MAGDA JJ, et al. A comparison of fluoroalkyl-derivatized imidazolium:TFSI and alkyl-derivatized imidazolium:TFSI ionic liquids: a molecular dynamics simulation study. *Phys Chem Chem Phys*, 2010, 12: 7064-7076.
[55] GARDAS RL, COUTINHO JAP. Extension of the Ye and Shreeve group contribution method for density estimation of ionic liquids in a wide range of temperatures and pressures. *Fluid Phase Equilibr*, 2008, 263: 26-32.
[56] YE CF, SHREEVE JM. Rapid and accurate estimation of densities of room-temperature ionic liquids and salts. *J Phys Chem A*, 2007, 111: 1456-61.
[57] GARDAS RL, COUTINHO JAP. A group contribution method for viscosity estimation of ionic liquids. *Fluid Phase Equilibr*, 2008, 266: 195-201.
[58] SMITH GD, BORODIN O, LI LY, et al. A comparison of ether- and alkyl-derivatized imidazolium-based room-temperature ionic liquids: a molecular dynamics simulation study. *Phys Chem Chem Phys*, 2008, 10: 6301-6312.
[59] APARICIO S, ATILHAN M, KARADAS F. Thermophysical Properties of Pure Ionic Liquids: Review of Present Situation. *Ind Eng Chem Res*, 2010, 49: 9580-9595.
[60] ROONEY D, JACQUEMIN J, GARDAS R. Thermophysical Properties of Ionic Liquids in KIRCHNER B. Ionic Liquids. Springer Berlin / Heidelberg. 2010: 185-212.
[61] CARLISLE TK, BARA JE, GABRIEL CJ, et al. Interpretation of CO_2 solubility and selectivity in nitrile-functionalized room-temperature ionic liquids using a group contribution approach. *Ind Eng Chem Res*, 2008, 47: 7005-7012.
[62] MAHURIN SM, DAI T, YEARY JS, et al. Benzyl-Functionalized Room Temperature Ionic Liquids for CO_2/N_2 Separation. *Ind Eng Chem Res*, 2011, 50: 14061-14069.

[63] BARA JE, LESSMANN S, GABRIEL CJ, et al. Synthesis and performance of polymerizable room-temperature ionic liquids as gas separation membranes. *Ind Eng Chem Res*, 2007, 46: 5397-5404.
[64] BEGG CG, GRIMMETT MR, WETHEY PD. The thermally induced rearrangement of 1-substituted imidazoles. *Aust J Chem*, 1973, 26: 2435-2446.
[65] ANDERSON JL, DIXON JK, MAGINN EJ, et al. Measurement of SO_2 solubility in ionic liquids. *J Phys Chem B*, 2006, 110: 15059-15062.
[66] WANG C, CUI G, LUO X, et al. Highly Efficient and Reversible SO_2 Capture by Tunable Azole-Based Ionic Liquids through Multiple-Site Chemical Absorption. *J Am Chem Soc*, 2011, 133: 11916-11919.
[67] SHIFLETT MB, YOKOZEKI A. Chemical Absorption of Sulfur Dioxide in Room-Temperature Ionic Liquids. *Ind Eng Chem Res,* 2010, 49: 1370-1377.

6.6 Appendix:

Table of Contents Graphic:

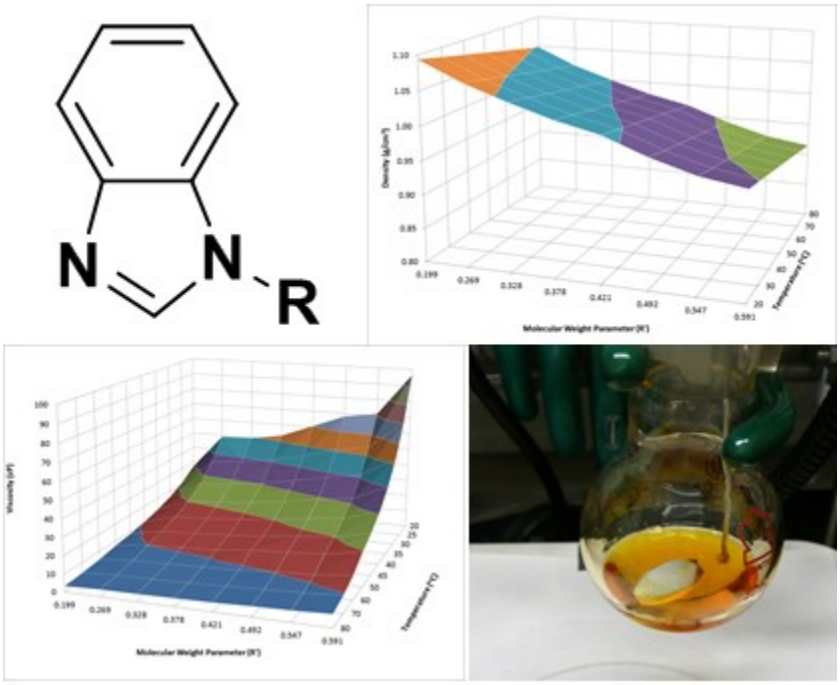

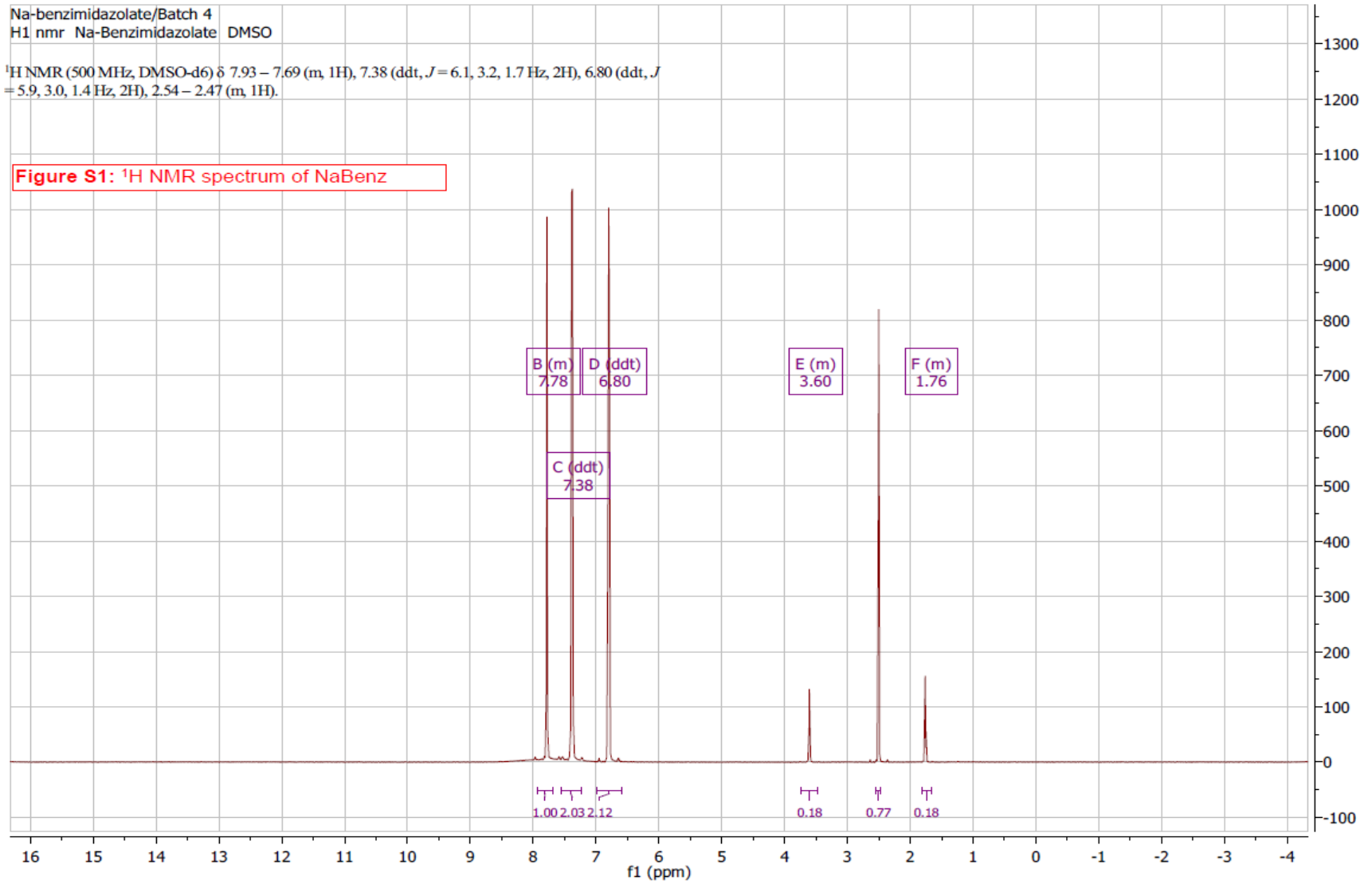

Figure S1: H[1]NMR spectrum of Na-benzimidazolate.

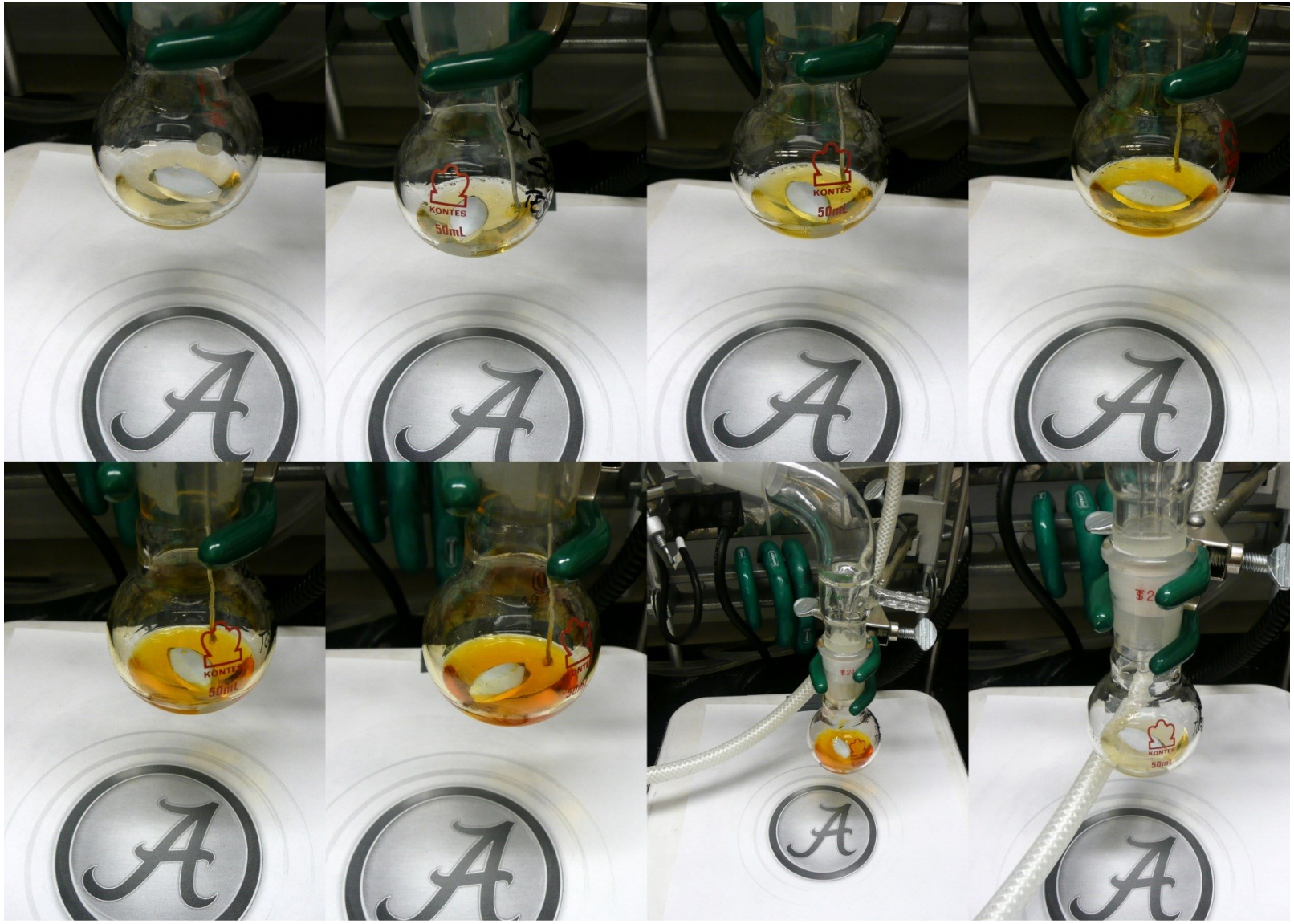

Figure S2: Larger view of Figure 6 from main manuscript.

CHAPTER SEVEN

[†]Properties and Performance of Ether-functionalized Imidazoles as Physical Solvents for CO_2 Separations

Matthew S. Shannon,[1] Jason M. Tedstone,[2,4] Scott P. O. Danielsen,[3,4]
Michelle S. Hindman[1] & Jason E. Bara[1*]

1. Department of Chemical & Biological Engineering, University of Alabama, Tuscaloosa AL USA 35487-0203
2. NSF-REU Site: Engineering Solutions for Clean Energy Generation, Storage and Consumption, Department of Chemical & Biological Engineering, University of Alabama, Tuscaloosa AL USA 35487-0203
3. Department of Chemical & Biomolecular Engineering, Clemson University, Clemson, SC USA 29634
4. Department of Chemical & Biomolecular Engineering, University of Pennsylvania, Philadelphia PA USA 19104-6315

Abstract

Previously, we investigated 1-*n*-alkylimidazoles as low viscosity, low vapor pressure physical solvents for CO_2/CH_4 separation and noted a decrease in performance as the length of the *n*-alkyl chain was extended. Here, we examine imidazoles featuring oligo(ethylene glycol) substituents ("PEG_n-imidazoles") as an opportunity to improve upon the separation performance of this class of molecules. In the current work, we have characterized density and viscosity of PEG_n-imidazoles over the range of 20-80°C. PEG_n-imidazoles are slightly more viscous than 1-*n*-alkylimidazoles but still fall below 20 cP. Ideal gas solubilities of CO_2 and CH_4 were measured in PEG_n-imidazoles at gas partial pressures of ~5 bar and temperatures of 25-70°C. Solubilities of CO_2 and CH_4 were both found to decrease with increasing temperature, with a stronger dependence for CO_2. However, better CO_2/CH_4 selectivity was achieved in PEG_n-imidazoles at lower operating temperatures than was observed for 1-*n*-alkylimidazoles. Physical properties and gas separation performances were correlated with fractional free volume calculated via COSMOtherm as well as solubility parameters. The results show trends of decreased FFV when polar ether groups comprise the substituent, and that CO_2 solubility and solubility selectivity for CO_2/CH_4 are improved compared to their non-polar, hydrocarbon-based analogues.

Keywords
Natural gas, imidazoles, ionic liquids, carbon dioxide (CO_2) capture, solvents

[†]*Energy & Fuels, 2013, 27, 3349-3357*.

7.1. Introduction: U.S. production of natural gas is approaching 1 trillion m^3 (STP) per year, with world consumption near 3 trillion m^3 (STP) per year.[1] Methane (CH_4) is the major component (75-90%) of natural gas streams along with other species such as water, carbon dioxide, nitrogen, hydrogen sulfide, and approximately 1-3% hydrocarbon content (ethane, propane, butane, etc.).[2, 3] Approximately 20% of raw natural gas contains CO_2, with U.S. pipeline standards only allowing no more than 2 vol%.[1-3] The leading technology for acid gas (i.e. CO_2, H_2S, etc.) removal is solvent absorption,[2, 3] where chemical (i.e. reactive) solvents such as aqueous amines are most commonly used, especially at lower contaminant partial pressures and/or when complete removal of CO_2 and/or H_2S is vital.[4] Physical (i.e. non-reactive) solvent absorption is employed at higher contaminant gas partial pressures, where they are more advantageous for bulk removal of CO_2 due to a more energy-efficient solvent regeneration than that of chemical solvents.[4-6] Examples of physical solvents used commercially include dimethyl ethers of poly(ethylene glycol) (DMPEG) and MeOH in the Selexol® and Rectisol® processes, respectively. Physical solvents are also used for pre-combustion CO_2 capture in the integrated gasification combined cycled (IGCC) process and syngas clean-up (CO_2/H_2 separation).[7, 8]

Ionic liquids (ILs) have been the subject of large research effort focused on the design of novel physical and/or chemical solvents for natural gas treating, pre- and post-combustion CO_2 capture and other gas separations applications due to their very low vapor pressures and tunable structures.[9-12] The low volatility of ILs is similar to that of DMPEG[6, 13] and is desirable for solvent regeneration as it lowers latent heat duties and minimizes fugitive solvent emissions. "Tuning" ILs structures through cation and/or anion functionalization provides a degree of control over IL thermophysical properties such as density, viscosity, heat capacity, gas solubility, etc.[9, 10, 14, 15] ILs have been shown to exhibit CO_2/CH_4 selectivities that compete with the most selective physical organic solvents.[10-12] ILs are at least an order of magnitude more viscous than most organic solvents,[13, 16, 17] and the solubility CO_2 in ILs on a molality basis (i.e. mol CO_2 $(kg\ IL)^{-1}$) is less than small (i.e. volatile) organic solvents[10, 18] but comparable to larger, nonvolatile organic solvents (e.g. large alkanes).[19] However, ILs are likely to be a more expensive alternative than conventional organic solvents due to the number of synthetic/purification steps required and the use of some uncommon starting materials.[20]

N-functionalized imidazoles (i.e. the precursors to imidazolium-based ILs) also present a readily accessible,[21] tunable solvent platform that can offer some advantages relative to ILs and other organic solvents for gas separations.[13, 22-24] Previously, we investigated the properties of 1-*n*-alkylimidazoles, the neutral analogues to 1-*n*-alkyl-3-methylimidazolium-based ($[C_nmim][X]$) ILs.[24] 1-*n*-alkylimidazoles were found to be an order of magnitude less viscous than their analogous ILs, while exhibiting up to 10-20%

improvement in CO_2 solubility per solvent volume.[24] We also examined CO_2/CH_4 separation performance of 1-*n*-alkylimidazoles,[13] with dissolution of both CO_2 and CH_4 found to be thermodynamically favorable (i.e. exothermic), although extending the *n*-alkyl chain proved to be detrimental to both CO_2 solubility and CO_2/CH_4 selectivity. Of the 1-*n*-alkylimidaozles studied, only 1-methylimidazole (i.e. the smallest compound) appears to favorably compete with other commercially employed physical solvents based on a comparative analysis of typical thermophysical properties associated with process design.[5, 6, 13]

However, it is now well-known that *n*-alkyl chains are just one of many possible substituents that can be appended to imidazoles or imidazolium-based ILs.[25-27] Bara, et al. first demonstrated that ILs with ether groups appended to an imidazolium cation exhibited a favorable increase in CO_2/CH_4 and CO_2/N_2 solubility selectivities relative to analogous ILs with similar length *n*-alkyl groups attached to the cation.[25] This effect was attributed to a reduction in CH_4 and N_2 solubilities, rather than an increase in CO_2 solubility, suggesting repulsion between the ether groups and the non-polar CH_4 and N_2 and/or reduced free volume in which the larger CH_4 and N_2 are not accommodated.[25, 28]

In addition to the use of DMPEG (Selexol®) as a commercial solvent for CO_2 removal, ether-based polymers such as poly(ethylene glycol) (PEG, also known as poly(ethylene oxide) (PEO)) have been extensively studied as gas separation membranes.[18, 29-31] PEG membranes have demonstrated high CO_2 permeability and permselectivity for CO_2/N_2 and CO_2/CH_4, which is known to be favored by solubility differences rather than diffusion.[18, 29, 30]

Thus, the inclusion of ether functionality within imidazoles and its effects on the solubility of CO_2 and other gases is certainly of interest. We have already shown that ether-functionalized imidazoles (and benzimidazoles) exhibit vapor pressures that are reduced by nearly an order of magnitude when compared to analogous 1-*n*-alkylimidazoles.[27, 32-34] These reductions in vapor pressure can prove to be advantageous for gas treating applications provided that other properties such as viscosity, CO_2 solubility and CO_2/CH_4 selectivity are not negatively impacted. Herein we report the physical properties and CO_2 separation performance of a series of imidazoles with oligo(ethylene glycol) repeat units, "PEG_n-imidazoles" (Figure 7.1).

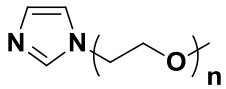

n = 1, 2, 3

Figure 7.1: Structures of PEG_n-imidazoles examined in this work.

Compared to analogous 1-*n*-alkylimidazoles, densities of PEG_n-imidazoles were found to be 12-21% larger, while their viscosities are ~40% larger on average.[24] However, the highest viscosity recorded was only ~18 cP for PEG_3-imidazole at 293.15 K. Like 1-*n*-alkylimidazoles, the densities and viscosities of PEG_n-imidazoles can be well-modeled as a function of temperature and proportional molecular weight (MW) of the side chain to that of the entire molecule.[24] At 298.15 K, the solubility of CO_2 in each of the PEG_n-imidazoles is larger than the corresponding 1-*n*-alkylimidazole with an equivalent number of atoms in the side chain (e.g. PEG_1-imidazole & 1-butylimidazole). Solubility of CO_2 in PEG_n-imidazoles is observed to decrease as the number of ether groups increases, although much less so than was observed for 1-*n*-alkylimidazoles.[24] CH_4 solubility in PEG_n-imidazoles exhibited a slight increase between PEG_1-imidazole and PEG_2-imidazole, followed by a reduction for PEG_3-imidazole. Consequently, PEG_1-imidazole provided the highest CO_2 solubility at any temperature, while PEG_3-imidazole exhibited the largest CO_2/CH_4 selectivity. These results can be rationalized through solubility parameters determined from vaporization enthalpies for PEG_n-imidazoles[27] and an analysis of fractional free volume (FFV) calculated via COSMOtherm.

7.2 Experimental

7.2.1 Materials: PEG_n-imidazoles were synthesized from sodium imidazolate and oligo(ethylene glycol) monomethyl ether monotosylates[35] according to our previously published procedures.[21] As with our prior work, purity of the compounds were > 98% by mass.

7.2.2. Density Measurements: Density values for each PEG_n-imidazole were obtained via a Mettler Toledo DM45 DeltaRange density meter per methodology described in our previous work.[24] Densities were recorded over the temperature range of 293.15-353.15 K (20.00-80.00^{o}C) at 10.00 K increments. The uncertainty in this measurement is +/- 0.00005 g cm^{-3} at all temperatures.

7.2.3. Viscosity Measurements: Viscosity data were obtained via a Brookfield DV-II+ Pro viscometer per methodology described in our previous work.[24] Viscosities were recorded within the temperature range of 293.15-353.15 K (20.00-80.00^{o}C), with an accuracy of +/- 1% of the measurement with a repeatability of +/- 0.2%.

7.2.4. CO_2 and CH_4 Solubility Measurements: Solubilities of CO_2 and CH_4 in each PEG_n-imidazole were measured using the same apparatus and methodology as described in our previous works.[13, 22, 24, 36] Solubility experiments were conducted at temperatures of 298.15, 313.15, 328.15, and 343.15 K (25.00, 40.00, 55.00, and 70.00°C, respectively). For each experiment, an initial charge of gas was fed to the apparatus at the initial temperature of 298.15 K and an equilibrated pressure of ~5 bar (75 psia). This equilibrated pressure was chosen as it represents the beginning of the regime where physical solvents become applicable for CO_2 removal.[4, 6] Similar to an experimental methodology provided by Finotello, solubility values at all temperatures were calculated based on initial charge of gas and pressure change upon heating.[37] Propagation of error based on experimental parameters and measurements was used to calculate respective errors of Henry's Constants (H_i) and volumetric solubility (S_i). Similar to our previous results for 1-*n*-alkylimidazoles, errors in CO_2 solubility measurements compared to CH_4 were 1-3% and 5-13%, respectively.[13, 24]

7.3 Computational Methods: COSMOTherm version C30_1301 (COSMOlogic GmbH, Leverkusen, Germany) was employed to simulate densities, viscosities, molar volumes and COSMO volumes for PEG_n-imidazoles at 298.15 K. CO_2 solubilities were simulated with a mole fraction of 0.075 CO_2 at 298.15, 313.15, 328.15 and 343.15 K, so as to correspond with the experimental conditions. Our group developed COSMO files for PEG_n-imidazoles using TURBOMOLE[38] to generate optimized structures with the triple-zeta valence potential (TZVP) basis set[39] with the Becke and Perdew (b-p)[40, 41] functional at the density functional theory (DFT) level. COSMO calculations were performed at the TZVP level, which has been used in our previous works[36] and other published reports on ILs and other solvents that have employed COSMOtherm.[42-49]

7.4 Results & Discussion

7.4.1 Densities of PEG_n-imidazoles and Empirical Model: The experimentally determined density values for PEG_n-imidazoles within the temperature range of 293.15-353.15 K are provided as tabulated data within the Supporting Information.

Densities for each compound decrease linearly with increasing temperature, and density increases at a given temperature as the PEG_n-chain length is extended. This is in distinct contrast to 1-*n*-alkylimidazoles and 1-*n*-alkylbenzimidazoles,[22, 24, 50] where density monotonically decreases as the *n*-alkyl chain is extended. Previously, we employed a dimensionless parameter (*R'*) to account for the influence of the substituent on density and viscosity. *R'* is determined from the ratio of the molecular weight of the side

chain to the molecular weight of the entire molecule (Eqn. 1). Relevant data for each PEG_n-imidazole are presented in Table 7.1.

$$R' = \frac{MW(PEG_n \text{ chain})}{MW(PEG_n \text{ - imidazole})} \quad (1)$$

Table 7.1: Molecular weight and *R'* values for PEG_n-imidazoles.

PEG_n-imidazole	MW (g mol^{-1})	*R'*
1	126.16	0.468
2	184.24	0.636
3	242.31	0.723

As utilized in our prior work,[24] the influence of temperature and side chain length on density of PEG_n-imidazoles are well-accounted for within a simple planar model (Eqn. 2),

$$\rho(T, R') = AT + BR' + C \quad (2)$$

where ρ [=] kg m^{-3}, T [=] K, and R' is dimensionless. The model coefficient values are as follows: A = -0.8574 kg m^{-3} K^{-1}, B = 90 kg m^{-3}, and C = 1276 kg m^{-3}, with an absolute average percent deviation (AAPD) of 0.063% within this temperature range. The surface fit relating density, temperature and R' in PEG_n-imidazoles is depicted in Figure 7.2.

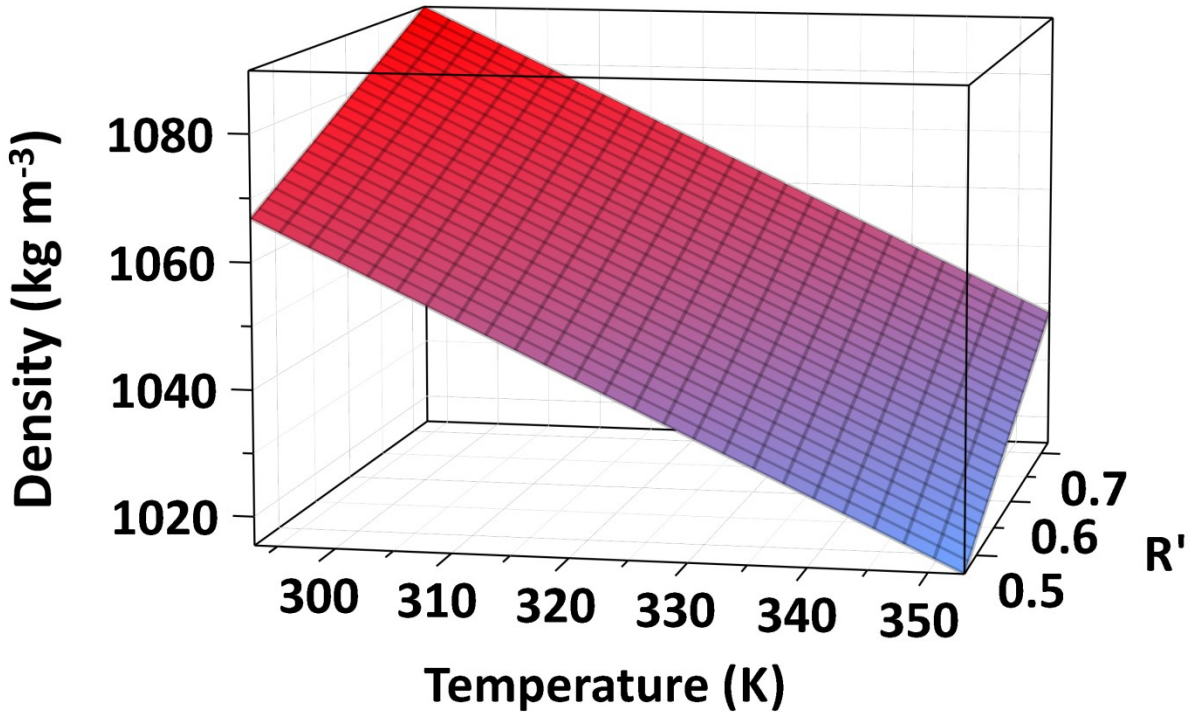

Figure 7.2: Surface fit of PEG_n-imidazole density with respect to temperature and R'.

Comparing the density behavior of PEG_n-imidazoles to analogous 1-*n*-alkylimidazoles, PEG_n-imidazoles exhibit increases that range from 12-21%. As 1-*n*-alkylimidazole have very similar MWs to analogous PEG_n-imidazoles with the same number of atoms in the side chain (e.g., 4 atom side chain: 1-butylimidazole = 124.18 g mol^{-1} and PEG_1-imidazole = 126.16 g mol^{-1}), the increased density is primarily due to the presence of the more dense ether repeat unit. The same contrast in density trends observed for PEG_n-imidazoles and 1-*n*-alkylimidazoles is also prevalent for other polar molecules. Polar entities present as end groups of alkyl chains (e.g. alcohols, nitriles, carboxylates) exhibit a decrease in density as the alkyl chain-length increases. However, molecules of a homologous series with incremental ethylene glycol units (i.e. 2-methoxyethanol, 2-(2-methoxyethoxy)ethanol, etc.) shows increased density as the number of repeat units is extended.

Additional intra- and intermolecular interactions may also occur within PEG_n-imidazoles based on analogy to ether-functionalized imidazolium-based ILs.[26, 28] We hypothesize that polar ether groups could allow for H-bonding to occur between the Lewis-basic ether oxygen atoms and the weakly acidic proton present at C(2) position of the imidazole ring. COSMOTherm can be used to aid in validating this hypothesis

by examining the distribution of electron-rich and electron-poor areas on the charge screening surface of each molecule, referred to as the σ-surface (sigma surface). Figure 7.3 presents a comparison of the σ-profiles (electron distribution per area) for PEG_1-imidazole (blue) and 1-butylimidazole (red) as calculated by COSMOTherm. The plot indicates that PEG_1-imidazole molecules feature more electron rich and electron poor surface area as indicated by peaks that lie at more negative and more positive values of σ (x-axis). In contrast, 1-butylimidazole shows a distribution that is more centered about σ = 0 as the *n*-alkyl chain presents a largely electroneutral surface that would not experience H-bonding interactions with the imidazole ring. Additional comparisons of σ-profiles and images of the σ -surfaces of the individual PEG_n-imidazoles and 1-*n*-alkylimidazole molecules are provided as Supporting Information.

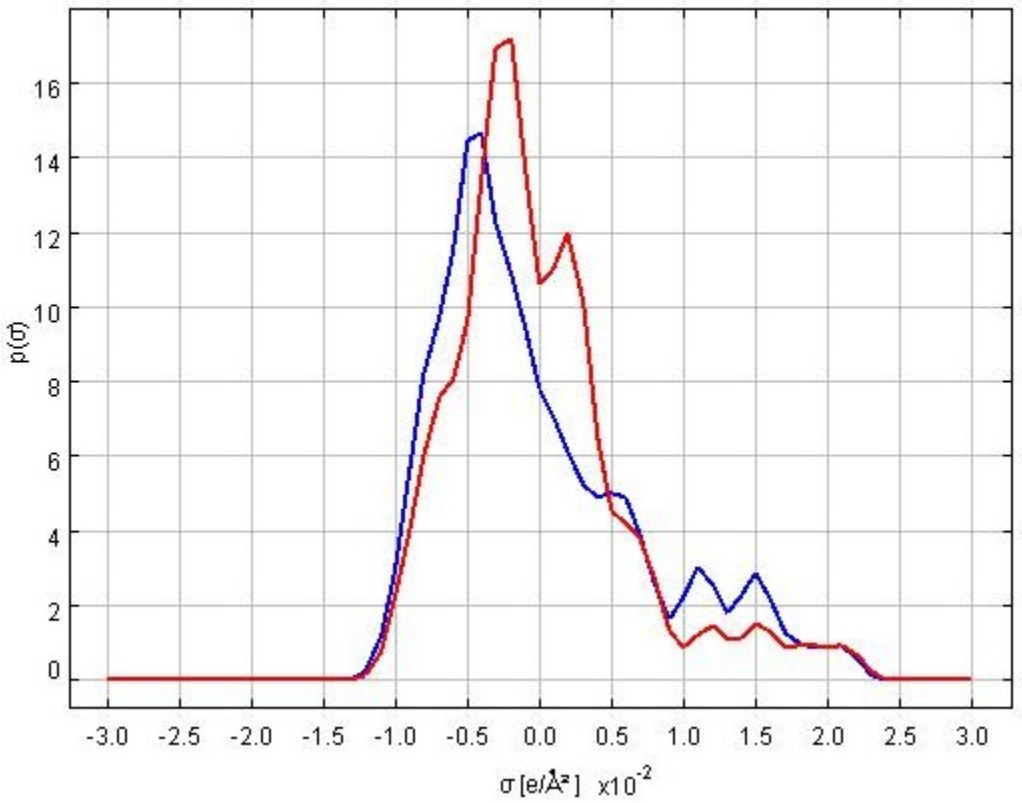

Figure 7.3: Comparison of σ-profiles for PEG_1-imidazole (blue) and 1-butylimidazole (red).

Turner, et al. recently showed that for 1-*n*-alkylimidazoles, the C(2) position of the imidazole ring bears a partial positive charge of +0.386,[50] which would suggest Lewis acid – Lewis base interactions in PEG_n-imidazoles are possible. Interactions of ether oxygen atoms with the C(2) position of the imidazole ring have been demonstrated in simulations of [PEG_n-mim][Tf_2N], where a partial positive charge on the C(2) is also present.[28] This increase in molecular interactions could also be supported by the observance of a reduced

FFV in PEG_n-imidazoles compared to 1-*n*-alkylimidazoles,[51] with further discussion presented in Section 7.4.4.

7.4.2 Viscosities of PEG_n-imidazoles and Empirical Model: The experimentally determined viscosity values for PEG_n-imidazoles over the temperature range of 293.15-353.15 K (20.00-80.00°C) are provided as Supporting Information. All measured viscosities for PEG_n-imidazoles are below 20 x 10^{-3} kg m^{-1} s^{-1} (20 cP) within this temperature range. As seen in our previous work with 1-*n*-alkylimidazoles, viscosity of each compound decreases non-linearly with increasing temperature.[24] Also, viscosity is highly dependent on PEG_n chain length (i.e. *R'*) with differences of ~3x and ~2x observed between PEG_1-imidazole and PEG_3-imidazole at 20.00°C and 80.00°C, respectively. A Litovitz-based viscosity model was employed that provides an excellent estimation of viscosity in PEG_n-imidazole compounds based on temperature and R' (Eqn. 6).[24, 52, 53] The empirical fit constants are shown in Table 7.2, and the model has an AAPD = 4.1%.

$$\mu(T, R') = (aR'+b)\exp((mR'+n)T^{-3}) + p \quad (3)$$

Table 7.2: Empirical constants for viscosity model (Eqn. 3) of PEG_n-imidazoles

Constant	Value
a	1.24x10^{-4} kg m^{-1} s^{-1}
b	2.29x10^{-4} kg m^{-1} s^{-1}
m	1.02 x 10^8 K^3
n	2.68 x 10^7 K^3
p	-5.9x10^{-5} kg m^{-1} s^{-1}

Figure 7.4 illustrates the surface plot of PEG_n-imidazole viscosity with respect to temperature and *R'*. PEG_n-imidazole viscosities within this temperature range are all slightly higher than analogous 1-*n*-alkylimidazoles, although all measured viscosities for both sets of compounds lie below 20 x10^{-3} kg m^{-1} s^{-1} (20 cP) in this temperature range,[24] implying they are considerably less viscous than $[C_n mim][X]$ or $[PEG_n mim][X]$ ILs, particularly at low temperatures.[15-17] PEG_3-imidazole shows the largest viscosity span, with 82% difference from highest to lowest recorded values. The viscosity of PEG_1mim-imidazole at 298.15 K (4.86 cP) is less than that of the commercially used oligo(ethylene glycol)-based solvent, DMPEG (Selexol®) (~5.8 cP),[6, 13] although the viscosities of PEG_2-imidazole and PEG_3-imidazole are ~2x and ~3x more viscous than DMPEG, respectively.

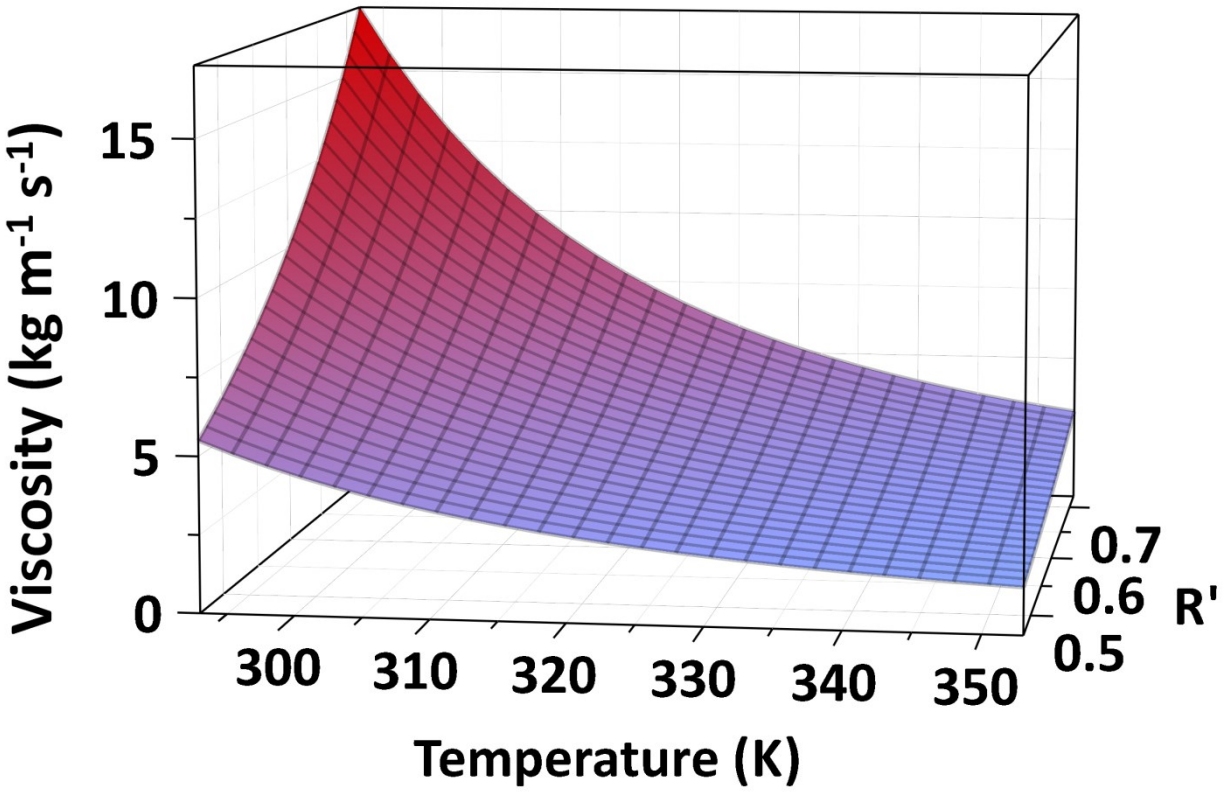

Figure 7.4: Surface plot of PEG_n-imidazole viscosity (cP) relative to temperature (K) and molecular weight parameter (*R'*).

7.4.3 CO_2 and CH_4 Solubility and Selectivity: Henry's constants (H_j) (bar) and volumetric solubilities (S_j) (m^3 (STP) (m^3 solvent)$^{-1}$ bar^{-1}) of both CO_2 and CH_4 in PEG_n-imidazoles for the temperature range of 298.15-343.15 K (25.00-70.00^{o}C) are presented in Table 7.3 as the average of three replicates with uncertainty as one standard deviation of the average. Ideal (i.e. single gas) CO_2/CH_4 separation selectivities are presented in Table 7.4.

Table 7.3: Solubilities (H_j) and (S_j) of CO_2 and CH_4 in PEG_n-imidazoles (1-3) at partial pressure of ~5 bar and temperatures from 298.15 – 343.15K.

		CO_2				CH_4			
PEG_n	T (K)	H_{CO_2} (bar)	±[a]	S_{CO_2} [b]	±[a]	H_{CH_4} (bar)	±[a]	S_{CH_4} [b]	±[a]
1	298.15	81.0	1.0	2.43	0.03	856	48	0.22	0.02
	313.15	118	2	1.64	0.03	760	57	0.25	0.02
	328.15	156	3	1.12	0.02	817	55	0.23	0.02
	343.15	197	4	0.86	0.02	768	60	0.24	0.02
2	298.15	64.3	1.0	2.34	0.05	568	67	0.25	0.02
	313.15	100	3	1.48	0.04	516	77	0.28	0.02
	328.15	144	5	0.99	0.03	542	77	0.26	0.02
	343.15	195	7	0.85	0.03	570	76	0.25	0.02
3	298.15	57.9	0.9	2.11	0.03	730	42	0.16	0.02
	313.15	84.3	2	1.43	0.03	551	58	0.21	0.02
	328.15	116	2	1.00	0.02	584	57	0.20	0.02
	343.15	152	3	0.80	0.02	609	56	0.19	0.01

[a] Uncertainty represents one standard deviation of the average value. [b] S [=] (m^3 gas (STP)) (m^3 solvent)$^{-1}$ bar^{-1}

Table 7.4: Ideal CO_2/CH_4 solubility selectivities in PEG_n-imidazoles for given temperatures

T (K)	PEG_1-imidazole	PEG_2-imidazole	PEG_3-imidazole
298.15	11	9.5	13
313.15	6.6	5.4	6.9
328.15	4.9	3.8	5.1
343.15	3.6	3.4	4.3

Uncertainty in selectivities from propagation of error = ~10%

As shown in Table 7.3, PEG_1-imidazole exhibits the highest CO_2 solubility (moles per solvent volume) within the experimental temperature range, while CH_4 exhibited the greatest solubility in PEG_2-imidazole. This trend of gas solubilities directly correlates with the results from our previous work with 1-*n*-alkylimidazoles, where the molecule with the shortest side group displayed the highest CO_2 solubility at any given temperature, while an intermediate length group displayed the highest CH_4 solubility.[13] Solubility of

CO_2 in each PEG_n-imidazole decreased with increasing temperature, while CH_4 solubility was essentially constant with temperature.

Mole fraction-based solubilities in the form of Henry's constants for both gases are also provided in Table 7.3. Decreasing values of H_{CO2} (at a given temperature) correlated with increasing the number of ether repeat units implies that the mole fraction of CO_2 increases as the PEG_n chain is extended. However, as discussed in previous works from our group and others,[10, 19, 54] the increase in CO_2 mole fraction in molecules with a propagating structure is primarily attributable to incrementally the larger MW of the solvent. Thus, metrics that normalize solubility on a basis of moles per solvent volume (e.g. molarity) or moles per solvent mass (e.g. molality) are most appropriate for formulating direct comparisons of solvent performances.

In examining the S_{CO2} data, each PEG_n-imidazole has a very similar working capacity for CO_2 if a temperature swing is applied at constant pressure. An ~65% decrease in CO_2 solubility is observed for CO_2 solubility in PEG_1-imidazole over 25-70^{o}C, with comparable results also observed for PEG_2-imidazole and PEG_3-imidazole (64% and 62%, respectively). Furthermore, it is likely that in practice, PEG_n-imidazole solvents would be heated to a temperature > 70^{o}C as a means of achieving even better regeneration (i.e. more complete release of CO_2). Garist, et al. measured vapor pressures of PEG_n-imidazoles at temperatures as high as 408.7 K (~135^{o}C) with no degradation noted,[27] and the maximum operating temperature for DMPEG has been reported to be 175^{o}C.[6] These results imply PEG_n-imidazoles can be used for gas absorption quite efficiently under just typical operating conditions (moderate to mild heating/vacuum).

Polar groups (ethers, nitriles, etc.) are typically more effective for selective separation of CO_2 when compared to hydrocarbon groups,[10, 18, 55] and modest (10-15%) improvements in CO_2 solubility were noted for PEG_n-imidazoles compared to their corresponding 1-*n*-alkylimidazoles (i.e. 1-butylimidazole, 1-heptylimidazole and 1-decylimidazole) at a given temperature.[13] Additionally, up to 30% reductions in CH_4 solubility are also observed for PEG_n-imidazoles relative to 1-*n*-alkylimidazoles at lower temperatures (298.15 K and 313.15 K).[13] As shown previously via comparisons of $[PEG_nmim][Tf_2N]$ and $[C_nmim][Tf_2N]$ ILs, the presence of ether groups resulted in little to no improvement in CO_2 solubility relative to alkyl groups.[25] Yet, in PEG_n-imidazoles, as with $[PEG_nmim][Tf_2N]$ ILs, although there is only a minor positive effect on CO_2 solubility, the ether groups have a more appreciable impact on improving CO_2/CH_4 solubility selectivity through reductions in CH_4 solubility at lower temperatures. Figure 7.5 shows that unlike CO_2 solubility, which slightly decreases with respect to PEG_n chain length but more significantly decreases with increasing temperature, CH_4 solubility is essentially independent of temperature and shows only a small dependence on chain length. A maximum CH_4 solubility was observed in PEG_2-imidazole, although it is much less

pronounced than the maximum that was observed to occur between 1-hexylimidazole and 1-octylimidazole in 1-*n*-alkylimidazoles.[13]

This result appears to suggest that a maximum for CH_4 solubility occurs in *N*-functionalized imidazoles when the length of the side chain is between 6-8 atoms, which might imply a change in the solution structure and/or significant side chain aggregation occurs at or near this size range which could influence gas solubility and selectivity behaviors. Padua, et al. showed that in imidazolium-based ILs, as the length of the alkyl side chain was 6 atoms or more, the connectivity between the non-polar domains became nearly continuous.[56] However, simulations involving ether-functionalized ILs have shown a more homogeneous distribution of tails throughout the bulk solvent.[28] Ether-functionalized ILs have tended to exhibit better CO_2 selectivity than alkyl-functionalized analogues,[25] and solution structure may play a role in this behavior. We see a need for similar studies comparing alkyl and ether-functionalized imidazoles to better elucidate the relationships between molecular structure, solvent aggregation, free volume, free volume distribution and gas solubility.

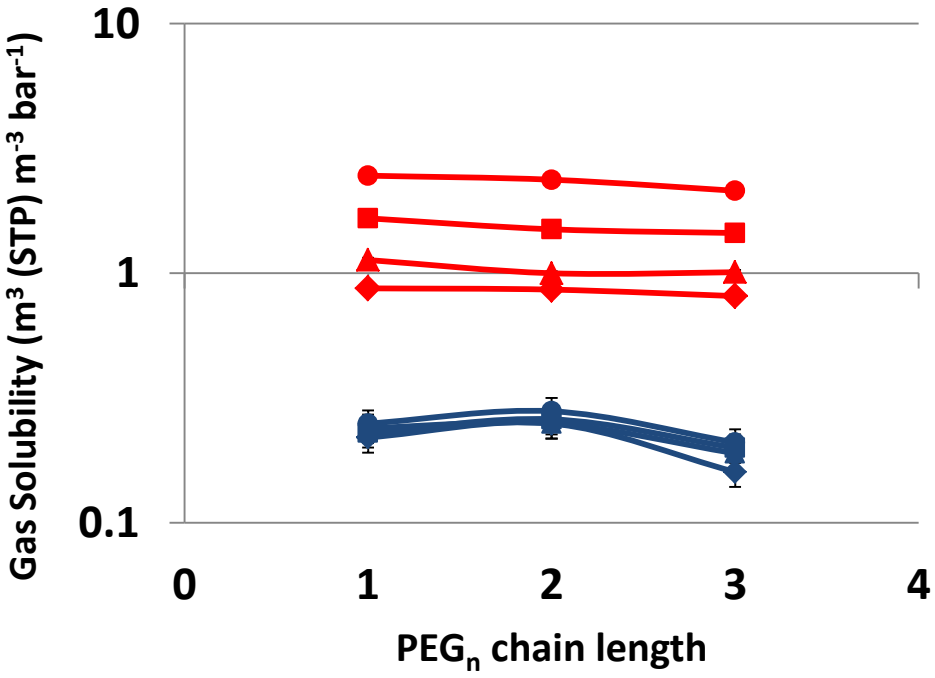

Figure 7.5: Relationship between volumetric solubilities (S_i) of CO_2 (red) and CH_4 (blue) in PEG_n-imidazoles at 298.15 K (circles), 313.15 K (squares), 328.15 K (triangles) and 343.15 K (diamonds) with respect the number of ether repeat units (PEG_n). Error bars for CO_2 solubility are within symbols.

Table 7.4 shows that CO_2 selectivity decreased with increasing temperature implying the dissolution of CO_2 in PEG_n-imidazole solvents is exothermic while the enthalpies of solution for CH_4 are minimally endothermic, a result similarly observed in our prior work with 1-*n*-alkylimidazoles.[13] Using the van't Hoff equation, average enthalpies of solution (ΔH_{soln}) for CO_2 in PEG_n-imidazoles between -16.8 and -19.7 kJ mol^{-1} were calculated, although the value for each compound is within the respective error of the others. These values are slightly more exothermic (and more favorable for CO_2 absorption at lower temperatures) than those observed for CO_2 + 1-*n*-alkylimidazoles (-15 +/- 2 kJ mol^{-1}),[13] but are still indicative of weak solute-solvent interactions (i.e. a physical solvent). Average ΔH_{soln} values for CH_4 in PEG_n-imidazoles calculated via the same manner are -1 +/- 2 kJ mol^{-1}, slightly more endothermic (and less favorable for CH_4 absorption at lower temperatures) than values for 1-*n*-alkylimidazoles (-5 +/- 5 kJ mol^{-1}).[13]

At all temperature conditions, PEG_3-imidazole proved to be the most selective under all temperatures, with an overall maximum separation factor of CO_2/CH_4 = 13 at 298 K, while PEG_2-imidazole was found to be the least selective under all conditions. Bara, et al. observed a similar effect in $[PEG_nmim][Tf_2N]$ ILs where CO_2/N_2 and CO_2/CH_4 solubility selectivities decreased between PEG_1 and PEG_2 ILs, but then increased in the PEG_3 IL.[25]

For the lowest experimental temperature (25°C), CO_2/CH_4 selectivity for PEG_n-imidazoles proved to be greater than those of 1-*n*-alkylimidazoles.[13] However, selectivities for PEG_n-imidazoles prove to be lower than 1-*n*-alkylimidazoles at the higher experimental temperatures, with up to 39% difference. This appears to be primarily due to the stronger temperature dependence of CO_2 solubility in PEG_n-imidazoles, as seen in Figure 7.5. Our observation can also be correlated to single gas solubilities of olefins and paraffins in a polar solvent (THF) relative to a non-polar solvent (*n*-hexane).[30] Lin, et al. showed that the solubility of an olefin (i.e. a polar solute) in THF decreased in a non-linear fashion and more rapidly than the non-polar paraffin with increasing temperature. In *n*-hexane, both olefin and paraffin solubility decreased linearly with increasing temperature. This implies that lowering the operating temperature below 25°C (i.e. the lower limit of this study) could significantly increase the separation selectivity for CO_2 in PEG_n-imidazoles. However, chilling PEG_n-imidazoles (and other physical solvents) to sub-ambient temperatures to improve solubility and solubility selectivity must be considered in tandem with increased solvent viscosity and the energy requirements of refrigeration.

7.4.4 Comparison of Experimental Data with COSMOTherm Calculations: Previously, we have shown that COSMOTherm is a useful tool for estimating physical and chemical properties (e.g. density, viscosity, CO_2 solubility, pK_a, vapor pressures, etc.) of 1-*n*-alkylimidazoles and 1-*n*-alkylbenzimidazoles,[32, 51] including

estimating vapor pressures and vaporization enthalpies of PEG_n-imidazoles.[27] By validating COSMOTherm calculations with experimental data, this approach can provide a level of confidence in the design of new molecules *in silico* by identifying species likely to have desirable properties prior to attempting their synthesis.

Table 7.5 presents a comparison of experimental density and viscosity data at 298.15 K to COSMOTherm estimates for PEG_n-imidazoles. The percent difference columns in Table 7.5 (%diff) are calculated as the quotient of the difference between the experimental and COSMO values (numerator) and the experimental value (denominator) multiplied by 100%.

Table 7.5: Comparison of experimental and COSMO density and viscosity for PEG_n-imidazoles at 298.15 K.

PEG_n-imidazole	ρ expt. (kg m^{-3})	ρ COSMO (kg m^{-3})	%diff ρ	μ expt. (kg m^{-1} s^{-1})	μ COSMO (kg m^{-1} s^{-1})	%diff μ
1	1064	1067	-0.319	4.86	3.82	21.5
2	1077	1086	-0.855	9.12	10.77	-18.1
3	1086	1096	-0.972	14.71	30.21	-105

For density (ρ) of PEG_n-imidazoles, COSMO provides an estimation at 298.15 K that is within 1% of the experimental value, with all species slightly overestimated in the calculations. Previously, we observed that COSMO achieved a similar level of accuracy (+/- 1%) for densities of 1-*n*-alkylimidazoles, but both under- and overestimations occurred. Nonetheless, this study provides further validation that COSMO yields very reliable estimates for densities of *N*-functionalized imidazoles.

As can be seen in Table 7.5, COSMO also provides reasonable estimates (at 298.15 K) for viscosity of PEG_1-imidazole and PEG_2-imidazole. Although the percent difference for these two compounds is approximately +/- 20%, the magnitude of error to the experimental value is within +/- 2 cP, indicating that COSMO is capable of providing an initial estimate for the smaller members of a series of molecules with a propagating structure. These results are comparable to those previously obtained for 1-*n*-alkylimidazoles with chains as larger as octyl.[51] However, COSMO predictions widely diverge from experimental values at longer chain lengths, where a difference of > 100% (15 cP overestimate) was given for PEG_3-imidazole. This is also consistent with COSMO viscosity estimates for larger 1-*n*-alkylimidazoles (e.g. decyl, dodecyl, tetradecyl) which were also overestimated by as much as 100%.[51]

As we have previously noted, although COSMO has been used to estimate Henry's Constants for CO_2 in IL solvents,[42-46, 57-60] a generally poor agreement was observed between experimentally determined CO_2

solubilities in 1-*n*-alkylimidazoles and COSMO calculations.[51] COSMO calculations yield an essentially constant value at a given temperature for the Henry's Constant of CO_2 (H_{CO2}) for 1-*n*-alkylimidazoles with chain lengths of butyl or larger. However, when the temperature dependence of H_{CO2} was examined through COSMOTherm, the results did provide a reasonable estimate for the enthalpy of solution for CO_2 in 1-*n*-alkylimidazoles, with a value of -16 +/- 1 kJ mol^{-1}, where the experimental values of solution enthalpy were in the range of 13 +/- 1 kJ mol^{-1} (except for 1-methylimidazole, -16 kJ mol^{-1}).[13, 51] For PEG_n-imidazoles, we also observed similar results in the use of COSMOTherm to predict H_{CO2}. At a given temperature, there was almost no difference in the simulated value of H_{CO2} obtained from COSMOTherm, which is clearly inconsistent with experimental data (Table 7.3). However, in examination of the temperature dependence of H_{CO2} calculated by COSMOTherm, enthalpies of solution for CO_2 in PEG_n-imidazoles between -15 and -16 kJ mol^{-1} are calculated. These values are less than the experimentally-derived values, as COSMO tends to underestimate the value of H_{CO2} for PEG_n-imidazoles. The agreement between COSMO and experimental H_{CO2} data is best for PEG_3-imidazole at lower temperatures. The COSMO data for H_{CO2} in PEG_n-imidazoles are provided as Supporting Information.

In order to compare the effect of molecular structure on gas solubility, we can also calculate solubility parameters (δ) of PEG_n-imidazoles from the cohesive energy density (Eqn. 4),[61]

$$\delta = \sqrt{\frac{\Delta H_{vap} - RT}{V_m}} \tag{4}$$

where ΔH_{vap} is the enthalpy of vaporization, R is the gas constant, T is absolute temperature and V_m is the molar volume. The solubility parameter provides an indication of the miscibility of solute and solvent (i.e. as the absolute value of $\delta_2 - \delta_1$ approaches zero a maximum in solubility will occur).[62] However, it has been observed that tailoring the molecular structures of molecules such as ILs and imidazoles so that the solubility parameters of these molecules match that of CO_2 (δ = 21.8 $MPa^{1/2}$)[18] does not increase solubility of CO_2 in these solvents, and decreases in CO_2 solubility are observed.[10, 55]

We have previously proposed that this decrease in solubility is associated with a decreasing free volume or an increase in free volume but with cavities which do not favor CO_2 absorption,[50] since the effect of incrementally extending a molecular structure results in a liquid solvent with more polymer-like character.[10] Thus, we also have considered FFV in tandem with solubility parameters to interpret the trends in gas solubility in solvents as ILs and *N*-functionalized imidazoles.[51] Previously, we have shown that COSMOTherm can provide a rapid and accurate estimation of FFV from Eqn. 5,[36, 51]

$$FFV = \frac{V_m - V_{COSMO}}{V_m} \quad (5)$$

where V_m represents the molar volume and V_{COSMO} represents the volume enclosed by the charge screening surface for that solvent as calculated by the density module within COSMOtherm. At 25°C, V_m values estimated by COSMOTherm were found to be within 1-2% of the experimental values (see Supporting Information).

Table 7.6 provides solubility parameters calculated from the experimentally determined enthalpies of vaporization in Garist, et al. and FFV values from COSMOtherm for PEG_n-imidazoles.

Table 7.6: COSMOtherm FFV values and solubility parameters determined from enthalpies of vaporization for PEG_n-imidazoles.

PEG_n-imidazole	δ ($MPa^{1/2}$)	FFV
1	24.1	0.163
2	21.9	0.155
3	20.6	0.153

For PEG_n-imidazoles, δ and FFV decrease with increasing number of repeat units. However, 1-*n*-alkylimidazoles show the opposite trend with slightly increasing FFV values as the *n*-alkyl chain is extended. The FFV values for PEG_n-imidazoles approach those reported by Lin for crosslinked PEO (0.12-0.14), indicating that FFV values determined from COSMO for molecules with a propagating chemical structure will approach the experimentally determined FFV of polymer at a sufficient number of repeat units. FFV values for PEG_n-imidazoles are also considerably lower than those calculated for 1-*n*-alkylimidazoles (0.19-0.20). A smaller free volume in PEG_n-imidazoles is supported by increased density and viscosity relative to 1-*n*-alkylimidazoles.[24] Although the solubility parameter for PEG_2-imidazole is very close to that of CO_2, the solubility of CO_2 in this solvent is less than in PEG_1-imidazole (mols per volume basis). Thus, tuning the solubility parameter is counteracted by a decreased FFV. Yet, while the FFV values in PEG_n-imidazoles are smaller than analogous 1-*n*-alkylimidazoles, CO_2 is still more soluble and CO_2/CH_4 selectivities are improved as PEG_n-imidazoles have more polar sites, which provides a more favorable environment for CO_2 dissolution. It should be noted that COSMO only provides an estimate of total free volume and other, more-detailed methods are required to gain a perspective of cavity sizes/shapes and distributions.[50]

However, as 1-methylimidazole had the best combination of CO_2 solubility and CO_2/CH_4 selectivity amongst all of the PEG_n-imidazoles and 1-*n*-alkylimidazoles,[13] it is apparent that small molecules are most advantageous, and that if a larger molecule is required (i.e. to suppress vapor pressure) then the inclusion of polar groups such as ethers will outperform *n*-alkyl groups for CO_2 separations.

7.5 Conclusions: We have analyzed the physical properties and CO_2/CH_4 separation performances of PEG_n-imidazoles. PEG_n-imidazoles are slightly more dense and viscous than analogous 1-*n*-alkylimidazoles, likely due to intra- and intermolecular interactions of polar groups with the imidazole ring. Both density and viscosity can be well-modeled as a function of temperature and *R'*. As seen in our previous study with 1-*n*-alkylimidazoles, CO_2 solubility decreases with increasing number of ether repeat units, although PEG_3-imidazole exhibited the greatest CO_2/CH_4 selectivity. The driving forces for CO_2 solubility and CO_2/CH_4 selectivity have been considered in terms of solution enthalpies, solubility parameters and FFV, suggesting distinct differences between polar PEG_n-imidazoles and the largely non-polar 1-*n*-alkylimidazoles. However, although PEG_n-imidazoles are likely to be more suitable candidates for CO_2/CH_4 separations than analogous 1-*n*-alkylimidazoles (i.e. 1-butyl, 1-heptyl and 1-decylimidazole), 1-methylimidazole is still the most promising *N*-functionalized imidazole solvent studied thus far. Further research on the effects of tailoring imidazoles for CO_2 separations will focus on substitution of one or more of the three carbons within the imidazole ring structure.

Acknowledgment

Partial support for this work provided by: ION Engineering, LLC; United States Department of Energy – National Energy Technology Laboratory (DE-FE0005799); and NSF Research Experiences for Undergraduates (EEC-1062705) is gratefully acknowledged.

7.6 References:

1. Baker, R. W.; Lokhandwala, K., Natural Gas Processing with Membranes: An Overview. *Ind. Eng. Chem. Res.* 2008, *47*, 2109-2121.
2. Astarita, G.; Savage, D. W.; Bisio, A., *Gas Treating with Chemical Solvents*. John Wiley & Sons: New York, 1983.
3. Kidnay, A. J.; Parrish, W. R., *Fundamentals of Natural Gas Processing*. CRC Press: Taylor & Francis Group: Boca Raton, FL, 2006.
4. Tennyson, R. N.; Schaaf, R. P., Guidelines can help choose proper process for gas-treating plants. *Oil Gas J.* 1977, *75*, 78-86.
5. Bucklin, R. W.; Schendel, R. L., Physical Solvent Processes Can Be Very Useful for Acid Gas Removal Applications. *Energy Progress* 1984, *4*, 137-142.

6. Burr, B.; Lyddon, L., A Comparison of Physical Solvents for Acid Gas Removal. In *Gas Processors' Association Convention*, Grapevine, TX, 2008.
7. Heintz, Y. J.; Sehabiague, L.; Morsi, B. I.; Jones, K. L.; Luebke, D. R.; Pennline, H. W., Hydrogen Sulfide and Carbon Dioxide Removal from Dry Fuel Gas Streams Using an Ionic Liquid as a Physical Solvent. *Energy Fuel* 2009, *23*, 4822-4830.
8. NETL DOE/NETL Advanced Carbon Dioxide Capture R&D Program: Technology Update May 2011. http://www.netl.doe.gov/technologies/coalpower/ewr/pubs/CO2CaptureTechUpdate051711.pdf (2 September 2011),
9. Bara, J. E.; Camper, D. E.; Gin, D. L.; Noble, R. D., Room-Temperature Ionic Liquids and Composite Materials: Platform Technologies for CO_2 Capture. *Acc. Chem. Res.* 2010, 43, 152-159.
10. Bara, J. E.; Carlisle, T. K.; Gabriel, C. J.; Camper, D.; Finotello, A.; Gin, D. L.; Noble, R. D., Guide to CO_2 Separations in Imidazolium-Based Room-Temperature Ionic Liquids. *Ind. Eng. Chem. Res.* 2009, 48, 2739-2751.
11. Karadas, F.; Atilhan, M.; Aparicio, S., Review on the Use of Ionic Liquids (ILs) as Alternative Fluids for CO_2 Capture and Natural Gas Sweetening. *Energy Fuel* 2010, *24*, 5817-5828.
12. Ramdin, M.; de Loos, T. W.; Vlugt, T. J. H., State-of-the-Art of CO_2 Capture with Ionic Liquids. *Ind. Eng. Chem. Res.* 2012, *51*, 8149-8177.
13. Shannon, M. S.; Tedstone, J. M.; Danielsen, S. P. O.; Bara, J. E., Evaluation of Alkylimidazoles as Physical Solvents for CO_2/CH_4 Separation. *Ind. Eng. Chem. Res.* 2012, *51*, 515-522.
14. Holbrey, J. D.; Rogers, R. D.; Mantz, R. A.; Trulove, P. C.; Cocalia, V. A.; Visser, A. E.; Anderson, J. L.; Anthony, J. L.; Brennecke, J. F.; Maginn, E. J.; Welton, T., Physicochemical Properties. In *Ionic Liquids in Synthesis*, 2nd ed.; Wasserscheid, P.; Welton, T., Eds. Wiley-VCH: Weinheim, Germany, 2008.
15. Aparicio, S.; Atilhan, M.; Karadas, F., Thermophysical Properties of Pure Ionic Liquids: Review of Present Situation. *Ind. Eng. Chem. Res.* 2010, *49*, 9580-9595.
16. Gardas, R. L.; Coutinho, J. A. P., A group contribution method for viscosity estimation of ionic liquids. *Fluid Phase Equilibr.* 2008, *266*, 195-201.
17. Seddon, K. R.; Stark, A.; Torres, M. J. Viscosity and density of 1-alkyl-3-methylimidazolium ionic liquids. In Clean Solvents—Alternative Media for Chemical Reactions and Processing; Abraham, M. A., Moens, L., Eds.; American Chemical Society: Washingtion, DC, 2002; Vol. 819,pp 34-49.
18. Lin, H. Q.; Freeman, B. D., Materials selection guidelines for membranes that remove CO_2 from gas mixtures. *J. Molec. Struct.* 2005, 739, 57-74.
19. Carvalho, P. J.; Coutinho, J. o. A. P., On the Nonideality of CO_2 Solutions in Ionic Liquids and Other Low Volatile Solvents. *J. Phys. Chem. Lett.* 2010, *1*, 774-780.
20. Bara, J. E., What chemicals will we need to capture CO_2? *Greenh. Gas Sci. Technol.* 2012, *2*, 162-171.
21. Bara, J. E., Versatile and Scalable Method for Producing N-Functionalized Imidazoles. *Ind. Eng. Chem. Res.* 2011, *50*, 13614-13619.
22. Shannon, M. S.; Hindman, M. S.; Danielsen, S. P. O.; Tedstone, J. M.; Gilmore, R. D.; Bara, J. E., Properties of alkylbenzimidazoles for CO_2 and SO_2 capture and comparisons to ionic liquids. *Sci. China Chem.* 2012, *55*, 1638-1647.
23. Shannon, M. S.; Bara, J. E., Reactive and Reversible Ionic Liquids for CO_2 Capture and Acid Gas Removal. *Sep. Sci. Technol.* 2012, *47*, 178-188.
24. Shannon, M. S.; Bara, J. E., Properties of Alkylimidazoles as Solvents for CO_2 Capture and Comparisons to Imidazolium-Based Ionic Liquids. *Ind. Eng. Chem. Res.* 2011, *50*, 8665-8677.
25. Bara, J. E.; Gabriel, C. J.; Lessmann, S.; Carlisle, T. K.; Finotello, A.; Gin, D. L.; Noble, R. D., Enhanced CO_2 separation selectivity in oligo(ethylene glycol) functionalized room-temperature ionic liquids. *Ind. Eng. Chem. Res.* 2007, 46, 5380-5386.
26. Tang, S.; Baker, G. A.; Zhao, H., Ether- and alcohol-functionalized task-specific ionic liquids: attractive properties and applications. *Chem. Soc. Rev.* 2012, *41*, 4030-4066.

27. Garist, I. V.; Verevkin, S. P.; Samarov, A. A.; Bara, J. E.; Hindman, M. S.; Danielsen, S. P. O., Building Blocks for Ionic Liquids: Vapor Pressures and Vaporization Enthalpies of Alkoxy Derivatives of Imidazole and Benzimidazole. *Ind. Eng. Chem. Res.* 2012, *51*, 15517-15524.
28. Smith, G. D.; Borodin, O.; Li, L. Y.; Kim, H.; Liu, Q.; Bara, J. E.; Gin, D. L.; Nobel, R., A comparison of ether- and alkyl-derivatized imidazolium-based room-temperature ionic liquids: a molecular dynamics simulation study. *Physical Chemistry Chemical Physics* 2008, *10*, 6301-6312.
29. Lin, H.; Freeman, B. D., Gas and Vapor Solubility in Cross-Linked Poly(ethylene Glycol Diacrylate). *Macromolecules* 2005, *38*, 8394-8407.
30. Lin, H.; Freeman, B. D., Gas solubility, diffusivity and permeability in poly(ethylene oxide). *J. Membr. Sci.* 2004, *239*, 105-117.
31. Hu, X.; Tang, J.; Blasig, A.; Shen, Y.; Radosz, M., CO_2 permeability, diffusivity and solubility in polyethylene glycol-grafted polyionic membranes and their CO_2 selectivity relative to methane and nitrogen. *J. Membr. Sci.* 2006, 281, (1+2), 130-138.
32. Garist, I. V.; Verevkin, S. P.; Bara, J. E.; Hindman, M. S.; Danielsen, S. P. O., Building Blocks for Ionic Liquids: Vapor Pressures and Vaporization Enthalpies of 1-(n-Alkyl)-benzimidazoles. *J. Chem. Eng. Data* 2012, *57*, 1803-1809.
33. Emel'yanenko, V. N.; Portnova, S. V.; Verevkin, S. P.; Skrzypczak, A.; Schubert, T., Building blocks for ionic liquids: Vapor pressures and vaporization enthalpies of 1-(n-alkyl)-imidazoles. *J. Chem. Thermodyn.* 2011, *43*, 1500-1505.
34. Verevkin, S. P.; Zaitsau, D. H.; Emel'yanenko, V. N.; Paulechka, Y. U.; Blokhin, A. V.; Bazyleva, A. B.; Kabo, G. J., Thermodynamics of Ionic Liquids Precursors: 1-Methylimidazole. *J. Phys. Chem. B* 2011, *115*, 4404-4411.
35. Ouchi, M.; Inoue, Y.; Wada, K.; Iketani, S.; Hakushi, T.; Weber, E., M Molecular Design of Crown Ethers .4. Syntheses and Selective Cation Binding of 16-Crown-5 and 19-Crown-6 Lariats. *J. Org. Chem.* 1987, *52*, 2420-2427.
36. Shannon, M. S.; Tedstone, J. M.; Danielsen, S. P. O.; Hindman, M. S.; Irvin, A. C.; Bara, J. E., Free Volume as the Basis of Gas Solubility and Selectivity in Imidazolium-Based Ionic Liquids. *Ind. Eng. Chem. Res.* 2012, *51*, 5565-5576.
37. Finotello, A.; Bara, J. E.; Camper, D.; Noble, R. D., Room-temperature ionic liquids: Temperature dependence of gas solubility selectivity. *Ind. Eng. Chem Res.* 2008, *47*, 3453-3459.
38. Ahlrichs, R.; Bär, M.; Häser, M.; Horn, H.; Kölmel, C., Electronic structure calculations on workstation computers: The program system turbomole. *Chem. Phys. Lett.* 1989, *162*,165-169.
39. Schafer, A.; Huber, C.; Ahlrichs, R., Fully optimized contracted Gaussian basis sets of triple zeta valence quality for atoms Li to Kr. *J. Chem. Phys.* 1994, *100*, 5829-5835
40. Becke, A. D., Density-functional exchange-energy approximation with correct asymptotic behavior. *Phys. Rev. A* 1988, *38*, 3098-3100.
41. Perdew, J. P., Density-functional approximation for the correlation energy of the inhomogeneous electron gas. *Phys. Rev. B* 1986, *33*, 8822-8824.
42. Sumon, K. Z.; Henni, A., Ionic liquids for CO_2 capture using COSMO-RS: Effect of structure, properties and molecular interactions on solubility and selectivity. *Fluid Phase Equilibr.* 2011, *310*, 39-55.
43. Palomar, J.; Gonzalez-Miquel, M.; Polo, A.; Rodriguez, F., Understanding the Physical Absorption of CO_2 in Ionic Liquids Using the COSMO-RS Method. *Ind. Eng. Chem. Res.* 2011, *50*, 3452-3463.
44. Sistla, Y. S.; Khanna, A., Validation and Prediction of the Temperature-Dependent Henry's Constant for CO_2–Ionic Liquid Systems Using the Conductor-like Screening Model for Realistic Solvation (COSMO-RS). *J. Chem. Eng. Data* 2011, *56*, 4045-4060.
45. Shimoyama, Y.; Ito, A., Predictions of cation and anion effects on solubilities, selectivities and permeabilities for CO_2 in ionic liquid using COSMO based activity coefficient model. *Fluid Phase Equilibr.* 2010, *297*, 178-182.

46. Zhang, X. C.; Liu, Z. P.; Wang, W. C., Screening of ionic liquids to capture CO_2 by COSMO-RS and experiments. *AIChE J.* 2008, *54*, 2717-2728.
47. Miller, M. B.; Chen, D.-L.; Luebke, D. R.; Johnson, J. K.; Enick, R. M., Critical Assessment of CO_2 Solubility in Volatile Solvents at 298.15 K. *J. Chem. Eng. Data* 2011, *56*, 1565-1572.
48. Yamada, H.; Shimizu, S.; Okabe, H.; Matsuzaki, Y.; Chowdhury, F. A.; Fujioka, Y., Prediction of the Basicity of Aqueous Amine Solutions and the Species Distribution in the Amine−H_2O−CO_2 System Using the COSMO-RS Method. *Ind. Eng. Chem. Res.* 2010, *49*, 2449-2455.
49. Miller, M. B.; Chen, D.-L.; Xie, H.-B.; Luebke, D. R.; Karl, J. J.; Enick, R. M., Solubility of CO_2 in CO_2-philic oligomers; COSMOtherm predictions and experimental results. *Fluid Phase Equilibr.* 2009, *287*, 26-32.
50. Turner, C. H.; Cooper, A.; Zhang, Z.; Shannon, M. S.; Bara, J. E., Molecular Simulation of the Thermophysical Properties of N-Functionalized Alkylimidazoles. *J. Phys. Chem. B* 2012, *116*, 6529-6535.
51. Bara, J. E.; Moon, J. D.; Reclusado, K. R.; Whitley, J. W., COSMOTherm as a Tool for Estimating the Thermophysical Properties of Alkylimidazoles as Solvents for CO_2 Separations. *Industrial & Engineering Chemistry Research*. Accepted Pending Minor Revisions.
52. Ghatee, M. H.; Zare, M.; Moosavi, F.; Zolghadr, A. R., Temperature-Dependent Density and Viscosity of the Ionic Liquids 1-Alkyl-3-methylimidazolium Iodides: Experiment and Molecular Dynamics Simulation. *J. Chem. Eng. Data* 2010, *55*, 3084-3088.
53. Litovitz, T. A., Temperature dependence of the viscosity of associated liquids. *J. Chem. Phys.* 1952, 20, 1088-1089.
54. Bara, J. E., Considering the Basis of Accounting for CO_2 Mole Fractions in Ionic Liquids and Its Influence on the Interpretation of Solution Nonideality. *Ind. Eng. Chem. Res.* 2013, *52*, 3522-3529.
55. Carlisle, T. K.; Bara, J. E.; Gabriel, C. J.; Noble, R. D.; Gin, D. L., Interpretation of CO_2 solubility and selectivity in nitrile-functionalized room-temperature ionic liquids using a group contribution approach. *Ind. Eng. Chem. Res.* 2008, *47*, 7005-7012
56. Canongia, L. J. N. A.; Padua, A. A. H., Nanostructural Organization in Ionic Liquids. *J. Phys. Chem. B* 2006, 110, 3330-3335.
57. Gonzalez-Miquel, M.; Talreja, M.; Ethier, A. L.; Flack, K.; Switzer, J. R.; Biddinger, E. J.; Pollet, P.; Palomar, J.; Rodriguez, F.; Eckert, C. A.; Liotta, C. L., COSMO-RS Studies: Structure-Property Relationships for CO_2 Capture by Reversible Ionic Liquids. *Ind. Eng. Chem. Res.* 2012, *51*, 16066-16073..
58. Gonzalez-Miquel, M.; Palomar, J.; Omar, S.; Rodriguez, F., CO_2/N_2 Selectivity Prediction in Supported Ionic Liquid Membranes (SILMs) by COSMO-RS. *Ind. Eng. Chem. Res.* 2011, 50, (9), 5739-5748.
59. Diedenhofen, M.; Klamt, A., COSMO-RS as a tool for property prediction of IL mixtures-A review. *Fluid Phase Equilibr.* 2010, 294, (1-2), 31-38.
60. Palomar, J.; Ferro, V. R.; Torrecilla, J. S.; Rodríguez, F., Density and Molar Volume Predictions Using COSMO-RS for Ionic Liquids. An Approach to Solvent Design. *Ind. Eng. Chem. Res.* 2007, 46, (18), 6041-6048.
61. Hansen, C. M., *Hansen Solubility Parameters: A User's Handbook*. 2nd ed.; CRC Press: Boca Raton, FL, 2007.
62. Prausnitz, J. M.; Lichtenthaler, R. N.; Gomes de Azevedo, E., *Molecular Thermodynamics of Fluid-Phase Equilibria*. 3rd ed.; Prentice-Hall: Upper Saddle River, NJ, 1999.

7.7 Appendix:

Table S1: Experimental density data for PEG_n-imidazoles with temperature.

	Density (kg m^{-3}) at given temperature		
T (K)	PEG_1-imidazole	PEG_2-imidazole	PEG_3-imidazole
293.15	1068	1081	1090
303.15	1059	1072	1081
313.15	1050	1064	1073
323.15	1041	1055	1065
333.15	1033	1047	1056
343.15	1024	1038	1048
353.15	1015	1030	1039

Table S2: Experimental viscosity data for PEG_n-imidazoles with temperature.

	Viscosity (kg m^{-1} s^{-1} x 1000) at given temperature		
T (K)	PEG_1-imidazole	PEG_2-imidazole	PEG_3-imidazole
293.15	5.65	10.84	18.03
298.15	4.86	9.12	14.71
303.15	4.21	7.69	12.11
308.15	3.73	6.57	10.15
313.15	3.30	5.67	8.61
318.15	2.94	4.95	7.39
323.15	2.65	4.37	6.39
333.15	2.18	3.48	4.93
343.15	1.84	2.85	3.93
353.15	1.57	2.37	3.21

Table S3: Experimental CO_2 solubility data used to calculate enthalpies of solution from van't Hoff Equation. (x CO_2 at 5 bar).

PEG_1-imidazole + CO_2 (ΔH_{soln} = -16.8 +/- 0.6 kJ mol^{-1})						
H (bar)	+/-	T (^oC)	T (K)	1/T (K^{-1})	x CO_2	ln (x CO_2)
81.0	1.0	25	298.15	0.00335	0.061728	-2.78501
118	2	40	313.15	0.00319	0.042373	-3.16125
156	3	55	328.15	0.00305	0.032051	-3.44042
197	4	70	343.15	0.00291	0.025381	-3.67377
PEG_2-imidazole + CO_2 (ΔH_{soln} = -19.7 +/- 3.1 kJ mol^{-1})						
H (bar)	+/-	T (^oC)	T (K)	1/T (K^{-1})	x CO_2	ln (x CO_2)
64.3	1.0	25	298.15	0.00335	0.07776	-2.55412
100	3	40	313.15	0.00319	0.05000	-2.99573
144	5	55	328.15	0.00305	0.034722	-3.36038
195	7	70	343.15	0.00291	0.025641	-3.66356
PEG_3-imidazole + CO_2 (ΔH_{soln} = -17.8 +/- 0.4 kJ mol^{-1})						
H (bar)	+/-	T (^oC)	T (K)	1/T (K^{-1})	x CO_2	ln (x CO_2)
57.9	0.9	25	298.15	0.00335	0.086356	-2.44928
84.3	2.0	40	313.15	0.00319	0.059312	-2.82494
116	2	55	328.15	0.00305	0.043103	-3.14415
152	3	70	343.15	0.00291	0.032895	-3.41444

Table S4: COSMOTherm CO_2 solubility predictions used to calculate enthalpies of solution from van't Hoff Equation. (x CO_2 at 5 bar).

PEG_1-imidazole + CO_2 (ΔH_{soln} = -16.0 kJ mol^{-1})					
H (bar)	T (^oC)	T (K)	1/T (K^{-1})	x CO_2	ln (x CO_2)
53.87042459	25	298.15	0.00335	0.092815	-2.37714
73.93187807	40	313.15	0.00319	0.06763	-2.69371
97.91267385	55	328.15	0.00305	0.051066	-2.97464
125.76623046	70	343.15	0.00291	0.039756	-3.22499
PEG_2-imidazole + CO_2 (ΔH_{soln} = -15.7 kJ mol^{-1})					
H (bar)	T (^oC)	T (K)	1/T (K^{-1})	x CO_2	ln (x CO_2)
54.2689962	25	298.15	0.00335	0.093354	-2.37135
74.0217181	40	313.15	0.00319	0.068443	-2.68176
97.47649992	55	328.15	0.00305	0.051974	-2.95701
124.55013948	70	343.15	0.00291	0.040676	-3.20211
PEG_3-imidazole + CO_2 (ΔH_{soln} = -15.5 kJ mol^{-1})					
H (bar)	T (^oC)	T (K)	1/T (K^{-1})	x CO_2	ln (x CO_2)
53.88205973	25	298.15	0.00335	0.094025	-2.3642
73.19443493	40	313.15	0.00319	0.069216	-2.67052
96.0201029	55	328.15	0.00305	0.052762	-2.94196
122.25276311	70	343.15	0.00291	0.041441	-3.18349

PEG_n-imidazole	1-*n*-alkylimidazole analogue
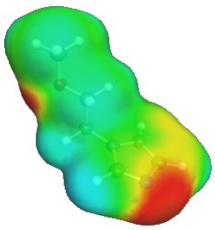 Figure S1: PEG_1-imidazole	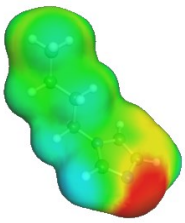 Figure S4: 1-butylimidazole
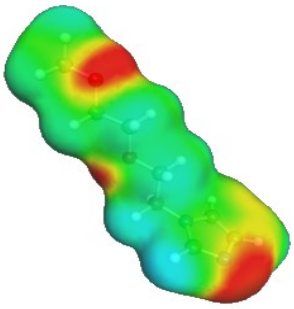 Figure S2: PEG_2-imidazole	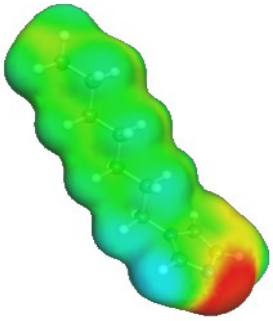 Figure S5: 1-heptylimidazole
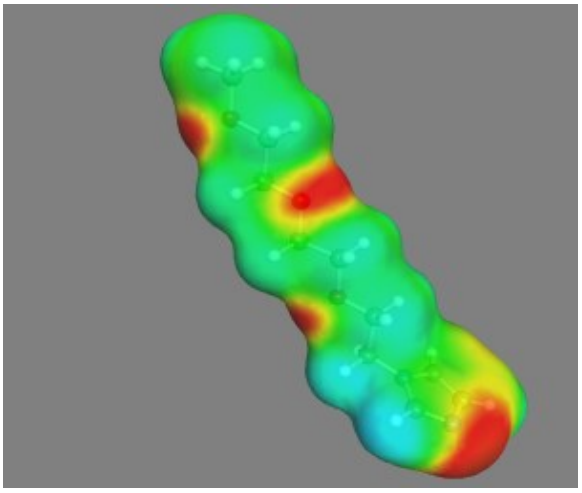 Figure S3: PEG_3-imidazole	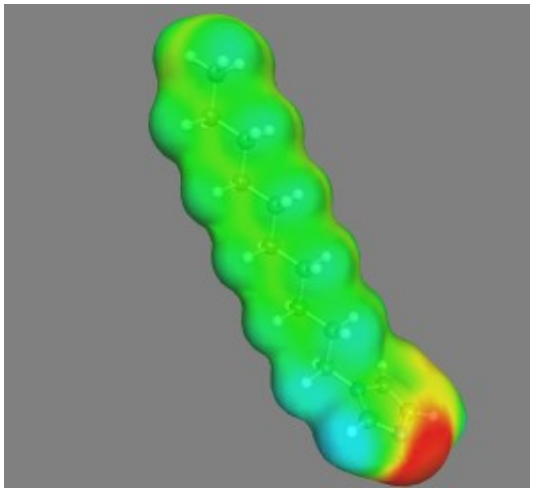 Figure S6: 1-decylimidazole

Figures S1-S6: σ-surfaces of PEG_n-imidazoles and 1-*n*-alkylimidazole analogues from COSMOTherm.

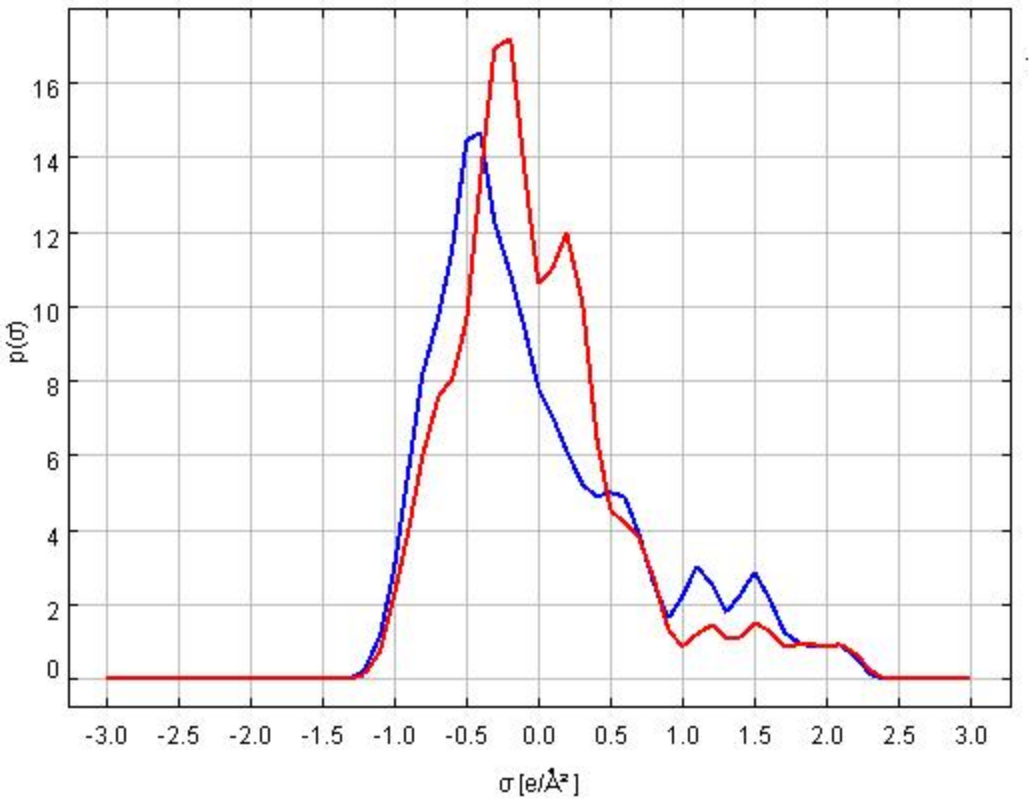

Figure S7: Comparison of σ-profiles of PEG_1-imidazole (blue) and 1-butylimidazole (red).

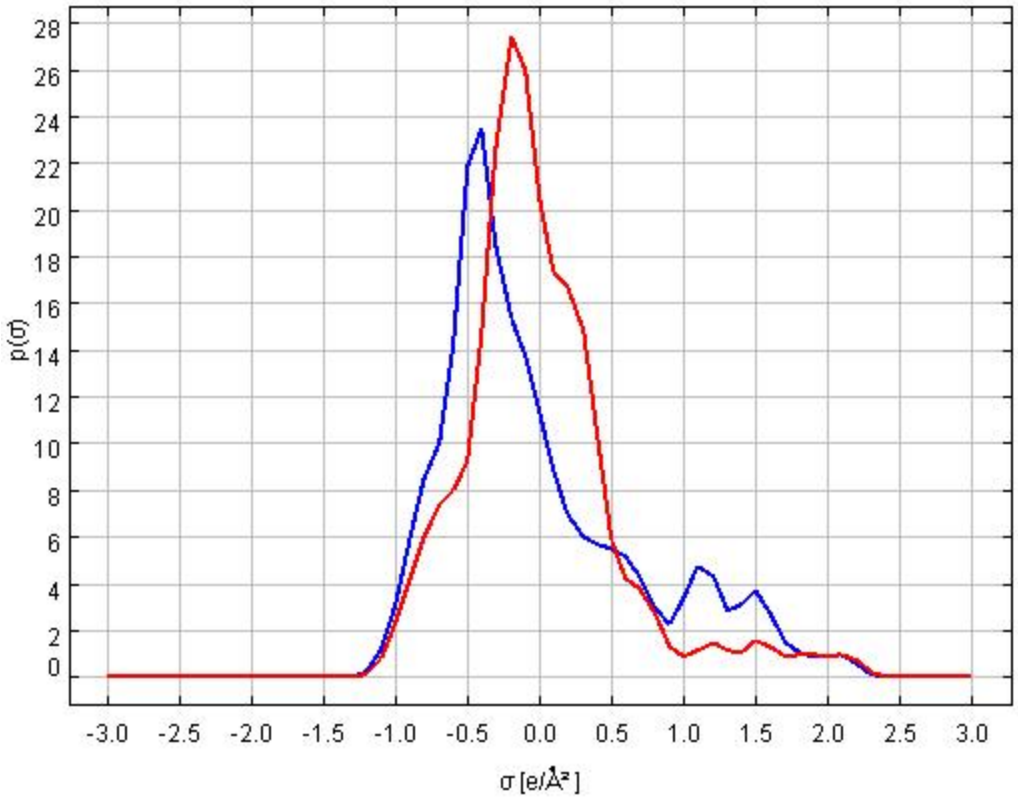

Figure S8: Comparison of σ-profiles of PEG_2-imidazole (blue) and 1-heptylimidazole (red).

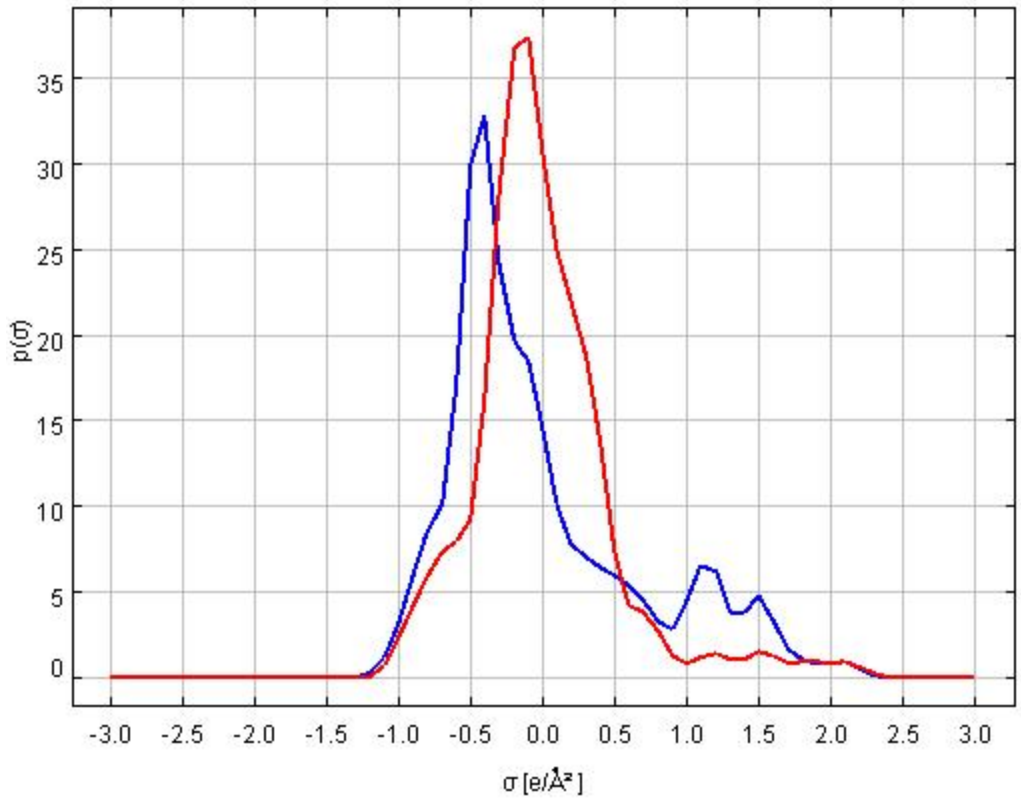

Figure S9: Comparison of σ-profiles of PEG_3-imidazole (blue) and 1-decylimidazole (red).

CHAPTER EIGHT

SO_2 Solubility in *N*-Functionalized Imidazoles and Molecular-level Characterization of Neutral Heterocyclic Structures

Matthew S. Shannon, A. Christopher Irvin, Joshua D. Moon, Haining Liu, C. Heath Turner, Jason E. Bara*

Department of Chemical & Biological Engineering

The University of Alabama, Tuscaloosa, AL USA 35487-0203

Abstract

The effects of functionalizing C(1,2,4) positions of the imidazole structure with alkyl and oligo(ethylene glycol) groups were studied to determine underlying principles of how exocyclic substituents govern SO_2 absorption and desorption capacities and kinetics. Equilibrium SO_2 solubility values in all *N*-functionalized imidazoles approach a 1:1 molar complex, especially given stronger vacuum conditions or inert gas sweep. The $\%mass_{SO2}$ (chemical only) was found to be inversely proportional to R', implying the highest SO_2 weight fraction is observed in less substituted imidazoles with smaller molecular weights (e.g. 1-methylimidazole). All SO_2-loaded samples are reversible as shown with the *N*-functionalized imidazoles given elevated temperature conditions (>100°C) and continuously under vacuum, yielding the original neat solvent. Solution enthalpies (ΔH_{SO2}) were calculated from SO_2 solubility data for the temperature range of 25-70°C, with the all imidazole molecules assumed to be saturated with SO_2 at a 1:1 molar complex and included in the mole fraction as the actual solvent. All calculated solution enthalpies (i.e. heats of absorption) were within the range of -8 to -14 (kJ mol^{-1}), thus, accounting for the additional "physical" dissolution of SO_2 being thermodynamically-favorable (i.e exothermic). Highly-branched imidazole structures proved to possess the most favorable SO_2 dissolution, which can be correlated to the presence of additional EDGs and in the increase in measureable pKa values and proton affinity at the N(3) site. FTIR measurements and analysis of neat and SO_2-loaded imidazole solvents explicitly highlights the distinguishable peak signatures for the presence of SO_2 as a stable complex in the far-IR region. DFT calculations and molecular-level computations were performed to yield optimized structures and determine the SO_2 binding energies to *N*-functionalized imidazoles, with all energies being between -40 and -50 kJ mol^{-1}, being comparable to that of SO_2 with tertiary amines (e.g. trimethylamine). Also, both complexes have similar S-N bond distances, with a slight negative charge observed for SO_2, thus, suggesting the N(3) site of the imidazole ring acting as a Lewis base with acidic SO_2 gas. Functionalizing the C(2) position of the imidazole structure had the most prevalent effect towards increasing the proton affinity experimentally and based on DFT calculations. Computational results along with equilibrium SO_2 solubility data and FTIR spectra analysis conclude and confirm the observed 1:1 molar complex of SO_2 to the imidazole ring at a much greater binding strength than that of physical gas dissolution.

Keywords

Imidazole solvents, sulfur dioxide, SO_2 capture, ionic liquids, gas separations

8.1 Introduction: Environmental detriment from the burning of fossil fuels and acid gas (i.e. CO_2, SO_2) pollution has led to awareness of the overall ecosystem stability and human health effects. SO_2 emissions from the combustion of fossil fuels as a pollutant promotes acid rain formation, affecting the water supply and causes soil contamination and erosion of man-made structures over time. With CO_2 emissions gaining the most attention as a large contributor to the greenhouse gas effect and global warming[1-4], novel capture and sequestration techniques have undergone extensive research for the past few decades. In post-combustion carbon capture, as from coal-fired power plants, removal of SO_2 from flue gas is also necessary to prevent atmospheric and environmental issues as stated in the Clean Air Act of 1990.[5] Typical CO_2 and SO_2 concentrations in post-combustion flue gas conditions are 10-14 vol% and 0.2 vol% (500-2000 ppm), respectively.[5]

Current CO_2 capture techniques utilize aqueous amine solvents, such as monoethanolamine (MEA), as a direct chemical sorbent to remove 75-90% of the bulk CO_2.[6] However, major processing issues occur using amine-based solvents, including corrosion, solvent degradation, and irreversible reactions with SO_2, reducing CO_2 absorption capacity. Flue gas desulfurization (FGD) techniques and processes are currently implemented prior to industrial-scaled CO_2 scrubbing. Current methods of SO_2 capture as utilized in power plants consists of direct scrubber systems containing alkaline slurries, such as limestone ($CaCO_3$), lime, or sodium hydroxide.[7,8] In the case of limestone scrubbing, the $CaCO_3$ slurry undergoes an oxidation reaction with SO_2 to form the fully-oxidized product of $CaSO_4$, which is commonly sold as gypsum dry-wall. Disadvantages with current SO_2 scrubbing techniques utilizing alkaline (i.e. limestone) slurries are low scavenging efficiency and gypsum waste products that are not truly economically-favorable. Recent novel approaches focus on reactive and reversible techniques as sustainable processes replacing conventional FGD systems that use more of a discarding approach. The presence of water during flue gas desulfurization must be considered due to a decrease in SO_2 desorption and increase in sulfuric acid byproducts.[9,10] Another currently utilized sorbent for industrial FGD is *N*,*N*-dimethylaniline (DMA), that has a moderate affinity for SO_2 and can readily be regenerated via heat.[11-14] DMA, however, is highly toxic, and during this process, some solvent loss is observed due to evaporation and wastewater dissolution. Citrate materials have also been considered for SO_2 scrubbing by forming buffer solutions;[15-17] however, defects occur in scaled-up processes, including fouling of piping and equipment, as well as SO_2 oxidation.

Ionic liquids (ILs) have gained consideration over the past few decades in several areas of engineering research and are now a main focus in the field of gas separations due to their unique properties, including low vapor pressure, chemical stability, and tunable platforms.[18-21] Room-temperature ionic liquids (RTILs) also present novel and favorable properties over amine-based solvents, such as thermal and

regeneration advantages and being less corrosive.[22-24] Several groups have extensively studied novel IL solvents as new, environmentally-benign sorbents to capture SO_2 efficiently and reversibly, as well as reducing fugitive solvent emissions that impact the environment. Wu et al.[25] first pioneered the area of SO_2 solubility in ILs based on N-S complexing. Wu et al. showed that 1,1,3,3,-tetramethylguanidine lactate ([TMG]L) reached a maximum SO_2 capacity of 0.978 mol mol^{-1} at 40°C and 1 bar of mixed gas (92% N_2, 8% SO_2). Dong An et al.[26] reported SO_2 absorption in 1,1,3,3-tetramethylguanidine acrylate (TMGA) and poly(TMGA) at 50°C, yielding nearly double SO_2 molar absorption in the polymeric material (~1.1 mol mol^{-1}). However, this guanidine-based polymer does exhibit a high viscosity of over 13,000 cP. Unlike most ILs and other physical solvents, [TMG]L undergoes chemical interaction with SO_2, which has been verified via FTIR and NMR analysis for both neat and SO_2-loaded IL. The proposed mechanism consists of hydrogen bonding between the NH_2 group of the cation and SO_2.

Brennecke et al.[27] reported high SO_2 solubilities in pyridinium- and imidazolium-based ILs as a function of temperature and pressure. The highest SO_2 mole fraction recorded of 0.90 was in 1-hexyl-3-methylimidazolium bis(trifluromethylsulfonyl)imide ([hmim][Tf_2N]) near the SO_2 saturation pressure of 3.44 bar and 25°C. Under these same conditions, the mole fraction of CO_2 in [hmim][Tf_2N] is only 0.10,[28] and the solubility of N_2 is sufficiently low and practically unmeasurable. This implies the likelihood of removing both SO_2 and CO_2 in a single processing step for post-combustion separations. Ionic liquids typically exhibit physical gas solubility/loading, implying a larger driving force (i.e. SO_2 partial pressure) is required to be implemented as a feasible gas separation solvent. With SO_2 being scrubbed from power plant flue gas initially from approximately 2000 ppm down to 50-100 ppm, chemically-interacting solvents are most optimal.

Novel solvents such as *N*-functionalized imidazoles provide a reversible and reactive platform for direct SO_2 recovery, thus, eliminating solids handling for flue gas desulfurization (FGD). In our previous work[29-32], we explored the imidazole platform for CO_2 gas separations in post-combustion capture and natural gas applications. This study investigates the effects of additional functionalization at the C(1), C(2), and C(4) positions of the imidazole ring for time- and temperature-dependent SO_2 solubility, as well as validating the overall SO_2 complexing mechanism. Additional functional groups appended to the imidazole ring can govern and tune the SO_2 absorption and desorption kinetics based on which groups are added, electron donating groups (EDGs) or electron withdrawing groups (EWGs).[33]

8.2 Experimental Section

8.2.1 Materials: All *N*-functionalized imidazoles were synthesized in our laboratory as noted and detailed in our previous work.[34] Purity of compounds were >98% by mass. Research grade SO_2 was purchased from AirGas (Radnor, PA, USA).

8.2.2 SO_2 Solubility Measurements: For each SO_2 solubility experiment, approximately 5-7 g of each *N*-functionalized imidazole was added to a 25 mL round bottom flask with a stir bar and clamped over a stir plate to ensure homogenous and continuous mixing. SO_2 gas at ~6 psig was bubbled through 1/16" stainless steel tubing, which was fully enclosed within Swagelok fittings through a ground glass joint that was securely connected to the round bottom flask. The mass of the flask (including the solvent and gas absorbed) was recorded over time at 5 min intervals, ranging from 35 to 110 minutes for different solvents, until equilibrium was achieved. Any observed color change associated with dissolution of SO_2 was also noted. The absorbed SO_2 was then immediately desorbed from the solvent via vacuum pump for approximately 24 hours until a final equilibrium was achieved. The error associated with the mass measurements is within +/- 0.01 g, implying an approximate 1% error in the calculated values for $\%mass_{SO2}$ and $mol_{SO2}/mol_{imidazole}$.

Also, temperature effects were studied in a select few of these *N*-functionalized imidazoles by measuring equilibrated SO_2 absorption at 25, 40, 55, and 70°C. The $\%mass_{SO2}$ in these selected imidazoles was observed to decrease with increasing temperature. Heats of absorption (i.e. solution enthalpy, ΔH_{SO2}) for each imidazole were determined via the integrated form of the van't Hoff equation (Eqn. 1) by calculating the slope from the plot of $\ln(x_{SO2})$ vs 1/T.

$$\ln(x_{SO2}) = -\frac{\Delta H_{SO2}}{RT} + B \quad (1)$$

8.3 Results and Discussion

8.3.1 SO_2 Solubility and Comparisons: Previously, we began initial SO_2 absorption experiments in both 1-hexylimidazole[35] and 1-butylbenzimidazole[31] for primary candidates as SO_2 gas scavengers. In 1-hexylimidazole, ~1 psig of SO_2 gas was bubbled through the continuously mixing solvent (~5.00 g) for only 5 minutes and reached a gas loading of 1.17 mol_{SO2}/mol 1-hexylimidazole. The SO_2 loaded solvent was then swept with a N_2 stream for several hours at room temperature and reached an equilibrated loading of ~0.5 mol_{SO2}/mol 1-hexylimidazole, implying a complex being formed at room temperature and ambient pressure consisting of 2 imidazole molecules binding one SO_2 molecule at each N(3) site. The chemically-bound SO_2 can readily be released reversibly by elevated temperatures (>100°C) and/or continuous N_2 sweep or

vacuum. However, more rigorous experiments are needed to validate this observed molar complex ratio of 2:1 imidazole to SO_2 as a function of higher partial pressures of SO_2.

SO_2 solubility in 1-butylbenzimidazole was also evaluated under similar methodology, in which SO_2 was again bubbled at ~1 psig in 5.00 g of solvent at room temperature. The mass of the flask and its contents along with color change were recorded at different time intervals over a 20 minute period. After equilibrating at a SO_2 absorption ratio of 0.96 mol_{SO2}/mol 1-butylbenzimidazole, the flask and its contents were then swept with N_2 for a 40 minute period, flushing all SO_2 out and returning the contents to neat imidazole. Although low pressure SO_2 can be readily absorbed and desorbed in 1-*n*-alkylbenzimidazoles, these solvents do not undergo the same chemical reaction as observed in 1-*n*-alkylimidazoles. The lack of this stable complex being formed in 1-*n*-alkylbenzimidazoles is due to the deactivation of the reactive N(3) site by the additional aromatic ring, causing the imidazole to act less as a nucleophile (i.e. decrease in basicity). An overall consensus of the observed color change when exposed to SO_2 still validates that *N*-functionalized imidazoles are useful as visual indicators in the presence of SO_2.

Table 8.1: SO_2 Solubility Data in *N*-functionalized Imidazoles at 25°C

	$mol_{SO2}/mol_{imidazole}$			$\%mass_{SO2}$				
Compound	Chemical	Chemical + Physical	%Diff.	Chemical	Chemical + Physical	%Diff.	MW	R'
1-methylimidazole	1.32	2.35	44%	51%	65%	22%	82.1	0.183
1,2-dimethylimidazole	-	1.25	-	-	45%	-	96.13	0.302
1-ethylimidazole	1.31	2.61	50%	47%	63%	27%	96.13	0.302
1-ethyl-2-methylimidazole	1.57	2.88	45%	48%	63%	24%	110.16	0.391
1-ethyl-4-methylimidazole	1.17	2.37	51%	41%	58%	30%	110.16	0.391
1,2-diethyl-4-methylimidazole	1.11	2.64	58%	34%	55%	38%	138.21	0.515
1-propyl-2-methylimidazole	1.15	1.69	32%	37%	47%	20%	124.18	0.460
PEG_1-imidazole	1.28	2.46	48%	39%	56%	29%	112.13	0.402
PEG_1-4-methylimidazole	1.19	2.70	56%	35%	55%	36%	126.16	0.468
PEG_2-imidazole	1.39	3.11	55%	33%	52%	37%	156.18	0.570
PEG_2-4-methylimidazole	1.1	2.93	62%	26%	49%	46%	170.21	0.606

Table 8.1 presents the measured SO_2 solubility in these *N*-functionalized imidazoles at room temperature as molar ratios and mass percentages. The term "chemical" refers to the residual amount of SO_2 left in each solvent after vacuuming, implying a permanent, reactive complex formed. The term "chemical + physical" accounts for the total observed and equilibrated amount of absorbed SO_2 in each solvent. The highest SO_2 molar absorption (chemical complexation) is observed in 1-ethyl-2-methylimidazole at 1.57 $mol_{SO2}/mol_{imidazole}$. However, all chemical SO_2 absorption values in these *N*-functionalized imidazoles are considered to be equilibrated under aforementioned methodology and would tend to approach a final molar complex of 1:1 if swept more with N_2 or undergone stronger vacuum conditions. The highest maximum (chemical +physical) SO_2 molar absorption is observed in PEG_2-imidazole, followed by PEG_2-4-methylimidazole, 3.11 and 2.93, respectively. Also, as can be concluded from the data in Table 8.1, functionalizing the C(2) position seems to have the most prevalent and optimal effect. With 1,2-dimethylimidazole being a solid at room temperature, this solvent recrystallized immediately upon continuous exposure to SO_2, implying no true chemical solubility was attainable along with desorption data. The highest $\%mass_{SO2}$ (chemical only) is seen in 1-methylimidazole having the smallest molecular weight, and the lowest $\%mass_{SO2}$ is seen in PEG_2-4-methylimidazole having the largest molecular weight. This observation is almost similar in $\%mass_{SO2}$ (chemical + physical), however, an overall trend cannot be made, especially with increasing molecular weight. With the chemical-only SO_2 mass fraction increasing with decreasing molecular weight, our previously used molecular weight parameter[29] (*R'*) can be revisited and used for modeling this observation. A decreasing, linear trend is observed with $\%mass_{SO2}$(chemical) vs *R'*, as seen in Figure 8.1, implying that mass of SO_2 absorbed is best in smaller molecular weight solvents (i.e. higher FFV, lower viscosity, etc). By comparing neat viscosities of these *N*-functionalized imidazoles, a similar trend can also be made to the "chemical only" SO_2 solubility, with $\%mass_{SO2}$ decreasing with increasing solvent viscosity. However, with this observation being somewhat intuitive, all neat viscosities fall below 10 cP, implying non-viscous media. Also, it should be noted that several SO_2-loaded samples were heated to elevated temperatures (~100^{o}C) while remaining under vacuum until the weight returned to that of the neat solvent, thus, showing the reversibility of this gas-binding complex.

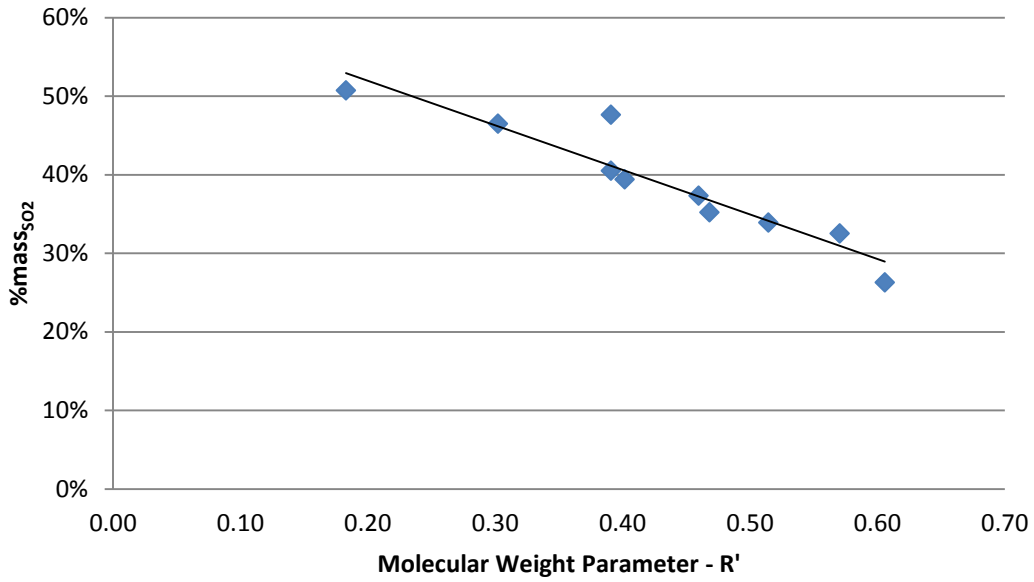

Figure 8.1: Linear regression of %mass$_{SO2}$ vs. *R'*.

SO_2 solubility within the temperature range of 25-70°C was measured in some *N*-functionalized imidazoles, in which gas solubility exhibited to decrease with temperature. Calculated solution enthalpies (ΔH_{SO2}) from the integrated form of the van't Hoff equation (Eqn. 1) better explains this temperature dependence, as previously explained in detail by Finotello et al.[36] As seen from Table 8.1, both "chemical" and "chemical + physical" SO_2 solubility measurements (molar ratios and mass percentages) at room temperature are noted, implying that the "physical only" SO_2 solubility term can be calculated as well. The "physical" SO_2 solubility known at 25°C for each *N*-functionalized imidazole accounts substantially for the overall measured mole fraction of SO_2 at each recorded temperature. As aforementioned regarding the SO_2 solubility data presented in Table 8.1, each SO_2-imidazole complex would approach a 1:1 molar ratio given sufficient time and vacuum/sweep conditions. Under this premise, all imidazole molecules are considered completely saturated and complexed with SO_2 for the temperature range provided, implying elevated temperature and vacuum conditions are needed to remove all SO_2, thus, yielding the neat solvent. The SO_2-imidazole complex is included in the mole fraction for solution enthalpy calculations, which are explained in more detail in Section 8.6 (Appendix), along with tabulated results of ΔH_{SO2}.

The calculated heats of absorption for select *N*-functionalized imidazoles ranged from -8 to -14 (kJ mol^{-1}), with all values being negative (i.e. exothermic), implying favorable SO_2 dissolution. Also, it can be noted that the more favorable SO_2 dissolution is observed in more highly branched imidazoles. This correlates with the effects of functionalizing the imidazole ring with electron donating groups (EDGs) vs electron

withdrawing groups (EWGs) and proton affinity at the N(3) site.[33] Liu et al. previously performed density functional theory (DFT) calculations on 1-methylimidazole with exocyclic substituents (EDGs and EWGs) and their effects on proton affinity (i.e. CO_2-philicity) and correlation to pK_a values. The presence of EDGs (*n*-alkyl groups) appended to the C(2), C(4), and/or C(5) sites does promote and increase in proton affinity compared to just 1-methylimidazole, with these effects being additive and directly proportional to empirical pK_a values. However, any presence of EWGs has a more significant impact in decreasing the proton affinity. With CO_2 and SO_2 capture and removal simply being an acid/base scavenging process, the overall consensus promotes the functionalization of the imidazole platform with EDGs to increase CO_2 uptake.

Brennecke et al.[27] noted that both CO_2 and SO_2 solubilities in pyridinium- and imidazolium-based ILs are quite similar when compared in reduced pressures and equifugacity. With an order of magnitude of difference in saturation pressures of CO_2 and SO_2, this explains the higher SO_2 solubility observed. Also, partial molar enthalpies of solution for both SO_2 and CO_2 were calculated, ranging from -11 to -20 kJ mol^{-1}, and fall within the regime of physical gas dissolution. Most of the calculated solution enthalpies for *N*-functionalized imidazoles are also within this range for physical-based gas dissolution in the SO_2-complexed solvent.

Yuan and Zhang investigated hydroxyl ammonium ionic liquids for SO_2 absorption, as well as analyzed FTIR spectra of various SO_2-loaded IL samples.[37] The highest SO_2 solubility measured was in tri-(2-hydroxyethyl)ammonium lactate with a mole fraction of 0.4957 at ambient pressure and temperature. Based on FTIR spectra analysis of both neat and SO_2-loaded IL solvent, SO_2 binds with the NH_2 group of the cation and is easily released via vacuum and/or heat. The absorption peak around 1580 cm^{-1} is significantly diminished after the IL solvent is loaded with SO_2, which is proportional to the disappearance of -C=O-O- molecules. Also, the respective absorption peaks for -C=O-OH and N-S=O- molecules appearance are more prevalent.

FTIR measurements were obtained for each neat and SO_2-loaded *N*-functionalized imidazole sample at room temperature for comparison and analysis of the SO_2-imidazole complex observed. Figure 8.2 shows the comparison of FTIR spectra between neat 1-methylimidazole and the effects of SO_2 complexing with 1-methylimidazole. Section 8.6 (Appendix) discusses all other FTIR spectra for the remaining *N*-functionalized imidazoles. Prominent IR peak differences are distinct, especially within the range of ~1500-1400 cm^{-1} for neat 1-methylimidazole, which are signatures for the N(3) site bonding with the neighboring carbons C(2) and C(3).[38] It also should be noted that at the last distinguishable peak observed for the lowest wavenumber occurs at ~619 cm^{-1}, with the SO_2-loaded sample exhibiting peaks at lower wavenumber values (550-500 cm^{-1}). This region corresponds to the far-IR spectra which is indicative of N-S bonds and/or SO_2

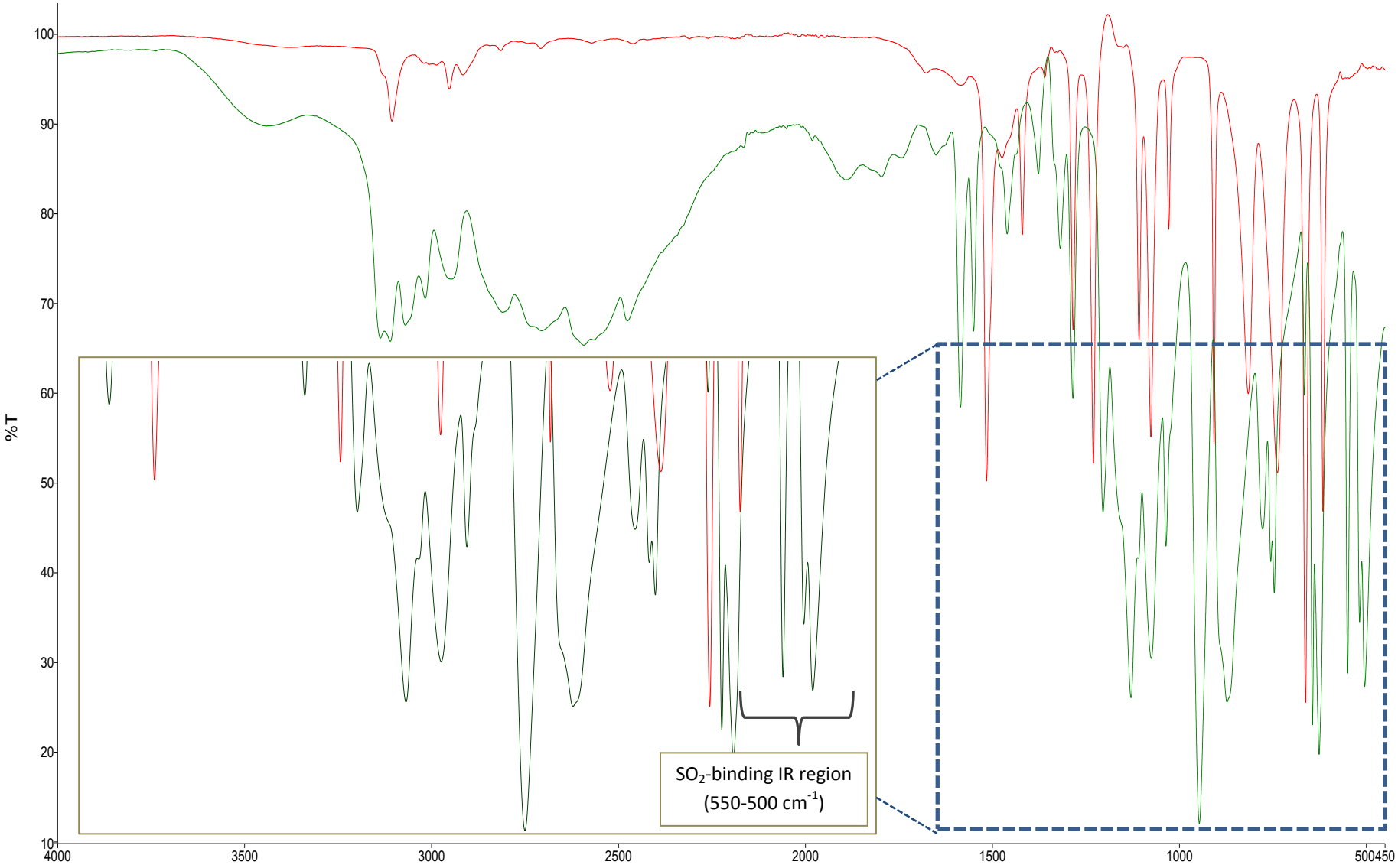

Figure 8.2: FTIR spectra for 1-methylimidazole sample: neat (red) and SO_2-loaded (green)

complex. These FTIR spectra obtained for *N*-functionalized imidazoles were compared to spectra of sulfur-containing compounds (i.e. sulfonamides) with similar structures as compiled in the Spectral Database for Organic Compounds (SDBS) by AIST.[39] Comparing the SO_2-loaded FTIR spectra in Figure 8.2 to that of IR spectra for simple examples of sulfonamides (i.e. *N*,*N*-dimethylmethanesulfonamide and methanesulfonamide) shows similarities in distinguishable peaks, particularly for the lower range of 550-500 cm^{-1}. These peaks are signatures for the presence of the SO_2 group, thus, implying a stable complex is indeed formed between SO_2 and 1-methylimidazole. This observation was also compared to another IR compilation for several compounds, including sulfonamides and other sulfur-containing solvents, as presented by Colthup et al.[40] Again, these compounds have prevalent IR peaks occurring in the far-IR spectra, including those correlating to the presence of SO_2 groups (~600-500 cm^{-1}). The significance of the observed SO_2 complex with *N*-functionalized imidazoles and the relevance to sulfonamides is discussed in more detail in Section 8.3.3.

8.3.2 SO_2 Binding Energies and Simulation Calculations: The Gaussian 09 computational suite was used to perform calculations and determine the optimized structures of selected neutral functionalized imidazoles with alkyl and poly(ethylene glycol) substituents using Density Functional Theory (DFT). All calculations were performed using the M06-2X functional with the 6-31++G(d,p) split-valence double zeta basis set with polarization and diffuse functions. While the B3LYP functional is more commonly used for DFT optimizations, it is less accurate than M06-2X at describing moderate-range non-covalent interactions and van der Waals complexes.[41,42] The optimized geometries and energies were calculated for each substituted imidazole in addition to each structure with an SO_2 molecule complexed at the N(3) position, with binding energies being corrected for zero-point vibrational energies (ZPVEs). An example of the optimized structure of 1-methylimidazole complexed with SO_2 is shown below in Figure 8.3.

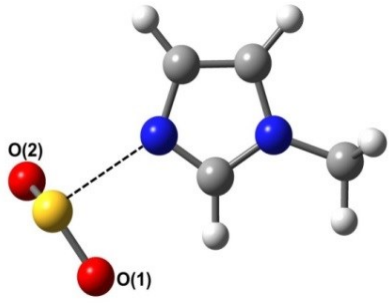

Figure 8.3: Optimized structure of 1-methylimidazole bound with SO_2.

The SO_2 binding energies were calculated by taking the difference between the enthalpies at 298 K of the unbound substituents and that of the complex. The calculated binding energies (kJ mol^{-1}), distance between N(3) and S (Å), NBO charge on N(3), proton affinity of N(3) (kJ mol^{-1}), and total charge on SO_2 are listed below. All of the binding energies were determined to be between -40 and -50 kJ mol^{-1}. This matches closely with the binding energy of SO_2 with trimethylamine, which is known to be -40.6 ± 1.7 kJ mol^{-1} from experiment and -39.1 kJ mol^{-1} from DFT calculations at the B3LYP/6-31G(2df,p) level with a BSSE (Basis Set Superposition Error) correction.[43] Additionally, the bond distance between S and N(3) was calculated to be between 2.319 and 2.497 Å, which is comparable to that of 2.417 Å for the SO_2-NMe_3 interaction.[43] The chemical binding of SO_2 with the imidazole ring, therefore, appears to occur with a similar strength to that of SO_2-amine binding. Furthermore, the SO_2 acquired a slightly negative net charge of -0.08 to -0.13, supporting the idea that it is acting as an electron acceptor in a Lewis acid-base interaction.

Table 8.2. Calculated SO_2 Binding Energies at 298 K.

	Binding energy	r(N_3···S)	NBO charge on N_3	PA	NBO charge on SO_2
1-CH_3	-40.3	2.488	-0.56248	952.9	-0.08069
1-CH_2CH_3	-41.6	2.470	-0.56253	959.6	-0.08521
1,2-CH_3	-43.5	2.372	-0.56579	972.5	-0.11098
1-CH_2CH_3-2-CH_3	-44.8	2.361	-0.56751	977.7	-0.11497
1-$CH_2CH_2CH_3$-2-CH_3	-44.8	2.368	-0.56851	980.2	-0.11333
1-CH_2CH_3-4-CH_3	-45.1	2.380	-0.56952	973.0	-0.11144
1-CH_2CH_3-5-CH_3	-43.9	2.436	-0.55798	974.0	-0.09554
1-CH_2CH_3-2-CH_2CH_3-4-CH_3	-49.9	2.402	-0.57575	994.5	-0.10815
1-CH_2CH_3-2-CH_2CH_3-5-CH_3	-49.7	2.319	-0.56413	995.0	-0.1312
1-peg1	-41.1	2.491	-0.55602	954.0	-0.07947
1-peg1-4-CH_3	-45.2	2.399	-0.56724	968.5	-0.10489
1-peg1-5-CH_3	-42.0	2.444	-0.55989	969.1	-0.09272
1-peg2	-42.1	2.497	-0.55952	955.1	-0.07748
1-peg2-4-CH_3	-43.4	2.392	-0.56693	968.7	-0.10623
1-peg2-5-CH_3	-42.1	2.461	-0.55556	969.8	-0.08815

The presence of an ethyl or methyl group at C(2) had a statistically-significant impact on the N-S binding characteristics, though adding methyl group at C(4) or C(5) had no significant impact except when an alkyl group was also present at C(2). This computational result is analogous to our empirical SO_2 solubility data and comparisons, in which *N*-functionalized imidazoles with a short, *n*-alkyl chain appended at the C(2) position displayed the most prevalent and optimal effect towards SO_2 solubility. The 1,2,4(5)alkylimidazole had the strongest binding energy and proton affinity due to the presence of several electron-donating alkyl groups on the imidazole ring that enhance the nucleophilic character of N(3), resulting in a greater affinity for acidic SO_2 molecules and strengthening the resulting bond through an increased binding enthalpy. The presence of an alkyl group at C(2) increased the binding energy by an average of 3.86 kJ mol^{-1} and increased the magnitude of the negative charge acquired by the SO_2 by 0.024. Additionally, replacing the C(1) alkyl group with PEG_1 or PEG_2 had a significant but opposite impact, as the binding energy was reduced by an average of 2.19 kJ mol^{-1} and the magnitude of the negative charge of the SO_2 was reduced by an average of 0.014.

The computational results therefore strongly support the 1:1 chemical binding of SO_2 to the imidazole ring as observed in experiment. The sulfur appears to bind to the imidazole ring with a strength much greater than that of physical solvation due to the nucleophilic nature of the N(3) atom and electrophilic nature of the S atom. Furthermore, the presence of an electron-donating alkyl group at the C(2) position enhances the effect by increasing the negative character of the nitrogen, while the PEG-group slightly deactivates the nitrogen from acting as a basic site, causing the SO_2-imidazole interaction to be slightly weaker.

8.3.3 Novel and Reversible SO_2 Removal via Imidazole Complexes as Potential Sulfa Drug Precursors: *N*-functionalized imidazoles as SO_2 scavenging solvents are presented in this work as reversible and efficient sorbents that can inevitably complex with SO_2 at an equilibrated molar ratio of 1:1 under ambient conditions. However, another consideration for this novel SO_2 capture approach and mechanism observed is towards the pharmaceutical field as potential precursors for sulfonamides and other sulfa drugs. Sulfa drugs, such as sulfonamides as seen in Figure 8.4, are synthetic antimicrobial agents inhibiting bacterial growth. The 1939 Nobel Prize winner Gerhard Domagk was able to successfully synthesize the first commercially-available sulfonamide, Prontosil, while researching at Bayer Laboratories.[44] Since his novel discovery, several sulfa drugs have been developed as antibacterial medication, including the mass production of penicillin in the early years of sulfonamides.[45] As of 2007, over 50 million kg of penicillin is

produced per year worldwide (over 100,000 kg per day).[46] Current mass production and preparation of sulfonamides includes reacting sulfonyl chloride with ammonia or amines.

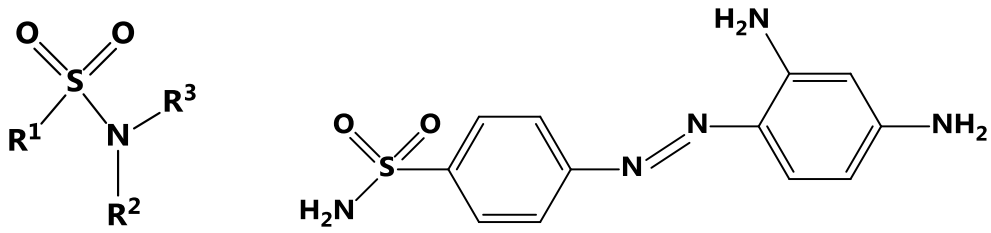

Figure 8.4: Structures of sulfonamide (left) and Prontosil (right).

Almost all pharmaceuticals are currently produced in batch and semi-batch processes, which can lead to higher production costs and excessive inventory of raw materials. With fossil fuel-based industries, such as coal-fired power plants, producing SO_2 continuously as a byproduct, SO_2 scavenging from these sources presents a continuous and readily-available feedstock for sulfa drug production. With an average-size fossil-fueled power plant (~600 MW) emitting an average flue gas flow rate of 500 m^3/s and with SO_2 concentrations as high as 0.2 vol.%, an excessive amount of SO_2 needs to be removed as a contaminant, reaching in the millions of kilograms of SO_2 being removed from just one power plant per day. With the experimental observations, FTIR analysis, and computational calculations supporting the 1:1 molar complexing of SO_2 to the N(3) site of the imidazole ring, *N*-functionalized imidazoles offer a promising platform for SO_2 capture from flue gas as either a reversible and renewable sorbent, ridding production of less economically-favorable byproducts (i.e. gypsum), or an innovative approach to feasibly and continuously produce sulfur-based pharmaceuticals. The similar, basic structure of the SO_2-imidazole complex compared to sulfonamide provides an opportunity for novel chemistry techniques to be utilized to synthesize several types of sulfa drugs with numerous tunable and tailored imidazole platforms available.

8.4 Conclusions: *N*-functionalized imidazoles present a reversible and reactive platform for direct SO_2 recovery, eliminating solids handling in current FGD processes that utilize alkaline slurries in direct scrubber systems. Environmentally-benign solvents such as imidazole-based solvents and ILs show promise for removing SO_2 and CO_2 in a single process step, thus, eliminating disadvantages with current scrubbing systems, including low scavenging efficiency, less favorable byproduct commodities (e.g. gypsum), and irreversible side reactions with amine-based solvents for CO_2 capture. This study investigated the effects of functionalizing C(1,2,4/5) positions with alkyl and oligo(ethylene glycol) groups to the imidazole ring that

govern SO_2 absorption and desorption capacities and kinetics. Equilibrium SO_2 solubility values in all *N*-functionalized imidazoles approach a 1:1 molar complex, being completely reversible given more intense vacuum conditions or inert gas sweep and at elevated tempertures (>100^oC), as shown for all imidazole solvents. Solution enthalpies (ΔH_{SO2}) calculated for the temperature range of 25-70^oC fell within the range of -8 to -14 (kJ mol^{-1}), including the 1:1 molar SO_2-imidazole complex in these calculations. Highly-branched imidazole structures are most favorable for SO_2 solvation due to the presence of additional EDGs, thus, correlated to the increase in measureable pK_a values and proton affinity at the N(3) site. Also, FTIR spectra of neat and SO_2-loaded imidazole solvents distinctly confirms peak signatures for the presence of SO_2 as a stable complex in the far-IR region. Based on DFT calculations and molecular-level computations, SO_2 binding energies to *N*-functionalized imidazoles were found to be fall between -40 and -50 (kJ mol^{-1}), being similar to that of SO_2 binding with tertiary amines (e.g. trimethylamine), as well as both complexes having similar S-N bond distances. A partial negative charge is observed for the SO_2 molecule, implying the Lewis acid-base chemistry of the N(3) site of the imidazole ring with acidic SO_2 gas. Functionalizing the C(2) position of the imidazole structure displayed the most prevalent effect towards increasing the SO_2 affinity, with the most substituted *N*-functionalized imidazole (1,2-diethyl-4-methylimidazole) exhibiting the strongest binding energy and highest proton affinity by enhancing the nucelophilicity of the N(3) site. The *N*-functionalized imidazole platform warrants further investigation and research as a novel and reversible SO_2 scavenging solvent for post-combustion FGD applications and potential use as an innovative source of sulfur-based pharmaceutical precursors.

8.5 References:

(1) Yeh, A. C.; Bai, H. L. Comparison of ammonia and monoethanolamine solvents to reduce CO_2 greenhouse gas emissions. *Sci. Total Environ*. 1999, *228*, 121-133.

(2) Blok, K.; Worrell, E.; Cuelenaere, R.; Turkenbur, W. The cost effectiveness of CO_2 emission reduction achieved by energy conservation. *Energy Policy* 1993, *21* (6), 656-667.

(3) Parson, E. A.; Keith, D. W. Fossil Fuels Without CO_2 Emissions. *Science* 1998, *282*, 1053-1054.

(4) Wolsky, A. M.; Daniels, E. J.; Jody, B. J. CO_2 capture from the flue gas of conventional fossil-fuel-fired power plants. *Environ*. *Prog*. 1994, *13*, 214-219.

(5) Merkel, T. C.; Lin, H.; Wei, X.; Baker, R. Power plant post-combustion carbon dioxide capture: An opportunity for membranes. *Journ*. *Mem*. *Sci*. 2010, *359*, 126-139.

(6) Rao, A. B.; Rubin, E. S. A technical, economic, and environmental assessment of amine-based CO_2 capture technology for power plant greenhouse gas control. *Environ*. *Sci*. *Technol*. 2002, *36*, 4467-4475.

(7) Ma, X.; Kaneko, T.; Tashimo, T.; Yoshida, T.; Kato, K. Use of Limestone for SO_2 Removal from Flue Gas in the Semidry FGD Process with a Powder-Particle Spouted Bed. *Chem*. *Eng*. *Sci*. 2000, *55*, 4643.

(8) Stergarsek, A.; Horvat, M.; Kotnik, J.; Tratnik, J.; Frkal, P.; Kocman, D.; Jacimovic, R.; Fajon, V.; Ponikvar, M.; Hrastel, I.; Lenart, J.; Debeljak, B.; Cujez, M. The role of flue gas desulphurisation in mercury speciation and distribution in a lignite burning power plant. *Fuel* 2008, *87* (17-18) 3504-3512.

(9) Ren, S.; Hou, Y.; Tian, S.; Wu, W.; Liu, W. Deactivation and Regeneration of an Ionic Liquid during Desulphurization of Simulated Flue Gas. *Ind*. *Eng*. *Chem*. *Res*. 2012, *51*, 3425.
(10) Ren, S.; Hou, Y.; Wu, W.; Chen, X.; Fan, J.; Zhang, J. Effect of H_2O on the Desulfurization of Simulated Flue Gas by an Ionic Liquid. *Ind*. *Eng*. *Chem*. *Res*. 2009, *48*, 4928.
(11) Balej, J.; Regner, A. Das System Schwefeldioxid-Dimethylanilin. 1. Die Absorptionsisothermen. *Collect*. *Czech*. *Chem*. *C* 1956, *21*, 1545.
(12) Basu, R. K.; Dutta, B. K. Kinetics of Absorption of Sulfur Dioxide in Dimethylaniline Solution. *Can*. *J*. *Chem*. *Eng*. 1987, *65*, 27.
(13) Bhattacharya, S.; Dutta, B. K.; Shyamal, M.; Basu, R. K. Absorption of Sulfur Dioxide in Aqueous Dispersions of Dimethyl Aniline. *Can*. *J*. *Chem*. *Eng*. 1996, *74*, 339.
(14) Luis, P.; Garea, A.; Irabien, A. Sulfur Dioxide Non-Dispersive Absorption in *N*,*N*-Dimethylaniline Using a Ceramic Membrane Contactor. *J*. *Chem*. *Technol*. *Biotechnol*. 2008, *83*, 1570.
(15) Erga, O. SO_2 Recovery by a Sodium Citrate Solution Scrubbing. *Chem*. *Eng*. *Sci*. 1980, *35*, 162.
(16) Nissen, W.; Crocker, L.; Oden, L. Citrate Process for Flue Gas Desulfurization; United States. Bureau of Mine, Bulletin 686; U.S. Department of the Interior, Bureau of Mines: Washington, DC, 1986.
(17) Bekassy-Molnar, E.; Marki, E.; Majeed, J. Sulphur Dioxide Absorption in Air-Lift-Tube Absorbers by Sodium Citrate Buffer Solution. *Chem*. *Eng*. *Process* 2005, *44*, 1039.
(18) Olivier-Bourbigou, H.; Magna, L. Ionic liquids: perspectives for organic and catalytic reactions. *J*. *Mol*. *Catal*. *A*: *Chem*. 2002, *182* (1), 419-437.
(19) Sheldon, R. Catalytic reactions in ionic liquids. *Chem*. *Commun*. 2001, 2399-2407.
(20) Dupont, J.; de Souza, R. F.; Suarez, P. A. Z. Ionic Liquid (Molten Salt) Phase Organometallic Catalysis. *Chem*. *Rev*. 2002, *102*, 3667-3692.
(21) Earle, M. J.; Esperanca, J.; Gilea, M. A.; Lopes, J. N. C.; Rebelo, L. P. N.; Magee, J. W.; Seddon, K. R.; Widegren, J. A. The distillation and volatility of ionic liquids. *Nature* 2006, *439*, 831–834.
(22) Holbrey, J. D.; Rogers, R. D.; Mantz, R. A.; Trulove, P. C.; Cocalia, V. A.; Visser, A. E.; Anderson, J. L.; Anthony, J. L.; Brennecke, J. F.; Maginn, E. J.; Welton, T. Physicochemical properties. In *Ionic Liquids in Synthesis*, 2nd ed.; Wasserscheid, P., Welton, T., Eds.; Wiley-VCH: Weinheim, Germany, 2008.
(23) Bara, J. E.; Camper, D. E.; Gin, D. L.; Noble, R. D. Room-temperature ionic liquids and composite materials: Platform technologies for CO_2 capture. *Acc*. *Chem*. *Res*. 2010, *43*, 152–159.
(24) Bara, J. E.; Carlisle, T. K.; Gabriel, C. J.; Camper, D.; Finotello, A.; Gin, D. L.; Noble, R. D. Guide to CO_2 separations in imidazolium-based room-temperature ionic liquids. *Ind*. *Eng*. *Chem*. *Res*. 2009, 48, 2739–2751.
(25) Wu, W.; Han, B.; Gao, H.; Liu, Z.; Jiang, T.; Huang, J. Desulfurization of Flue Gas: SO_2 Absorption by an Ionic Liquid. *Angew*. *Chem*., Int. Ed. 2004, *43*, 2415.
(26) An, D.; Wu, L.; Li, B.-G.; Zhu, S. Synthesis and SO_2 Absorption/Desorption Properties of Poly(1,1,3,3-tetramethylguanidine Acrylate). *Macromolecules* 2007, *40*, 3388.
(27) Anderson, J. L.; JaNeille, K. D.; Maginn, E. J.; Brennecke, J. F. Measurement of SO_2 Solubility in Ionic Liquids. *Journ*. *Phys*. *Chem*. *B* 2006, *110*, 15059-15062.
(28) Hert, D. G.; Anderson, J. L; Aki, S.; Brennecke, J. F. Enhancement of oxygen and methane solubility in 1-hexyl-3-methylimidazolium bis(trifluoromethylsulfonyl) imide using carbon dioxide. *Chem*. *Commun*. 2005, 2603-2605.
(29) Shannon, M. S.; Bara. J. E. Properties of Alkylimidazoles as Solvents for CO_2Capture and Comparisons to Imidazolium-Based Ionic Liquids. *Industrial & Engineering Chemistry Research,* 2011, *50*, 8665-8677.
(30) Shannon, M.S.; Tedstone, J. M.; Danielsen, S. P. O.; Bara, J. E. Evaluation of Alkylimidazoles as Physical Solvents for CO_2/CH_4 Separation. *Industrial & Engineering Chemistry Research* 2012, *51*, 515–522.

(31) Shannon, M. S.; Hindman, M. S.; Danielsen, S. P. O.; Tedstone, J. M.; Gilmore, R. D.; Bara, J. E. Properties of Alkylbenzimidazoles for CO_2 and SO_2 Capture and Comparisons to Ionic Liquids. *Science China: Chemistry* 2012, *55*, 1638-1647.
(32) Shannon, M. S.; Tedstone, J. M.; Danielsen, S. P. O.; Hindman, M. S.; Bara, J. E. Properties and Performance of Ether-functionalized Imidazoles as Physical Solvents for CO_2 Separations. *Energy & Fuels* 2013, *27*, 3349-3357.
(33) Liu, H.; Bara, J. E.; Turner, C. H. DFT Study on the Effect of Exocyclic Substituents on the Proton Affinity of 1-Methylimidazole. *Chemical Physics* 2013, *416*, 21-25.
(34) Bara, J. E. Versatile and Scalable Method for Producing *N*-Functionalized Imidazoles. *Industrial & Engineering Chemistry Research*, 2011, *50*, 13614-13619.
(35) Shannon, M. S.; Bara, J. E. Reactive & Reversible Ionic Liquids for CO_2 Capture and Acid Gas Removal. *Separation Science & Technology* 2012, *47*, 178-188.
(36) Finotello, A.; Bara, J. E.; Camper, D.; Noble, R. D. Room-temperature ionic liquids: Temperature dependence of gas solubility selectivity. *Ind*. *Eng*. *Chem*. *Res*. 2008, *47*, 3453–3459.
(37) Yuan, X. L.; Zhang, S. J.; Liu, X. M. Hydroxyl Ammonium Ionic Liquids: Synthesis, Properties, and Solubility of SO_2. *J*. *Chem*. *Eng*. *Data* 2007, *52*, 596-599.
(38) Hasegawa, K.; Taka-aki, O.; Takumi, N. Vibrational Spectra and Ab Initio DFT Calculations of 4-Methylimidazole and Its Different Protonation Forms: Infrared and Raman Markers of the Protonation State of a Histidine Side Chain. *J*. *Phys*. *Chem*. *B* 2000, *104*, 4253-4265.
(39) Kinugasa, S.; Tanabe, K. Tamura, T. Spectral Database for Organic Compounds (SDBS) for IR Spectra. Tokyo, Japan: AIST, 2013. 13 Feb. 2014.
(40) Colthup, N. B. Spectra-Structure Correlations in the Infra-Red Region. *J*. *Opt*. *Sci*. *Am*. 1950, *40*, 397-400.
(41) Zhao, Y.; Truhlar, D. G. Density Functionals with Broad Applicability in Chemistry. *Acc*. *Chem*. *Res*. 2008, *41* (2), 157-167.
(42) Zhao, Y.; Truhlar, D. G. Density Functional for Spectroscopy: No Long-Range Self-Interaction Error, Good Performance for Rydberg and Charge-Transfer States, and Better Performance on Average than B3LYP for Ground States. *J*. *Phys*. *Chem*. *A* 2006, *110* (49), 13126-13130.
(43) Steudel, R.; Steudel, Y. Charge-Transfer Complexes between the Sulfur Molecules SO_2, S_2O, S_3, SONH, and $SOCl_2$ and the Amine Donors NH_3 and NMe_3 – A Theoretical Study. *Eur*. *J*. *Inorg*. *Chem*. 2007, *2007* (27), 4385-4392.
(44) Otten, H. Domagk and the development of the sulphonamides. *J. Antimicrob. Chemother.* 1986, *17* (6), 689–696
(45) Achilladelis, B. The dynamics of technological innovation: The sector of antibacterial medicines. *Research Policy* 1993, *22* (4), 279-308.
(46) Demain, A. L. The business of biotechnology. *Ind*. *Biotech*. 2007, *3*, 269-283.

8.6 Appendix: Supporting information is presented here for SO_2 solubility experiments and comparisons for *N*-functionalized imidazoles.

Table 8.6.1: Additional data and observations of SO_2 solubility in *N*-functionalized imidazoles.

Compounds	Equilibrated SO_2 Absorption Time (min)	Total Vacuum Time (hrs)	Color	Viscosity (cP)
1-methylimidazole	100	22.5	bright yellow	*solid
1,2-dimethylimidazole	35	-	white, powder	*solid
1-ethylimidazole	95	21.5	yellow	~1000
1-ethyl-2-methylimidazole	75	22.5	orange	*solid
1-ethyl-4-methylimidazole	95	21.5	yellow	*solid
1,2-diethyl-4-methylimidazole	75	21.9	burnt orange	*solid
1-propyl-2-methylimidazole	110	21.25	pale yellow, powder	*solid
PEG_1-imidazole	75	18	light green	*solid
PEG_1-4-methylimidazole	85	20	bronze	>1000
PEG_2-imidazole	60	20	green	<1000
PEG_2-4-methylimidazole	65	19	green	>1000

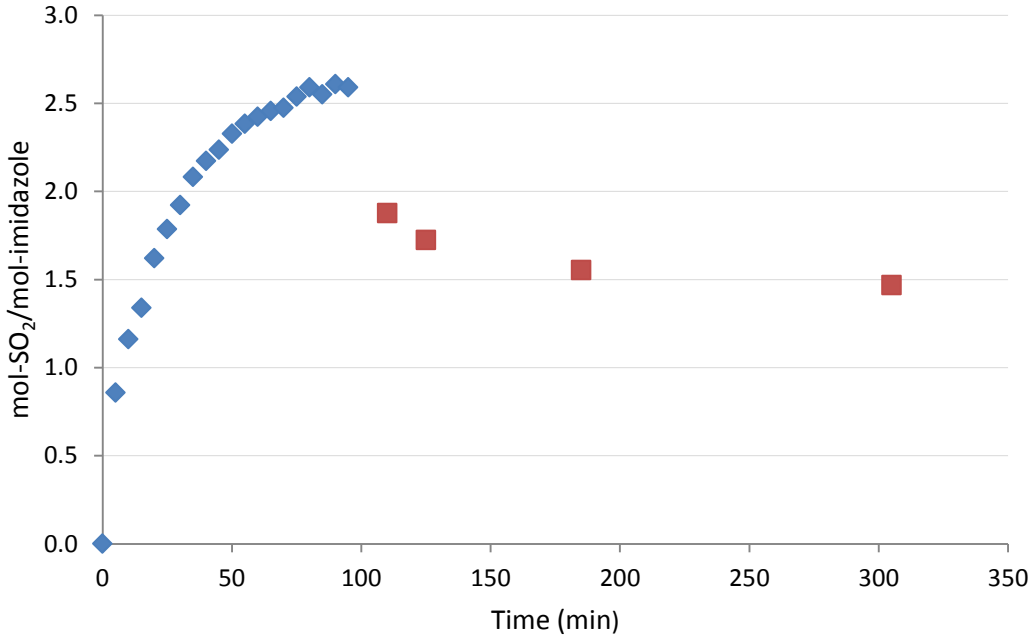

Figure 8.6.1: SO_2 absorption/desorption data for 1-ethylimidazole

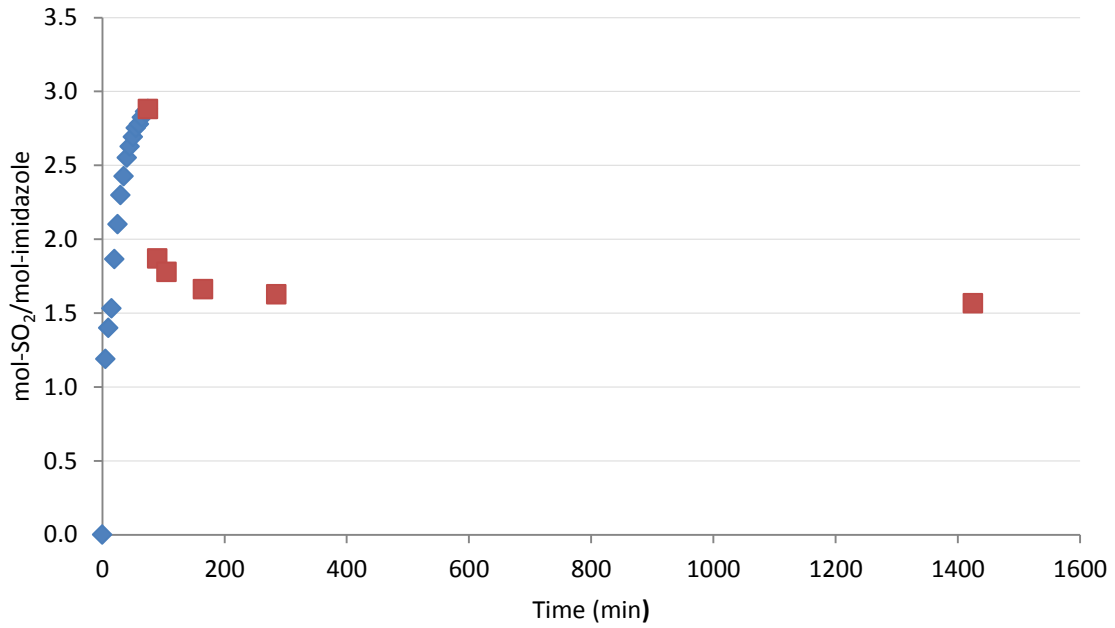

Figure 8.6.2: SO_2 absorption/desorption data for 1-ethyl-2-methylimidazole

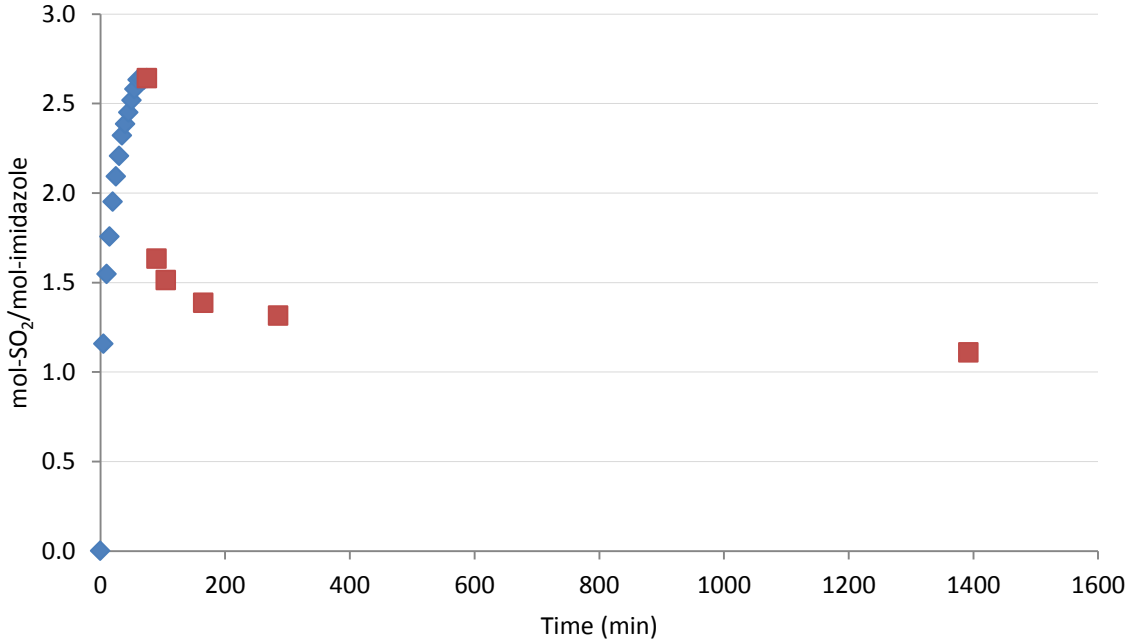

Figure 8.6.3: SO_2 absorption/desorption data for 1,2-diethyl-4-methylimidazole

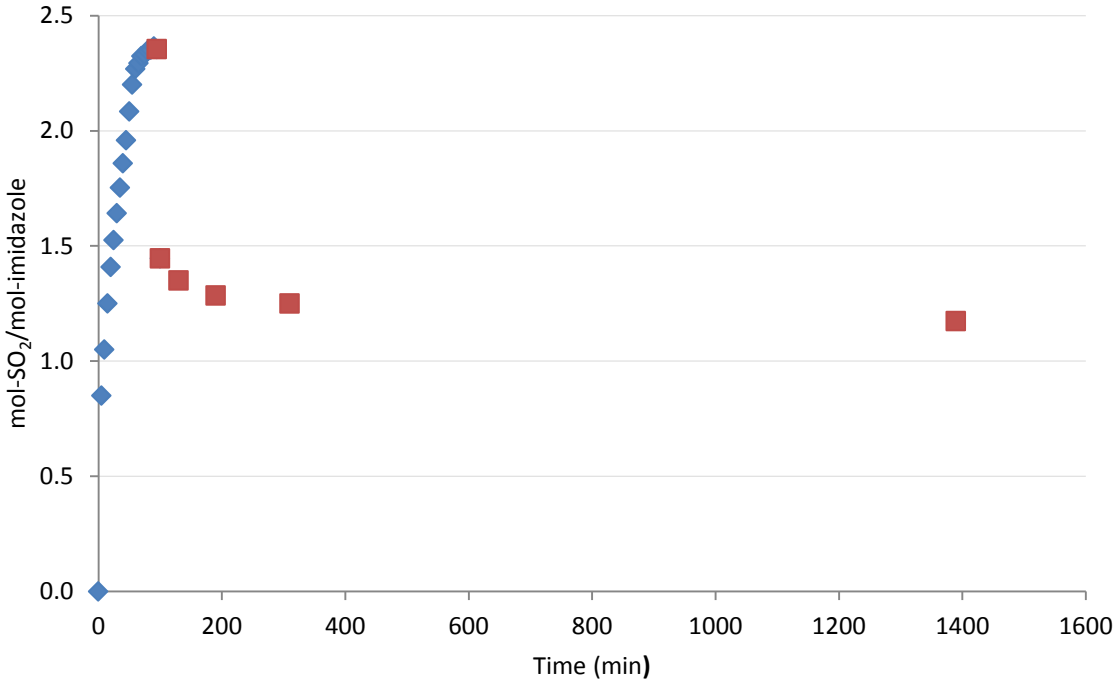

Figure 8.6.4: SO_2 absorption/desorption data for 1-ethyl-4-methylimidazole

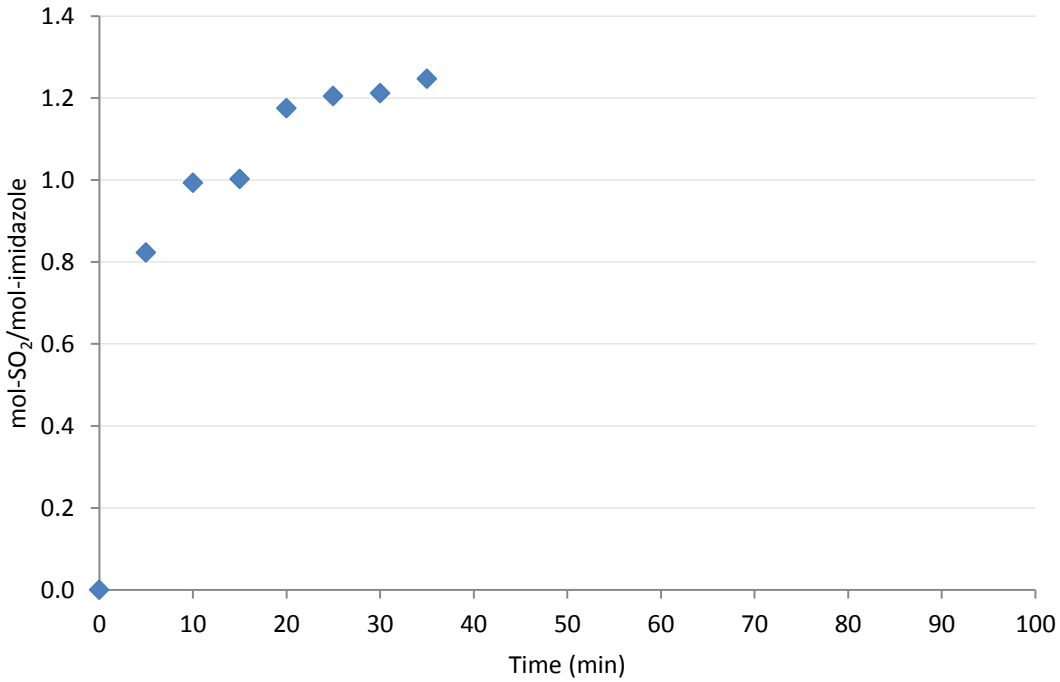

Figure 8.6.5: SO_2 absorption/desorption data for 1,2-dimethylimidazole

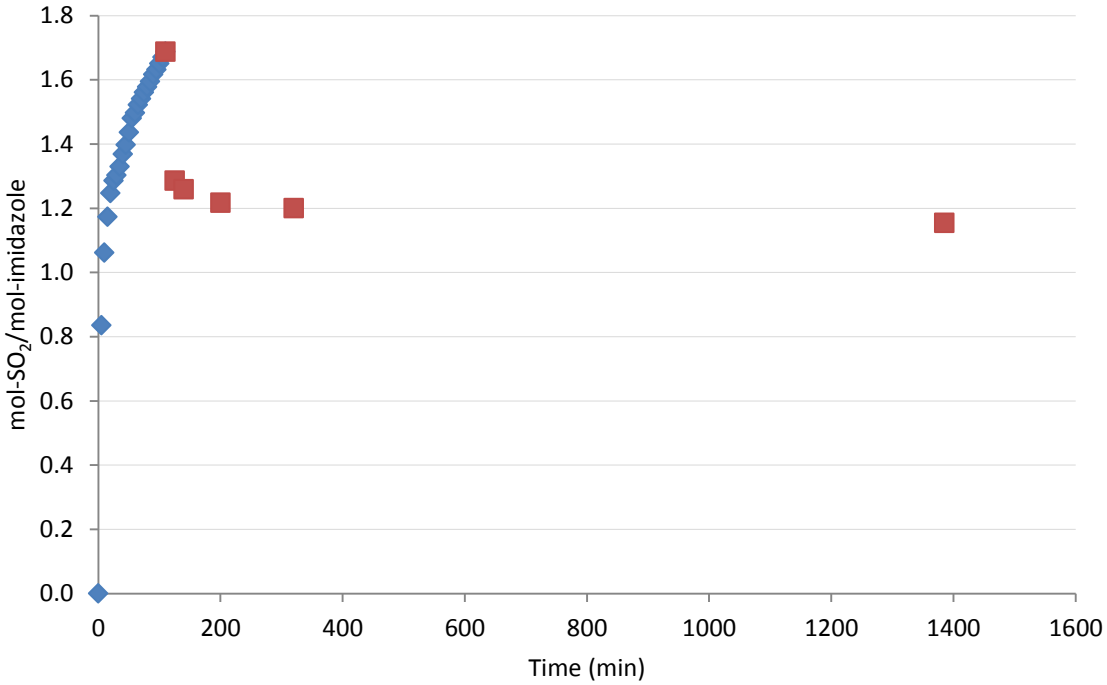

Figure 8.6.6: SO_2 absorption/desorption data for 1-propyl-2-methylimidazole

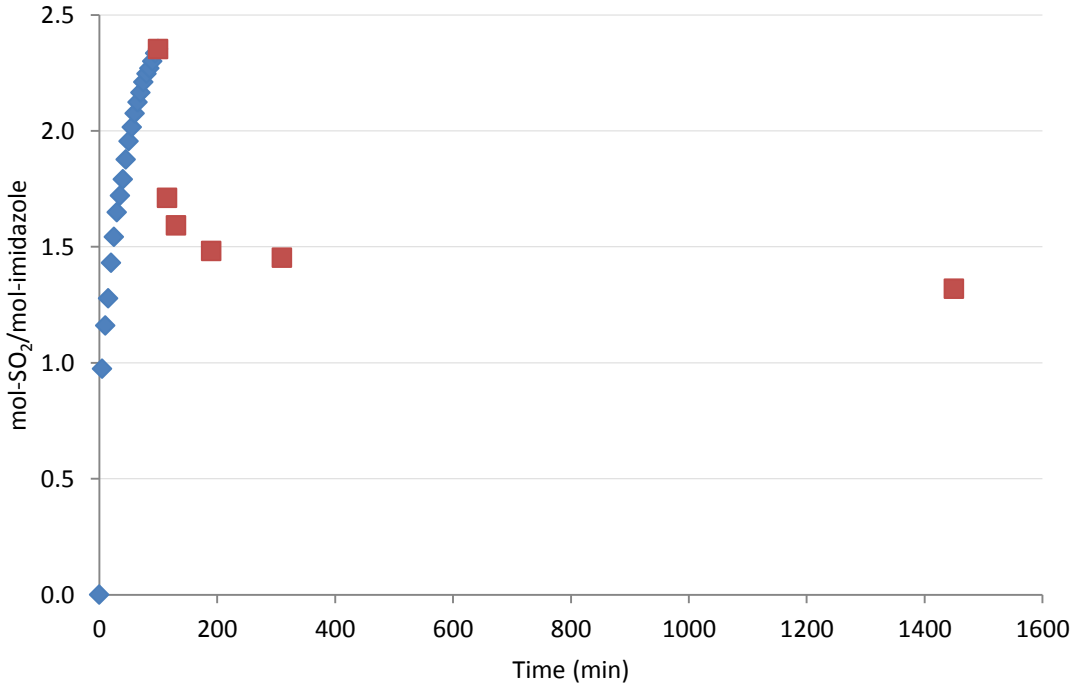

Figure 8.6.7: SO_2 absorption/desorption data for 1- methylimidazole

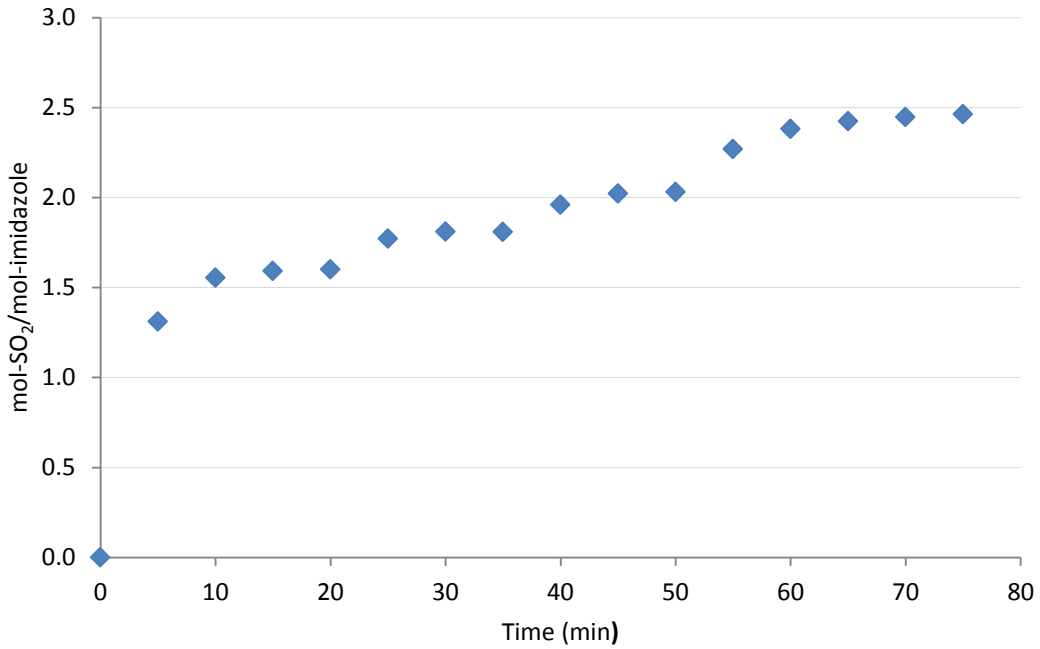

Figure 8.6.8: SO_2 absorption/desorption data for PEG_1-imidazole

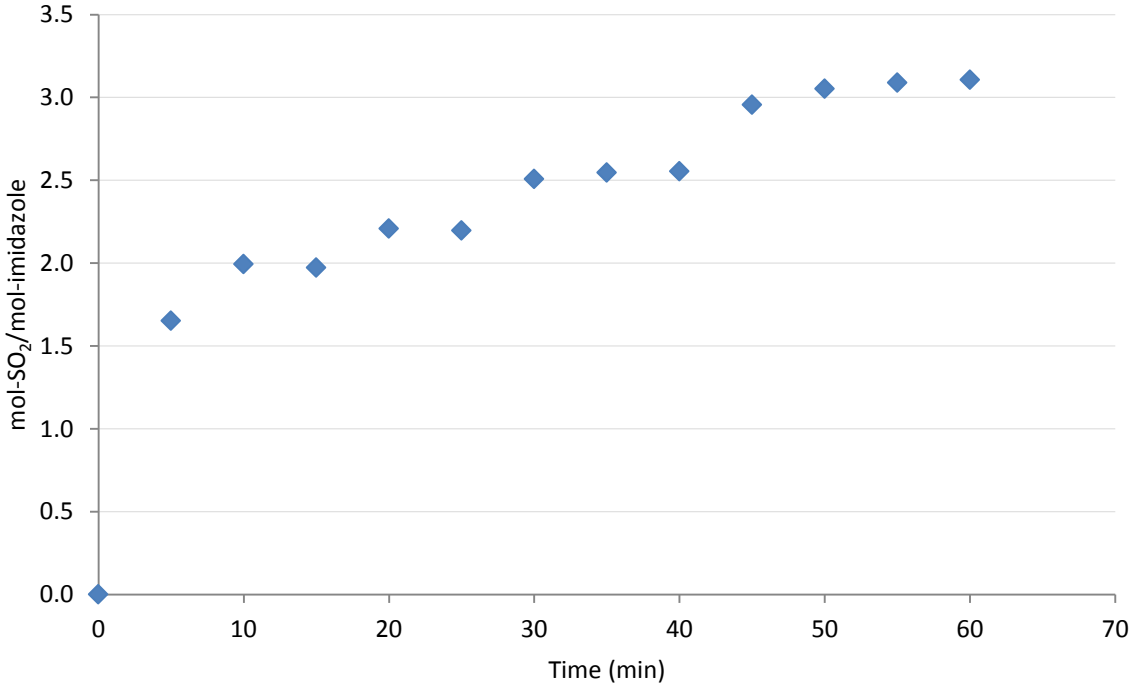

Figure 8.6.9: SO_2 absorption/desorption data for PEG_2-imidazole

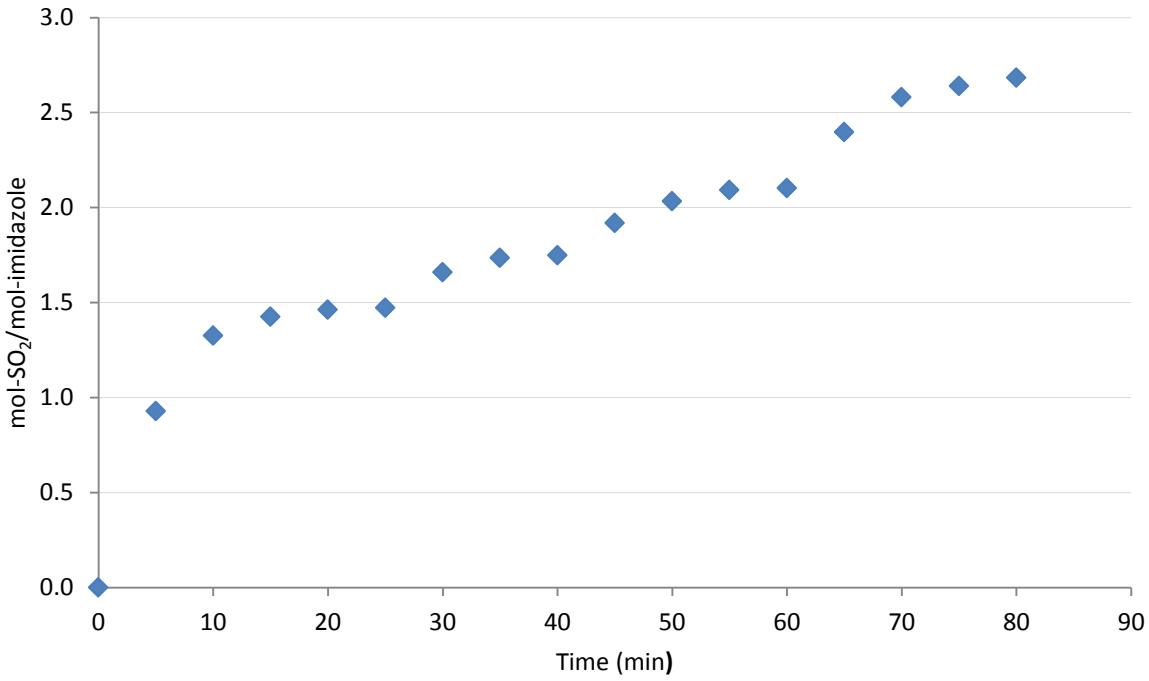

Figure 8.6.10: SO_2 absorption/desorption data for PEG_1-4-methylimidazole

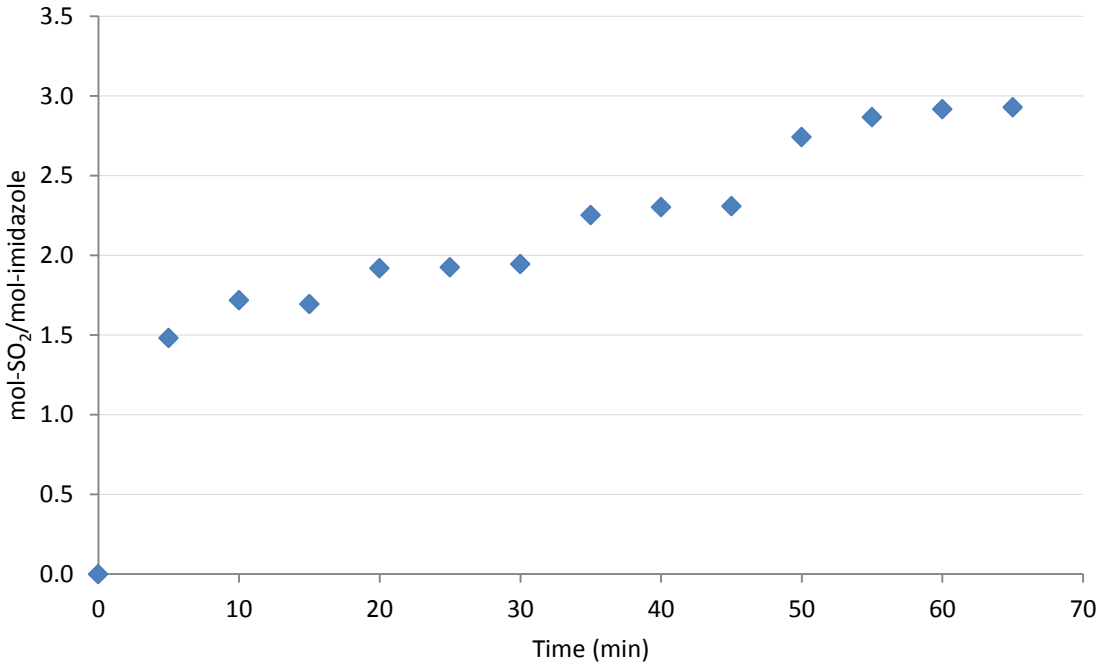

Figure 8.6.11: SO_2 absorption/desorption data for PEG_2-4-methylimidazole

Table 8.6.2: Calculated enthalpies of solution for *N*-functionalized imidazoles with SO_2.

Compound	ΔH_{Abs} (kJ/mol)
1-ethylimidazole	-5.42
1-ethyl-2-methylimidazole	-11.72
1,2-diethyl-4-methylimidazole	-12.33
PEG_1-imidazole	-11.18
PEG_1-4-methylimidazole	-16.34
PEG_2-imidazole	-8.25
PEG_2-4-methylimidazole	-11.71

**NOTE*: The error associated with calculated ΔH_{Abs} is 0.1%.

Sample Calculation of ΔH_{Abs} for PEG_2-imidazole

$$corrected, n_{SO2} = n_{SO2} - Imid.\ Init.\ Mole \quad => \quad \frac{1mol_{SO2}}{1mol_{imidazole}}$$

$$\Delta H_{Abs} = -(slope)(R) \qquad where\ R = 8.314 \frac{J}{mol\ K}$$

$$x_{SO2} = \frac{corrected,\ n_{SO2}}{corrected,\ n_{SO2} + 2(Imid.\ Init.\ Mole)}$$

$$\ln(x_{SO2}) \propto slope\left(-\frac{1}{T}\right)$$

$MW_{imidazole}$(g/mol)	170.21
MW_{SO2}(g/mol)	64.01

Imidazole Init. Wt. (g)	Imidazole Init. Mole (mol)	T(K)	$mass_{SO2}$ (g)	n_{SO2} (mol)	corrected,n_{SO2} (mol)
6.298	0.037	343	4.737	0.074	0.037
		328	5.249	0.082	0.045
		313	6.081	0.095	0.058
		298	7.361	0.115	0.078

x_{SO2}	$\ln(x_{SO2})$	1/T(K)	slope (K)	ΔH_{Abs} (J/mol)
0.332	-1.103	0.0029	992.35	-8250
0.377	-0.976	0.0030		
0.437	-0.827	0.0032		
0.513	-0.668	0.0034		

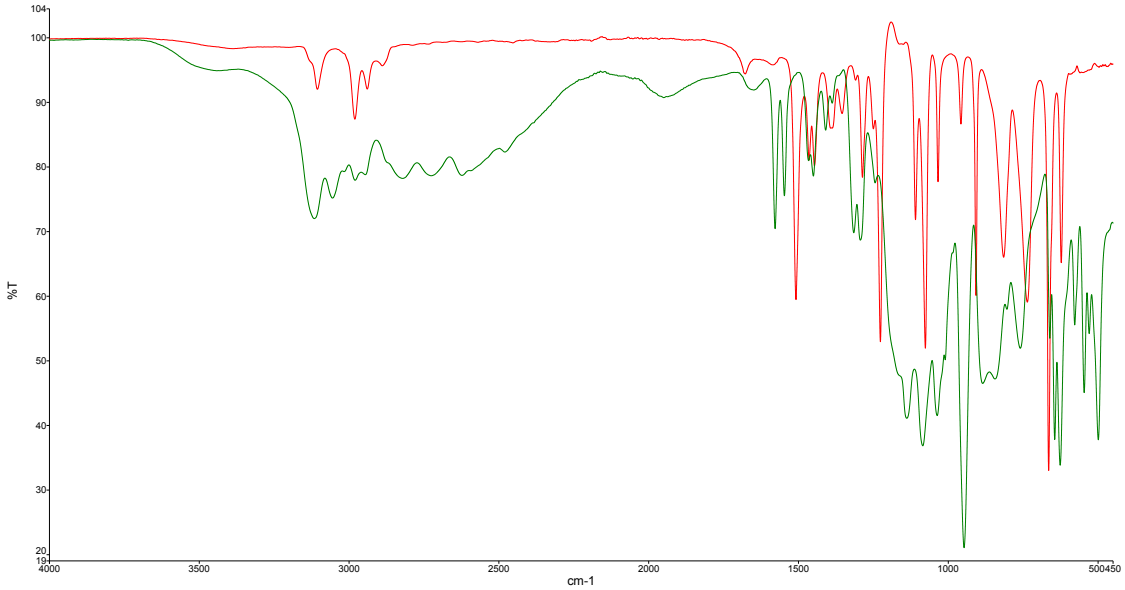

Figure 8.6.12: FTIR spectra for 1,2-diethyl-4-methylimidazole sample: neat (red) and SO_2-loaded (green).

Figure 8.6.13: FTIR spectra for 1,2-dimethylimidazole sample: neat (red) and SO_2-loaded (green).

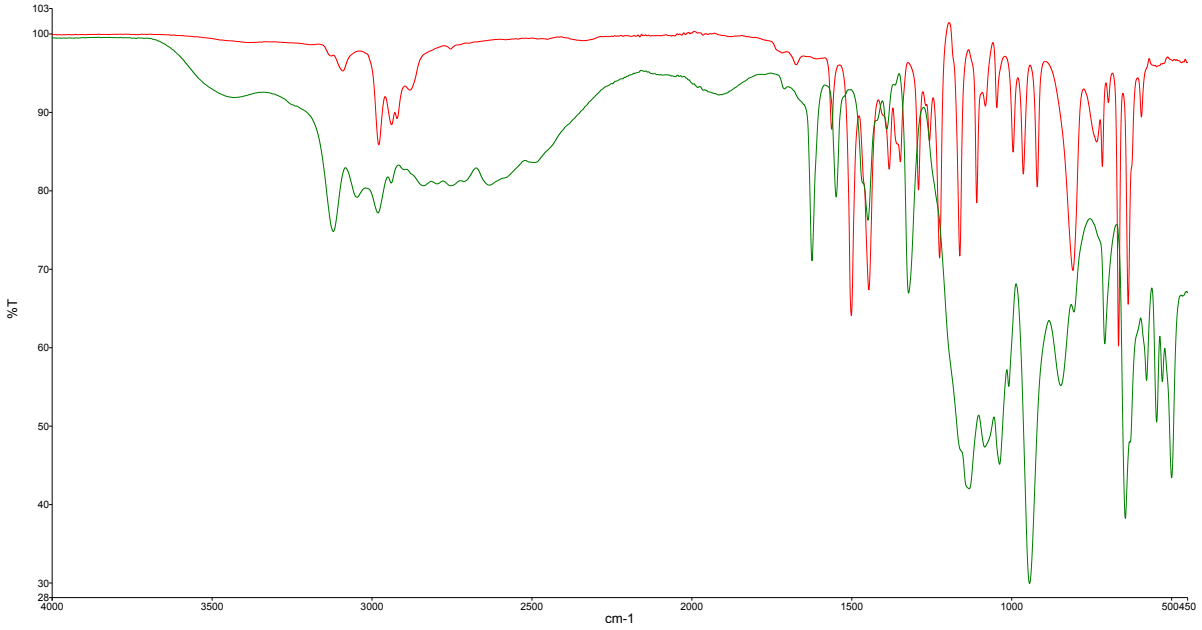

Figure 8.6.14: FTIR spectra for 1-propyl-2-methylimidazole sample: neat (red) and SO_2-loaded (green).

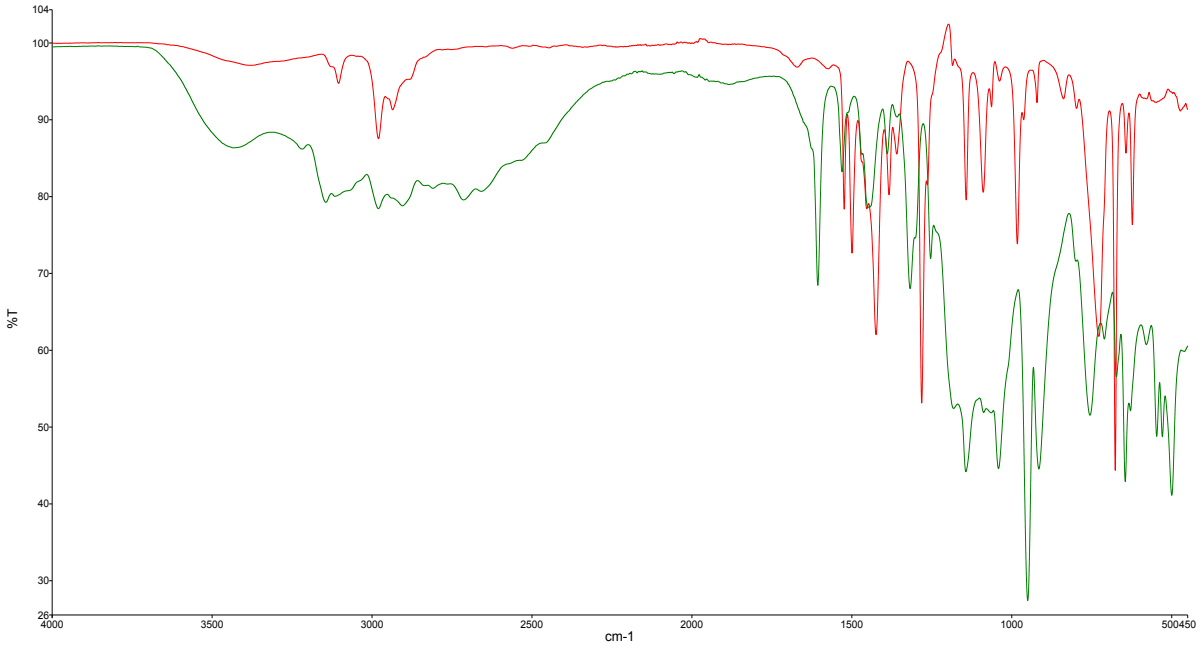

Figure 8.6.15: FTIR spectra for 1-ethyl-2-methylimidazole sample: neat (red) and SO_2-loaded (green).

Figure 8.6.16: FTIR spectra for 1-ethyl-4-methylimidazole sample: neat (red) and SO_2-loaded (green).

CHAPTER NINE

Imidazole-Based Polymeric Media and Novel Poly(ILs) for CO_2 Separation Applications

Matthew S. Shannon, W. Jeffrey Horne, John W. Whitley, Joshua D. Moon, Kristopher R. Reclusado, Michelle S. Hindman, Kelsey L. Terrill, Frank L. Foley, Jason E. Bara*

Department of Chemical & Biological Engineering

The University of Alabama, Tuscaloosa, AL USA 35487-0203

9.1 Introduction: The most prevalent technology utilized for industrial-scale CO_2 separations is chemical absorption, with aqueous amines being the most commonly used solvent for this application. Commercially-used aqueous amine solvents have been used for nearly a century for natural gas "sweetening", in which CO_2 contaminant is removed from raw CH_4 streams.[1-6] This technology and other absorption techniques have undergone extensive research in efforts to optimize the acid-base chemistry and improve the CO_2 affinity and physical properties of such solvents. However, even with aqueous amine technology being readily available and highly efficient at removing contaminant acid gases to low level specifications, these solvents are energy intensive mainly due to the high latent heat of water for solvent regeneration along with corrosion and volatility issue.[7] With more attention now on impacting CO_2 global emissions and greenhouse gas effects, novel chemical absorption technologies are being proposed to capture and mitigate CO_2 from industrial sources that burn fossil fuels. Coal-fired power plants are by far the largest source for CO_2 emissions, contributing to over half of the current greenhouse gas emissions world-wide. However, the scalability of chemical absorption is not practical or feasible for CO_2 capture from coal-fired power plants and such large sources of CO_2 emissions due to the vast flow rate to process and lack of a potential driving force (i.e. pressure differential). The average size of a power plant currently is ~600 MW, with a bulk flue gas flow rate of 500 m^3 s^{-1}, which correlates to approximately 460 tons of CO_2 per hour.[8] Also, flue gas emissions are at atmospheric pressure (CO_2 partial pressure, ~2 psia) implying that the process stream must be at least slightly compressed to increase the driving force for any type of novel separation technique.[9] For natural gas processing, gas streams are compressed to at least 100 psia and typically higher providing a sufficient driving force with CO_2 concentrations being around 30 v/v%.[10-12]

CO_2 separations via novel polymeric materials has gained recent consideration as an alternative approach for feasible post-combustion CO_2 capture, with commercially-available polymer membranes such as cellulose acetate modules being used in the natural gas industry since the late 1980s.[11,13] Currently, novel polyimide structures are replacing the latter technology as a more robust, CO_2 selective material.[14-18]

However, membrane separations are most feasible only for smaller-scale natural gas industries (<5 million standard cubic feet per day), where chemical absorption is currently utilized in large-scale processes being a more mature technology for gas separations.[8] Most of current membrane technologies suffer from low CO_2 permeability and selectivity for higher throughput of gas streams to be considered feasible for larger-scaled processes but can potentially offer a more energy efficient option with ongoing research as a fixed media for CO_2 capture.

Our current research incorporates and explores the concept of imidazole-based polymeric materials to enhance CO_2 uptake compared to commercially-available polymers that are currently used in industrial gas separations. We previously began exploring the concept of imidazole-based polymeric materials to enhance CO_2 uptake compared to commercially-available polymer materials that are currently. Most utilized polymeric materials for such gas separations are solution-diffusion based (Eqn. 1), implying the permeability or rate of transport of a gas species at a given pressure and volume will be affected and very dependent upon the material and gas (e.g. penetrant molecular kinetic diameter).

$$P = S \times D \tag{1}$$

Diffusivity typically governs gas permeability, except in the presence of polar gases/higher pressures, with solubility influencing the gas separation factor (i.e. selectivity).[19] Gas selectivity is impacted by molecular structures of polymers, including backbone stiffness and interchain spacing.[20] The presence of functional imidazole groups can increase the CO_2 separation performance via facilitated transport mechanism with water and the formation of bicarbonate. Characterization of these imidazole-based polymers includes gas solubility performance, water-inclusion solubility runs, DSC thermograms to obtain glass transition temperatures (T_g), FTIR analysis, and SEM imagery. Also, new strategies for designing CO_2 selective poly(ILs) are presented in this work, along with solvent swelling properties and enhanced photopolymerization via a coordinating pseudo IL mechanism. Ideal gas permeability and selectivity results for imidazole-based copolymers are discussed and compared to previously synthesized poly(IL) materials and gas separation performance in Section 9.2. Our recent research efforts focus with novel condensation polymerization and polyimide chemistry forming highly networked poly(ILs) for gas separations. This unique electrolyte-based polymer synthesis is discussed in detail in Section 9.3 along with projected research applications for CO_2 gas separations.

9.2 Novel imidazole-based polymeric materials for CO_2 separations: All imidazole and IL starting materials were synthesized and purified as detailed in our previous work.[21] Imidazole-styrene monomer synthesis is shown in Scheme 1, and 1-*n*-alkyl-3-methylimidazolium IL-styrene monomer synthesis is shown in Scheme 2, with both being reacted with *p*-chloromethylstyrene in solution at elevated temperatures. Each monomer underwent photopolymerization at 254 nm UV light in the presence of ~1 wt.% photoinitiator (i.e. 2-hydroxy-2-methylpropiophenone).

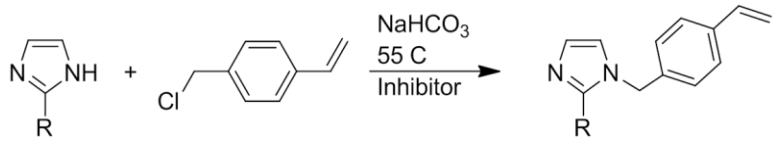

Scheme 1: 2-methylimidazolestyrene monomer synthesis

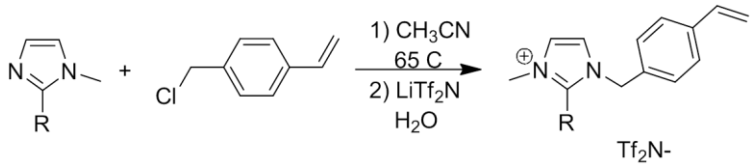

Scheme 2: 1-*n*-alkyl-3-methylimidazolium RTIL monomer synthesis

Commercially-available siloxane coating was applied to two 6-inch diameter quartz plates, making the surface hydrophobic to inhibit adhesion during membrane synthesis. Approximately 1-1.5 g of each monomer was placed on an oversized piece of porous nylon support material (Nylaflo™, 0.45 µm pore-size, porosity of 0.8) and placed between both quartz plates, followed by at least one hour of 254 nm UV polymerization. After curing, the quartz plates were carefully separated, and the thin-film supported polymer was peeled off and punched into a 47 mm diameter membrane for gas permeability experiments. Monomer synthesis and thin-film polymer membrane methodology along with ideal gas permeability measurements obtained via a time-lag apparatus are also noted in previous works.[22,23] Novel membranes need to be very thin (typically < 0.5 µm) and are processed as hollow fiber modules to maximize surface area and achieve high CO_2 throughput for industrial-scaled processes.[8,9] Based on current models, membranes with permeances (*P* in Barrers divided by membrane thickness in µm) surpassing 1000 gpu and CO_2/N_2 selectivities > 50 can present favorable economics for post-combustion CO_2 capture.[8]

Ideal gas permeability experiments were conducted at 3 atm for various concentrated copolymer membranes consisting of poly(ethylene glycol) methyl ether acrylate (M_n = 480, (PEG-MEA)) and 2-methylimidazolestyrene (2-MIS). PEG-MEA:2-MIS copolymer membrane concentrations (by wt%)

considered are as follows: 100-0, 90-10, 80-20, 70-30, and 50-50. Table 9.1 presents the permeability and selectivity data for each aforementioned copolymer concentration. PEG-based membranes composed of hydrophilic ethylene glycol repeat units range in CO_2 permeability (200-600 Barrers)

Table 9.1: Gas separation performance observed in PEG-MEA:2-MIS copolymer membranes.

Membrane	P_{CO2}	P_{N2}	P_{CH4}	$\alpha_{CO2/N2}$	$\alpha_{CO2/CH4}$
100% PEG	277 ± 1.5	3.9 ± 0.04	13.8 ± 0.21	70.2 ± 0.89	20.1 ± 0.32
90-10%	233 ± 10	8.6 ± 0.02	26.0 ± 1.3	27.1 ± 1.9	8.94 ± 0.58
80-20%	415 ± 23	88 ± 0.8	138 ± 3.5	4.70 ± 0.26	3.01 ± 0.18
70-30%	90.8 ± 3.4	8.1 ± 0.3	16.5 ± 0.11	11.2 ± 0.57	5.50 ± 0.21
50-50%	12.9 ± 0.24	0.18 ± 0.01	0.478 ± 0.01	73.6 ± 5.3	27.0 ± 2.0

Permeability (P) values are in reported in Barrers (10^{-10} cm^3(STP) cm/cm^2 s cmHg). Selectivity (α) values are defined as the ratio of P_{CO2} to P_j (light gas).

due to the vast difference in available chain length/molecular weights of PEG polymers (M_n can range from ~280 to ~500,000), with a CO_2/N_2 selectivity of ~50, thus, favoring the solubility of CO_2.[24-26] At the PEG-MEA:2-MIS concentration of 80-20%, gas permeability is observed to reach a maximum for both CO_2 (at least 50% higher) and N_2 (up to 3 orders of magnitude higher). Figure 9.1 shows the ideal gas selectivities and compares the separation performance at each copolymer concentration. Minima are observed for both CO_2/N_2 and CO_2/CH_4 selectivities at the 80-20% concentration due to the significant increase in gas permeability and throughput for all gases considered. Based on previous theory and calculations, we hypothesize the optimum PEG-MEA:2-MIS concentration to be between 70-30 to 80-20% due to PEG-MEA and 2-MIS approximately being at a 1-to-1 molar ratio. To increase the selectivity at this optimum concentration range, a facilitated transport mechanism can be utilized with the inclusion of water and low partial pressure CO_2, as observed in flue gas conditions. With PEG-MEA being hydrophilic by nature, water is strongly attracted to these tethered ether sites. As observed in our previous works with CO_2 solubility in imidazole solvents, the pyridine-like nitrogen N(3) site can interact and has a strong infinity for CO_2.

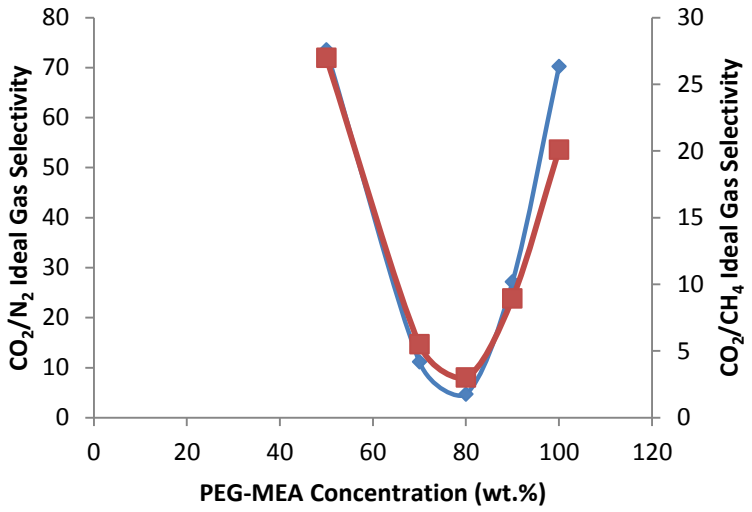

Figure 9.1: Ideal CO_2/N_2 (blue diamond) and CO_2/CH_4 (red square) Selectivities at Varying PEG-MEA:2-MIS Copolymer Concentration

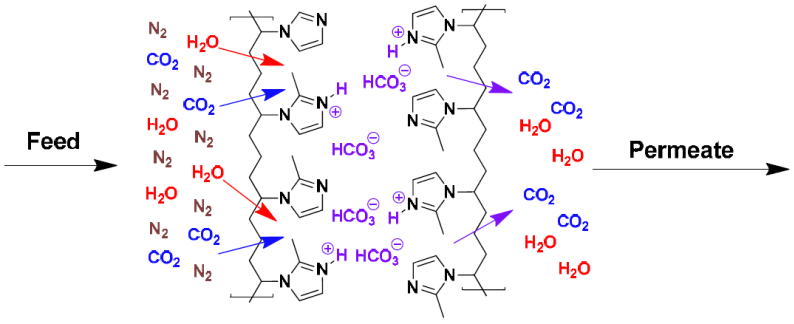

Figure 9.2: Mechanism for Facilitated Transport in Imidazole-Functionalized Membrane

Figure 9.2 displays how CO_2 is selectively transported through the polymer matrix via the formation of bicarbonate as reversible mechanism to the permeate side. The "hopping" mechanism selectively separates CO_2 from light gases and can then be dehydrated and processed for further use. However, at higher partial pressures, these sites can become saturated, thus, impeding this proposed mechanism. Due to complex copolymer morphology, the ideal and optimum concentration around 80-20% could be actually trapping gas in these sites yielding in overall high permeabilities for all tested gases (i.e. lowers selectivity). This implies that sub-atmospheric permeability experiments should be conducted to show if the results are affected and that the selectivity becomes more favorable at the proposed, optimum polymer concentration.

As compared to industrially-used amine-based materials, the interaction between CO_2 and the imidazole N(3) is weaker and more energetically favorable requiring only a minimal driving force (i.e.

pressure gradient). Primary (1°) and secondary (2°) amines can achieve high levels of CO_2 uptake (up to 0.5 mol CO_2/mol amine) even at the low partial pressures of CO_2 found in flue gas (~2 psia).[9] The reaction between CO_2 and amine is not readily-reversible at lower operating temperatures, primarily due to the inherent stability of the carbamate.[2,3] At elevated temperatures (>100°C) where the carbamate is reversible, diffusion of other light gases (e.g. N_2, CH_4) become much more rapid as the polymer becomes more rubbery, negating any effect of facilitated transport of CO_2. An alternative approach to increasing CO_2 solubility in polymer membranes is by using tertiary (3°) amines or other bases that do not form carbamates, but form of a bicarbonate (HCO_3^-) anion.[2,3] The reaction can be readily reversed at low to moderate temperatures and/or with mild vacuum conditions,[27] thus, being far more favorable for energy efficient CO_2 capture under post-combustion conditions.[9] However, the promoted bicarbonate mechanism under low CO_2 partial pressures can prove to be less efficient, with a lack of polymeric materials that possess only 3° amines or other basic groups in the appropriate pK_a range (~7.0-9.5). Typically, amines are also readily and irreversibly degraded by oxidizing agents such as O_2, SO_2 and NO_x, that are typically present in flue gas and rapidly diminish the lifetime of amine-based materials.[9]

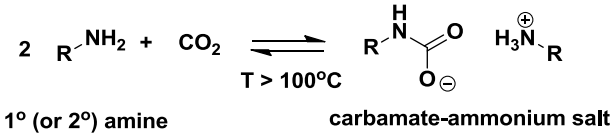

Scheme 3: Carbamate-ammonium salt formation.

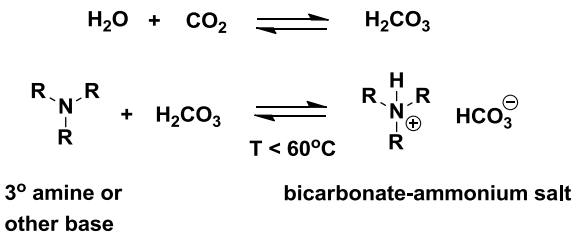

Scheme 4: Carbonic acid formation, with subsequent neutralization to form bicarbonate-ammonium salt.

We previously reported CO_2 solubility in a series of 1-*n*-alkylimidazoles (*n*=1-14), and in anhydrous conditions, these imidazole solvents exhibited physical CO_2 dissolution being comparable to other common organic solvents and ILs.[28] However, in the presence of a 1° or 2° amine, 1-*n*-alkylimidazoles were capable of acting as proton (H^+) acceptors, forming carbamate-imidazolium salts, as seen in Scheme 1.[1] Tomizaki et al.[27] showed that 1-methylimidazole and 1,2-dimethylimidazole in aqueous solutions form reversible bicarbonate-imidazolium salts in the presence of CO_2 (Scheme 3), with all CO_2 easily desorbed by applying vacuum and mild heating (70°C). The reported heat of reaction as observed for Scheme 3 for the formation

of bicarbonate-imidazolium salt is ~55 kJ mol^{-1}, as compared to the heat of reaction of the less reversible reaction of CO_2 with monoethanolamine (MEA) being ~85 kJ mol^{-1}.[27] This implies the feasibility of the presented bicarbonate mechanism for facilitated transport in imidazole-base polymers being readily reversible with minimal energy requirements. For example at 40°C and 2 psia, 1-methylimidazole (pK_a = 7.21) would exhibit lower loading (~0.15 mol CO_2/mol) but with a lower heat of reaction (~45 kJ/mol CO_2), while 1,2,4-trimethylimidazole (pK_a = 8.64) and 1,2,4,5-tetramethylimidazole (pK_a = 9.20) would be expected to be >> 0.40 mol CO_2/mol, but with increased heat of reaction (> 65 kJ/mol).[27] The pKa will essentially govern the rate of CO_2 uptake through the extent and heat of reaction for the bicarbonate mechanism. The addition of imidazole carrier sites could potentially increase the permeability to 4000-10000 Barrers with a selectivity for CO_2/N_2 of at least 50.

To validate the compatibility with water and increased CO_2 affinity, volumetric solubility experiments were performed with aqueous solutions of copolymers. Methodology of CO_2 solubility runs were similar to as detailed in our previous work. With all copolymers considered being mainly comprised of PEG-MEA, all samples favored the aqueous phase and formed uniform mixtures in solution. For each run, 50 mL of deionized water (47.7 g) was used, initially for a tare CO_2 solubility measurement and then with each subsequent run.

Table 9.2: CO_2 solubility in aqueous-copolymer solutions.

Comp.	CO_2 mass in solution (g)	CO_2 mass increase (g)	Polymer mass (g)	$mass_{CO2}/mass_{polymer}$	$mass_{CO2}/mass_{imidazole}$	$mol_{CO2}/mol_{imidazole}$
Water	0.15	-	-	-	-	-
100-0	0.16	0.01	1.500	0.009	-	-
90-10	0.16	0.01	1.448	0.005	0.055	0.249
80-20	0.17	0.03	0.507	0.049	0.247	1.111

**NOTE*: Error in masses is +/- 0.001 g

As seen from Table 9.2 and based on the CO_2 solubility in neat water, a significant increase in CO_2 uptake is observed in the 80-20% concentration. This ratio of PEG-MEA to 2-MIS again correlates to 1:1 mol-to-mol and is most optimal for the proposed facilitated transport mechanism via bicarbonate formation. No significant amount of CO_2 uptake was noted in 100-0% (pure PEG-MEA) or 90-10%, even with approximately 3X more polymer material by mass in solution compared to that for 80-20%. With the polar ether sites of PEG-MEA and the reversibly-reactive N(3) site of the imidazole ring, the facilitated bicarbonate reaction is

favored in the presence of water. For post-combustion CO_2 capture conditions, the average molar ratio of CO_2 to H_2O is 1 mol-CO_2 to 1 mol-H_2O, implying the feasibility of this proposed facilitated transport mechanism via novel copolymers.

FTIR analysis was employed to determine the degree of polymerization (D.P.) of the synthesized monomers. Table 9.3 shows respective IR absorption spectra of initial monomer and polymer samples for both neat 2-MIS and PEG-MEA. For determining the degree of polymerization in photopolymers, both monomer and polymer samples must be measured for distinct peaks (presence/disappearance of vinyl group and bulk reference group) and compared as shown in Eqn. 2 as a ratio of the disappearance of the reacting vinyl group to the reference group. Both neat 2-MIS and PEG-MEA reach nearly complete conversion.

$$D.P. = 1 - \frac{\left(\frac{A_{poly}}{A_{mono}}\right)_{vinyl}}{\left(\frac{A_{poly}}{A_{mono}}\right)_{reference}} \quad (2)$$

Table 9.3: FTIR spectra analysis for degree of polymerization (D.P.)

2-MethylImidazoleStyrene						
Monomer			Polymer			Degree of
Peak Id.	Wave number	Area	Peak Id.	Wave number	Area	Polymerization
Vinyl	909.65	821.74	Vinyl	909.65	66.9	97.0%
Styrene	3002.74	1484.86	Styrene	2924.74	3982.25	
Poly(ethylene glycol) methyl ether acrylate						
Monomer			Polymer			Degree of
Peak Id.	Wave number	Area	Peak Id.	Wave number	Area	Polymerization
Acrylate	809.10	155.14	Acrylate	809.1	6.41	98.3%
Carbonyl	1726.36	812.71	Carbonyl	1726.36	1934.60	

Glass transition temperature (T_g) is another applicable polymer property that defines the transition of amorphous materials from a brittle-like, glassy state to more that of a rubber. The plot below in Figure 9.3 shows the relative heating curves for the copolymers 100-0% and 90-10%. The T_g values for both concentrations are -15.33^{o}C and -11.36^{o}C, respectively.

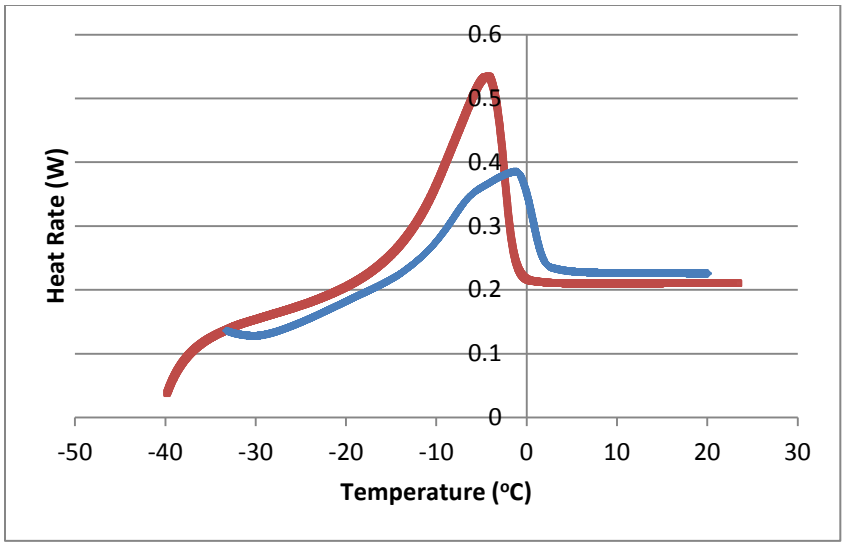

Figure 9.3: DSC thermograms of 100-0% (red) and 90-0% (blue)

This implies that the 100% PEG-MEA polymer is more rubbery than the imidazole-comprised copolymers, which become glassier as the imidazole concentration increases.

Scanning electron microscopy (SEM) was performed on all experimented membrane samples, including the standard nylon support, to determine the approximate thickness and topography. The measured thickness ranged from 74.1 µm for the nylon support up to 125 µm for the 100% PEG-MEA membrane. This implies the polymerized material absorbed into the support as well as deposited a measureable thin film throughout the nylon support.

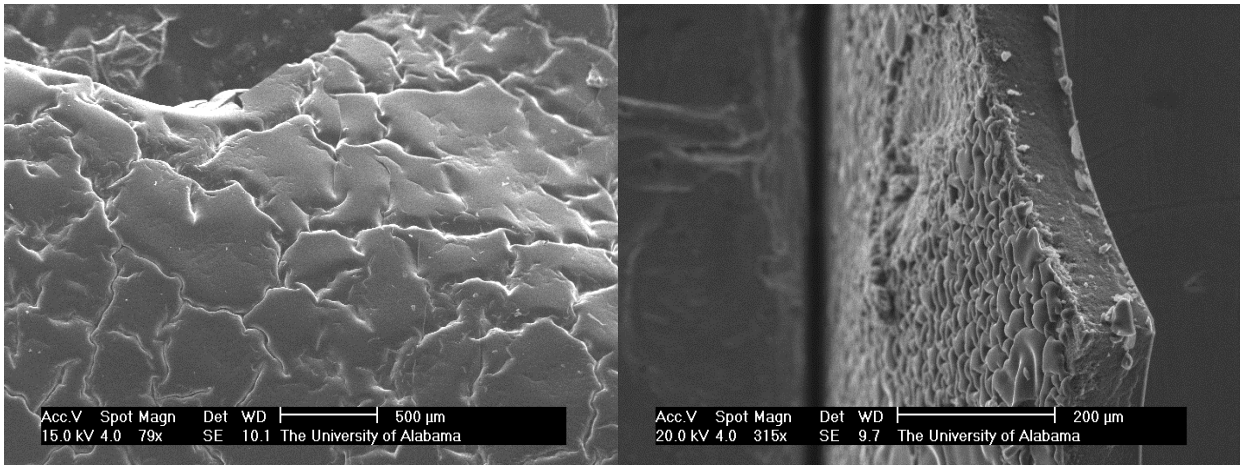

Figure 9.4: SEM Images of PEG-MEA:2-MIS Copolymers

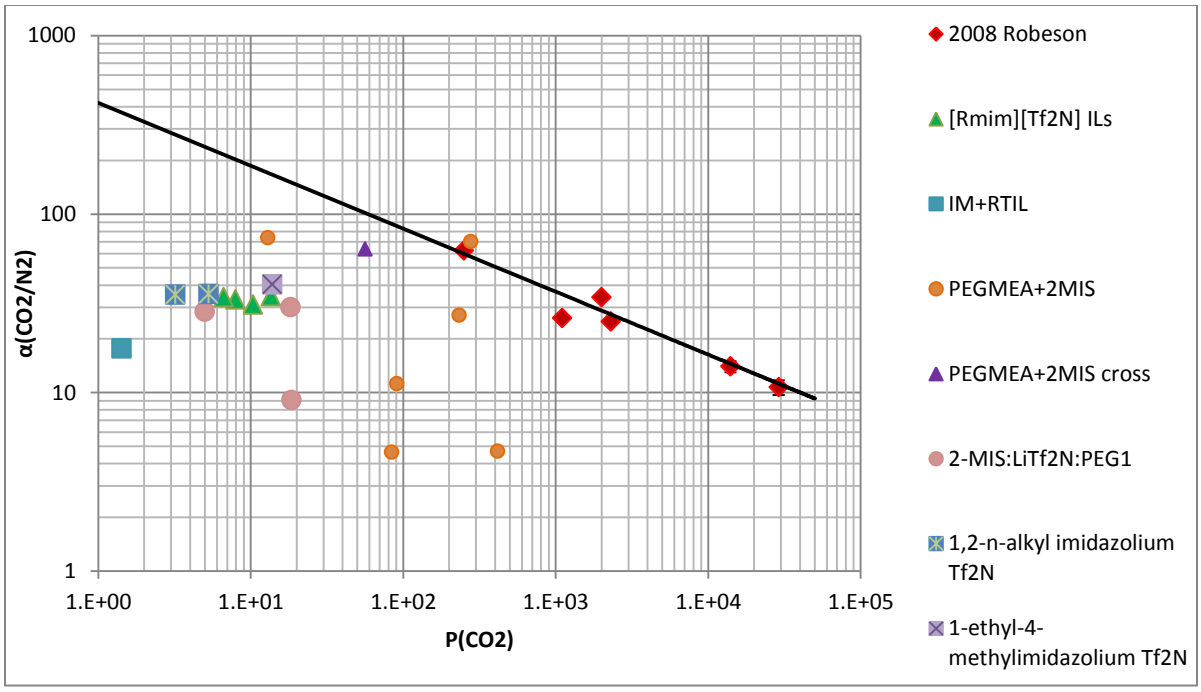

Figure 9.5: Upper bound trade-off plot for comparisons in CO_2/N_2 separation performance

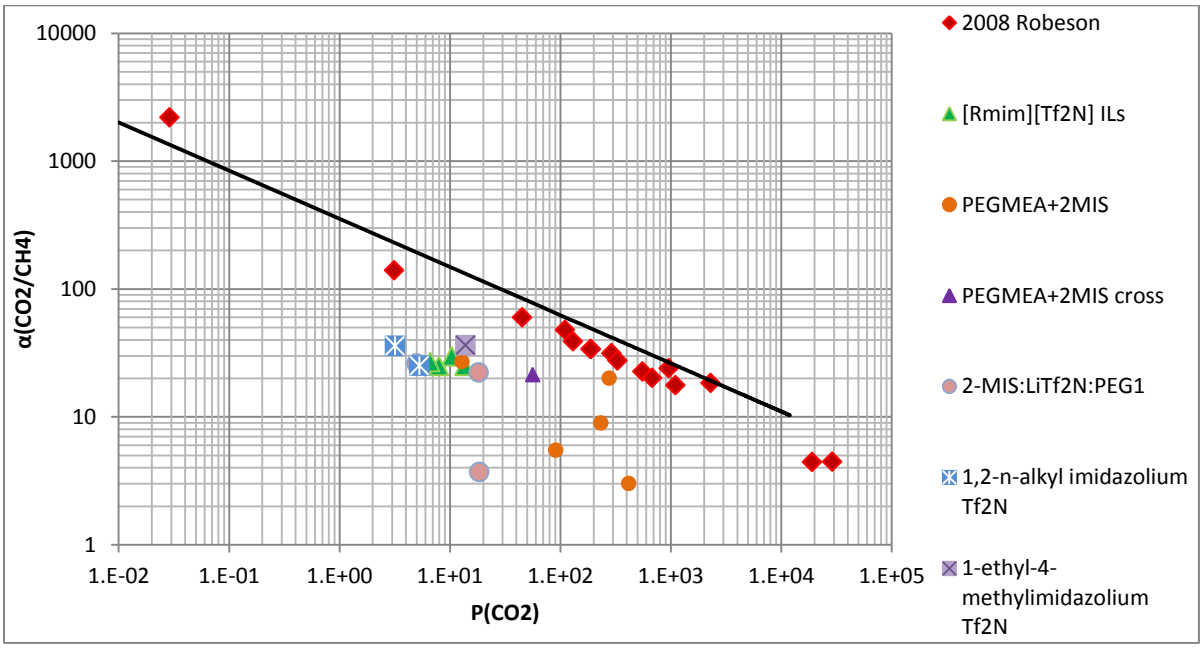

Figure 9.6: Upper bound trade-off plot for comparisons in CO_2/CH_4 separation performance

Comparisons of constantly-improving gas separation performance in novel polymeric materials is observed in upper bound plots, relating gas selectivity to penetrant permeability.[29] An inverse relationship between gas selectivity and permeability was first introduced by Robeson[19] implying a "trade-off" exists in

gas separation performance. Improvements in membrane technology continue to shift the upper bound, with thermally-rearranged (TR) polymers and fluorocarbon-base materials leading the forefront of CO_2 separations based on molecular sieving effects that are governed by size exclusion of gas molecules.[29] Figures 9.5 and 9.6 display the CO_2/N_2 and CO_2/CH_4 gas separation performance of various imidazole- and IL-based polymers compared to the current upper bound, respectively. The slope of the upper bound can be correlated to the difference in gas penetrant kinetic diameters[29], with this slope being independent to temperature implying more favorable gas selectivity at lower operating temperatures.[30]

Most of these novel polymers we studied as shown in Figures 9.5 and 9.6 tend to approach the upper bound, with 100-0% PEG-MEA essentially lying on the upperbound. Imidazole-based materials tend to exhibit higher permeabiliteis yet lower selectivities when compared to that of presented IL-base polymers. However, imidazole-based polymers consisting 2-MIS, $LiTf_2N$, and mobile PEG_1-imidazole approach that of poly(IL) gas separation performance. This is due to the adverse effect of imidazole-based polymer in the presence of $LiTf_2N$ forming a more structured (i.e. crystalline-like) and glassier material that inherently decreases the gas permeability (i.e. CO_2 solubility) yet increasing in selectivity. The effects of crosslinking PEG-MEA:2-MIS copolymers also exhibits a similar effect by decreasing the CO_2 permeability by an order of magnitude but increasing in selectivity by an order of magnitude. Overall, the premise for the proposed and continuous research employing imidazole-based polymers for CO_2 separations is based on the hypothesis of the advantageous facilitated transport via the bicarbonate mechanism in the presence of water, as in post-combustion flue gas conditions.

9.3 Electrolyte-based polymers utilizing diimide chemistry for CO_2 capture: Polyimides are a class of stable polymers based on condensation chemistry formed by di-functional monomers, with the polymers possessing stiff aromatic backbones. Synthesis of polyimides consists of reacting a dianhydride with a diamine typically in a dipolar aprotic solvent.[31] Their industrial applications include electronics, natural gas "sweetening", medical tubing, semiconductors, fuel cells, etc. For the area of novel gas separations, polyimides were introduced to the natural gas industry for CO_2 separations during the 1990s[8,11,12] and have been at the forefront of current research efforts in optimizing the polyimide structures for higher gas uptake and selectivity. Koros et al.[15] compared gas separation performances of polyimide, polycarbonate, and polypyrrolone families (Figure 9.7). Families of the 6-FDA (hexafluoropropane dianhydride) polyimide materials were shown to outperform various polycarbonates (PC) in respect to CO_2/CH_4 selectivity. The increase in CO_2 uptake in polyimides is primarily due to the increase in solubility. Also, CO_2 interactions are higher in the presence of carbonyl groups, as observed in higher CO_2 solubility in polyimides compared to

polypyrrolones. This observation can also be correlated to the molecular structure of polyimides resulting in heterogeneous packing and irregular domains formed, thus, exhibiting size/shape exclusion towards target gas penetrants (e.g. CO_2). The long, flat, and rigid chain segments of polyimides inhibit packing and decrease CO_2 plasticization effects at elevated pressures.

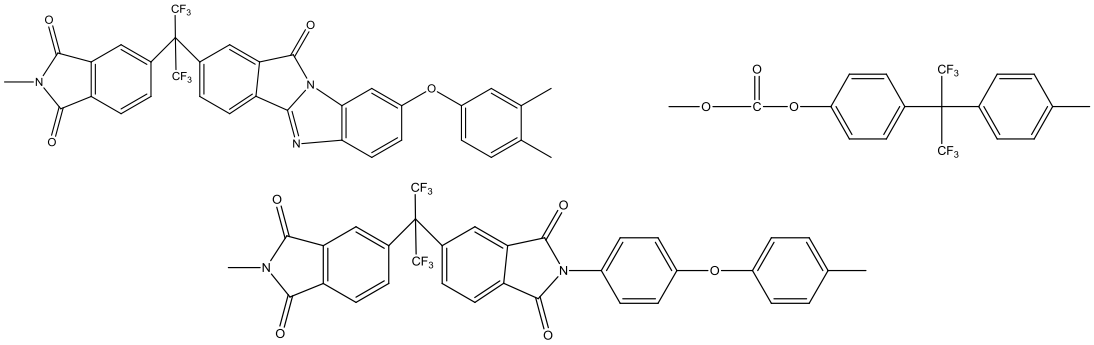

Figure 9.7: Basic structures of polypyrrolone (6FDA-TADPO), polycarbonate (HFPC), and polyimide (6FDA-ODA), respectfully.

Our ongoing work and research with novel polymer structures for CO_2 capture applications will investigate the characteristics and performance of polyimide-based materials functionalized as poly(ILs). Scheme 5 details the chemistry involved for the synthesis of the pyridine-based diimide, as detailed in previous works by Dinolfo et al.[33] Scheme 6 shows the novel synthesis of these poly(ILs) forming a pyridinium-based material reacting with a dihalide-containing compound. A similar premise to the synthesis of poly(ILs) with a polyimide-based backbone has only been recently noted by Imaizumi et al.[32] work with printable polymer acutators using these polymers as novel electrode materials for fuel cell research. Sulfonated polyimides (SPIs) were reacted with 1-ethyl-3-methylimidazolium bis(trifluoromethanesulfonyl) amide [C_2mim][Tf_2N] and bis[4-(3-aminophenoxy)phenyl] sulfone to form a networked poly(IL) copolymer material. These electroactive polymers (EAPs) possess unique thermophysical properties as seen in ILs, including low volatility, high electrochemical stability, and high ionic conductivity. SPI-ILs make for strong films due to rigid, aromatic backbone as seen in polyimides.

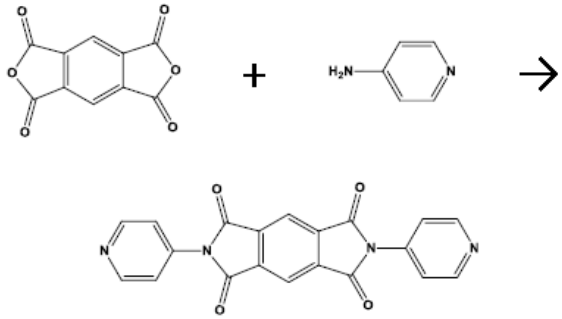

Scheme 5: Formation of N,N'-di-(4-pyridyl)-1,2,4,5-benzenetetracarboxydiimide via reacting pyromellitic dianhydride and 4-aminopyridine in aprotic solvent, as according to Ref (33).

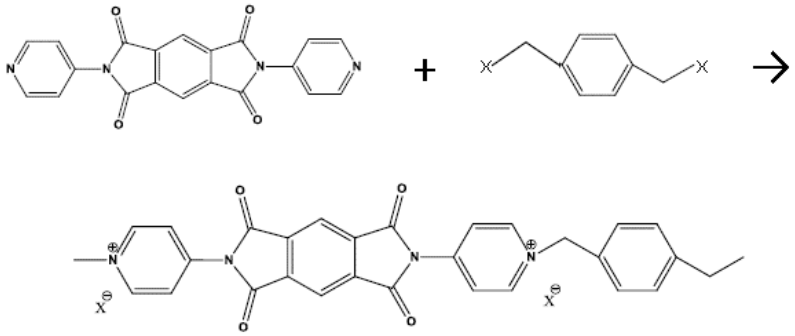

Scheme 6: Pyridinium-based poly(IL) reaction.

This study will include successful synthesis of precursors and diimide monomers to form novel poly(ILs). Thin-film membranes will result from polymer-solvent casting techniques in order to obtain ideal gas permeability data for CO_2 and light gases (e.g. N_2, CH_4). Similar polymer synthesis steps and experimental methodology is explained in detail in previous works.[23] Also, as acquired for aforementioned imidazole-base polymers, characterization of these novel poly(ILs) will include SEM imagery and DSC thermography. T_g is a good indication of FFV effects, with higher T_g materials exhibiting more restrictions in chain mobility.[16] Variations of the bridged structure of the symmetric diimide molecule will be explored for optimization in polymeric material properties and the effects on ideal gas separations.

9.4 Conclusions: Given the numerous imidazole-based homopolymers, co-polymers, and electrolyte-based poly(IL) materials that can be synthesized and tested as potential membranes for CO_2 uptake and separations, fundamental understandings of these novel materials must be developed, empirically and at a molecular level. Functionalized imidazole-based polymers are driven by the hypothesis of the bicarbonate mechanism presented as a form CO_2 facilitated transport, with experimental pK_a of each material being

correlated to the efficiency and performance of CO_2 uptake. Also, molecular-level computations will allow underlying polymer microstructures and local reactivity to be uncovered to validate and model trends in these properties governing CO_2 separation. With polyimides being a diverse polymeric material used for several applications and having high thermal stability and significant tensile strength, the premise of novel polyimide-based electrolytic polymers warrant further investigation for gas separation properties.

9.5 References:

(1) Rochelle, G. T. Amine Scrubbing for CO_2 Capture. *Science* 2009, 325, 1652-1654.
(2) Astarita, G.; Savage, D. W.; Bisio, A. *Gas Treating with Chemical Solvents*. John Wiley & Sons: New York, 1983.
(3) Kidnay, A. J.; Parrish, W. R. *Fundamentals of Natural Gas Processing*. CRC Press: Taylor & Francis Group: Boca Raton, FL, 2006.
(4) Teng, T. T.; Maham, Y.; Hepler, L. G.; Mather, A. E. Viscosity of Aqueous-solutions of N-Methyldiethanolamine and of Diethanolamine. *J. Chem. Eng. Data* 1994, *39*, 290-293.
(5) Jou, F. Y.; Mather, A. E.; Otto, F. D. The solubility of CO_2 in a 30-Mass-Percent Monoethanolamine Solution. *Can J. Chem. Eng.* 1995, *73*, 140-147.
(6) Vrachnos, A.; Kontogeorgis, G.; Voutsas, E. Thermodynamic modeling of acidic gas solubility in aqueous solutions of MEA, MDEA and MEA-MDEA blends. *Ind. Eng. Chem. Res.* 2006, *45*, 5148-5154.
(7) NETL DOE/NETL Advanced Carbon Dioxide Capture R&D Program: Technology Update 9/2010. www.netl.doe.gov/technologies/coalpower/ewr/pubs/CO2%20Capture%20Tech%20Update%20Final.pdf (Accessed 1 February 2014)
(8) Merkel, T. C.; Lin, H. Q.; Wei, X. T.; Baker, R., Power plant post-combustion carbon dioxide capture: An opportunity for membranes. *Journal of Membrane Science* 2010, *359* (1-2), 126-139.
(9) NETL DOE/NETL Advanced Carbon Dioxide Capture R&D Program: Technology Update May 2011. http://www.netl.doe.gov/technologies/coalpower/ewr/pubs/CO2CaptureTechUpdate051711.pdf (accessed 10 February 2014).
(10) Bernardo, P.; Drioli, E.; Golemme, G., Membrane Gas Separation: A Review/State of the Art. *Industrial & Engineering Chemistry Research* 2009, *48* (10), 4638-4663.
(11) Baker, R. W., Future Directions of Membrane Gas Separation Technology. *Industrial & Engineering Chemistry Research* 2002, *41* (6), 1393-1411.
(12) Baker, R. W.; Lokhandwala, K., Natural Gas Processing with Membranes: An Overview. *Industrial & Engineering Chemistry Research* 2008, *47* (7), 2109-2121.
(13) Spillman, R. W., ECONOMICS OF GAS SEPARATION MEMBRANES. *Chemical Engineering Progress* 1989, *85* (1), 41-62.
(14) Favre, E., Carbon dioxide recovery from post-combustion processes: Can gas permeation membranes compete with absorption? *Journal of Membrane Science* 2007, *294* (1-2), 50-59.
(15) Koros, W. J.; Walker, D. R. B. Gas Separation Membrane Material Selection Criteria: Weakly and Strongly Interacting Feed Component Situations. *Poly. Journ*. 1991, *23* (5), 481-490.
(16) Bickel, C. S.; Koros, W. J. Improvement of CO2/CH4 separation characteristics of polyimides by chemical crosslinking. *Journal of Membrane Science* 1999, *155*, 145-154.
(17) Hirose, T.; Mi, Y.; Stern, S. A. The solubility of carbon-dioxide and methane in polyimides at elevated pressures. *Journal of Polymer Science Part B: Polymer Physics* 1991, *29* (3), 341-347.
(18) Coleman, M. R.; Koros, W. J. Isomeric polyimides based on fluorinated dianhydrides and diamines for gas separation applications. *Journal of Membrane Science* 1990, *50*, 285-297.

(19) Robeson, L. M. Correlation of separation factor versus permeability for polymeric membranes. *Journal of Membrane Science* 1991, *62*, 165-185.
(20) Freeman, B. D. Basis of Permeability/Selectivity Tradeoff Relations in Polymeric Gas Separation Membranes. *Macromolecules* 1999, *32*, 375-380.
(21) Bara, J. E. Versatile and Scalable Method for Producing *N*-Functionalized Imidazoles. *Industrial & Engineering Chemistry Research*, 2011, *50*, 13614-13619.
(22) Bara, J. E.; Lessmann, S.; Gabriel, C. J.; Hatekeyama, E. S.; Noble, R.D.; Gin, D. L. Synthesis and Performance of Polymerizable Room Temperature Ionic Liquid Gas Separation Membranes. *Industrial & Engineering Chemistry Research*, 2007, *46*, 5397-5404.
(23) Carlisle, T. K.; Bara, J. E.; LaFrate, A. L.; Gin, D. L.; Noble, R. D. Main-Chain Imidazolium Polymer Membranes for CO2 Separations: An Initial Study of a New Ionic Liquid-Inspired Platform. *Journal of Membrane Science*, 2010, *359*, 37-43.
(24) Lin, H. Q.; Freeman, B. D., Materials selection guidelines for membranes that remove CO2 from gas mixtures. *Journal of Molecular Structure* 2005, *739* (1-3), 57-74.
(25) Lin, H.; Freeman, B. D., Gas and Vapor Solubility in Cross-Linked Poly(ethylene Glycol Diacrylate). *Macromolecules* 2005, *38* (20), 8394-8407.
(26) An, W.; Turner, C. H., Linking Carbon and Boron-Nitride Nanotubes: Heterojunction Energetics and Band Gap Tuning. *Journal of Physical Chemistry Letters* 2010, *1* (15), 2269-2273.
(27) Tomizaki, K.-y.; Shimizu, S.; Onoda, M.; Fujioka, Y., Heats of Reaction and Vapor−Liquid Equilibria of Novel Chemical Absorbents for Absorption/Recovery of Pressurized Carbon Dioxide in Integrated Coal Gasification Combined Cycle−Carbon Capture and Storage Process. *Industrial & Engineering Chemistry Research* 2009, *49* (3), 1214-1221.
(28) Shannon, M. S.; Bara, J. E., Properties of Alkylimidazoles as Solvents for CO_2 Capture and Comparisons to Imidazolium-Based Ionic Liquids. *Industrial & Engineering Chemistry Research* 2011, *50* (14), 8665-8677.
(29) Robeson, L. M. The upper bound revisited. *Journal of Membrane Science* 2008, *320*, 390-400.
(30) Rowe, B. W.; Robeson, L. M.; Freeman, B. D.; Paul, D. R. Influence of temperature on the upper bound: Theoretical considerations and comparison with experimental results. *Journal of Membrane Science* 2010, *360*, 58-69.
(31) Ratta, V. Stancik, E. J.; Ayambem, A. A melt-processable semicrystalline polyimide structural adhesive based on 1,3-bis(4-aminophenoxy)benzene and 3,3 ',4,4 '-biphenyltetracarboxylic dianhydride. *Polymer* 1999, *40* (7), 1889-1902.
(32) Imaizumi, S.; Ohtsuki, Y.; Yasuda, T.; Kokubo, H.; Watanabe, M. Printable polymer actuators from ionic liquid, soluble polyimide, and ubiquitous carbon materials. *Appl. Mater. Interfaces* 2013, *5* (13), 6307-6315.
(33) Dinolfo, P. H.; Williams, M. E.; Stern, C. L.; Hupp, J. T. Rhenium-based molecular rectangles as frameworks for ligand-centered mixed valency and optical electron transfer. *J. Am. Chem. Soc*. 2004, *126*, 12989-13001.

CHAPTER TEN

CONCLUSION AND RECOMMENDATIONS

The novel CO_2 separation performance and properties of imidazole-based media are presented in this work as an alternative approach to capture and mitigate fugitive, anthropogenic CO_2 emissions from post-combustion flue gas, as well as applied to natural gas purification processes. With current technologies (e.g. absorption, adsorption, cryogenics, and polymer separations) not being practical or feasible for full-scale post combustion CO_2 capture, emerging research efforts must consider other techniques and platforms with advanced chemistry and properties by increasing the affinity and uptake of CO_2 over light gases (e.g. N_2, CH_4). Physical properties of 1-*n*-alkylimidazoles, including density and viscosity, were measured and modeled as a function of temperature and molecular weight (i.e. *R'*). Alkylimidazoles prove to be comparable to analogous IL counterparts in terms of CO_2 solubility, low volatility, and tunable structure, however, exploiting the additional proton accepting capabilities for significant increases in CO_2 uptake as hybrid solvents with readily-available amine solvents. However, reactive and reversible (e.g. in situ) ILs show promise as advanced materials for efficient CO_2 separations, being synthesized readily by available chemical stock. Ideal CO_2 and CH_4 solubilities in 1-*n*-alkylimidazoles as functions of temperature present favorable gas separation performance for natural gas sweetening when compared to currently used organic solvents and IL families. Several cation and anion combinations for imidazolium- based ILs were also examined to determine underlying structure properties correlated to gas solubility via COSMOTherm software package, thus, revaluating prior RST-based CO_2 solubility and selectivity models. Fractional free volume (*FFV*) calculated during this study proved to be a better suited dependent variable for aforementioned models than previously considered molar volume (V_m). Novel imidazoles including oligo(ethylene glycol) substituents (e.g. PEG_n-imidazoles) were investigated for improved CO_2/CH_4 separations due to inclusion of polar chains having higher affinity for CO_2. *N*-funcitonalized imidazoles also presented a reversible and reactive mechanism with SO_2 for direct recovery in flue gas desulfurization (FGD), forming a stable 1:1 molar complex under ambient conditions unlike other common organic solvents or ILs and can be considered for novel synthesis of sulfur-based pharmaceutical precursors. All aforementioned CO_2 capture performance in imidazole solvents can also be applied to novel imidazole-based polymeric materials as fixed media for gas separations. Imidazole-based co-polymers offer an innovative platform for facilitated transport via a bicarbonate mechanism in the presence of water for post-combustion CO_2 capture, with tunability and pK_a of varying structures governing CO_2 uptake and polymeric material properties. Also, electrolyte-based polymers can readily be formed with the imidazole platform as based on diimide chemistry and will be explored as alternative materials for CO_2 separations.

REFERENCES

(1) Ozgur, E., Gumrah, F. Energy Sources, Part A: Recovery, Utilization, and Environmental Effects, 31, 698-709, 2009.

(2) Figueroa, J. D.; Fout, T.; Plasynski, S.; McIlvried, H.; Srivastava, R. D., Advancesn in CO2 capture technology - The US Department of Energy's Carbon Sequestration Program. *International Journal of Greenhouse Gas Control* 2008, *2* (1), 9-20.

(3) de Visser, E.; Hendriks, C.; Barrio, M.; Molnvik, M. J.; de Koeijer, G.; Liljemark, S.; Le Gallo, Y., Dynamis CO2 quality recommendations. *International Journal of Greenhouse Gas Control* 2008, *2* (4), 478-484.

(4) The Future of Coal - Options for a Carbon Constrained World. MIT Interdisciplinary Study: 2007.

(5) U. S. Environmental Protection Agency (EPA), Inventory of U. S. greenhouse gas emissions and sinks: 1990-2009, Executive Summary 5, tbl. ES-2.

(6) Herzog, H., What future for carbon capture and sequestration? *Environmental Science & Technology* 2001, *35* (7), 148A-153A.